UNIVERSITY
of
GLASGOW

The effect of pharmacological modulation of the sarcoplasmic reticulum on left ventricular function in the isolated working rabbit heart

Allen Kelly, BSc

Submitted in fulfilment of the requirements for the degree Doctor of Philosophy to the Faculty of Veterinary Medicine, University of Glasgow, U.K.

Research completed within the Glasgow Cardiovascular Research Centre, University of Glasgow, U.K.

Abstract

This work described in this thesis investigated the role of the sarcoplasmic reticulum (SR) in the regulation of normal mechanical function of the isolated heart, with the focus of the work resting on the Ca^{2+} release channel, the ryanodine receptor (RyR) and the SR Ca^{2+} pump, the sarco-endoplasmic reticulum Ca^{2+} ATPase (SERCA). This was performed by characterising left ventricular mechanical function in an isolated working heart model in the face of pharmacological manipulation of the above intracellular SR proteins. The following were the aims of this project.

1. Characterisation of *ex vivo* working heart left ventricular mechanical function using miniaturised single and multi-segment pressure-conductance technology
2. Characterisation of working heart mechanical function under conditions where SR Ca^{2+} cycling is altered; i) perfusion with elevated $[Ca^{2+}]_o$ and β-adrenergic stimulation to induce SR Ca^{2+} loading and ii) in a rabbit coronary artery ligation model of left ventricular dysfunction. Following this, the influence of acute perfusion of the compound K201 in healthy hearts and in the above experimental conditions was investigated.
3. Investigation of the specific contribution of SR Ca^{2+} uptake to normal left ventricular contractility and relaxation by specific pharmacological blockade of SERCA in the isolated working heart.

Hearts from male New Zealand White rabbits were cannulated via the aorta and a pulmonary vein ostium and perfused in working heart mode. Contractile function and changes in left ventricular volume during the cardiac cycle were assessed using a 3F pressure-conductance catheter inserted into the left ventricle via the aorta. The isolated working heart was found to produce a maximal stroke volume under identical loading conditions and and pacing frequency using a volume of air within the compliance chamber of 15 ml of air. Using an atrial filling pressure of 7.4 mmHg and an afterload of 60 mmHg the preparation was also found to have stable function in working mode for 60 – 90 min with <10% decline in cardiac output.

To assess the effect of the compound K201 on cardiac mechanical function isolated working hearts were perfused with increasing concentrations of K201 (0.3, 1.0 and 3.0) for 4 min at each concentration. When normalised to control hearts paced at equivalent rates 0.3 μM K201 led to a significant increase in end diastolic pressure (EDP) but did not alter other indices of mechanical function. 1.0 μM and 3.0 μM K201 led to a significant decline

in left ventricular peak pressure and dP/dt_{max}, impairment of relaxation (reduced dP/dt_{min}, increased EDP and τ) and a depression of heart rate and stroke volume. At 3.0 μM depression of mechanical function was of a sufficient extent as to cause cessation of forward flow (aortic flow) in 3 of the 8 hearts studied. In a subset of experiments where heart rate was kept constant via electrical stimulation of the right atrium, exposure to 1.0 μM K201 led to a decline in mechanical function that was of a similar degree to that of unpaced hearts.

High Ca^{2+} loading conditions were simulated by raising $[Ca^{2+}]_o$ from 2.5 mM to 4.5 mM, followed after 5 min by addition of 150 nM isoproterenol (ISO). Increasing $[Ca^{2+}]_o$ led to a sustained increase in stroke volume and systolic function (dP/dt_{max} and peak systolic pressure) with no steady state change in dP/dt_{min} or end diastolic pressure. Addition of ISO led to a transient improvement in all indices of mechanical function lasting approximately 20s. In hearts perfused with 4.5 mM $[Ca^{2+}]_o$ and ISO only (n=11) mechanical function declined thereafter such that by 600s post-ISO addition aortic flow had ceased in all but 5 of the 11 hearts in this group. In contrast, hearts perfused with 1.0 μM K201 30s after addition of ISO (n=9) all maintained aortic flow and demonstrated significantly improved peak systolic pressure, dP/dt_{max} and dP/dt_{min} at 600s post-ISO in comparison to hearts not perfused with K201. In addition, mean inter-peak interval variability determined from left ventricular pressure recordings (used as an index of arrhythmicity) was significantly lower in K201 treated hearts 600s post-ISO addition in comparison to non-treated hearts. K201 also led to a preservation of left ventricular peak pressure and stroke volume when applied 300s post-ISO. Despite being detrimental to mechanical function in healthy hearts K201 preserved function in a pharmacological model of high calcium loading.

Left ventricular dysfunction was surgically induced in rabbits by coronary artery ligation. *Ex vivo* mechanical function was assessed 8 weeks post-op using a 3 segment multi-segmental pressure-conductance catheter inserted into the left ventricle with each segment delineating 3 discrete functional regions within the ventricular chamber; apex, mid and base. Hearts were paced at 200 $beats.min^{-1}$ throughout. 8 week ligation hearts exhibited a significantly reduced ejection fraction and higher end systolic volumes in comparison to sham operated controls. Assessment of regional mechanical function in 8 week ligation hearts revealed that a significantly greater proportion of total stroke volume and stroke work was performed by the mid segment *vs.* the apex, while regional function was similar between all segments in the sham operated controls. Treatment with 1.0 μM K201 led to a decline in systolic function and impairment of relaxation (decreased dP/dt_{min} and increased

τ) in sham operated control hearts similar to that shown in chapter 3. In contrast, aside from dP/dt_{max} which was significantly reduced from baseline, K201 had no significant effect on mechanical function in 8 week ligation hearts. No region specific effects of K201 were detected, as the percentage contribution of each region to total stroke volume and stroke work remained unchanged in both groups after treatment with K201. The effects of K201 on mechanical function in hearts with left ventricular dysfunction appear to be altered in comparison to both healthy and sham operated hearts.

SR Ca^{2+} uptake was inhibited in an isolated working rabbit heart model using the specific pharmacological SERCA2a inhibitor thapsigargin (TG). Hearts were paced at 220 beats.min throughout the investigation. The experimental endpoint for TG treated hearts was reached when hearts no longer produced an aortic flow. Hearts perfused in working heart mode with the thapsigargin vehicle for 60 min acted as controls. At the end of each experiment left ventricular tissue samples were homogenised in a protease-phosphatase inhibitor cocktail and stored for subsequent analysis. A significant decline in systolic and diastolic functional parameters was evident 5 min after addition of TG, with no significant changes demonstrable in the vehicle control group at this timepoint. In TG treated hearts function had declined even further by the endpoint. In a subset of TG treated hearts end systolic and end diastolic volumes were shown to decline over time, indicative of impaired left ventricular filling and diastolic abnormalities. Analysis of SERCA uptake by Elliott *et al*. (2009) using tissue homogenates from the current investigation revealed that at the time of aortic flow cessation SERCA activity was < 10 %, suggesting that SR Ca^{2+} uptake may decrease to very low levels before working heart function fails.

Table of Contents

List of Tables

List of Figures

Acknowledgements

Firstly I would like to thank both Mike Dunne and Aileen Rankin for their excellent technical support throughout my PhD. It cannot be overemphasised the critical role the Technicians play within research. Aileen especially deserves a mention for her tireless efforts to help me overcome the myriad small problems which cropped up throughout my 3 years and as well for lending an ear (and a cup of tea) whenever I was feeling down.

To my supervisors, Dr Chris Loughrey and Professor Godfrey Smith, I can offer nothing but my praise and admiration. Over the past 3 years I have come to appreciate that success in academic research takes a certain driven attitude extending beyond simply understanding of the field, and I have recognised in both my supervisors a passion and commitment to science that is inspirational for anyone who works closely with them. To Chris especially I would like to extend my gratitude for his constant help and support in both my academic and personal life, and a seemingly unwavering belief in my ability which has kept me going through these past three years. I feel in both my supervisors I have not only gained a mentor, but also a good friend and trusted colleague.

To Elspeth Elliott, who has not only been an excellent lab partner and teacher to me, but also a great friend. Whether it be the subtle nuances of an experimental protocol, or possibly even the latest fashion advice, you were always willing to go out of your way to offer help and advice and I can't thank you enough. Remember to keep checking your taps.

I have made some incredible friends during my time in the lab who have all helped me with their love and support in more ways that they can know. I want to thank every one of them for making the hard times seem just that little less difficult; Niall MacQuaide, Iffath Ghouri, Dave Farmer, Helen Chick, Luisa Frei, Sarah Kettlewell, Rachel Myles, Naouki Ohtani, Toshiya Matsuda, Hisashi Hasumi, Soontaree Petchdee, Jenny Greig and Jennifer M^{c}Lachlan. I especially want to thank Kirsty Foote and Stuart M^{c}Intyre, who over the past year have offered so much of their time, effort and friendship to keep me focussed and drag me out of the lows whenever necessary. Thank you.

Finally I wish to thank my family; my mum and dad, my sister Yvonne, and my brother-in-law Mark, for supporting me and being there whenever I needed a helping hand.

Author's Declaration

The experimental work described in this thesis was carried out by myself and has not been presented as part of any other degree. Some results during the period of research have been presented in abstract form and are detailed below.

A. Kelly, T. Matsuda, A. Rankin, G. L. Smith, and C. M. Loughrey: Calcium overload induces ectopic electrical activity and abnormalities of left ventricular function in an isolated working heart. Abstract – Biophysical Society annual meeting Long Beach, California. *Biophysical Journal* 2008; **94(2):** 518-527

A. Kelly, T. Matsuda, A. Rankin, G. L. Smith, and C. M. Loughrey: K201 maintains cardiac function during Ca^{2+} overload in an isolated working rabbit heart. Abstract – Physiological Society annual meeting Cambridge, *J Physiol* 2008; Proc Physiol Soc 11: PC25

E. Elliott, A. Kelly, A. Rankin, G. L. Smith, and C. M. Loughrey. A quantitative assessment of selective pharmacological inhibition of SERCA in isolated rabbit working hearts. Abstract – Biophysical Society annual meeting Boston, Massachusetts, *Biophysical Journal* 2009; **96(3):** 515a

Definitions/Abbreviations

AP	Action potential
APD	Action potential duration
ATP	Adenosine triphosphate
ATPase	Adenosine triphosphatase
Ba^{2+}	Barium ion
C-terminal	Carboxy-terminal
Ca^{2+}	Calcium ion
Ca^{2+} ATPase	Calcium pump
CaMKII	Ca^{2+}/Calmodulin-dependent protein kinase II
cAMP	cyclic adenosine monophosphate
CCh	carbachol chloride
CICR	Calcium-induced calcium release
COS-1	CV-1 (simian) cell line containing SV-40 genetic material
CPA	Cyclopiazonic acid
CPK	Creatine phosphokinase
CPVT	Catecholaminergic polymorphic ventricular tachycardia
DAD	Delayed afterdepolarisation
DIDS	4,4'-diisothiocyanatostilbene-2,2'-disulfonic acid
DKO	double knockout
DM-Nitrophen	1-(2-Nitro-4,5-dimethoxyphenyl)-1,2-diaminoethane-N,N,N,',N'-tetraacetic acid
DMSO	Dimethyl sulfoxide
dP/dt_{max}	Maximum rate of left ventricular pressure rise
dP/dt_{min}	Maximum rate of left ventricular pressure fall
EC coupling	Excitation-contraction coupling
EDP	End diastolic pressure
EDPVR	End diastolic pressure-volume relationship
EDV	End diastolic volume
EF	Ejection fraction
EGTA	Ethyleneglycol-*bis*(β-aminoethyl)-N,N,N',N'-tetraacetic acid
E_m	Membrane potential
ESPVR	End systolic pressure-volume relationship
ESV	End systolic volume
FKBP12	FK506 binding protein (12 kDa)
FKBP12.6	FK506 binding protein (12.6 kDa)

HR	Heart rate
IAA	Iodoacetate
IR	Ischaemia-reperfusion
ISO	Isoproterenol
K^+	Potassium ion
K_{Ca}	Calcium dissociation constant
LDH	Lactate dehydrogenase
Li^+	Lithium ion
LTCC	L-type Ca^{2+} channel
LV	Left ventricular
LVDP	Left ventricular developed pressure
LVEDP	Left ventricular end diastolic pressure
MI	Myocardial infarction
mM	Millimolar (concentration)
MPTP	Mitochondrial permeability transition pore
mRNA	Messenger ribonucleic acid
Na^+	Sodium ion
NCX	Na^+/Ca^{2+} exchanger
NHE	Na^+/H^+ exchanger
Ni^+	Nickel ion
nM	Nanomolar (concentration)
NO	Nitric oxide
NOS	Nitric oxide synthase
pCa	-log $[Ca^{2+}]$
PCr	Phosphocreatine
P_i	Inorganic phosphate
PKA	Protein kinase A
PKC	Protein kinase C
PKC-δ	Delta-isoform of protein kinase C
PLB	Phospholamban
PMCA	Plasma membrane Ca^{2+} ATPase
P_o	Open probability
PSP	Peak systolic pressure
RyR	Ryanodine receptor
RyR2	Cardiac ryanodine receptor
SEM	Standard error of the mean
SERCA	Sarco-endoplasmic reticulum Ca^{2+} ATPase
SR	Sarcoplasmic reticulum
SV	Stroke volume

TBQ	2,5-Di(*tert*-butyl)-1,4-Benzohydroquinone
TG	Thapsigargin
TnC	Troponin C
TnI	Troponin I
TnG	Transgenic
T-tubule	Transverse tubule
VLA	Ventricular long axis
V_{max}	Maximum velocity
VSL	Variable segment length
WT	Wild type
µM	Micromolar (concentration)
ºC	Degree Celcius

1 Introduction

1.1 Excitation-Contraction Coupling

In life the heart is responsible for the continuous flow of blood throughout the body, allowing transport of vital nutrients, hormones, signalling factors etc. to and from the tissues of the body. During the normal cardiac cycle the chambers of the heart contract and relax in a tightly regulated fashion in order to pump blood as efficiently as possible. The millions of cardiac myocytes which comprise the chambers of the heart are tightly coupled to one another forming a functional syncytium which allows electrical activation of the heart, beginning at the sino-atrial node, to spread quickly through the conduction system of the heart, resulting in near synchronous depolarisation and subsequent contraction of the atria and then the ventricles. The heart is a complex organ however, with decades of research devoted to elucidating the underlying mechanisms which link electrical excitation of the cardiac tissue to activation of the myofilament machinery, a process known as excitation-contraction (EC) coupling. It is now widely accepted that cardiac muscle is most likely activated by a process known as calcium-induced calcium release (CICR), described in detail by Fabiato using mechanically skinned canine cardiomyocytes (Fabiato, 1983; Fabiato, 1985). Calcium ions are key second messengers in the mechanisms linking electrical excitation of the cardiac myocyte to contraction of the heart. Regulation of Ca^{2+} cycling between the myoplasm, intracellular organelles and the extracellular space is critical for the control of heart rhythm and cardiac contractile force both in health and in cardiac disease states such as heart failure.

The following chapter is intended to give the reader an introduction to a number of intracellular Ca^{2+}-handling processes relevant to this thesis and from this attempt to address some of the key outstanding issues which will be discussed in the proceeding chapters. While the complex nature of cardiac EC coupling does not allow discussion of each component to be given equal weighting this is not intended to suggest that certain elements are more important than others. Rather this reflects the focus of the thesis and the subject matter which has been investigated and discussed in the forthcoming chapters.

1.1.1 Calcium-Induced Calcium release

Research over the past 30 years has provided more detailed insight into the specific processes involved in cardiac E-C coupling at the myocyte level. Information is now available on the locations and relative contributions of specific ion transport mechanisms within the cardiac myocyte, as well as the regulation of specific transporters and release

channels by subsidiary proteins, small molecules and second messengers. A schematic of the basic processes intrinsic to myocyte contraction and relaxation is shown in Figure 1.1. The cardiac action potential spreads as a wave of depolarization across the surface sarcolemma and down into surface membrane invaginations known as T-tubules. Depolarisation of voltage-sensitive Ca^{2+} channels located there triggers an influx of Ca^{2+} into the cell as an inward Ca^{2+} current (I_{Ca}). This influx of Ca^{2+} in turn activates the release of a proportionately greater amount of Ca^{2+} from the sarcoplasmic reticulum in a process known as Ca^{2+}-induced Ca^{2+} release. This process is critical in determining the amount Ca^{2+} released and therefore the strength of contraction.

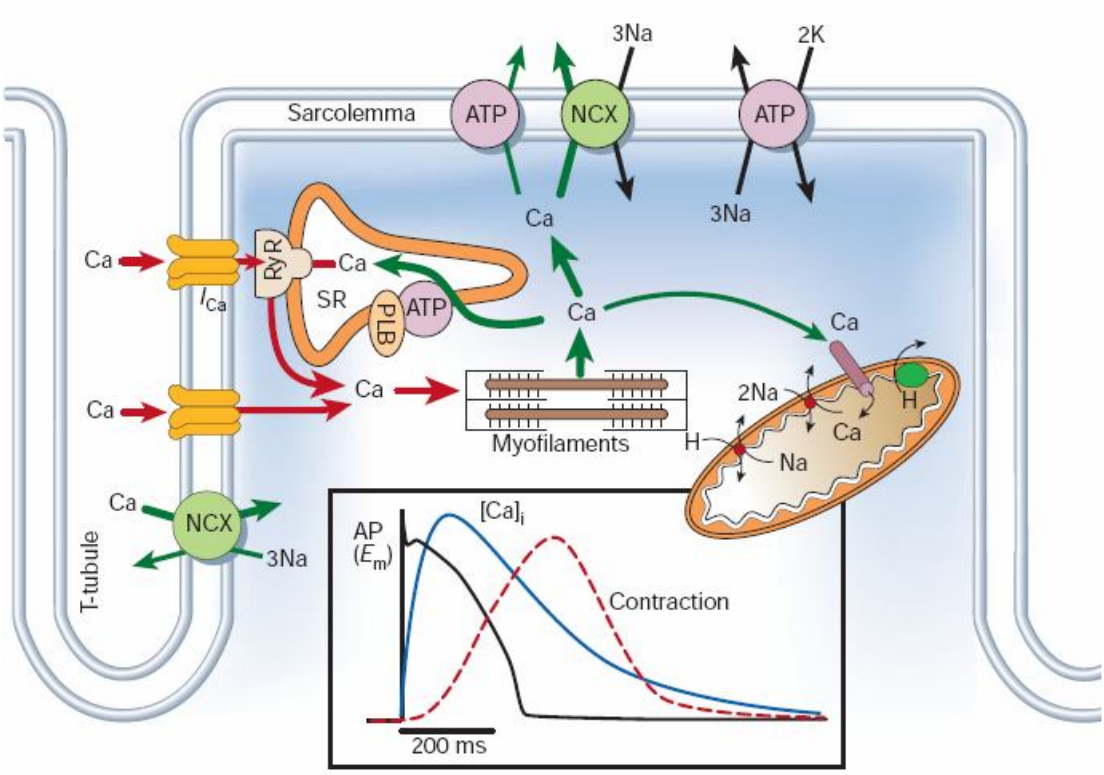

Figure 1.1 Ca^{2+} dynamics within the ventricular myocyte. Schematic representation of major Ca^{2+} transport fluxes within the myocyte, with inset showing time course of rabbit ventricular myocyte action potential (black line), intracellular Ca^{2+} transient (blue line) and contraction (red dashed line). (ATP, ATPase; NCX, Na^+/Ca^{2+} exchange; PLB, phospholamban; SR, sarcoplasmic reticulum; RyR, Ryanodine receptor). (Figure taken from Bers (2002) *Nature* 415, 198-205).

1.1.1.1 Ca^{2+} Influx via the L-Type Ca^{2+} channel

The main source of trigger I_{Ca} for CICR originates from Ca^{2+} influx via L-type Ca^{2+} channels (LTCCs) which are located primarily in the T-tubule membrane in close proximity to the SR terminal cisternae (Carl *et al.*, 1995). Contribution of the T-type Ca^{2+} channels to EC coupling mechanisms in adult ventricular myocytes is believed to be negligible, with small to undetectable levels of T-type channel protein present in guinea-

pig, rabbit and rat (Bers & Perez-Reyes, 1999). I_{Ca} is dependent on membrane potential (E_m), becoming activated at -40 mV and reaching a peak at approximately +10 mV, declining thereafter as the channel approaches its reversal potential at approximately +60 mV (Beuckelmann & Wier, 1988). This results in the appearance of a bell-shaped relationship between E_m and peak I_{Ca} as is shown in Figure 1.3.

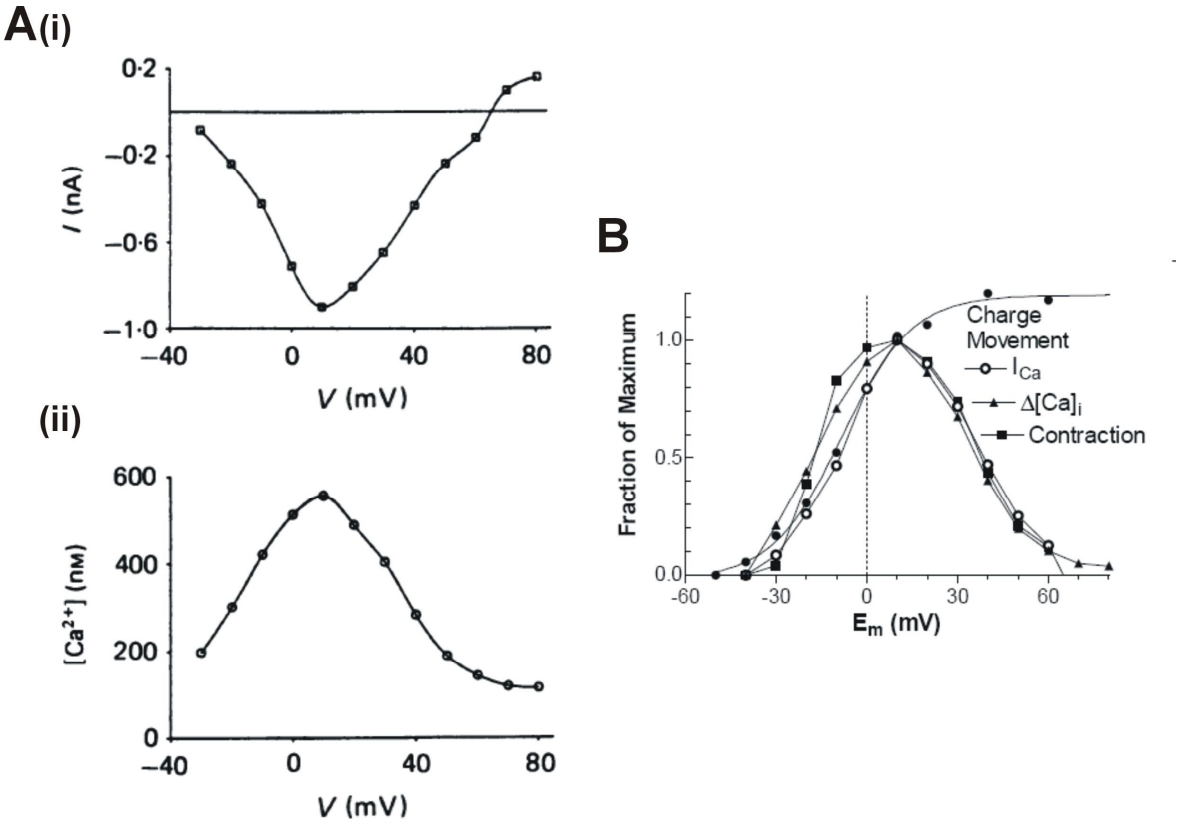

Figure 1.2 Voltage dependence of I_{Ca} in cardiac muscle. Both I_{Ca} (A(i)) and $[Ca^{2+}]_i$ (A(ii)) exhibit a bell-shaped dependence on voltage (or E_m). B. Despite the sigmoidal relationship between E_m and charge movement, normalised I_{Ca}, intracellular Ca^{2+} transient and myocyte contraction all demonstrate a bell-shaped appearance in relation to E_m illustrating that charge movement is not responsible for Ca^{2+}-induced release of Ca^{2+} from the SR. (Adapted from (A) Bueckelmann *et al.* (1988) *J.Physiol*. 405 233-255, and (B) Bers (2001) Excitation-Contraction coupling and Cardiac Contractile Force, 2nd edition, Kluwer Academic, Dortrecht, The Netherlands).

The amount of Ca^{2+} entering the cell in most cases would not be sufficient to activate the myofilament contractile machinery as has been demonstrated in skinned cardiac myocyte preparations (Fabiato, 1983). Data from intact myocytes predicts an estimated total Ca^{2+} influx into the cytosol of ~60 µmol/l cytosol for activation of a normal twitch in ventricular myocytes, corresponding to approximately 40 % of maximal developed force at 25-30ºC (Harrison & Bers, 1989). Quantification of Ca^{2+} entry via LTCCs during the action potential has yielded estimates for rabbit ventricular myocytes between 21 and 25 µmol Ca/l cytosol (Yuan *et al.*, 1996), however these values are thought to be an overestimation

as EGTA, a Ca^{2+} chelator, was present in the intracellular environment which may reduce Ca^{2+}-dependent inactivation of LTCCs (Bers & Perez-Reyes, 1999). More physiological estimates for the total amount of Ca^{2+} entering during the action potential have been placed at ~12 μmol/l cytosol in rabbit ventricular myocytes (Puglisi *et al.*, 1999). Therefore, the Ca^{2+} required for activation of the myofilaments must come from a separate source.

1.1.2 The Sarcoplasmic Reticulum

The sarcoplasmic reticulum (SR) is an extensively networked, tubular organelle enclosed entirely within the intracellular space of the cardiac myocyte. Its main function is the storage and release of calcium which is a requirement for normal contractile function of the heart. In cardiac myocytes the sarcolemmal membrane and SR couple closely in junctions known as dyads. Estimates suggest that in ventricular myocytes from rabbits, rats and mice the junctional couplings between the SR and T-tubules is 4 to 6 times greater than between the surface sarcolemma (Page & Surdyk-Droske, 1979). Between species, distribution is not equal; in rabbit the fraction of sarcolemmal membrane involved in dyadic junctions (4.6 % surface sarcolemma, 20.6 % T-tubular) is lower in comparison to mice and rats (6.5-7.7 % surface sarcolemma, 40-48 % T-tubular), reflecting the species-dependent differences in SR Ca^{2+} dependence for contraction (Bers, 1985; Page & Surdyk-Droske, 1979). In mammalian ventricular myocardium LTCCs located in the T-tubules are closely associated with large molecular weight proteins at the junctions between the SR and the sarcolemmal membrane, now known to be the SR Ca^{2+} release channel, the Ryanodine receptor.

1.2 Structure of the Ryanodine receptor

The cardiac ryanodine receptor exists as a large homotetrameric protein, consisting of 4 identical subunits of molecular weight 565 kDa. While three subtypes are known to exist in a variety of tissues, RyR2 is the predominant isoform in cardiac muscle. Figure 1.3 depicts a schematic representation of the RyR2 monomer. Around 90% of the channel is located in the N-terminal region, described as the foot-process noted in early electron micrographic images, in which a large number of regulatory proteins, including calmodulin, FKBP12.6 (calstabin-2), protein phosphatases 1 and 2A and protein kinase A (PKA) bind and coordinate channel function (Yano *et al.*, 2006). The C-terminal, composed of 4-10 transmembrane domains, comprises the remaining 10% of the channel.

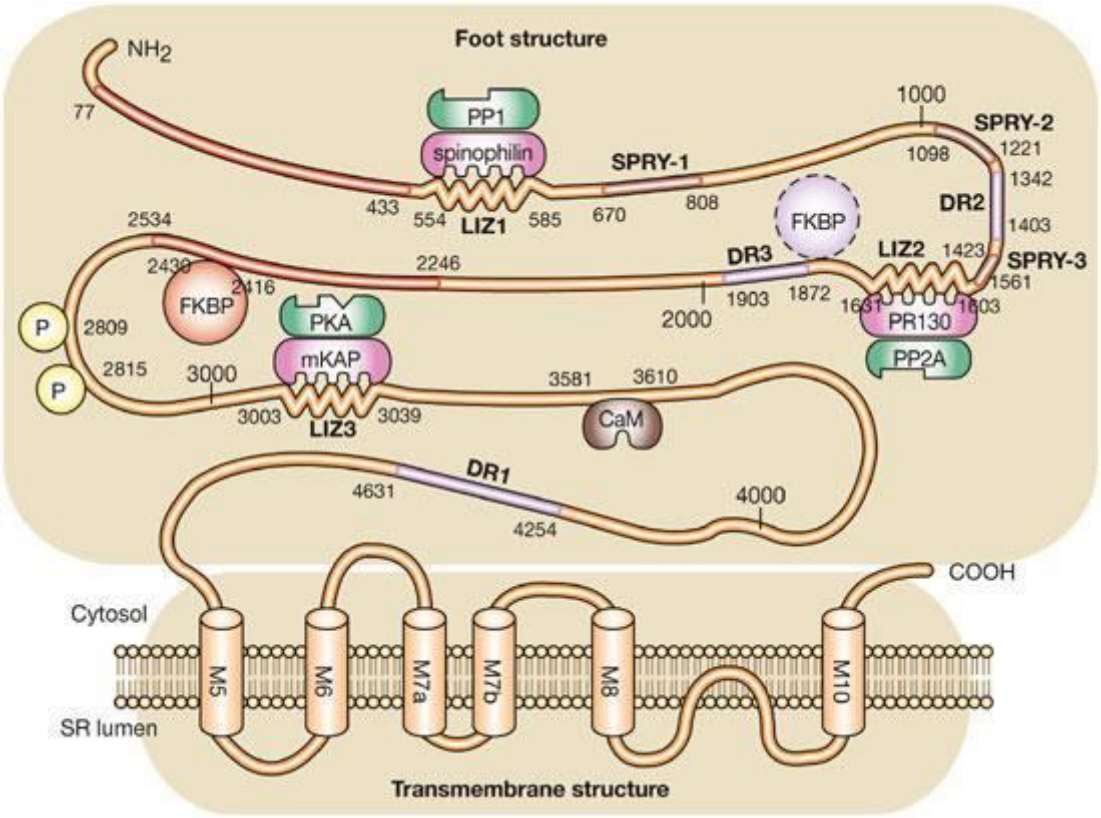

Figure 1.3 Schematic diagram of the cardiac RyR subunit. The large N-terminal domain of RyR2 contains binding sites for many regulatory proteins, including FKBP12.6, PKA, Calmodulin and protein phosphatases 1 and 2A. (Diagram taken from Yano *et al.* (2006) *Nat. Clin. Pract.* 3(1) 43-52).

1.2.1 Evidence for Ca^{2+}- Induced Ca^{2+} release

Fabiato demonstrated using skinned cardiac myocyte preparations that Ca^{2+} release from the SR and subsequently contraction could be induced by simulation of I_{Ca} using rapid Ca^{2+} application. The trigger for Ca^{2+} release from the SR was shown to be a function of the rate of change of [free Ca^{2+}]; rapid application induces SR Ca^{2+} release whereas slow gradual application only serves to load the SR (Fabiato, 1983). This is in contrast to the charge-coupled release mechanism proposed for skeletal muscle, where Ca^{2+} release from the SR is dependent on charge movement (Melzer *et al.*, 1986). Support for CICR as the mechanism of SR Ca^{2+} release in cardiac muscle (versus a charge-coupled release mechanism) comes from several experimental observations; 1. Buffering extracellular Ca^{2+} with 4 mM EGTA causes the LTCC to carry a large Na^{+} current, but while a measurable ionic current flows under these circumstances and there is charge movement due to LTCC activation, neither a $[Ca^{2+}]_i$ transient nor contraction are evoked (Nabauer *et al.*, 1989). The same scenario is encountered using Ba^{2+} as the charge carrier, highlighting the requirement for Ca^{2+} entry as the triggering stimulus for Ca^{2+} release from the SR. 2.

Flash photolysis of photolabile Ca^{2+} chelators (Nitr-5 and DM-nitrophen) has been demonstrated to induce $[Ca^{2+}]_i$ transients in intact ventricular myocytes. Valdeolmillos *et al*. (1989) demonstrated flash photolysis of Nitr-5 induced contractions in isolated rat ventricular myocytes that were sensitive to Ryanodine and could also be invoked in the presence of 10 mM Ni to block I_{Ca} (Valdeolmillos *et al.*, 1989). Similar experiments performed by Niggli & Lederer (1990) under a constant holding potential of -40 mV (to eliminate the possibility of depolarization-induced SR Ca^{2+} release) confirmed that photolysis of caged Ca^{2+} could induce CICR independent of depolarisation, highlighting the requirement for a sudden increase in $[Ca^{2+}]_i$ to induce SR Ca^{2+} release and contraction (Niggli & Lederer, 1990). Altering the holding E_m between -100, 0 or +100 mV also had no effect on the amplitude of the contractions invoked by photolysis of caged Ca^{2+}, providing further evidence that CICR is not influenced by a voltage-dependent mechanism.

1.2.2 CICR and the theory of 'Local Control'

Problems are encountered when attempting to explain the mechanisms governing calcium-induced calcium release. The theory itself implies a high gain positive feedback system, whereby the triggering of an initial release of Ca^{2+} from the SR will cause the system to feedback upon itself and allow release to continue to completion. On the contrary, experimental evidence shows that CICR is not an 'all-or-none' process, and SR Ca^{2+} release is graded by I_{Ca} (Lederer *et al.,* 1990). Furthermore, early termination of I_{Ca} leads to abbreviation of SR Ca^{2+} release. Simulated model systems have been proposed to try and explain this apparent dichotomy. **Common pool models** operate on the assumption that there is a single cytosolic pool of Ca^{2+} accessible to both the Ca^{2+} entering from the extracellular space and released from the SR, the concentration of which governs the release of Ca^{2+} from the SR (Stern, 1992). Such models however predict a system where very small adjustments in amplification would result in the appearance of spontaneous behaviour. The close juxtaposition of LTCCs and RyRs in the dyadic junctions allows prediction of an alternative model of CICR, where Ca^{2+} enters the dyadic cleft and is immediately in very close proximity to Ca^{2+} sensitive sites on the RyRs. This would permit these sites to be much less sensitive to global intracellular Ca^{2+} concentrations, reducing the likelihood of regenerative Ca^{2+} release occurring. This '**Local Control**' theory was advanced by Stern (1992), who proposed two models of CICR; a) a 'Ca^{2+}-synapse' model, where 1 LTCC triggered the release of Ca^{2+} from a single RyR, and b) a 'Cluster bomb' model, in which single LTCCs activated a cluster of RyRs (Stern, 1992). Gradation of release by the inward calcium current could be accounted for using both

models, however, in keeping with the high gain of CICR, single SR release channel Ca^{2+} flux using the Ca^{2+}-synapse model would have to be unfeasibly large. The Cluster bomb model therefore initially appeared more appropriate and was supported by reports which demonstrate the ratio of ryanodine receptors to LTCCs in junctional regions is approximately 1:4-10, depending on species (Bers & Stiffel, 1993; Wibo *et al.*, 1991).

1.2.3 Ca^{2+} sparks represent local release events from the sarcoplasmic reticulum

The idea of local control was supported by the description of visualised SR Ca^{2+} release events in ventricular myocytes known as Ca^{2+} sparks (Cheng *et al.*, 1993; Lukyanenko *et al.*, 2000; Parker *et al.*, 1996). The physical separation of individual clusters of RyR2s limits the possibility of Ca^{2+} release from one cluster activating neighbouring clusters due to Ca^{2+} diffusion limitations. The cumulative effect of thousands of Ca^{2+} sparks, temporally and spatially synchronised by the action potential and I_{Ca} are believed to produce the upstroke of the $[Ca^{2+}]_i$ transient. While the existence of these local release events aids the acceptance of CICR as the dominant mechanism for activation of contractile elements in cardiac EC coupling, the system described thus far is still regenerative. Further mechanisms must exist to explain termination of SR Ca^{2+} release. Currently several mechanisms have been proposed which may account for termination of Ca^{2+} sparks.

1. All of the RyR2s and L-type Ca^{2+} channels within a cluster may inactivate at the same time, a process termed 'stochastic attrition' (Stern, 1992). This process could potentially operate as a dominant mechanism for spark termination in the 'Ca^{2+}-synapse' model described above, as local $[Ca^{2+}]_i$ would decline quickly following closure of the SR Ca^{2+} release channel. While it is likely this process contributes to termination of SR Ca^{2+} release to some degree, as cluster size increases above 3-4 the probability that stochastic attrition alone could explain release termination is exponentially reduced (Stern, 1992).

2. SR Ca^{2+} levels become depleted preventing further release. This view has not gained acceptance as experimental evidence suggests that a significant releasable fraction of Ca^{2+} is still present following Ca^{2+} release. In addition, interventions which increase RyR sensitivity to activation induce long-lasting local Ca^{2+} release events (sparks) which maintain a similar amplitude throughout the period of release (Cheng *et al.*, 1993). While

the entire SR may not become depleted, it is possible that local depletion within the SR near a release cluster may occur (see below).

3. Ca^{2+}-dependent inactivation of release, first proposed by Fabiato (1985) (Fabiato, 1985) states that Ca^{2+} binds to a high affinity binding site on the RyR2 at a slow rate, inducing inactivation and refractoriness of the channel. While inactivation itself is not directly supported by experimental evidence, an extension of this idea was proposed known as Ca^{2+}-dependent adaptation of RyR. It has been noted in studies where RyRs are incorporated into planar lipid bilayers that prolonged elevation of $[Ca^{2+}]$ using flash photolysis of caged Ca^{2+} initially increases RyR open probability (P_o), but this gradually diminishes over time (Zahradnikova *et al.*, 1999). Further stimulating increases in $[Ca^{2+}]$ can however, elicit activation of the channels. These findings were explained by observations that RyRs exhibit three separate modes of gating, characterised by prolonged and frequent channel openings (high open probability, H-mode), short and infrequent opening (low open probability, L-mode) and no openings (inactivated, I-mode) (Fill *et al.*, 2000; Zahradnikova *et al.*, 1999). The major problem with adaptation is the time course over which it is believed to operate is ~10 times slower than the time course for termination of SR Ca^{2+} release within individual clusters of RyRs.

While the above mechanisms may operate to some extent in SR Ca^{2+} release termination none can adequately explain experimental findings from permeabilised and intact myocytes. Current investigations have begun to focus on the role of luminal $[Ca^{2+}]_{SR}$ in the control of Ca^{2+} release termination. Buffering SR Ca^{2+} with low-affinity Ca^{2+} buffers drastically altered the relationship between I_{Ca} and SR Ca^{2+} release, and significantly increased Ca^{2+} spark amplitude and duration, suggesting that SR luminal $[Ca^{2+}]$ determines SR release termination and refractoriness of RyR (Terentyev *et al.*, 2002). SR Ca^{2+} release termination is also markedly altered in intact myocytes expressing mutations of the SR Ca^{2+} buffering protein calsequestrin which reduce SR Ca^{2+} buffering, allowing quicker restoration of local SR $[Ca^{2+}]$ following release and reduction of luminal Ca^{2+}-dependent RyR refratoriness (Terentyev *et al.*, 2008). Moreover, Ca^{2+} release appears to terminate at the same threshold luminal [Ca] regardless of initial SR Ca^{2+} content (Terentyev *et al.*, 2008; Zima *et al.*, 2008). This recent work provides compelling evidence that local luminal SR $[Ca^{2+}]$ is a critical determinant of SR Ca^{2+} release termination although it does not completely explain termination of long-lasting release events. An alternative model of SR Ca^{2+} release termination was proposed earlier by Sobie *et al.* (2002) based on the observation of a coupled-gating mechanism between individual RyRs within a cluster in

both skeletal and cardiac muscle (Sobie *et al.*, 2002). In skeletal and cardiac muscle, RyRs within a cluster are functionally linked by unique FK506 binding proteins (FKBP), which exist in the RyR macromolecular complex in a 4:1 stoichiometry with the channel (1 FKBP molecule per channel subunit). Coupled gating, conferred in cardiac RyR2s by the specific binding protein FKBP12.6, provides a mechanism for termination of SR Ca^{2+} release within an entire cluster, whereby functionally linked RyRs open and close simultaneously, effectively inhibiting neighbouring individual channels from reactivating one another. Sobie *et al*. (2002) incorporated this observation into a mathematical model of SR Ca^{2+} release termination, termed the 'sticky cluster' hypothesis, additionally consolidating the potentially large variability in RyR cluster size. The model was successful in marrying many of the experimentally observed features of Ca^{2+} sparks with simulated data, including a robust termination of SR Ca^{2+} release and largely similar Ca^{2+} spark characteristics irrespective of cluster size. The model failed however, to approximate Ca^{2+} spark width closely, with simulated Ca^{2+} sparks appearing roughly half the width of those observed experimentally (Sobie *et al.*, 2002).

A coherent theory of SR Ca^{2+} release termination therefore has yet to be completely defined and further work is required to describe all features of SR Ca^{2+} release observed experimentally. It is likely however that termination of SR Ca^{2+} release involves several of the mechanisms described above.

1.3 Ca^{2+} removal from the cytosol

Activation of the contractile machinery occurs when $[Ca^{2+}]_i$ is elevated sufficiently to allow Ca^{2+} to bind to Troponin C (TnC), releasing the inhibitory binding of Troponin I with actin and enabling actin-myosin interaction and cross-bridge formation. Following activation of the myofilament contractile machinery and systolic contraction $[Ca^{2+}]_i$ must decline back to resting levels in order that the individual myocytes and ultimately the chambers of the heart may relax to fill with blood again before the initiation of the subsequent contraction. To this end there are four Ca^{2+} removal systems present within the intracellular environment, the relative contributions of which are varied and species-dependent (see below).

1. The sarcolemmal Ca^{2+}-ATPase is a 138 kDa P-type ion motive transport enzyme, deriving energy from ATP molecules which is transferred to a phosphorylated intermediate (an aspartyl residue), enabling transport of 1 Ca^{2+} ion across the sarcolemmal membrane

for every ATP molecule hydrolysed. The sarcolemmal Ca^{2+}-ATPase consists of 10 transmembrane domains accounting for ~20% of the total protein, with the cytosolic portion making up the remaining 80%. The carboxy terminal tail of the Ca^{2+}-ATPase includes a 30 amino-acid sequence believed to be the binding site for calmodulin, as well as the phosphorylation site for both PKA and PKC. The reported maximal transport rate (V_{max}) in intact rabbit ventricular myocytes is ~2 μmol/l cytosol/s (Bassani *et al.*, 1995).

2. The mitochondrial Ca^{2+}-uniporter. Uptake of Ca^{2+} into the mitochondria is driven by the large negative membrane potential across the mitochondrial membrane (Gunter & Gunter, 2001). Thus, Ca^{2+} entry into the mitochondria does not occur through ionic exchange mechanisms but simply by diffusion of Ca^{2+} down its electrochemical gradient (Gunter & Pfeiffer, 1990). Mitochondrial Ca^{2+} uptake can be inhibited by application of ruthenium red as well as Ru360, a distinct ruthenium compound. Ca^{2+} uptake velocity is close to zero below 200 nM cytosolic $[Ca^{2+}]$, and as such mitochondrial Ca^{2+} uptake does not occur at rest in cardiac myocytes, where diastolic $[Ca^{2+}]_i$ are in the order of 100-150 nM (Gunter & Gunter, 2001).

3. The Na^+/Ca^{2+} exchanger (NCX). The major mechanism of Ca^{2+} removal from the cell is via NCX, a transporter located on the sarcolemmal membrane at sites distinct from RyR clusters in the junctional cleft. NCX transports 3 Na^+ ions in exchange for 1 Ca^{2+} ion, thus creating a net positive charge and generation of current. Transport across the membrane occurs in a consecutive fashion. As an example, with the channel face on the outer membrane open 3 Na^+ ions bind and a conformational alteration in the channel transports these ions into the myocyte. 1 Ca^{2+} ion then binds to the now open face of the channel on the cytosolic side and the reverse conformational change transports this ion out of the myocyte, and one full channel cycle is completed (Bers, 2001). NCX exhibits $Ca^{2+}{}_i$-dependent activation characteristics such that regulatory $[Ca^{2+}]_i$ is required for the channel to operate regardless of the intracellular substrate being removed. High $[Na^+]_i$ causes inactivation of the channel although this may not be physiologically relevant as the $[Na^+]_i$ required to elicit such a response is >30 mM (Matsuoka & Hilgemann, 1992). The transport action of the channel is reversible and highly dependent on E_m. Thus, during the initial phases of the action potential when E_m is high Ca^{2+} influx via NCX is thermodynamically favoured. Under certain experimental conditions (rapid reduction of $[Na^+]_o$, elevation of $[Na^+]_i$) activation of contraction induced by large (or long depolarisations in voltage-clamped cells) can occur when LTCC blockade is imposed (Barcenas-Ruiz *et al.*, 1987; Chapman & Tunstall, 1980). The contribution of NCX to

contraction is thought to be limited under physiological conditions however, and may only become significant in circumstances where $[Na^+]_i$ is substantially increased (Bers *et al.*, 1988).

4. The sarco-endoplasmic reticulum Ca^{2+}-ATPase (SERCA). SERCA is responsible for re-sequestration of Ca^{2+} into the SR following the $Ca^{2+}{}_i$ transient. Like the sarcolemmal Ca^{2+}-ATPase SERCA belongs to the P-type family of ion-motive transport proteins, however the two pumps are structurally and functionally quite distinct. Transport of Ca^{2+} into the SR lumen is described using a two-state model proposed by Mackinose (1973) (Makinose, 1973). In the 'ground state' (E_1) 2 Ca^{2+} ions and 1 molecule of ATP bind to high affinity binding sites on the cytosolic surface of the enzyme. The terminal phosphate of ATP (γ-phosphate) is donated to an aspartyl residue (Asp^{351}) in the phosphorylation domain of SERCA, resulting in a conformational change which prevents Ca^{2+} escaping from the enzyme complex ($E_1P.2Ca^{2+}$). The enzyme undergoes a further transition from a high to low energy state (E_2P), resulting in transfer of the occluded Ca^{2+} ions from a high affinity binding site to low affinity binding sites facing the inner lumen of the SR, from which the 2 Ca^{2+} ions dissociate from the enzyme complex and enter the SR. As the phosphate is dissociated from the enzyme complex, SERCA returns to the E_1 state, restoring the high affinity Ca^{2+} binding sites to the cytosolic surface of the membrane. Species-dependent differences exist in the density of SR Ca^{2+} pump sites and probably reflect the relative dependence on SERCA for cytosolic Ca^{2+} removal (discussed below). Estimates of the pump density in rabbit and rat permeabilised ventricular myocytes using thapsigargin titration were 7.7 μM.kg wet $weight^{-1}$ and 54.6 μM.kg wet $weight^{-1}$, respectively (Hove-Madsen & Bers, 1993). Structural features and differences between SERCA isoforms are discussed in detail in section 1.4.

In cardiac myocytes of most mammalian species SR Ca^{2+} uptake via SERCA is the dominant mechanism of Ca^{2+} removal from the cytosol, however species variation does exist. Ca^{2+} efflux via NCX is ~2-3 fold faster in rabbit ventricular myocytes in comparison to rat, with SR Ca^{2+} uptake via SERCA exhibiting a similar increased rate of cytosolic Ca^{2+} removal in rat *vs.* rabbit myocytes. Estimates suggest that the relative contributions of SERCA and NCX to Ca^{2+} removal following the $Ca^{2+}{}_i$ transient to be approximately 70 % and 28 % respectively in rabbit ventricular myocytes, and 92 % and 7 % respectively in rat (Bassani *et al.*, 1994). In intact ventricular myocytes, blockade of NCX and SERCA function using 0 Na^+/0 Ca^{2+} solutions and perfusion with caffeine, respectively, revealed that decay time of the $Ca^{2+}{}_i$ transient was >20s (Bassani *et al.*, 1992). Further blockade of

either mitochondrial Ca^{2+} uptake (using FCCP and oligomycin) or sarcolemmal Ca^{2+} uptake (using 10-100 mM $[Ca^{2+}]_o$) lengthens the decay time of caffeine-induced transients to >60s. The combined contribution of the sarcolemmal Ca^{2+}-ATPase and the mitochondrial Ca^{2+} uniporter (dubbed the 'slow transport mechanisms') to normal decay of the $[Ca^{2+}]_i$ is therefore negligible, with estimates in both rat and rabbit ventricular myocytes suggesting a similar value of 1-2 % of the total Ca^{2+} removed (Bassani *et al.*, 1994).

1.4 The SR Ca^{2+} ATPase is responsible for Ca^{2+} uptake into the sarcoplasmic reticulum

A key feature of the sarco-endoplasmic reticulum Ca^{2+} ATPase along with other P-type ion-motive ATPases is the transfer of the terminal phosphate of ATP to an aspartyl residue located at the catalytic site, enabling a reversible conformational change of the enzyme (Inesi *et al.*, 2005). The SERCA pump is a 110-kDa protein, encoded by three distinct genes in vertebrate species, alternative splicing of which currently accounts for over 10 distinct splice variants. The SERCA1 gene encodes an adult (SERCA1a) and fetal (SERCA1b) isoform, expressed in fast-twitch skeletal muscle (Brandl *et al.*, 1986), whilst SERCA2 encodes a further two isoforms, SERCA2a, expressed mainly in cardiac and slow twitch skeletal muscle, and a ubiquitously expressed isoform SERCA2b. SERCA3 isoforms have also been identified in a number of non-muscle tissues (Periasamy & Kalyanasundaram, 2007; Treiman *et al.*, 1998). The different SERCA isoforms exhibit a high degree of structural homogeneity, with SERCA1a and 2a sharing approximately 84 % amino acid sequence conservation (Periasamy & Kalyanasundaram, 2007). A structural diagram of the SR Ca^{2+}-ATPase is shown in Figure 1.4. The protein consists of 10 transmembrane regions (M_1-M_{10}) with additional α-helical 'stalk' regions on segments M_1-M_5 facing the cytosolic side of the SR membrane. The high affinity Ca^{2+} binding sites are most likely located in the transmembrane regions M_4-M_6 which are believed to form a pore-like structure that traps Ca^{2+} during occlusion.

1.4.1 Phospholamban is an endogenous mediator of SR Ca^{2+} uptake in cardiac muscle

In cardiac muscle SR Ca^{2+} uptake via SERCA is regulated by the inhibitory protein phospholamban. Phospholamban (PLB) exists as a pentamer within the SR membrane consisting of 5 identical subunits stabilized by leucine-isoleucine zipper motifs between

the transmembrane α-helices of the protein. It is now widely recognized that PLB monomers confer inhibition of SERCA while the pentamer configuration acts as the PLB reservoir in cardiac muscle. Evidence to support this comes from the observation that PLB mutants in which the transmembrane leucine-isoleucine zipper interactions are disrupted inhibits pentamerisation, resulting in a greater inhibition of SERCA (Cornea *et al.*, 1997). Interaction of PLB with SERCA2a inhibits SR Ca^{2+} uptake by decreasing the affinity of SERCA for Ca^{2+} (increasing the K_{Ca} value). This inhibitory effect can be relieved through phosphorylation of PLB by PKA or Ca^{2+}/Calmodulin-dependent protein kinase II (CaMKII) as well as with the use of monoclonal antibodies for PLB. Removal of PLB's inhibitory effect on SR Ca^{2+} uptake by cAMP-dependent PKA phosphorylation is a major contributor to the positive inotropic effect mediated by β-adrenergic stimulation. PKA phosphorylation of PLB at Ser^{16} increases SERCA's affinity for Ca^{2+} (reduces K_{Ca}) resulting in an increase in the rate of Ca^{2+} uptake (Hicks *et al.*, 1979). PLB is also phosphorylated by CaMKII at Thr^{17}, resulting in a reduction in K_{Ca} similar to that produced by PKA phosphorylation at Ser^{16}. Genetic deletion of the PLB gene in transgenic mouse studies significantly enhances cardiac contractility and relaxation measured using isolated working heart preparations, however the ability to elicit a positive inotropic response using β-agonists is lost (Luo *et al.*, 1994), despite intact β-adrenergic receptor signalling pathways and comparable upregulation of cAMP and phosphorylation of Troponin I and C (Kiss *et al.*, 1997). PLB knockout mice also exhibit altered intracellular Ca^{2+} handling properties, including increased Ca^{2+} spark amplitude and frequency, and increased RyR sensitivity to trigger I_{Ca} (Santana *et al.*, 1997). These effects are almost exclusively mediated by an elevated SR Ca^{2+} load in PLB knockout, as reduction of SR Ca^{2+} content to wild type levels abolishes these differences.

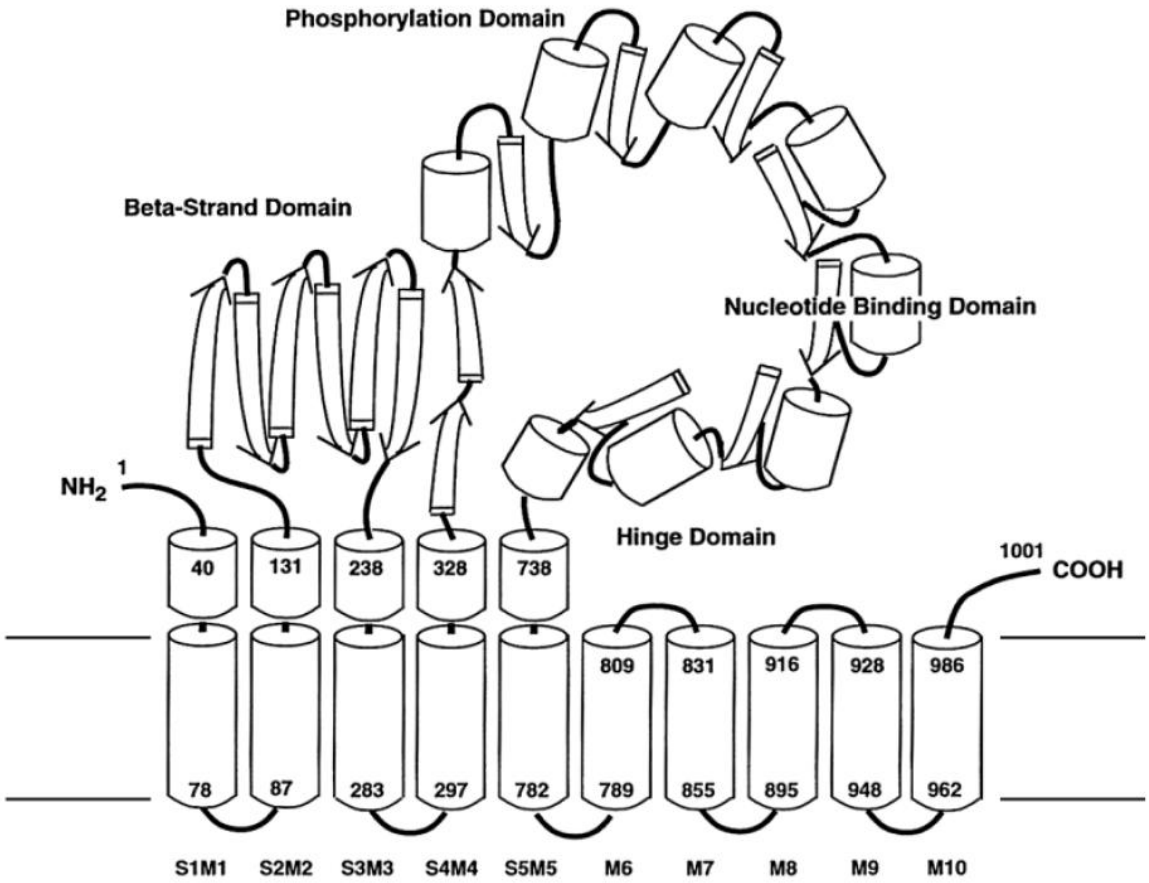

Figure 1.4 Structural diagram of SERCA. The protein consists of 10 transmembrane domains (M_1-M_{10}) the first 5 of which also include an α-helical 'stalk' region extending into the cytosolic face of the protein. The large cytosolic portion, consisting of the β-strand domain, the phosphorylation site, nucleotide binding domain and hinge domains, comprises the bulk of the molecule. Numbers indicate amino acid positions at the end of each transmembrane sequence. (Diagram taken from Tada (2003) *Circ. J.* 67(9) 729-737).

1.4.2 SERCA isoforms exhibit functional heterogeneity with regard to Ca^{2+}-transport properties

Despite a high level of sequence homology between SERCA isoforms, functional differences with regard to Ca^{2+} affinity and ATP turnover rates have been reported in a number of investigations. SERCA2b has been shown to have a lower ATP and Ca^{2+} turnover rate in comparison to SERCA2a (Lytton *et al.*, 1992) however it exhibits roughly 2-fold higher affinity for Ca^{2+} than SERCA2a (Verboomen *et al.*, 1992; Verboomen *et al.*, 1994). SERCA1a and SERCA2a demonstrate very similar Ca^{2+} dependence, however the Ca^{2+} uptake rate of SERCA1a is approximately twice as fast (Cavagna *et al.*, 2000). Due to the observed differences in Ca^{2+} uptake properties between isoforms a number of studies have elected to investigate the consequences of SERCA2a replacement with, or upregulation of, variant SERCA isoforms to normal myocyte Ca^{2+} handling and overall cardiac function (see below).

1.4.2.1 Overexpression of SERCA2a enhances cardiac contractility and Ca^{2+}-handling dynamics

The relationship between levels of SERCA and cardiac contractile function have been investigated using adenoviral gene transfection (Hajjar *et al.*, 1997) and transgenic over-expression in rat and mouse models (Baker *et al.*, 1998; He *et al.*, 1997; Maier *et al.*, 2005; Muller *et al.*, 2003). He *et al.* (1997) reported that transgenic mice expressing a rat SERCA2a gene demonstrated a 20% increase in SERCA2a protein levels relative to PLB expression (He *et al.*, 1997). This phenotype exhibited an increased rate of $[Ca^{2+}]_i$ transient decay and relaxation in isolated myocytes, with baseline left ventricular dP/dt_{max} and dP/dt_{min} increased, and a significantly reduced relaxation constant, τ. These functional differences between transgenic mice and controls were abolished following a low dose (1 ng) injection of isoproterenol, and the relaxation constant τ in transgenic mice under resting conditions was not significantly altered following isoproterenol, suggesting that the rate of relaxation in transgenic mice under resting conditions was almost maximal (He *et al.*, 1997). A similar study by Baker *et al.* (1998) found that transgenic over-expression of SERCA2a in mice resulted in enhanced LV contractility and relaxation, and an increase in the maximal rate of SR Ca^{2+} uptake (V_{max}), although the affinity of SERCA for Ca^{2+} was unchanged vs. controls (Baker *et al.*, 1998). Crucially, unlike the previous study the investigators found an increase in $Ca^{2+}{}_i$ transient amplitude and cell shortening, though this could be explained by the increased level of protein expression which was 1.5 fold greater than control, in comparison to the 20% increase reported in the previous investigation (He *et al.*, 1997). Enhanced LV function was also described by Muller *et al.* (2003) in a rat model of SERCA2a over-expression (Muller *et al.*, 2003). The investigators were also able to demonstrate a correlation between the levels of SERCA2a protein expression in aortic banded and sham operated transgenic rats, and the measured relaxation constant τ from isolated working heart experiments, suggestive of SERCA's critical role in active relaxation (Muller *et al.*, 2003). The enhancement of cardiac contractility seen following increased expression of SERCA2a has been shown to be beneficial in pressure-overload hypertrophy leading to heart failure (del Monte *et al.*, 2001; Miyamoto *et al.*, 2000; Muller *et al.*, 2003).

1.4.2.2 Expression of the SERCA1a isoform in small animal models

Ji *et al.* (1999) investigated the functional consequences of ectopic over-expression of SERCA1a in the heart using a transgenic mouse model (Ji *et al.*, 1999a). The generated model resulted in significant remodelling of the cardiac SR, expressing ~80% SERCA1a

and ~20% SERCA2a, with overall SERCA protein expression increased 2.5 fold. In agreement with previous studies using expression of SERCA isoforms in COS-1 cells, maximal rate of Ca^{2+} uptake (V_{max}) was 1.9-fold higher in cardiac homogenates from transgenic mice *vs.* non-transgenic controls, but the apparent Ca^{2+} affinity of SERCA was unchanged. The increase in V_{max} was explained by an increase in the total amount of active SERCA pumps in transgenic mouse cardiomyocytes (Ji *et al.*, 1999a). Lalli *et al.* (2001) investigated the consequences of SERCA1a expression in transgenic mouse hearts on intracellular Ca^{2+} handling and myocyte contractile function (Lalli *et al.*, 2001). Histological analysis revealed no significant differences between left ventricular myocytes from wild-type (WT) or transgenic (TnG) mice, and mortality curves were similar for both. While no changes were found in function or protein expression of NCX, RyR2 and L-type Ca^{2+} channel protein expression were reduced by ~20 % and ~30-35% in TnG mice respectively. This resulted in a decline in the maximal binding capacity of RyR2, as well as reduced peak $I_{Ca.L}$ compared to WT. Despite these alterations, the increased SR Ca^{2+} uptake kinetics present in TnG mice resulted in an increase in Ca^{2+} transient amplitude, faster Ca^{2+} removal and increased force production, consistent with an increased SR Ca^{2+} content in isolated myocytes, suggesting that ectopic expression of SERCA1a enhances contractility despite eliciting downregulation of other Ca^{2+} cycling proteins (Lalli *et al.*, 2001). Talukder *et al.* (2007) demonstrated a significant cardioprotective effect against ischaemia-reperfusion injury in isolated perfused mouse hearts overexpressing SERCA1a (Talukder *et al.*, 2007). Recovery of left ventricular developed pressure (LVDP) and end diastolic pressure (LVEDP) was significantly greater in SERCA1a$^{+/+}$ hearts vs. non-transgenics, with SERCA1a$^{+/+}$ hearts also exhibiting significantly reduced infarct size and duration of post-reperfusion arrhythmic episodes. In contrast to the apparent success of transgenic overexpression of SERCA1a with regards to improved cardiac function and cardioprotection, adenoviral-mediated gene transfer of the SERCA1a isoform has resulted in mixed findings (Logeart *et al.*, 2006; O'Donnell *et al.*, 2008). O'Donnell *et al.* (2008) reported a 34 ± 15 % increase in total SERCA levels in rat hearts 3 days after adenoviral gene transfer of SERCA1 (O'Donnell *et al.*, 2008). Aortic banding was used to induce LV hypertrophy in both gene transfected and untreated controls. While LVDP and dP/dt_{min} in isolated working heart preparations were shown to be improved in gene transfected rat hearts vs. controls, *in vivo* echocardiographic measurements revealed a 10-15 % increase in LV diastolic and systolic dimensions, and 17 % decrease in fractional shortening in gene transfected rats exposed to aortic banding compared to animals that underwent aortic banding alone. In this case compensatory mechanisms present *in vivo* may have resulted in

a masking of the beneficial effects of SERCA1a over-expression on cardiac function (O'Donnell *et al.*, 2008).

1.4.2.3 Expression of the SERCA2b isoform in transgenic animal models

The role of SERCA2b, a ubiquitously expressed SERCA isoform, in cardiac muscle was investigated by Greene *et al*. (2000) using a mouse model over-expressing the rat SERCA2b transgene (Greene *et al.*, 2000). They reported an 8-10 fold increase in protein levels of SERCA2b but no change in SERCA2a levels in comparison to wild-type controls. There was no detectable difference in the maximal uptake rate of Ca^{2+} (V_{max}) in SERCA2b-overexpressing mice, however the pump affinity for Ca^{2+} was significantly increased in transgenics. This alteration in uptake function translated into increased LV systolic and diastolic function (Greene *et al.*, 2000). The physiological importance of the SERCA2a isoform to normal cardiac function was further explored by replacement of SERCA2a with the SERCA2b isoform (Ver *et al.*, 2001). Mice lacking the SERCA2a isoform and instead expressing SERCA2b demonstrated a 49% reduction in overall SERCA2 protein expression and greater than 2-fold increase in PLB protein levels compared to wild type controls. Postnatal mortality was increased in transgenics, while mice surviving to adulthood exhibited signs of mild concentric hypertrophy, impairment of contractile and relaxation function and a reduction in maximal Ca^{2+} uptake rates by ~50%. A question remained over the role of increased PLB protein expression in this model. This may be responsible for the observed contractile dysfunction by working synergistically with the reduced cardiac SERCA2 expression, as removal of PLB's inhibitory effect on SERCA has been shown to improve cardiac function (Hoshijima *et al.*, 2002; Minamisawa *et al.*, 1999). Vangheluwe *et al*. (2006) investigated this hypothesis by studying a double knockout (DKO) mouse from cross-bred $PLB^{-/-}$ and $SERCA2^{b/b}$ transgenic mice (Vangheluwe *et al.*, 2006b). DKO mice exhibited significantly reduced life expectancy, increased concentric hypertrophy and development of diastolic dysfunction. B-Adrenergic stimulation using Dobutamine also failed to elicit a positive inotropic response in DKO mice, suggesting a lack of inotropic reserve in this model. It is now thought that the SR Ca^{2+} ATPase affinity for Ca^{2+} operates within a physiological range, with significant perturbation of this affinity in either direction resulting in a detrimental cardiac phenotype (Vangheluwe *et al.*, 2006a; Vangheluwe *et al.*, 2006b).

1.5 SR Ca^{2+} handling abnormalities significantly alter cardiac mechanical function

The observation that the SR contributes such a large proportion of the Ca^{2+} required for contraction in most mammalian species obviates the notion that alterations in the function of the SR Ca^{2+} release channel or in the Ca^{2+} uptake by SERCA could potentially impact on normal contractile function in the whole heart. Indeed, as described in the section above enhancement of SERCA2a expression and function in transgenic mouse models may result in a positive inotropic response and enhancement of cardiac contractility. Two such conditions are described below in which disruption of SR Ca^{2+} handling mechanisms are thought to be a major contributing factor to the development of contractile dysfunction; Ca^{2+} overload, and chronic myocardial infarction.

1.5.1 Ca^{2+} Overload

Ca^{2+} overload can be defined as an excessive increase in intracellular Ca^{2+} levels which overwhelms the Ca^{2+} regulatory mechanisms of the cell resulting in a depression of contractility and the appearance of abnormal electrical activity. Examples of both are well documented in the case of cardiac glycoside toxicity, which has allowed experimental characterization of Ca^{2+} overload, and which will be discussed in greater detail later in this chapter. The decline in peak force development and appearance of ventricular extrasystoles is linked to spontaneous Ca^{2+} release from the sarcoplasmic reticulum. Fabiato & Fabiato (1972) noted that in skinned cardiomyocytes from rat ventricle that bathing Ca^{2+} levels greater than 100 nM led to cyclic oscillations in cell contraction (Fabiato & Fabiato, 1972). Modification of free $[Ca^{2+}]_i$ by increasing EGTA concentrations led to a decline in this spontaneous contractile activity. These spontaneous contractions are now known to result from spontaneous Ca^{2+} release from the SR but by themselves do not necessarily indicate Ca^{2+} overload. Rat ventricular myocytes exhibit such spontaneous behaviour when bathed in physiological solution, but interventions resulting in elevated $[Ca^{2+}]_o$ levels (catecholamines, Na^+-K^+ pump inhibition) are required to elicit the same response in rabbit ventricular myocytes which exhibit far less spontaneous activity under resting conditions (Capogrossi & Lakatta, 1985; Kort & Lakatta, 1984).

1.5.1.1 Mechanical abnormalities and negative inotropy in Ca^{2+} overload

The consequences of increasing $[Ca^{2+}]_o$ levels in a ferret papillary muscle preparation were investigated by Allen *et al*. (1985) who concluded that the decrease in contractile force resulted from the spontaneous oscillatory Ca^{2+} release events from the SR contributing directly to a decrease in Ca^{2+} availability for subsequent stimulated contractions due to a decreased SR load (Allen *et al.*, 1985), a finding supported by several other investigations (Capogrossi *et al.*, 1987; Capogrossi & Lakatta, 1985). Capogrossi *et al*. (1986) investigated the impact of spontaneous Ca^{2+} release on electrically stimulated contractions in isolated rat and rabbit ventricular myocytes, demonstrating that when such spontaneous release events occur during the diastolic period between stimulation they have a negative impact on cell shortening amplitude (Capogrossi *et al.*, 1986). Diaz *et al*. (1997) demonstrated that the reduction in SR Ca^{2+} content during spontaneous release could be measured by assessing the integral of the Na^{+}-Ca^{2+} exchange (NCX) current following rapid application of caffeine to deplete SR stores (Diaz *et al.*, 1997). It was found that in rat ventricular myocytes a measureable decline in SR Ca^{2+} content was apparent following spontaneous release events, and that the amount of Ca^{2+} lost in this way can be accounted for by the amount removed from the cell via NCX (Diaz *et al.*, 1997). In Ca^{2+} overload conditions (bathing $[Ca^{2+}]_o$ at 10 mM) intact ventricular myocytes exhibit increased Ca^{2+} spark frequency and an increased propensity for initiation of Ca^{2+} waves (Cheng *et al.*, 1996). In multi-cellular preparations the decline in force may be complicated by heterogeneous activity between cardiomyocytes, as Ca^{2+} waves occurring in a large enough population of cells within multi-cellular preparations would result in asynchronous activation of contractile elements and an increase in diastolic tension, potentially contributing to a Ca^{2+}-dependent increase in diastolic tone (Stern *et al.*, 1988). Therefore a decline in peak force production and negative inotropy are, at least in part, explained by reduction in SR Ca^{2+} content following spontaneous Ca^{2+} release events from the SR along with an increase in diastolic tone. The SR is not the only structure believed to be susceptible to Ca^{2+} overload; Ca^{2+} accumulation within the mitochondria is thought to contribute to the negative inotropic effects of Ca^{2+} overload. Excessive mitochondrial Ca^{2+} uptake has been demonstrated to cause a reduction in oxidative phosphorylation, reducing the available levels of ATP for critical cellular processes (Holmuhamedov *et al.*, 2001). In agreement with this theory, metabolic inhibitors (NaCN, oligomycin) in small concentrations have little effect on developed force in Purkinje fibres bathed in physiological Tyrode's solution, but in the presence of Strophanthidin (a cardiac glycoside)

the initial inotropic response is lost, and force declines at a faster rate than in strophanthidin alone (Vassalle & Lin, 2004).

1.5.1.2 Electrical abnormalities in Ca^{2+} overload

Electrical disturbances associated with Ca^{2+} overload, like the negative inotropic effects already discussed, are mediated by spontaneous Ca^{2+} release from the SR. Activation of a transient inward current (I_{TI}) arises from ionic movements across the sarcolemmal membrane by electrogenic transporters (Berlin *et al.*, 1989) and is the mechanism responsible for the appearance of delayed after depolarisations (DADs) (Kass *et al.*, 1978; Schlotthauer & Bers, 2000). Zygmunt *et al.*, (1998), using canine mid-myocardial cells concluded that I_{TI} was the result of both inward NCX current ($I_{Na/Ca}$) and Ca^{2+}-dependent inward Chloride current ($I_{Cl(Ca)}$) with the relative contributions of I_{NaCa} and $I_{Cl(Ca)}$ reported as approximately 60 and 40 % respectively (Zygmunt *et al.*, 1998). Verkerk *et al.* (2000) examined the contribution of $I_{Na/Ca}$ and $I_{Cl(Ca)}$ to I_{TI} in sheep ventricular and purkinje fibres (Verkerk *et al.*, 2000). They found a component of I_{TI}, blocked by the anion channel inhibitor DIDS (4,4'-diisothiocyanatostilbene-2,2'-disulfonic acid) that could be attributed to a Chloride (Cl^-) current. The remainder of I_{TI} not blocked by DIDS (termed DIDS-insensitive current) could be abolished by replacement of $[Na^+]_o$ with Li^+. The fact that inhibition of I_{TI} was complete following the combination of these two manoeuvres led the authors to conclude that contribution by non-specific inward current to I_{TI} was most likely negligible (Verkerk *et al.*, 2000) Schlotthauer and Bers (2000) noted that in I_{TI}, membrane potential (E_m) is constant, whereas during DADs E_m changes throughout such that alteration of the electrochemical gradients which drive the aforementioned currents may have a profound effect on their relative contribution to DADs (Schlotthauer & Bers, 2000). The authors therefore investigated the contribution of $I_{Na/Ca}$ and $I_{Cl(Ca)}$ to delayed after depolarisations using caffeine-induced DADs (cDADs). They found that in rabbit ventricular myocytes, blockade of $I_{Na/Ca}$ with $0Ca^{2+}/0Na^+$ solution led to a >90 % reduction in cDAD amplitude, while specific blockade of $I_{Cl(Ca)}$ with niflumate (50 μM) could only account for < 10 % (Schlotthauer & Bers, 2000). This heavy reliance on $I_{Na/Ca}$ for generation of DADs appears to hold true for guinea pig ventricular myocytes also (Fedida *et al.*, 1987). Katra & Laurita (2005) attempted to better define the origin of triggered activity induced due to spontaneous SR Ca^{2+} release using optical mapping techniques in a canine left ventricular wedge preparation (Katra & Laurita, 2005). Under conditions of enhanced calcium entry (selective blockade of I_{Ks} and stimulation of the β-adrenergic system) spontaneous SR Ca^{2+} release and DADs resulted from a relatively large cluster of

cells and could also originate from multiple sites through the transmural wall (although mostly occurring closer to the endocardium). Sites of spontaneous Ca^{2+} release origin were also associated with slower Ca^{2+} uptake and higher diastolic Ca^{2+} levels (Katra & Laurita, 2005). The consequences of I_{TI} and DADs due to Ca^{2+} overload is ultimately the increased propensity for generation of an action potential leading to triggered arrhythmias (Kimura *et al.*, 1984; Schlotthauer & Bers, 2000).

1.5.2 When does Ca^{2+} Overload occur?

In addition to the influence of excessive β-adrenergic stimulation (discussed in detail in Chapter 4) a number of conditions have been shown to result in Ca^{2+} overload yet the mechanisms underlying each can be quite different.

1) **Cardiac glycosides.** It has long been established that the positive inotropic actions of cardiac glycosides are evoked through inhibition of the Na^+-K^+ ATPase, leading to a rise in $[Na^+]_i$ levels (Khatter *et al.*, 1989). This leads to a reduction in Ca^{2+} extrusion via NCX activity and a net increase in $[Ca^{2+}]_i$, which is effective in loading the SR and increasing SR Ca^{2+} content (Blaustein *et al.*, 1998). An increase in Ca^{2+} influx may also occur via NCX when $[Na^+]_i$ levels rise sufficiently (Satoh *et al.*, 2000). Cardiac glycoside toxicity results in the appearance of triggered arrhythmias and a reduction in Ca^{2+} transient amplitude (Terada *et al.*, 1994). Satoh *et al* (2000) demonstrated the influence of NCX-mediated Ca^{2+} influx on the toxicity of cardiac glycosides in rat ventricular myocytes by selective blockade of Ca^{2+} influx via NCX using KB-R7943 (Satoh *et al.*, 2000). KB-R7943 was selective for Ca^{2+} influx via NCX and did not alter Ca^{2+} efflux through the exchanger or normal EC coupling mechanisms. While KB-R7943 was able to prevent Ca^{2+} oscillations and arrhythmic activity induced by 50 μM strophanthidin, the inotropic effects of strophanthidin administration were not prevented, suggesting that a decrease in Ca^{2+} efflux following cardiac glycoside treatment (caused by an increase in $[Na^+]_i$ was sufficient to promote a positive inotropic response in rat ventricular myocytes, however net Ca^{2+} influx via NCX is required for cardiac glycoside-induced Ca^{2+} overload (Satoh *et al.*, 2000). Recent evidence has challenged the traditional view of cardiac glycoside action, suggesting that alternative intracellular interaction sites may exist (Nishio *et al.*, 2002; Nishio *et al.*, 2004; Sagawa *et al.*, 2002). Sagawa *et al.* (2002) demonstrated that digoxin and actodigin led to an increase in opening of cardiac Ryanodine receptors incorporated into planar lipid bilayers, without altering open duration (Sagawa *et al.*, 2002). Nishio *et al.*, (2002) found that Ouabain was capable of inducing its positive inotropic, and toxic

effects even in the absence of functional NCX or Na^+-K^+ ATPase (Nishio *et al.*, 2002). A follow-up investigation by the same group looked at the effects of Ouabain on SR Ca^{2+} release in intact and permeabilised cat ventricular myocytes (Nishio *et al.*, 2004). They discovered that Ouabain led to a reduction in Ca^{2+} spark frequency but enhanced SR Ca^{2+} leak in the complete absence of Na^+ in intact cells. Removal of potential sarcolemmal mechanisms with the use of permeabilised myocytes yielded similar results, suggesting that mechanisms other than Na^+-K^+ ATPase blockade may contribute to the effects of cardiac glycosides. This view was challenged by Altamirano *et al.*, (2006) however, who found no change in Ca^{2+} spark characteristics, and no significant inotropic effect in the absence of Na^+ or during blockade of NCX, suggesting that any secondary mechanisms of cardiac glycoside action do not significantly contribute to their inotropic effects (Altamirano *et al.*, 2006).

2) **Ischaemia-Reperfusion Injury.** Since the work of Zimmerman & Hulsmann (1966) on Langendorff-perfused rat hearts, it has been known that when solution containing normal [Ca^{2+}] is re-introduced to the mammalian heart following 5-10 min of perfusion with a Ca^{2+}-free medium this quickly leads to loss of contractile and electrical function and extensive myocardial tissue damage (Chapman & Tunstall, 1987; Zimmerman & Hulsmann, 1966). This phenomenon, known as the 'calcium paradox', is thought to arise from excessive cellular Ca^{2+} influx leading to Ca^{2+} overload. While it is highly unlikely such a situation would ever occur *in vivo*, with regards to the final outcome it shares striking similarities with the physiological phenomenon of ischaemia-reperfusion injury, both of which result in excessive accumulation of intracellular Ca^{2+}, severe sarcolemmal disruption, alteration of mitochondrial morphology and loss of high energy phosphates (Alto & Dhalla, 1979; Chapman & Tunstall, 1987). Prolonged periods of ischaemia (decreased blood supply to the tissues) followed by reperfusion have long been known to result in myocardial damage and necrosis. It has been demonstrated by a large number of studies that in myocardial tissue that has undergone severe disruption there is a significant increase in Ca^{2+} levels (Ferrari *et al.*, 1986; Meissner & Morgan, 1995; Tani, 1990). Ca^{2+} accumulation occurs following reperfusion (Higgins & Blackburn, 1984; Tani, 1990) and use of specific Ca^{2+} channel antagonists as well as calmodulin inhibition has been shown to be effective in limiting Ca^{2+} overload following ischaemia and reperfusion (Das *et al.*, 1989; Higgins & Blackburn, 1984). While Ca^{2+} overload from ischaemia-reperfusion results in contracture and increased propensity for arrhythmias as described above (Ferrier *et al.*, 1985), evidence also points toward specific accumulation of Ca^{2+} within the mitochondria (via the mitochondrial Ca^{2+}-uniporter) and not the cytosol per se as being in

part responsible for mediation of post-ischaemic reperfusion injury (Miyamae *et al.*, 1996; Miyata *et al.*, 1992). It is now understood that during ischaemia mitochondria switch from oxidative phosphorylation to anaerobic mechanisms in order to continue ATP synthesis, leading to accumulation of lactate within the cell which cannot be washed away. This leads to a decline in intracellular pH (pH_i) and acidosis (Baines, 2009). Stimulation of the Na^+/H^+ exchanger (NHE) occurs in an attempt to offset the decline in pH_i resulting in accumulation of Na^+ within the cell. Upon reperfusion there is a large influx of Na^+ in exchange for H^+ to re-establish pH_i to normal levels. This is thought to result in stimulation of NCX to remove Na^+ and bring in Ca^{2+}, leading to a large influx of Ca^{2+} and concomitant cell injury (Karmazyn *et al.*, 1999). Evidence for this view is supported by studies using NHE inhibitors such as cariporide (HOE642), and amiloride derivatives which limit intracellular Na^+ loading and reduce IR-induced injury (Hartmann & Decking, 1999; Meng & Pierce, 1990; Stromer *et al.*, 2000; ten Hove *et al.*, 2003) although studies also suggest that this effect may also be mediated by direct action on NHE within the inner mitochondrial membrane (Ruiz-Meana *et al.*, 2003). Accumulation of Ca^{2+} within the mitochondria has also been implicated in opening of the mitochondrial membrane permeability transition pore (MPTP) and cell necrosis. Moreover, Toda *et al*. (2007) demonstrated that cariporide was able to attenuate mitochondrial Ca^{2+} overload and significantly delay MPTP opening in a rat ventricular myocyte model of oxidative stress (Toda *et al.*, 2007). Ca^{2+} overload associated with ischaemia-reperfusion injury therefore represents an indirect mechanism of Ca^{2+} loading as a result of disruption of normal intracellular ion-handling processes. Although Ca^{2+} overload is not the only complication arising from ischaemia-reperfusion injury it is clearly a significant contributor to detrimental effects associated with this phenomenon, including a contributory role in cell apoptosis and necrosis.

1.5.3 Myocardial infarction alters intracellular Ca^{2+} handling properties

One of the leading causes of heart failure in humans is coronary artery disease leading to the formation of a myocardial infarct (MI). Significant modifications in the contractile and electrophysiological properties of cardiac myocytes are thought to underlie the advancement of contractile dysfunction and progressive decline in cardiac output. Animal models of myocardial infarction, the most prevalent of which is the coronary artery ligation model, have afforded greater insight into the cellular alterations underlying the development of contractile dysfunction in chronically infarcted hearts and a large body of

evidence now exists demonstrating that in infarcted hearts the viable myocytes undergo significant alterations with respect to intracellular Ca^{2+} handling properties. Depression or prolongation of the $[Ca^{2+}]_i$ transient is believed to play a significant role in the contractile dysfunction seen clinically in heart failure patients (Beuckelmann *et al.*, 1992; Gwathmey *et al.*, 1987) and in animal models of myocardial infarction (Ng *et al.*, 1998). The amplitude of the systolic $[Ca^{2+}]_i$ transient has been shown to be significantly reduced in patients with end stage heart failure, resulting from a significantly reduced SR Ca^{2+} content in comparison to non-failing myocytes (Lindner *et al.*, 1998; Pieske *et al.*, 1999). Similar findings are also reported in pacing, and coronary artery ligation-induced models of heart failure (Hobai & O'Rourke, 2001; Neary *et al.*, 2002b). These findings suggest that alteration in SR Ca^{2+} uptake and/or release mechanisms may play a significant role in the development of left ventricular dysfunction seen in heart failure.

1.5.3.1 SR Ca^{2+} uptake

A consistent finding in clinical and animal models of heart failure is an alteration in the expression and function of proteins involved in cytosolic Ca^{2+} removal, including SERCA (Currie & Smith, 1999; Hasenfuss *et al.*, 1994b; Schmidt *et al.*, 1998), its regulatory protein phospholamban (Currie & Smith, 1999), and NCX (Studer *et al.*, 1994a). Yamaguchi *et al.* (1997) demonstrated a reduced SR Ca^{2+} uptake rate in permeabilised ventricular myocytes from 8 week ligation rat hearts (Yamaguchi *et al.*, 1997). Afzal & Dhalla found that Ca^{2+} uptake in SR vesicles prepared from 16 week ligation rat hearts was reduced by ~65%, although protein expression was only reduced by 30% (Afzal & Dhalla, 1996). The study reported that the Ca^{2+} and ATP affinity of SERCA was unaltered, and that stimulation of Ca^{2+} uptake activity by exposing SR vesicles to PKA or calmodulin resulted in a significant greater % increase in SR Ca^{2+} uptake of failing SR vesicles in comparison to controls at all concentrations used. However, maximal Ca^{2+} uptake rate (V_{max}) remained significantly depressed in failing SR vesicles following PKA/calmodulin stimulation in comparison to controls. The authors concluded this was likely to have occurred due to an alteration in phospholamban expression or function although neither parameter was directly measured (Afzal & Dhalla, 1996). In a rabbit coronary artery ligation model of myocardial infarction, left ventricular dysfunction was evident 8 weeks after coronary artery ligation, with a significantly reduced ejection fraction in comparison to sham operated controls (41.1% vs. 73.8%) (Ng *et al.*, 1998). Peak systolic pressure and the maximal rates of pressure rise and fall (measured in isovolumically beating Langendorff perfused hearts) were also significantly depressed. This model was associated

with an ~50% reduction in SERCA and PLB protein expression, however the SERCA:PLB ratio was not evaluated. Isolated SR vesicle preparations from 8 week ligation animals also revealed that SR Ca^{2+} uptake was reduced to ~50% of that seen in sham hearts (Currie & Smith, 1999). A reduced level of protein expression and function of SERCA and its regulatory protein PLB therefore appears frequently in characterization of heart failure models and could explain the decline in SR Ca^{2+} content seen in a number of heart failure studies

1.5.3.2 The ryanodine receptor in heart failure

As described above, Ca^{2+} release from the sarcoplasmic reticulum provides a large proportion of the Ca^{2+} required for contraction and as such the function of the SR Ca^{2+} release channel, the Ryanodine receptor, is critical in maintaining the highly graded mechanism of CICR. B-adrenergic stimulation of the cardiac myocyte activates a signalling cascade resulting in activation of PKA which binds to the RyR and increases channel P_o. Marx *et al.* (2000) reported that PKA 'hyper-phosphorylation' of RyR at Ser^{2808} occurred in failing human hearts, resulting in dissociation of the regulatory protein FKBP12.6 from the channel complex, increased sensitivity to activation by luminal Ca^{2+} and the induction of channel sub-conductance states (Marx *et al.*, 2000). A similar finding was reported in a canine pacing-induced heart failure model, as well as a number of MI models (Obayashi *et al.*, 2006; Wehrens *et al.*, 2005; Yano *et al.*, 2000) The resultant conformational change in RyR induced significant Ca^{2+} leak through the channel. These findings lent weight to the theory that diastolic Ca^{2+} leak from the sarcoplasmic reticulum may contribute to altered contractile function in heart failure by participating in the decline of SR Ca^{2+} content, as well as increasing the propensity for diastolic Ca^{2+} release events to occur which may serve as a triggering mechanism for DADs and ventricular arrhythmias.

Several controversies have arisen however which suggest this may not be the complete story. Some studies have shown no effect of PKA hyper-phosphorylation at Ser^{2808} (Ser^{2809} in rabbits) on FKBP12.6 binding to RyR2 (Stange *et al.*, 2003; Xiao *et al.*, 2004). Furthermore, the enhanced diastolic Ca^{2+} leak following β-adrenergic stimulation has been demonstrated in a rabbit MI model of heart failure to be mediated through phosphorylation of RyR by CaMKII, not PKA (Ai *et al.*, 2005; Curran *et al.*, 2007). Recently, the idea of defective inter-domain interactions between the N and C-terminals of the RyR has been proposed in a number of studies (Tateishi *et al.*, 2009; Yamamoto *et al.*, 2008). In SR vesicles from normal canine hearts introduction of domain peptides which correspond to

the amino acid sequence of interacting zipper domains leads to a conformational change in the channel and the appearance of a significant Ca^{2+} leak without dissociating FKBP12.6 from the channel complex (Tateishi *et al.*, 2009). SR vesicles from failing canine hearts however already exhibited a similar Ca^{2+} leak profile which was not altered with addition of the same domain peptide. The relative roles of PKA phosphorylation of RyR2 and dissociation of FKBP12.6 from the channel complex to induction of diastolic Ca^{2+} leak in heart failure therefore remains controversial.

1.6 Isolated perfused heart preparations

Investigations using isolated single cell preparations have revealed an enormous amount of information regarding specific function of Ca^{2+} cycling proteins within the ventricular myocyte, their interaction in EC coupling, and alteration in disease states. How such observations impact cardiac function at the whole organ level however cannot be directly extrapolated from such work. A fuller understanding of how intracellular components of cardiac EC coupling impinge on the normal function of the heart may be obtained using more physiologically relevant *in vivo* models. Specific manipulation of cardiac function in the intact animal however is frequently complicated by alterations in vascular tone, circulating factors, and in the case of pharmacological interventions, non-specific extra-cardiac effects. In this respect the isolated perfused heart preparation offers a number of unique advantages to studying cardiac function. The basic preparation offers a high level of reproducibility and can be modified to allow measurement of a vast array of physiological indices. The major advantage lies in the ability to rigorously control the experimental conditions imposed on the heart without confounding systemic effects such as sympathetic and vagal stimulation, circulating factors and the potential influence of anaesthetic on the preparation. Since the perfusion medium of the heart (most commonly a crystalloid buffer solution) is strictly controlled by the investigator, isolated heart preparations are superbly suited to the investigation of cardiac responses to metabolic substrate supply, hypoxia and pharmacological interventions. Regional and global changes in coronary flow can readily be manipulated to induce ischaemia. Indeed, isolated heart preparations have proven to be an invaluable analytic tool in the study of ischaemia-reperfusion injury and associated phenomena, including myocardial stunning and preconditioning.

1.6.1.1 The isolated mammalian heart preparation according to Langendorff

In 1898 Oscar Langendorff described the isolated mammalian heart preparation, in which an excised intact heart (principally from cats, although he did employ rabbit and canine cardiac preparations) could be kept alive for a prolonged period by delivery of blood to the aortic root through a cannula attached to the ascending aorta (Skrzypiec-Spring *et al.*, 2007; Zimmer & Millar, 1998). Using a constant perfusion pressure head, blood was delivered to the aortic root in a retrograde fashion, causing the aortic valves to close and blood to flow through the coronary circulation, eventually exiting from the coronary sinus into the right atrium. Measurement of cardiac contractile function can be achieved using this preparation. Ventricular pressure parameters may be recorded by inflation of a latex balloon in the left ventricle as depicted in Figure 1.5, introduced via the left atrium, and recording of isovolumic ventricular pressure parameters through an attached microtip pressure transducer. One disadvantage of this is that isovolumic contractions are less energetically demanding in comparison to *in vivo* contractions which produce pressure-volume work during the cardiac cycle (Merx & Schrader, 2009).

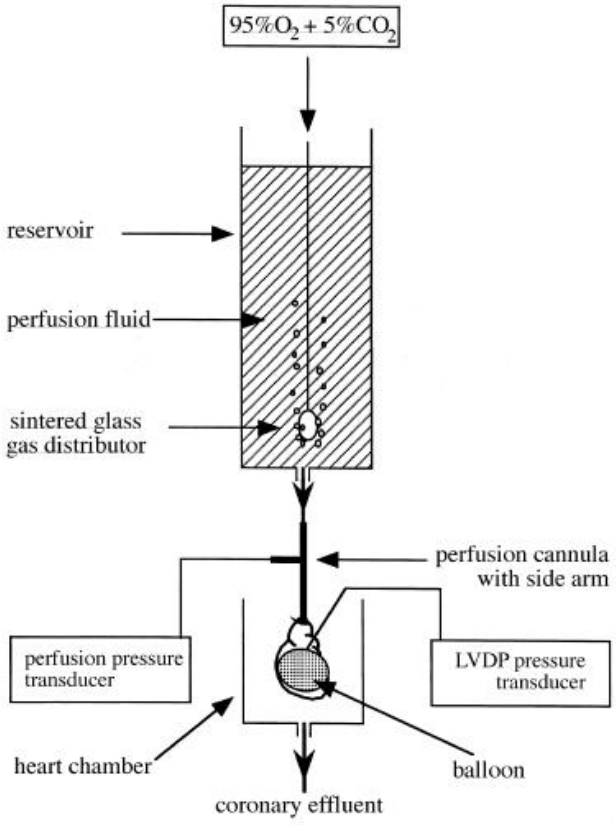

Figure 1.5 Isolated perfused heart according to Langendorff. The isolated heart is cannulated via the aorta and perfused from a constant pressure head using blood or crystalloid buffer perfusate (pictured). Insertion of a latex balloon into the LV attached to a pressure transducer allows the investigator to set end

diastolic pressure and measure isovolumetric contractions. (Diagram taken from Sutherland & Hearse (2000) *Pharmacol. Res.* 41(6) 613-627).

1.6.1.2 The isolated working heart preparation can be used to investigate cardiac mechanical function

The aforementioned problems associated with measurement of contractile function using Langendorff perfused hearts was addressed by Neely *et al*. (1967) who investigated the use an isolated heart preparation capable of performing *ex vivo* pressure-volume work (Neely *et al.*, 1967). This preparation, termed the isolated working heart, modified the existing setup described by Langendorff by additional cannulation of the pulmonary ostium separately and introduction of perfusion solution to the left atrium, where it would enter the left ventricle and be ejected out through the aorta against a hydrostatic pressure head. This setup is advantageous for investigation of cardiac mechanical function as the pressure-volume work performed by the heart is more physiologically relevant than the isovolumic pressure measurements attainable from the use of the balloon insertion method.

1.6.1.3 The pressure-volume loop allows description of the intrinsic contractile and relaxation properties of the left ventricle

The importance of ventricular volume with respect to contractility of the myocardium has been apparent since the classic description of the Frank-Starling mechanism, whereby an increase in filling pressure, induced by increasing the volume filling the heart, augments ventricular contractility and stroke volume. Due to the technical difficulty in obtaining accurate volume measurement within the heart however, the utility of the pressure-volume (PV) diagram for the description of intrinsic myocardial contractility did not receive much attention until the latter half of the 20th century, when a fundamental series of experiments using the isolated blood-perfused canine heart preparation revealed that intrinsic contractile and relaxation properties for any given ventricle could be described independent of load by fitting an appropriate relationship to the end systolic and end diastolic pressure-volume points obtained by altering the loading conditions imposed on the ventricle (Suga *et al.*, 1973; Suga & Sagawa, 1974; Sunagawa *et al.*, 1983). Simultaneous measurement of pressure and volume within the ventricular chambers of the heart (most commonly the left ventricle) allows the 4 phases of the cardiac cycle, isovolumic contraction, ejection, isovolumic relaxation and ventricular filling, to be conveniently visualised in a diagram known as the pressure-volume loop. From such a plot direct comparisons of a number of useful functional indices can be made between hearts exposed to varying experimental conditions, including ejection fraction and stroke volume. Crucially however, intrinsic

contractile properties of the ventricle independent of load can be obtained by transiently altering loading conditions imposed on the ventricle without altering myocardial contractility. The relationship between end-systolic and end-diastolic pressure volume points from the resultant family of PV loops may then be used to describe the intrinsic systolic (ESPVR) and diastolic (EDPVR) properties of the ventricle, as shown in Figure 1.7. The ESPVR is commonly described using a linear relationship with a unique slope (E_{es}) and volume intercept (V_o), while the EDPVR is inherently non-linear and is often described using a mono-exponential curve fit.

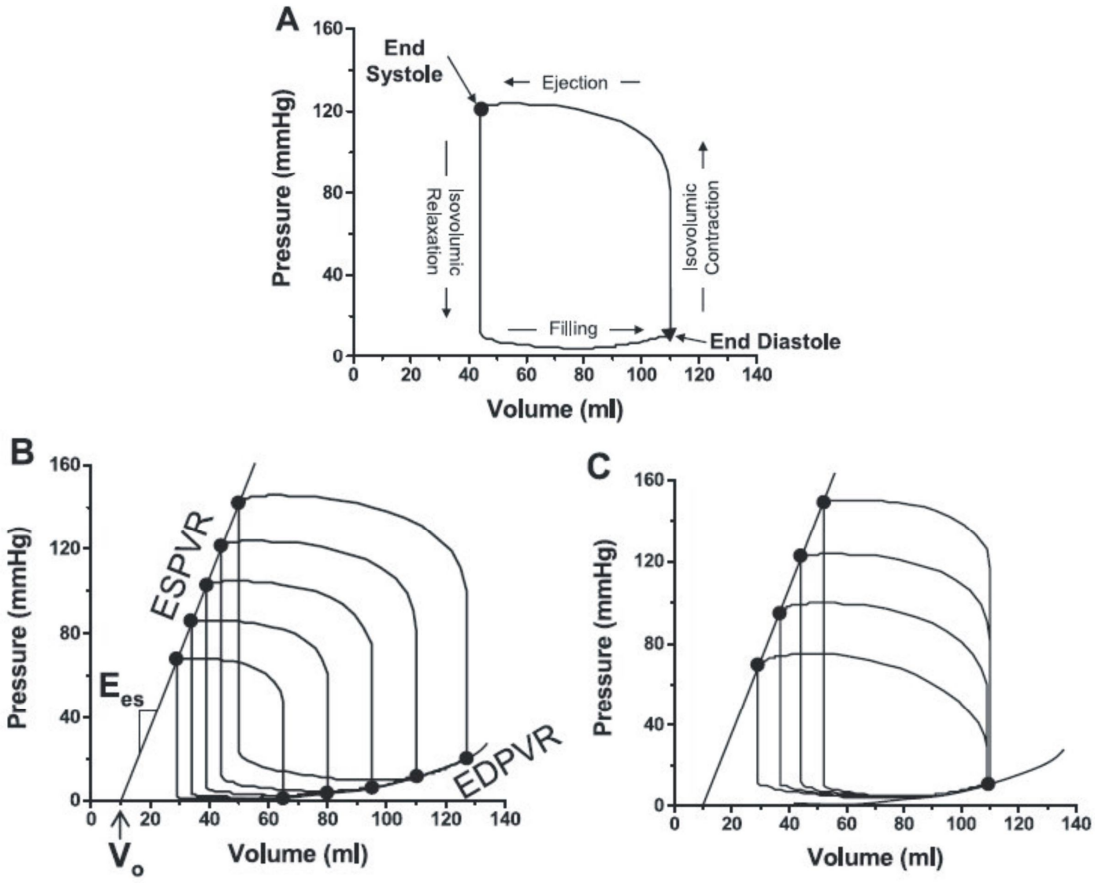

Figure 1.6 The pressure-volume loop. A. Idealised pressure-volume diagram highlighting the 4 phases of the cardiac cycle. End systole and end diastole are demarcated by the upper left and lower right hand corners of the loop, respectively. Transiently altering loading conditions by (B) preload reduction or (C) increasing afterload creates a family of PV loops. End systolic pressure volume points form a linear end-systolic pressure-volume relationship (ESPVR) characterised by a slope (E_{es}) and volume intercept (V_o), while the end diastolic pressure-volume points describe a non-linear end diastolic pressure volume relationship (EDPVR). (Panels adapted from Burkhoff *et al.* (2005) *Am. J. Physiol.* 289(2) 501-512).

A number of techniques now exist which allow determination of ventricular volume in the intact animal including echocardiography and magnetic resonance imaging. The disadvantage of such techniques with regard to volume analysis is that they rely on

averaging of steady state images and therefore lack the continuous volume signal required for transient loading/unloading manoeuvres. Conductance catheter technology overcomes this limitation by enabling instantaneous and continuous volume recording within the left ventricle, allowing assessment of ventricular pressure-volume relationships. The technique involves insertion of a multi-electrode catheter into the left ventricular chamber via the aorta to encompass the entire ventricular long axis. The catheter measures relative changes in the conductance of blood during the cardiac cycle, reflective of ventricular filling and ejection during the cardiac cycle, which is then calibrated to achieve a measure of true volume. The technical aspects of conductance catheter technology are described in detail in the General Methods chapter. While predominantly employed for *in vivo* studies, the use of combined pressure and volume measurement greatly enhances the potential of the isolated working heart for assessment of cardiac mechanical function, and several reports have validated its use in *ex vivo* working heart preparations from a number of species, including mice, dogs and swine.

1.7 Aims

Manipulation of intracellular Ca^{2+} handling dynamics, with particular emphasis on the sarcoplasmic reticulum Ca^{2+} release channel and the Ca^{2+} pump, has been extensively investigated using single cell preparations. The consequences of interventions which alter SR Ca^{2+} handling proteins to whole heart mechanical function are however, less well characterised. Therefore the initial aim of the work described in this thesis was to set up and characterise an isolated working heart preparation using rabbit hearts that would act as a platform for manipulation of SR function using various pharmacological approaches. In order to assess the impact of such interventions on mechanical function, this preparation was paired with a miniaturised pressure-conductance catheter which affords assessment of left ventricular function through analysis of both pressure and volume data instantaneously and continuously recorded within the left ventricle.

The next set of aims was to characterise the influence of the 1, 4-benzothiazepine derivative K201 on cardiac function in healthy hearts and under various experimental conditions where SR Ca^{2+} release via the RyR is believed to be altered. K201 has been demonstrated in single cell studies to interact with the cardiac RyR, stabilising the channel in its closed state and inhibiting SR Ca^{2+} release. Alteration of RyR function has been proposed to be a major contributor to arrhythmogenicity and contractile abnormalities in various cardiac disorders including ischaemic heart failure. The effects of this compound

on cardiac contractile function in healthy intact hearts however have yet to be described. Therefore the second aim was to characterise working heart mechanical function following exposure to varying concentrations of K201. The study then aimed to investigate the influence of acute perfusion of K201 under conditions where SR Ca^{2+} release is thought to be altered; 1) using elevated $[Ca^{2+}]_o$ and β-adrenergic stimulation, known to cause Ca^{2+} overload in intact ventricular myocyte preparations and 2) in a rabbit ligation model of left ventricular dysfunction.

The final set of aims was to assess the contribution of intact SR Ca^{2+} uptake to normal left ventricular contractility and relaxation by perfusion of isolated working hearts with the selective SERCA inhibitor thapsigargin to inhibit Ca^{2+} uptake into the SR.

2 General Methods

2.1 The isolated working heart technique

The technique is based on the principle that a heart isolated from the body can be studied *ex vivo* for a prolonged period of time provided the coronary circulation is perfused with oxygenated blood or equivalent physiological solution (Skrzypiec-Spring *et al.*, 2007). When perfusion solution is delivered to the coronary circulation in a retrograde fashion, also known as Langendorff perfusion, the heart will not perform external work (ejection of blood from the left ventricular chamber into the aorta) as no fluid will be present in the left ventricle (Merx & Schrader, 2009). Cannulating the left side of the heart and introducing perfusion solution into the left atrium, and subsequently the left ventricle allows the heart to perform pressure-volume work (Merx & Schrader, 2009).

2.1.1 Experimental Setup

Figure 2.1 shows the equipment setup used for the isolated working heart experiments. The setup was based upon an approach described by Neely *et al*. (Neely *et al.*, 1967). A dual-head peristaltic pump controlled the flow of perfusate directed towards a number of bubble traps, depicted in Figures 2.1 & 2.2. With a bubble trap open to air, any solution required by the heart would enter under a hydrostatic pressure head dictated by the height of the chamber, with the remainder returning to one of two reservoirs through an overflow. The system was capable of initially perfusing hearts in Langendorff mode (Figure 2.1 (ii)) under constant pressure, adjustable via the height of bubble trap B2. Flow could be redirected via several three-way taps located around the system to then establish working heart in non-recirculating mode (Figure 2.2 (i)). In this configuration hearts were provided with solution via the main 5 L reservoir, with smaller 2.5 L containers heated in a separate water bath providing a backup volume. For experiments requiring perfusion of a fixed volume the recirculating reservoir was filled and flow could be redirected back through the system via the second pump head to establish the working heart in recirculating mode (Figure 2.2 (ii)). Two 5 μm pore in-line filters (*Millipore*; *Billerica, MA*) arranged in parallel facilitated the removal of unwanted debris from the recirculating perfusate. This bypass configuration permitted the replacement of filter membranes during experiments where necessary. The recirculating volume in experiments where recirculation of solution was required was 540 ml. A defined length of tubing was present between the reservoirs and the heart used in either working heart mode which meant that there was a time delay between the addition of a drug or agent to the reservoir and that drug/agent reaching the heart and perfusing through the coronary circulation. This time was initially determined by

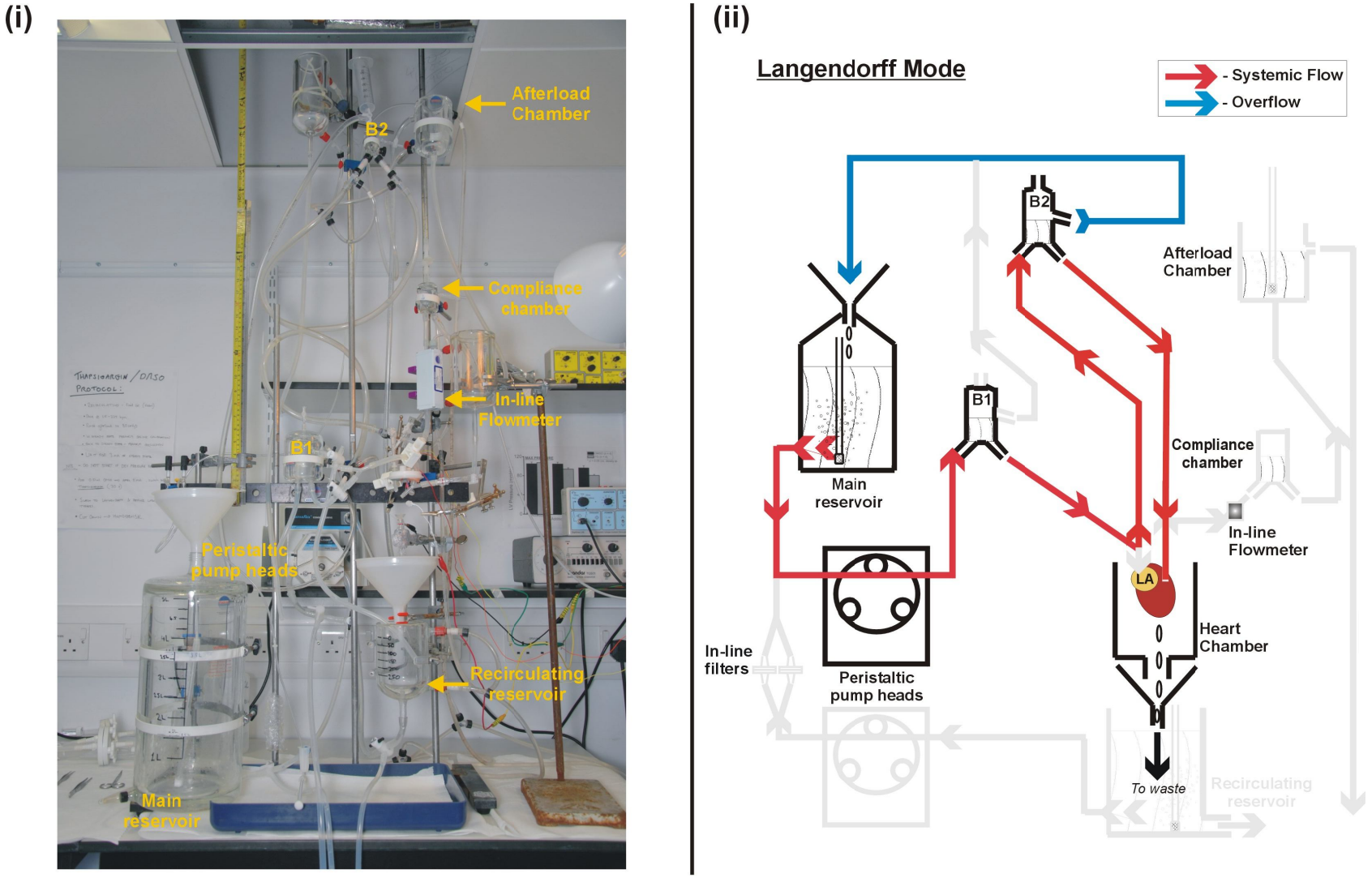

Figure 2.1 The isolated working heart system. (i) Picture of the perfusion system (ii) Perfusion pathway during retrograde (Langendorff) perfusion

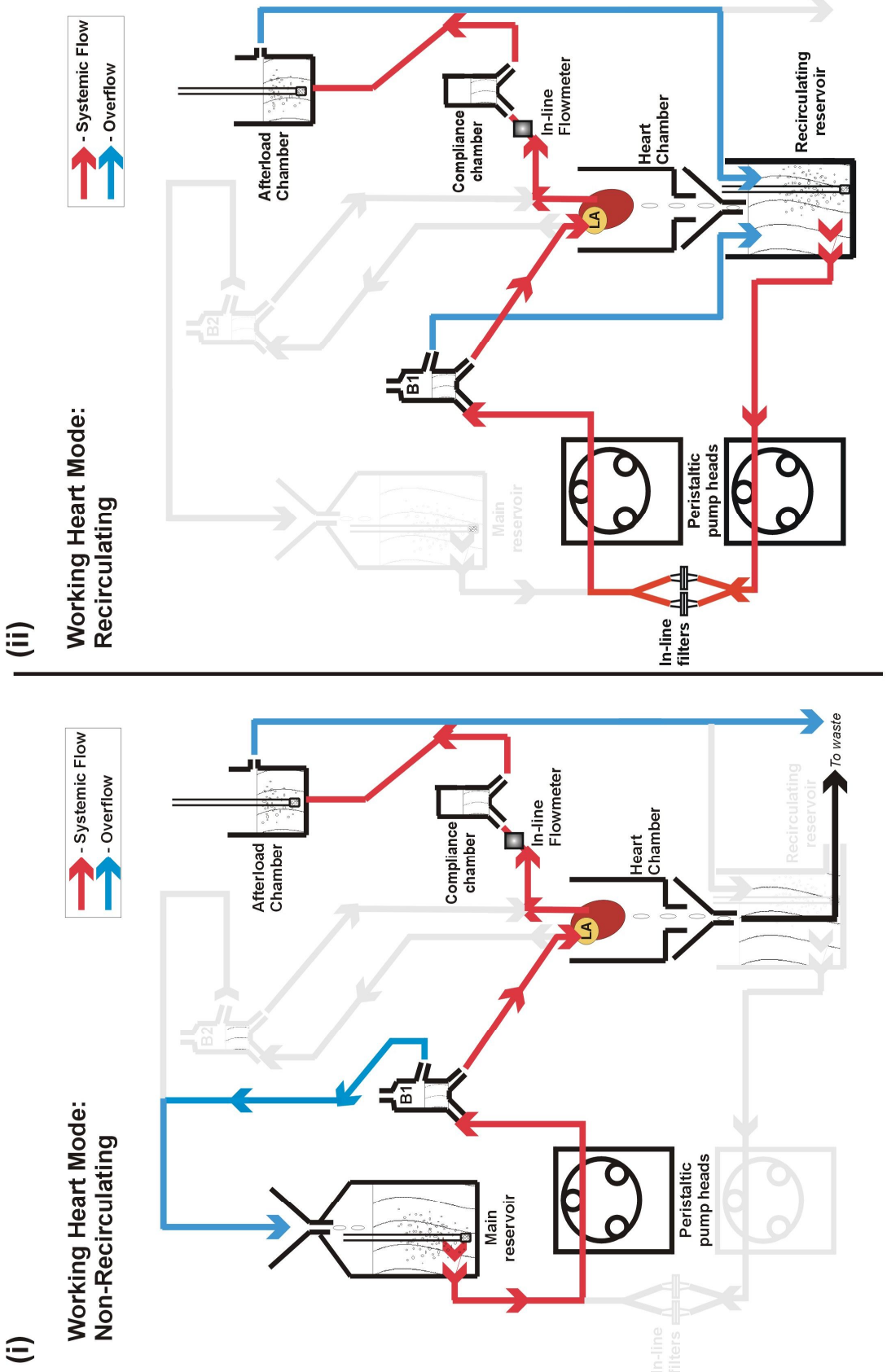

Figure 2.2 Schematic of working heart. Perfusion pathway in (i) non-recirculating and (ii) recirculating working heart modes

the speed of the peristaltic pump delivering solution to the preload chamber, with the rate of inflow into the heart contributing to the remaining delay. To eliminate differences in time delay between experiments the pump speed was adjusted to deliver 450 ml of solution per min during drug additions. This was calculated as a delay of 14.4 ± 0.5 s from addition to a reservoir to reaching the heart.

In both recirculating and non-recirculating working heart modes, left atrial filling pressure was dictated by the height of bubble trap B1. The afterload imposed on each heart was dictated by the height of the afterload chamber, which was also partially filled with perfusate. An in-line ultrasonic flowmeter (*Malema*; *Florida, US*) was located between the aortic cannula and the compliance chamber for continuous monitoring of aortic flow.

2.1.2 Perfusion of the isolated working heart

2.1.2.1 Inflow tract design

Cardiac output of the isolated working heart can be augmented under a diverse set of experimental conditions, for example by increasing left atrial filling pressure or by applying an inotropic agent to the perfusion medium. It was therefore essential that both the peristaltic pump and the left atrial cannula were able to provide a volume that would exceed the maximum cardiac output expected in the isolated working rabbit heart for any given inotropic state. This ensures that the cardiac output of the isolated heart is not limited by the constraints of the perfusion system itself. Values for mean cardiac output vary significantly between studies depending on the setup used, the perfusion medium and the loading conditions imposed for the individual investigation, however mean baseline cardiac outputs as high as 272 ± 32 $ml.min^{-1}$ have been reported for crystalloid buffer perfused working rabbit hearts (Vanagt *et al.*, 2007). *In vivo* cardiac outputs in the rabbit as assessed by thermodilution tend to be higher but are susceptible to variability depending on anaesthesia used (Chalmers *et al.*, 1967; Desager *et al.*, 1979; Edwards *et al.*, 1959; Neutze *et al.*, 1968). Reported values range from 110 $ml.kg^{-1}.min^{-1}$ (anaesthetized with sodium pentobarbital) to 215 $ml.kg^{-1}.min^{-1}$ (unanaesthetised) (Neutze *et al.*, 1968). The range of cardiac outputs expected in a 3 kg rabbit *in vivo* therefore would potentially be between 330 to 645 $ml.min^{-1}$. Using 5.5 mm internal diameter silicon tubing the peristaltic pump was capable of a maximum flow rate of 1500 $ml.min^{-1}$. 4.5 mm was found to be the largest internal diameter possible for the atrial cannula. Correct cannulation of the pulmonary orifice became very challenging with larger cannulae. Using a 4.5 mm internal diameter it was possible to achieve a maximum flow of 470 $ml.min^{-1}$ at a left atrial filling

pressure of 10 cmH_2O (7.4 mmHg), with stepwise increments of this maximum attained through increasing filling pressure.

2.1.2.2 Outflow tract design

The design of the aortic outflow tract is crucial in determining the aortic impedance experienced by the isolated working heart. The aorta and large arteries *in vivo* are partially distensible which allows the arterial lumen to increase in diameter during systole. This Windkessel or elastic reservoir effect serves to prevent excessive increases in blood pressure during systole. In the isolated working heart system, a compliance chamber partially filled with air was located in the aortic outflow line which provided an aortic Windkessel to compensate for the lack of elasticity of the outflow tubing (Belz, 1995; Podesser *et al.*, 1993). Previous investigators have shown that the pressure drop across the proximal portion of the aortic cannula is critical to the long-term stability of the isolated working heart (de Windt *et al.*, 1999; Van Bilsen *et al.*, 1991) and a major determinant of this is the internal diameter of the cannula. The largest possible internal diameter of the aortic cannula was 4.5 mm. Using this diameter ensured pressure drop was kept as low as possible whilst maintaining ease of cannulation of the aortic stub.

Both the aortic and left atrial cannulae were designed with offshoot arms, each fitted with a sealable plastic haemostasis valve, through which the pressure and conductance catheters were inserted. The side ports were also used for perfusion of various drugs and solutions where timing was critical and addition via the main reservoir was not possible. Cannulae were made of clear plastic which facilitated the detection and removal of air bubbles that formed in the openings prior to cannulation.

2.1.3 Experimental preparation

2.1.3.1 Solution preparation and system priming

Prior to beginning of experimentation thorough cleaning of the equipment and glassware was performed. 10 – 15 L of double-distilled water was perfused through the system followed by 2 L of boiling de-ionised water. A bicarbonate buffer based Tyrode's solution was prepared containing (in mM) NaCl (116), $NaHCO_3$ (20), Na_2HPO_4 (0.4), $MgSO_4$ (1), KCl (4), $CaCl_2$ (2.5) and Glucose (11), gassed with a 95% O_2 – 5% CO_2 mixture to maintain pH at 7.4. All solutions were suction filtered through a 5 μm pore filter using a 5L *Buchner* flask and a stainless steel filter apparatus before entering the system to remove any possible debris. A water bath was linked via a network of *Tygon* tubing connections to

all water-jacketed glassware components on the system, allowing solution temperature to be maintained at 37 ºC throughout. The isolated working heart system was primed prior to experiments to fill the system with Tyrode's solution for perfusion of the isolated heart. Care was taken to ensure no air bubbles were present in any of the tubing in order to prevent air emboli occurring in coronary circulation. Bubble traps were primed with solution up to the level of the overflow, leaving a volume of air to capture stray bubbles before they could enter the heart. After priming the afterload line and filling the compliance chamber with an appropriate volume of air, perfusion was switched to Langendorff mode before the outflow lines were clamped and the peristaltic pump stopped.

2.1.3.2 Heart Isolation and cannulation

Surgical removal of the heart was a licensed procedure, performed by one of two technicians (Aileen Rankin or Michael Dunne) licensed to carry out the procedure, with assistance provided by myself. New Zealand White rabbits weighing 3.0 – 4.0 kg, were injected with 0.5 ml Heparin (5000 $IU.ml^{-1}$) and an overdose of sodium pentobarbital (100 $mg.kg^{-1}$). Following thoracotomy hearts were quickly excised from the animal and submerged in a beaker containing cold (4 ºC) Tyrode's solution. Hearts were weighed before being moved to the working heart system. The peristaltic pump was started again and perfusate was allowed to flow freely through the aortic cannula, with a portion of the flow returning to the main reservoir via an overflow on bubble trap B2. Hearts were quickly cannulated via the aorta and perfused in a retrograde fashion at a pressure of 60 mmHg. The entire process from injection of the animal to initiation of perfusion took no longer than 3 min to achieve. A small cut was made in the base of the pulmonary artery to ensure unimpeded flow of the coronary perfusate exiting from the right side of the heart. Excess fat and lung tissue was removed to reveal a common pulmonary vein ostium. The left atrial inflow cannula was left to drip constantly to ensure no air bubbles were present during cannulation. The cannula was positioned over the ostium which was carefully cannulated, taking time to ensure there were no leaks present. A pair of platinum subdermal needle electrodes were positioned on the right atrium. These connected to a constant voltage isolated stimulator and train generator (*Digitimer*; *Hertfordshire, UK*) for experiments requiring electrical pacing of the heart.

2.1.4 Working heart perfusion and pressure-volume catheterization

2.1.4.1 Insertion of PV catheter

Following completion of the necessary preparatory steps, working heart was initiated. The aortic outflow tract was switched from Langendorff bubble trap B2 to the working heart afterload chamber. The air and overflow openings on bubble trap B1 were opened, perfusate was redirected to the left atrial cannula and working heart was established. Where appropriate, perfusate recirculation was instituted first. Hearts were then given a 5 min stabilization period to equilibrate. A 3F pressure-volume catheter (*Scisense*; *Ontario, Canada*) was situated in a haemostasis valve connected to the aortic cannula. The haemostasis valve was opened slightly to allow unrestricted movement of the catheter and the tip was slowly advanced past the aortic valves and into the left ventricular cavity. The haemostasis valve was then closed to secure the catheter within the left ventricle.

2.1.4.2 Establishment of baseline working heart function

Haemostasis valve positioning was manipulated in order to obtain a desirable pressure-volume loop, which was defined as the widest and straightest PV loop achievable. Using this rule allowed achievement of the largest stroke volume possible in order to minimize the calibration factor alpha (see Section 2.3.4). Afterwards the valve was clamped into position. Hearts were paced by switching on the isolated stimulator and train generator and setting the frequency of stimulation as required (usually 3.3 Hz). Afterload was then adjusted depending on the requirements of the experiment and hearts were left to equilibrate for 5 minutes.

2.1.4.3 Introduction of saline bolus

A 0.15 ml bolus of 20 % saline at 37 ºC was injected into the left atrial inflow line via a side-port to estimate parallel conductance. Hearts were then left for a further 5 minutes before baseline functional measurements were obtained. The entire process from initiation of working heart to measurement of baseline function took on average 30 min to complete. Parallel conductance estimation is explained in detail in Section 2.3.3 later in this chapter.

2.1.4.4 Estimation of left ventricular pressure-volume relations

Estimation of left ventricular pressure-volume relations was performed by transient occlusion of the left atrial inflow line to obtain a family of pressure-volume loops, and

commencement of the experimental procedure took place thereafter. Ventricular pressure volume relations are described in greater detail in Section 2.3.7 of this chapter. Coronary flow was measured at regular intervals throughout the experiment by manual timed collection of perfusate dripping from the heart into a graduated cylinder. Cardiac output was calculated as the sum of aortic flow and coronary flow and was used to estimate alpha in volume signal calibration (described in detail in Section 2.3.4). It should be noted that the sum of aortic flow and coronary flow was also equal to the inflow volume.

2.1.5 Data recording

All electrical and electronic recording equipment was connected to an 8-channel *Powerlab* A-D convertor (*ADInstruments*; *Oxfordshire, UK*), linked to a *Dell* Personal Computer. Data were captured at a sampling rate of 1000 Hz using *ADInstruments LabChart* Data Acquisition software version 5.5.6 and displayed throughout on a 22“ monitor connected to the PC. Following the end of experiments data were immediately saved to the PC and backed up on an external hard disk for off-line analysis.

2.2 Assessment of left ventricular function using miniaturised pressure-volume catheterisation.

Simultaneous measurement of pressure and volume is regarded as the most effective means of permitting extensive characterization of intact heart function experimentally (Georgakopoulos *et al.*, 1998; Kass, 1992). Currently the gold standard for assessment of intact heart function involves the use of pressure-volume catheters. Virtually all of the data gathered during this study stem from the use of miniaturized pressure-volume technology. The following sections will briefly explain the theory of pressure and volume catheterisation separately before describing calibration of each. While this technique has been used extensively *in vivo* in a large number of species including rabbit, there are very few descriptions of pressure-volume technology in isolated working heart preparations (Araki *et al.*, 2005; Burkhoff *et al.*, 1985; Grieve *et al.*, 2004; How *et al.*, 2005), with no description of its use in an isolated working rabbit heart preparation available at the time of writing. This therefore necessitated detailed characterization of miniaturized pressure-volume technology in relation to its application to the isolated working rabbit heart.

2.2.1 Why study the pressure-volume loop?

The advantage of instantaneous pressure-volume measurement lies in the ability to assess load-independent indices of contractility and relaxation. Measurement of volume and ventricular chamber dimensions obtained by echocardiography or MRI alone offer information about the pump function of the heart under a particular set of loading conditions, but these techniques rely on averaging of steady state images over several seconds and therefore do not provide load-independent assessment of contractility, which requires interventions that acutely alter loading conditions. The pressure-conductance catheter technique in contrast provides an instantaneous and continuous signal for pressure and volume. Occlusion manoeuvres performed during conductance catheterization permit assessment of end systolic and end diastolic pressure volume relationships (ESPVR and EDPVR respectively) allowing characterization of the intrinsic contractile properties of the ventricle and providing information useful for both clinical and basic research (Burkhoff *et al.*, 2005).

2.2.2 Pressure measurement by micromanometer pressure transducer

The current favoured method of pressure measurement in the intact heart is through the use of ultra-miniature pressure tipped transducers. These solid-state pressure transducers consist of a thin silicon diaphragm sensing apparatus with 2 implantable semiconductor strain gauges whose electrical resistance changes upon deformation, with the change corresponding linearly to a change in pressure (Zimmer & Millar, 1998). Measurement of left ventricular pressure was performed using a 3F *Scisense* variable segment length (VSL) combined pressure-volume catheter inserted into the left ventricular chamber via the aorta (segment lengths; 12, 15, 17 and 19 mm – Figure 2.3B(ii)). An SPR-320 2F micromanometer-tipped catheter (*Millar*; *Texas, US*) was inserted via a side-port haemostasis valve connected to the aortic cannula for measurement of aortic pressure. Measurement of atrial pressure was also performed by insertion of a *Millar* SPR-851 pressure-volume catheter into the left atrial cannula via a second side-port haemostasis valve. Pictures of the *Scisense* and *Millar* PV catheters and amplifier control boxes are shown in Figure 2.3. A third *Millar* pressure-volume catheter, SPR-878 (Figure 2.3B(i)) was used for calibration experiments (see Section 2.3.2) but was not included in the isolated working heart setup.

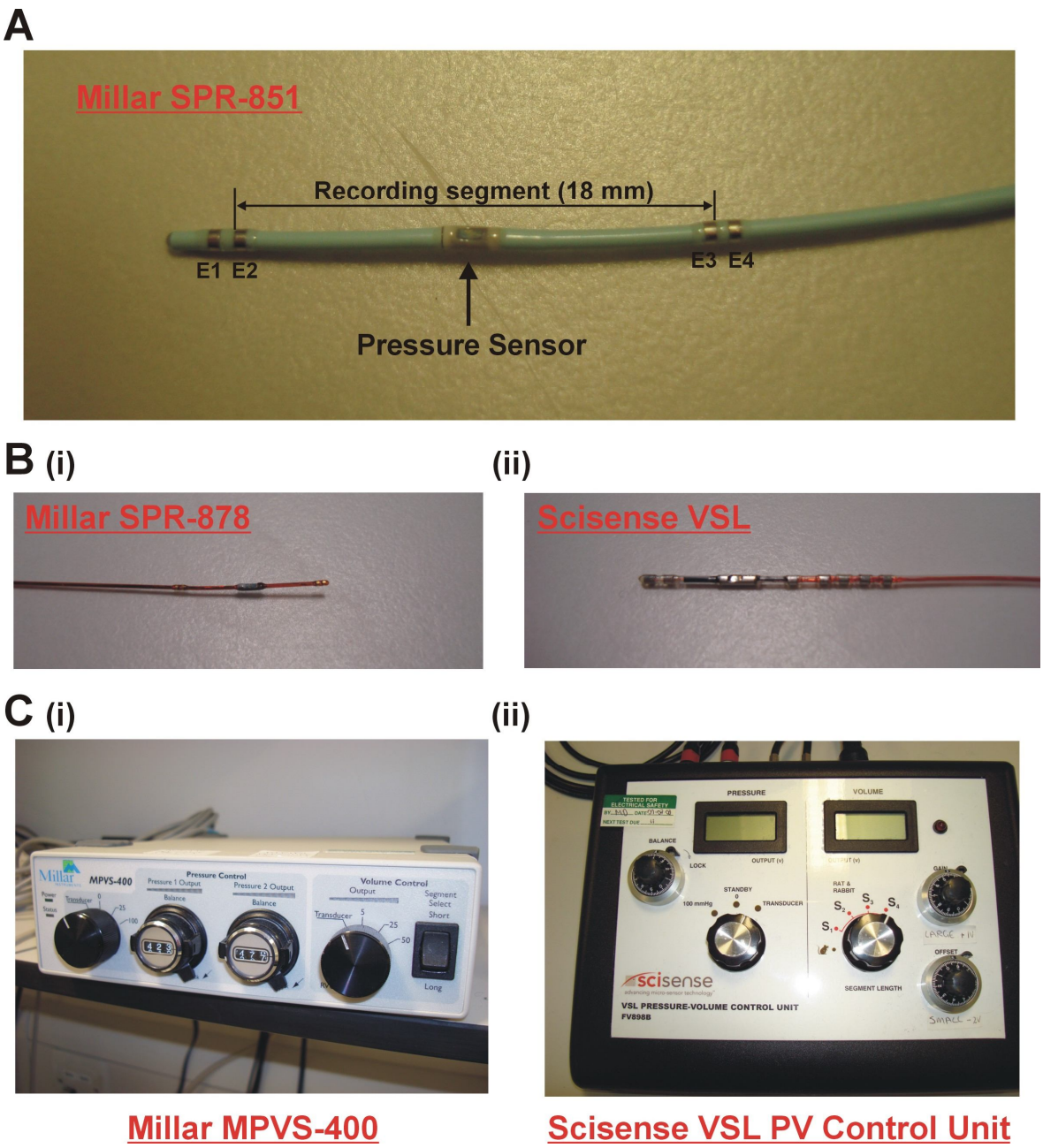

Figure 2.3 Pressure-volume catheter technology. A. *Millar* rabbit PV catheter. Typical pressure-volume catheter features are highlighted. B (i) *Millar* 12 mm rat PV catheter and (ii) *Scisence* VSL rabbit PV catheter. C. Control units for (i) *Millar* and (ii) *Scisense* PV catheters.

2.2.3 Pressure sensor calibration

Prior to each experiment catheters were connected to their respective pressure amplifiers, with each catheter tip left soaking in separate saline filled bijous floated in a water bath at 37 ºC. Catheters were left for at least 45 minutes prior to experiments to warm up. This ensured maximum stability of the pressure signal and prevented drift over long periods. Signal calibration was based on a 2-point linear calibration technique. Briefly, the input settings menu for each pressure channel was accessed individually within *LabChart* and the software displayed output voltages from each sensor with respect to time. Both the

Scisense and *Millar* pressure amplifiers were equipped with a calibration control switch that allowed output of preset voltage values corresponding to 0 and 100 mmHg. With the catheter tip bathed in 37ºC Tyrode's solution the calibration control switch was turned from 'Transducer' to '0'. After ensuring this 0 pressure voltage reference was captured by *Labchart*, the switch was then turned to '100'. The voltage values along with their corresponding pressure value were then entered into a units calibration interface. Using these two values *Labchart* would then create a linear calibration by drawing a straight line between the two points and calculating the slope. Calibration of both *Scisense* and *Millar* pressure sensors was performed in the same manner as described above, however it should be noted that the *Scisense* amplifiers have preset outputs of -2.86 V and -0.56 V for 0 and 100 mmHg respectively, while the *Millar* amplifier had preset outputs of 0 V and +1V for 0 and 100 mmHg respectively. Once a calibration curve was established, pressure sensors were balanced to 0 using a balance adjustment control switch found on the pressure amplifier. Sensors were balanced to 0 by holding the catheter with the sensor dipped under a meniscus of double distilled water at 37 ºC and adjusting the balance control switch until the *Labchart* output read 0 mmHg. At this point the pressure sensor was ready to be used.

2.2.4 Pressure sensor linearity and stability

The voltage-pressure linear relationship for both *Millar* and *Scisense* pressure sensors was tested using a *Delta-Cal* pressure transducer tester (*Utah Medical*; *Midvale, UT*). This handheld electronic device contains a built-in pre-calibrated solid state pressure transducer linked to an LCD display. Following calibration of the pressure sensors as described above in section 2.2.3, the catheters were placed inside a haemostasis valve which was then attached to the *Delta-Cal* via a side-port connector. A pneumatic pump within the *Delta-Cal* was used to generate a pressure that was applied to both the built-in transducer and the pressure sensor attached to the side port. The pressure applied to the internal transducer was increased from 0 to 100 mmHg in 10 mmHg steps and compared with the pressure output generated by the catheter. Figure 2.4 shows the results of the pressure generated by the *Delta-Cal* versus the pressure output from both *Scisense* and *Millar* catheters. Both sensors demonstrated excellent linearity and were in agreement with the independently generated pressures of the *Delta-Cal*. Provided catheters were warmed for 45 min to 1 hour before balancing, the *Scisense* and *Millar* pressure sensors were also stable over extended periods of time, demonstrating signal drifts of less than 1 mmHg per hour. These findings were in agreement with those of a previous study confirming the

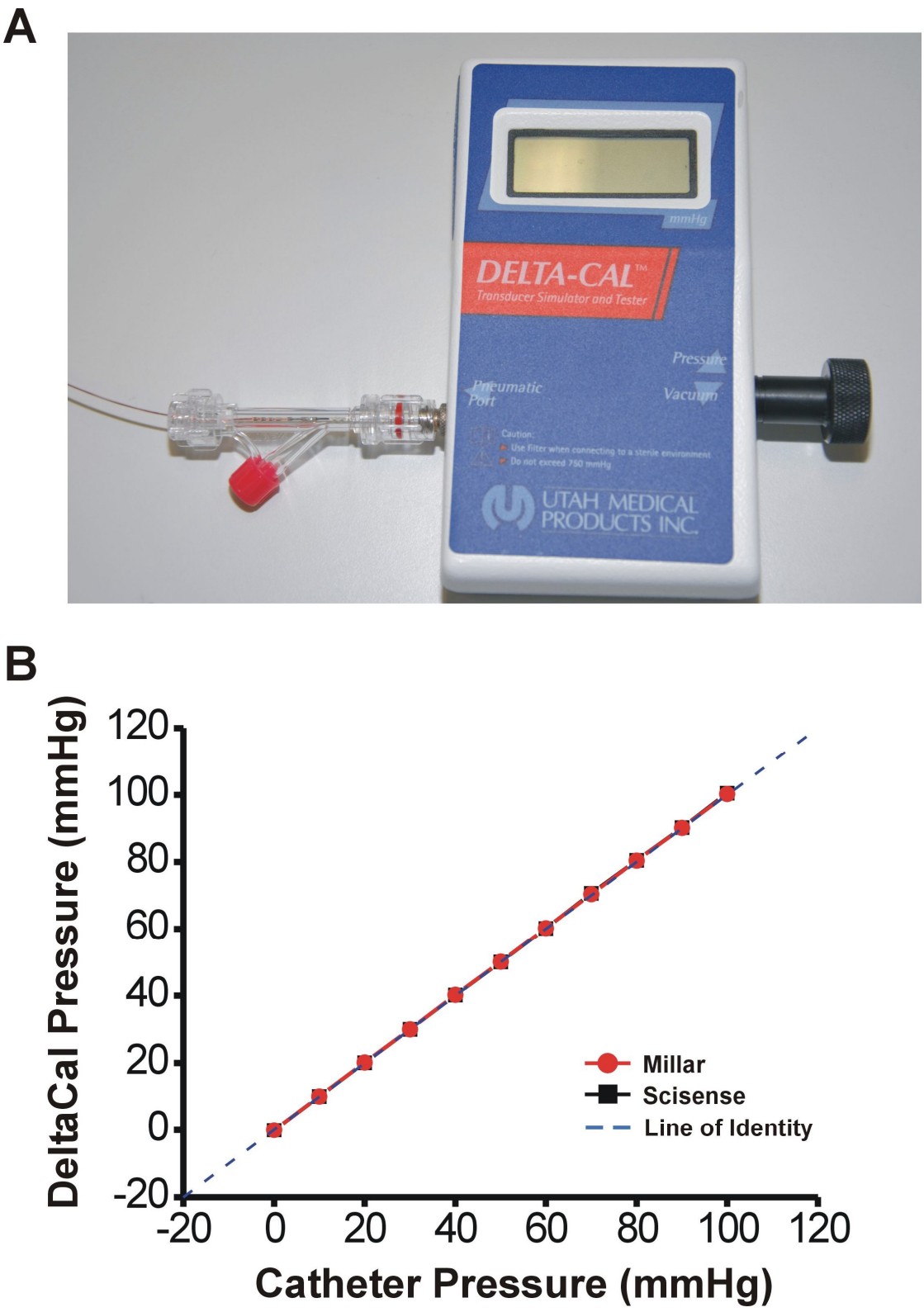

Figure 2.4 Pressure sensor linearity. A. *Scisense* VSL catheter attached via haemostasis valve to the *Delta-Cal*. B. *Delta-cal* pressure reading vs. *Millar* and *Scisense* catheters

accuracy and stability of solid-state pressure transducers from four separate manufacturers including *Scisense* and *Millar* (Hartley *et al.*, 2008).

2.3 Volume measurement by conductance catheter

Conductance catheter technology, originally developed by Jan Baan and colleagues (Baan *et al.*, 1981; Baan *et al.*, 1984) involves the insertion of a catheter with at least 2 pairs of ring electrodes, longitudinally into the left ventricle. Pressure-volume catheters used in this study are shown in Figure 2.3, with electrodes for the single segment *Millar* SPR-851 labeled E1 to E4. E4 is the proximal electrode (located closest to the catheter handle), with E1, the distal electrode located closest to the tip of the catheter. E2 and E3 lie in between E1 and E4 and comprise the volume sensing component of the catheter. A constant current is passed through E4 with E1 acting as a ground reference. This results in the generation of an electric field within the ventricular chamber. As blood is a conductive medium, the voltage between the inner pair of electrodes E2 and E3 can be measured throughout the cardiac cycle. Conductance (G) is related to voltage by the equation

$$G = \frac{1}{R} = \frac{I}{V} \qquad (1)$$

Where I is current (amps) V is voltage (volts) and R is resistance (Ω). The voltage measured between two recording electrodes is inversely proportional to the volume of blood surrounding the electrodes (Pacher *et al.*, 2008). As volume within the ventricle increases during diastole, the resistance (and therefore voltage) measured by the catheter decreases, and conductance increases. As blood is ejected during systole, the measured resistance of the blood pool increases and conductance decreases. Using this method it is therefore possible to measure instantaneous changes in conductance during the cardiac cycle. In order to convert this conductance signal into true volume the length of the recording segment, as well as the specific resistivity of blood must also be taken into account. The original equation proposed by Baan was

$$Vol = \rho L^2 G \qquad (2)$$

Where Vol is the instantaneously measured volume (ml), ρ is the specific resistivity of blood (Ω-cm), and L is the length of the recording electrode segment (mm). Two elements were incorporated into (2) to yield

$$Vol = \frac{1}{\alpha}\rho L^2 (G - G_P) \qquad (3)$$

Where α is a dimensionless constant used to correct the volume signal for non-uniformity of the electric field and G_p, also known as parallel conductance, is a term used to describe conductance measured by the catheter owed to structures other than the blood within the left ventricle. Calculation of these two parameters is discussed in detail later in this chapter.

2.3.1 Volume signal calibration

Calibrating the conductance signal to achieve actual volume measurements was performed by creating a 2 point calibration curve in the data acquisition software similar to the method previously described for the pressure sensor. This could be performed in two ways. The first utilizes solutions of equal volume but different known conductance values to create a linear relationship between voltage output and conductance, with the resulting conductance values then being applied directly to Baan's equation to obtain true volume. The second method requires the use of a conductance cuvette (pictured in Figure 2.5 A (i)), an acrylic block with precisely machined wells of matching depth but increasing diameter, and hence volume. Cuvette wells were filled with a saline solution matching the specific conductivity of the blood of the animal being studied. In the case of the isolated working heart, the Tyrode's solution made for each experiment was used directly. The catheter was placed in a well to display a voltage reading on the data capturing software being used. Great care was taken to ensure the catheter was central within the well as this was where the highest voltage signal was obtained. Slight deviation from centre would result in underestimation of the voltage signal. The purpose of this calibration was to establish a linear relationship between the raw analogue signal and measured volume, and then establish the slope of this line. Provided that the relationship is indeed linear, all points in between the 2 calibration values used will fall on this line. The total volume of solution that each well held was inconsequential, as the catheter only recorded volumes lying between the recording electrode segment (denoted by the symbol L in Baan's equation). The relationship between measured volume and cuvette diameter for some commonly used recording electrode segments can be seen in Figure 2.5 A(ii). Several factors were taken into account before commencing calibration using this method:

(1) The specific resistivity, ρ, of the solution being used is heavily temperature dependent, increasing by 2.1 % per degree Celsius as it cools from body temperature to room temperature. Calibrating cuvettes were fixed to the inside of the isolated working heart water bath, heating the solution within to 37 ºC. This eliminated the possibility of differences in solution conductivity between calibration and during the working heart experiment.

(2) The conductance signal measured by the catheter depends on the position of the catheter within the well, with the largest signal being achieved when the catheter was

central in a given well. To maintain the accuracy of the calibration care was taken when moving between wells to achieve the highest conductance signal possible.

2.3.1.1 Choosing lower and upper volume calibration limits

A custom design 3F *Scisense* variable segment length (VSL) catheter and two *Millar* pressure volume catheters (SPR-878, 12 mm spacing; SPR-852, 18 mm spacing) were calibrated using the 2-point calibration described above. The *Scisense* catheter permitted selection of the length of the recording segment from 14, 17, 20 and 23 mm in order to accommodate rabbit hearts of varying ventricular long axis (VLA) dimensions. A smaller *Scisense* VSL catheter featuring 12, 15, 17 and 19 mm electrode spacing was also available. Two cuvette wells of known diameter were chosen for an initial 2-point calibration using the *LabChart* software. The cuvette wells were chosen to represent the highest and lowest volumes expected from the isolated working rabbit heart, which were estimated from preliminary experiments. Cuvette wells of diameter 8.0 mm and 14.0 mm were chosen to represent the low and high volume limits of the linear relationship. Since the calibration volume varied depending on the segment length chosen the rationale for selecting these calibration volumes was based on the most commonly used electrode spacing segment, 19 mm, such that the low calibration volume was 955.04 µl, and the highest calibration volume 2925.82 µl.

2.3.1.2 Volume signal calibration procedure

The *Scisense* VSL pressure-volume control unit allowed adjustment of the volume signal gain and offset, a feature not available on the *Millar* MPVS-400. This permitted control of the voltage range or 'swing' that the catheter would operate within during a typical experiment. The *Scisense* control unit had a voltage range of +/- 5 V, and voltage swing used throughout the study was -2 V to + 1 V, corresponding to the 8 mm and 14 mm diameter cuvette wells respectively. This afforded plenty of room on the positive side of the control units' operational range without compromising signal resolution. Just prior to calibration, the temperature of solution within the cuvette wells was monitored using a 2000T electronic thermistor (*Digitron*; *Devon, UK*). Desired segment length was chosen using a control switch on the front of the *Scisense* control unit, labelled S1 for the shortest segment, up to S4 for the largest. With *Labchart* recording, the catheter tip was submerged in the largest cuvette well, ensuring all electrodes were enclosed within the well. The tip was positioned as centrally as possible and the voltage reading on the control units' digital display was noted. The catheter was then moved into the small well, centred, and the

voltage noted. To achieve the desired voltage swing of -2V to +1V, the gain and offset balance controls were adjusted using a simple rule of moving between each well and adjusting the offset when the catheter is in the smallest well, while adjusting the gain in the largest well. Eventually a reading of -2V and +1V was achieved by submerging the catheter tip in the 8 mm and 14 mm diameter cuvette wells respectively. To complete the 2-point calibration, the voltage values were entered into the *LabChart* units calibration interface and associated with a specific volume. The volume associated with this measured voltage was dependent upon the recording segment length chosen and calculated using the equation describing the volume of a cylinder

$$Vol = \pi r^2 L \tag{4}$$

Where *Vol* is volume (µl), *r* is the cuvette radius (mm) and *L* is the recording segment length (mm). Calibration using this method was advantageous in that the values of 'ρ' and '*L*' from Baan's equation were automatically incorporated into the calibration being intrinsic properties of the calibration solution and the catheter being used, respectively. Conversion of measured volume to true volume was simplified to

$$V_T = \frac{1}{\alpha}(V_C - V_P) \tag{5}$$

Where V_T is the true volume (ml), V_c is the volume measured by the catheter (ml) and V_p is the volume owed to parallel conductance (ml).

Calibration of the *Millar* pressure-volume catheter was performed in a different manner to the *Scisense* equipment. The MPVS-400 control unit was equipped with preset calibration values for volume similar to the in-built pressure calibration settings found on both systems, the units of which were expressed in RVU or relative volume units. The calibration procedure for this was identical to that of the pressure sensor calibration described above.

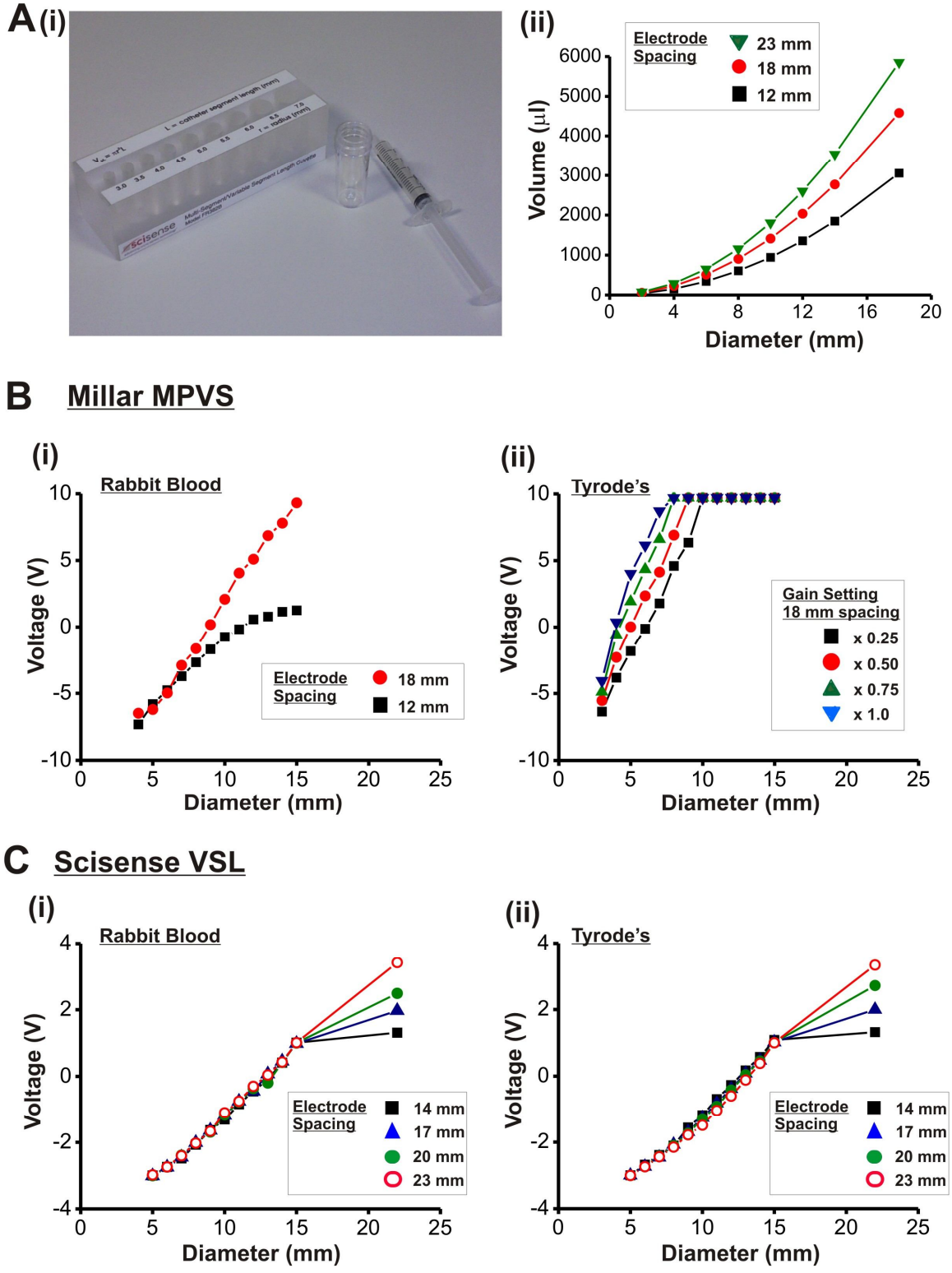

Figure 2.5 Cuvette volume calibration. A(i). Acrylic calibration cuvette and calibration wells. A(ii). Cuvette diameter vs. volume relationship for several recording segments. Linearity and range of volume measurement of *Millar* (B) and *Scisense* (C) catheter systems using either rabbit blood (B (i) and C (i)) or Tyrode's solution (B (ii) and C (ii)).

2.3.2 Volume range and linearity by the cuvette calibration method

2.3.2.1 Comparison of Millar vs. Scisense volume measurement

The control units for the volume portion of the *Millar* and *Scisense* catheters described above were based on the same technology, however the capabilities of the two systems were unknown prior to initiation of the experimental study. Direct comparison of the two systems was undertaken by the cuvette calibration method described in the previous section using two different calibration media; Tyrode's solution and heparinised rabbit blood.

2.3.2.2 Resistivity of Tyrode's solution and rabbit blood

The specific resistivity of rabbit blood and Tyrode's solution was measured using an electronic conductivity meter (*Amber Science*; *Eugene, Oregon*). It was found that while rabbit blood at 37 ºC had a measured resistivity of 163.93 $\Omega.cm^{-1}$, Tyrode's solution resistivity was lower, measuring 68.49 $\Omega.cm^{-1}$. The effect this difference in conductivity between the two media had on the performance of the *Millar* and *Scisense* catheter systems was investigated by performing a cuvette volume linearity experiment.

2.3.2.3 Cuvette well linearity calibration

The calibration cuvette provided by *Scisense* was secured in the isolated working heart water bath at 37 ºC, and each cuvette well was filled with the calibration solution of interest. Cuvette wells ranged from 3.0 to 14.0 mm in diameter, in 1 mm increments. To extend the range of testing permitted by the cuvette wells, a cylindrical well of diameter 15 mm was included. Starting from the smallest cuvette well and moving in sequence to the largest well, catheter tips were fully submerged and centred in each cuvette well with the voltage output recorded on *LabChart*. This procedure was repeated with each segment length of the *Scisense* VSL and for both *Millar* PV catheters using Tyrode's solution and heparinised rabbit blood.

2.3.2.4 Millar PV system has a limited range using Tyrode's solution

Using heparinised rabbit blood (Figure 2.5 B(i)) both *Millar* catheters were capable of recording values across the range of cuvette well diameters provided. The 12 mm SPR-878 (black filled squares) was linear only over a limited range (between 4 and 10 mm cuvette well diameter) while the 18 mm SPR-851 remained linear up to the 15 mm

diameter cuvette. The non-linear behaviour of the SPR-878 was the result of the electric field generated by the catheter reaching its theoretical limits and becoming insensitive to further increases in volume. This concept is discussed in more detail in the next section. Figure 2.5B(ii) shows the same experiment performed using the 18 mm *Millar* catheter bathed in Tyrode's solution, with the output gain of the MPVS control unit set to four different values; 0.25, 0.5, 0.75 and 1.0. The voltage signal of the 18 mm catheter at a gain of 1.0 (blue filled triangles) reaches a maximum in the 7 mm diameter cuvette using Tyrode's solution, as demonstrated by the voltage remaining constant in the larger cuvette wells. This problem persisted even when the gain on the MPVS was reduced to as little as ¼ its original value (black filled squares). This observation was due to the increased electrical conductivity of Tyrode's solution in comparison to heparinised rabbit blood. From Figure 2.5A(ii), using an 18 mm catheter the highest volume capable of being measured would be ~ 1.4 ml which is unsuitable for an isolated working rabbit heart where stroke volume alone may exceed this value. Preliminary experiments with the *Millar* catheter confirmed this limitation, with the volume signal reaching the limits of the control units' operational range before end diastole, resulting in a truncated volume signal and PV loop.

2.3.2.5 Scisense PV system remains within operational range using either blood or Tyrode's solution

Figure 2.5C(i) and (ii) show the cuvette well calibrations performed with the Scisense VSL catheter using heparinised rabbit blood and Tyrode's solution, respectively. Each segment length was calibrated using the voltage span of -2V to +1V as described above. All segment lengths demonstrated linearity up to and including the 15 mm diameter cuvette. An additional cylinder with a diameter of 22 mm was included to extend the range of testing with this system. The sensitivity of all but the 23 mm recording segment was reduced using the 22 mm cuvette (Figure 2.5B(i) and (ii), black squares, green circles and blue triangles), however the recording segments all remain within the operational voltage range of the *Scisense* control unit. The range of cuvette diameters (and hence volumes) that the *Millar* system could work within was therefore restricted when using Tyrode's solution. In contrast, the *Scisense* VSL catheter remained within its operational range of +/- 5V in all cuvette wells, using all four recording segments. The ability to fine tune gain and offset values using the *Scisense* control unit proved this system had superior utility compared to the *Millar* volume measurement technology in our isolated working heart setup and was therefore used for all subsequent volume measurements.

2.3.2.6 Limitations of electric field generated by conductance catheter

Panels C(i) & (ii) in Figure 2.5 illustrate the limitations of the electric field generated by the *Scisense* VSL catheter when placed within a relatively large cylindrical well of diameter 22 mm. Although the chosen recording segment lengths demonstrated linearity in cuvette wells up to 15 mm in diameter, all segment lengths except for the 23 mm become non-linear at the last well used. Of note from Figure 2.5C(i) and (ii) is that non-linearity decreased as segment length increased, indicating that in larger diameter wells the sensitivity of the catheter is increased with increasing segment length.

2.3.2.7 Electric field heterogeneity in conductance catheter studies

For the 2-point volume calibration to remain valid, it is critical that linearity exists between the volume measured by a conductance catheter and the actual volume present. A number of studies have established that while Baan's equation assumes a homogenous electric field distribution within the ventricle by the conductance catheter, in reality does not hold true *in vivo* (Steendijk *et al.*, 1993; Wei *et al.*, 2005; Wu *et al.*, 1997). While this heterogeneity could potentially lead to error in the estimation of true volumes within the ventricle, Baan *et al.* (1984) demonstrated there was no significant deviation in catheter volume estimation compared to cine-angiography and stroke volume estimation via electromagnetic flow probe (Baan *et al.*, 1984). While it can be seen that electric field heterogeneity does contribute as a source of error, conductance catheter measurements demonstrate linearity over a range of volumes in a number of publications using different species (Abe *et al.*, 1995; Burkhoff *et al.*, 1985; Ito *et al.*, 1996; Yang *et al.*, 2001) and provided the correct catheter spacing is employed this may not be a significant problem. To assess the relationship between volume measured by the catheter and true volume, the 2-point calibrations established prior to assessment of the voltage/cuvette well diameter relationships above and stored in *LabChart* were applied to all previously generated voltage data to obtain the calibrated volume measurement for each segment length using Tyrode's solution. The results in Figure 2.6 demonstrate that each recording segment demonstrates linearity over a large range of measured volumes, such that the effects of electric field heterogeneity do not create a significant source of error in volume estimation by conductance catheter within the range of volumes expected in the rabbit working heart.

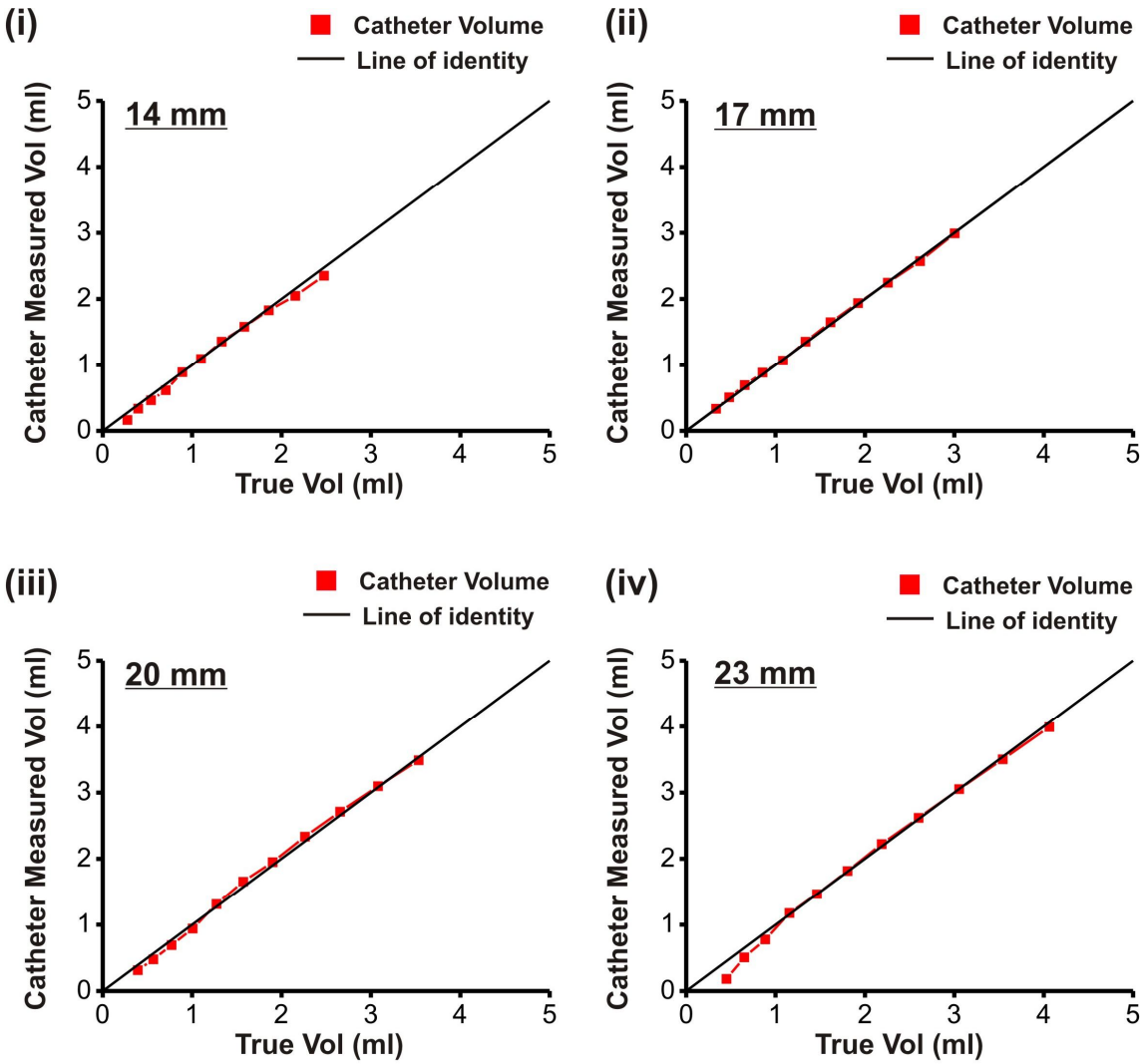

Figure 2.6 Catheter volume linearity. Relationship between true cuvette volume and cuvette volume as estimated by conductance catheter for (i) 14 mm, (ii) 17 mm, (iii) 20 mm and (iv) 23 mm recording segments

2.3.3 Estimation of parallel conductance

Two correction terms which had to be estimated for calculation of the true volume signal were parallel conductance and alpha. Parallel conductance arises from the observation that the myocardial tissue as well as structures surrounding the heart will conduct electricity, and a significant offset of the conductance signal will occur as a result. Since only the blood conductance signal is desired, the offset owing to parallel conductance must be estimated and subtracted from the total conductance (or volume) signal measured by the catheter. The most common method of estimating parallel conductance *in vivo* involves injection of a bolus of hypertonic saline (10 to 30 %) into the pulmonary artery (Pacher *et al.*, 2008; Steendijk *et al.*, 2001; Steendijk & Baan, 2000). The highly conductive saline washes into the left ventricle leading to a transient increase in the conductivity of the blood over several beats that will be recorded by the catheter. The saline bolus must be of

sufficient volume such that it leads to a transient increase in the measured left ventricular volume signal without altering pressure within the chamber. Calculation is performed offline and yields a single value for the parallel conductance.

2.3.3.1 Verification of the hypertonic saline method for parallel conductance estimation

The merits of the hypertonic saline bolus for parallel conductance estimation lie in the ease with which it can be performed as well as its reproducibility, however it relies on the assumption that parallel conductance remains constant throughout the cardiac cycle. Under normal circumstances parallel conductance is estimated from just 2 points on the volume signal, the maximum and minimum volume points. Lankford *et al*. (1990) noted that potential errors could emerge if the value for parallel conductance at these 2 points was not the same (Lankford *et al.*, 1990). The group therefore investigated this claim by dividing the systolic period of each cardiac cycle during the saline injection into 20 equal time intervals (demarcated by dP/dt_{max} and dP/dt_{min} from the ventricular pressure trace), and obtaining time varying parallel conductance ($V_p(t)$) values by linear extrapolation of each of these time points between successive cardiac cycles (Lankford *et al.*, 1990). Using both isolated supported canine hearts and *in vivo* canine measurements the investigators demonstrated that parallel conductance determined from multiple points in the cardiac cycle correlated very highly with determination from just a single estimation, concluding that parallel conductance does not vary to a significant degree during the cardiac cycle.

2.3.3.2 Ideal conditions for parallel conductance estimation

Hypertonic saline bolus remains the most routinely used method of parallel conductance estimation and is still recommended for current conductance catheter studies (Pacher *et al.*, 2008). To improve reproducibility and minimize error between studies optimal experimental conditions for saline bolus calibration have been investigated. Herrera *et al*. (1999) investigated the effect of saline temperature and concentration on parallel conductance estimation by performing three injection manoeuvres in closed-chest dogs (Herrera *et al.*, 1999). They found that the saline bolus yields better results when kept as close to body temperature as possible, as the temperature gradients induced by cold (22 ºC) saline may increase blood resistivity by as much as 10%. Bolus concentrations that caused the greatest dispersion of the volume signal (4.5 M and 6 M NaCl, approximately 26 and 35 % respectively) yielded more consistent V_p estimations between injections, and were the concentrations recommended by the study (Herrera *et al.*, 1999).

2.3.3.3 Saline bolus injection in the isolated working heart

In the isolated working heart setup described here, only the left side of the heart was perfused. This immediately limited the injection sites for saline bolus to two locations on the working heart system; i) The haemostasis valve located on the left atrial cannula, or ii) the preload chamber. Injection via the preload chamber was chosen as it was more successful in yielding 5 – 7 cardiac cycles where solution conductivity changed without eliciting a change in peak pressure. Using a thin plastic French catheter attached to a 1 ml syringe, a 0.15 ml bolus of 20 % saline bolus was injected at the entrance to the left atrial inflow line such that injection of the bolus did not alter the filling pressure during the manoeuvre.

2.3.3.4 Calculation of parallel conductance

So far the offset in the volume signal owing to structures other than the solution within the heart has been termed parallel conductance. However the calibration procedure described above takes into account the blood resistivity, ρ and electrode segment length, L, from Baan's original equation, allowing the parallel conductance term (G_p) to be exchanged for parallel volume (V_p) in the conversion to absolute volumes. As described in Section 2.3.1.2 the equation for estimation of true volume becomes

$$V_T = \frac{1}{\alpha}(V_C - V_P) \qquad (5)$$

Where V_T is the true volume (ml), V_c is the volume measured by the catheter (ml) and V_p is the volume owed to parallel conductance (ml). The term parallel volume will be used from this point onwards to describe the volume offset due to structures other than perfusion solution within the left ventricle. A plastic bijou was filled with 5 ml of 20 % saline solution and held at 37 ºC in a water bath. V_p estimation was performed after establishing stable baseline function. Timing of the saline bolus was necessitated by the terminal nature of many experiments during this study which prevented post-experimental determination. A 1 ml syringe was partially filled with 20 % saline solution. A plastic French catheter attached to the syringe was primed with saline and fed into the working heart preload chamber just inside the left atrial inflow line. 0.15 ml of saline was injected into this line while pressure and volume traces were carefully monitored to ensure the injection had worked correctly. The concentration of saline injected is not taken into account during calculation of V_p and is therefore not critical in that respect. However bolus concentration, along with the volume injected, will impact on the success of the manoeuvre; too low a concentration and the volume dispersion will not be sufficient to

correctly estimate V_p, too high and there is an increased risk of causing irreversible depression of contractile function. An example of pressure-volume loops obtained following a saline bolus injection in the isolated working heart, along with the resultant V_p estimation is shown in Figure 2.7, with mean V_p and r-values for 7 control isolated working hearts displayed in Table 2.1. The aim was to achieve the largest number of cycles where V_c was changing without any alteration in left ventricular pressure. 0.15 ml of 20 % saline solution injected into the left atrial inflow line allowed consistent achievement of a period of 5 – 7 beats where alteration in V_c was visible while peak pressure remained stable. V_p was estimated offline using PVAN pressure-volume analysis software version 3.6. Parallel conductance was calculated as follows:

1) The maximum (V_{max}) and minimum (V_{min}) volumes determined by the catheter during the wash-in phase of the hypertonic saline injection were displayed by PVAN with V_{min} plotted as a function of V_{max}, as shown in Figure 2.7 B.

2) V_p is solved using the observation that volume measured by the catheter, V_c, is linearly related to Tyrode's solution conductivity (σ_T - the reciprocal of resistivity). The hypertonic saline bolus causes a transient increase in V_c on a beat to beat basis owed exclusively to an increase in solution conductivity, however the actual volume within the ventricle remains constant.

3) PVAN establishes a linear relationship between successive V_{min} and V_{max} points for each cardiac cycle where σ_T is increasing. This relationship is then extrapolated to the point where it crosses the line of identity, where $V_{max} = V_{min}$. Where these two lines meet the volume within the left ventricle is 0, and therefore the volume measured by the catheter at this point must be due to surrounding structures, or V_p.

Measured volume calibration constants - Control group (n = 7)		
V_p	**R-value**	**α**
1150.4 ± 187.13	0.94 ± 0.03	0.87 ± 0.04

Table 2.1 Mean values for parallel conductance and correction factor α

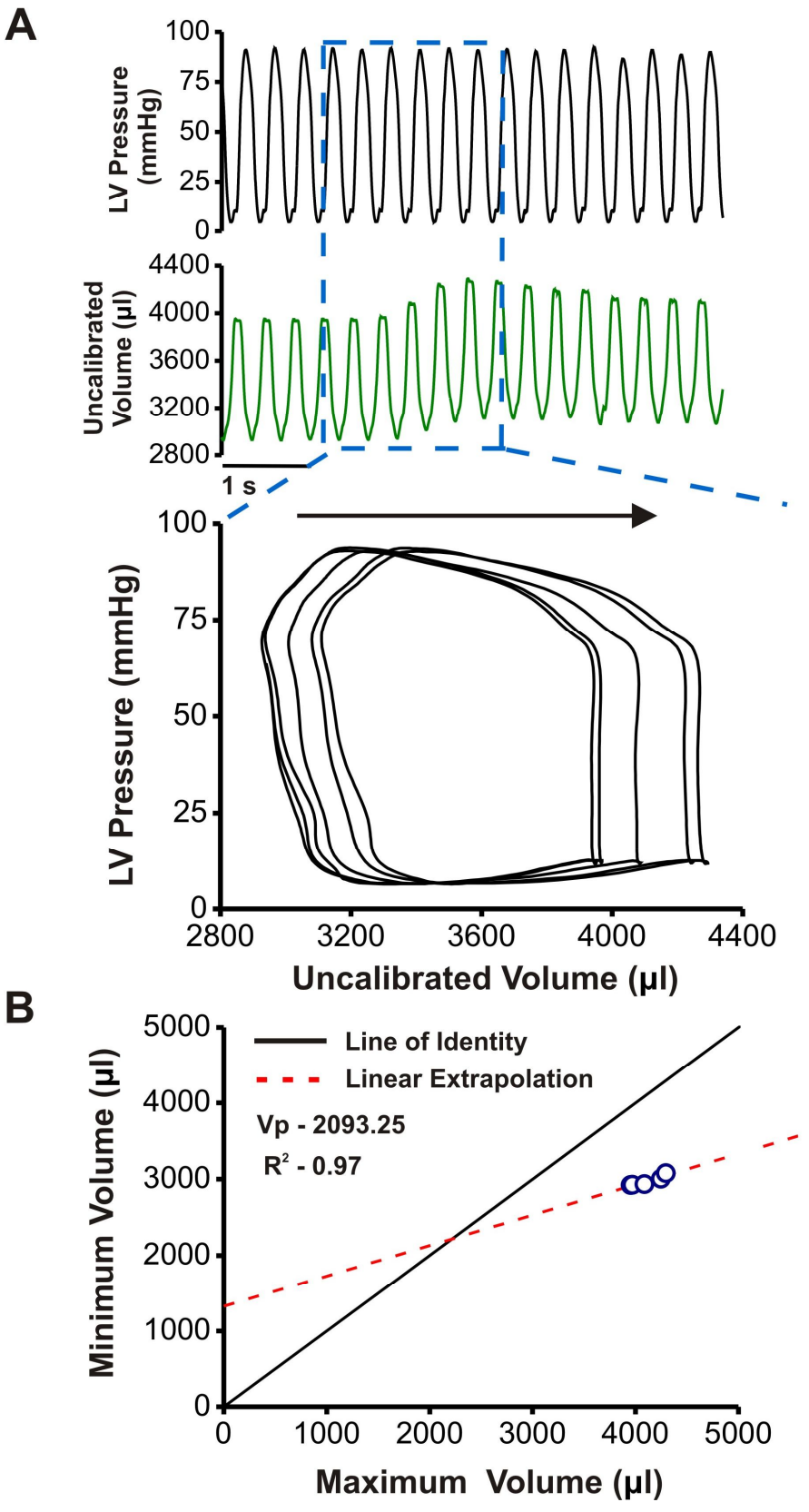

Figure 2.7 Parallel volume estimation. A. Conductivity change after saline bolus injection. B. Parallel volume estimation from maximum and minimum volumes by linear extrapolation

2.3.4 Estimation of α

The effects of electric field heterogeneity have already been described in this chapter as a possible source of error when estimating absolute left ventricular volumes. An associated source of error stems from the chosen catheter recording electrode segment length and its relation to the ventricular long axis (VLA) length. Ideally the recording electrode segment would encompass the entire long axis of the ventricle but if an inappropriate recording segment length is chosen this may not be the case and may contribute to underestimation of absolute volumes. The original equation proposed by Baan and colleagues (1984) included a calibration term known as α, a dimensionless constant used to correct the measured volume signal for the errors introduced by electric field heterogeneity as described above (Baan *et al.*, 1984). In practice α is calculated by forcing the stroke volume measured by the catheter, SV_c to equal stroke volume as measured by an independent means, most commonly an electromagnetic flow probe. Therefore:

$$\alpha = \frac{SV_C}{SV_{True}} \qquad (6)$$

Where SV_c is the volume measured by the catheter, and SV_{True} is the independently measured true stroke volume. In the isolated working heart setup, α was measured in this manner by independent assessment of cardiac output. In the isolated working heart cardiac output was defined as the sum of aortic flow and coronary flow. Coronary flow was assessed by timed measurement of perfusate dripping from the heart. Aortic flow was measured continuously throughout the experiment using an ultrasonic in-line flow meter.

2.3.4.1 Ultrasonic flow meter calibration

The flow meter utilized two in-built piezoelectric transducers located at either end of the flow probe tubing. When electrically stimulated they produced a vibration that alternately propagates along the length of the tubing both with and against the flow of liquid. The velocity with which the wave propagates is proportional to the flow and was therefore used to calculate flow. The measured flow value was then transmitted to a control unit and displayed on a 5 digit LCD output that updated once every 1 s. The output voltage of the ultrasonic flow meter changed linearly with measured volume and continuous recording of flow was made through *LabChart* by connecting the flow meter to the 8-channel *Powerlab* A/D board and performing a 2-point linear calibration similar to that described for pressure and volume. After priming of the working heart system afterload line the peristaltic pump was stopped briefly dropping flow to 0. *LabChart* software was set to record the baseline voltage output from the flow meter when flow was 0 ml/min. The pump was then

switched on and flow commenced. Flow was adjusted via the dial on the peristaltic pump such that the flow meter would display a reading of 200 ml/min. Both low and high voltages recorded by *LabChart* were then entered into the units calibration interface and associated with 0 and 200 ml/min respectively, creating the appropriate linear calibration.

2.3.4.2 Calculation of heart rate for assessment of stroke volume

Heart rate was calculated from the left ventricular pressure trace by measuring the interval between the cyclical rise and fall of the pressure waveform with respect to time. Stroke volume was then calculated using the formula

$$SV_{True} = \frac{CO}{HR} \qquad (7)$$

Where SV_{True} is the true stroke volume (ml), CO is cardiac output ($ml.min^{-1}$) and HR is heart rate ($beats.min^{-1}$). Values recorded for SV_{True} and SV_c during each experiment were entered into equation (6) to obtain α.

2.3.5 Selection of catheter segment length

The correction term α allows for conversion of relative volume to absolute volume. However, steps were taken to avoid reliance on α and ensure the absolute volume measurements obtained were as representative of volume within the entire left ventricle as possible. This was achieved through selection of a catheter whose recording segment length matched as closely as possible the VLA distance of the animal being studied. Isolated rabbit heart VLA distances were assessed during the initial setup of the working heart system. Upon completion of an isolated working heart experiment, hearts were removed from the system and a cut was made longitudinally along the left ventricular wall to reveal the chamber. The distance from apical endocardium to the aortic valve leaflets was measured using a small plastic measuring device fashioned from a millimeter ruler. Figure 2.8A shows the spread of VLA distances recorded from 39 hearts isolated from stock animals with a mean body weight of 3.41 ± 0.06 kg and mean age of 152 ± 3 days. VLA distances ranged from 20 to 24 mm, with a mean value of 22.00 ± 0.20 mm, representing a potential error of 4 mm between animals. The most suitable VSL catheter available was defined as one which could match the 20 – 24 mm range closest. Initially this appeared to be the VSL catheter with 14, 17, 20 and 23 mm recording segments. The largest electrode segments almost completely span the range of measured VLA distances in isolated hearts. Dead space at the catheter tip however was 4.25 mm. Factoring this into the total distance spanned by the catheter the 23 mm spacing was unsuitable for isolated

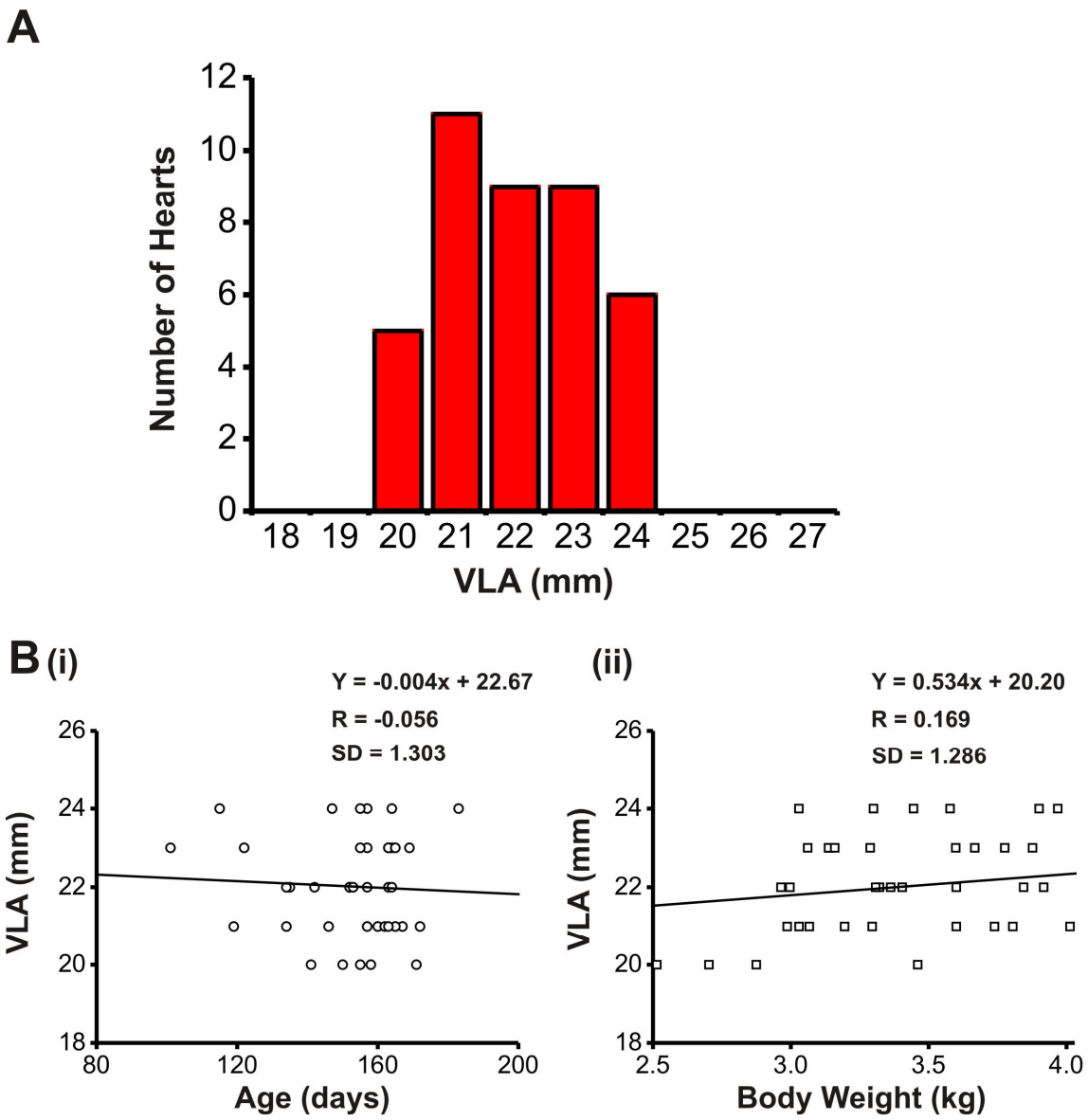

Figure 2.8 Isolated rabbit heart VLA measurements. A. Spread of VLA lengths in isolated rabbit hearts (n = 39). B. Correlation between measured VLA versus (i) animal age and (ii) body weight (n = 39)

working heart experiments, at least on stock animals. A second VSL catheter with recording segments of 12, 15, 17 and 19 mm was manufactured. The dead space at the tip of this catheter was 2 mm, meaning the largest segment did not become redundant. While there was argument for use of the larger VSL catheter in bigger hearts, with the majority of isolated hearts having a VLA of less than 24 mm the 19 mm spacing of the smaller catheter would offer greater accuracy in most cases. The lengthy warm-up time of the catheters and lack of a second PV control unit meant that swapping between the two was not feasible. VLA distances of each heart were plotted against the age and body weight of the donor animal to investigate existence of a correlation that could be used to predict the VLA of an isolated heart prior to the experiment. Results are shown in Figure 2.8B(i) and (ii).

Neither parameter demonstrated correlation with VLA distance meaning selection of recording segment length could not be made on that basis. The catheter recording segment chosen for each experiment was set at 19 mm. Where a smaller segment length was appropriate the catheter was removed from the isolated working heart system and the volume signal quickly recalibrated in *LabChart* to accommodate the new segment. Mean values for 7 control isolated working hearts are shown in Table 2.1. Mean values for α using this approach were 0.87, with values as high as 0.95 being recorded in some cases, demonstrating very good representation of volumes within the entire left ventricular cavity prior to correction with α.

2.3.6 Multi-segmental volume measurement

Due to size of the ventricular cavity in large animals and humans, volume estimation in these species is performed using a conductance catheter with multiple sets of recording segments. This allows the volume signal to be split up into discrete segments, each representing a particular portion of the left ventricular cavity. The resulting segmental volumes are then summed to obtain the total volume signal for the entire left ventricle. The advantage of this technique is that it may permit assessment of regional changes in cardiac function following a localized intervention. Size limitations (due to minimum electrode segment lengths possible) prevent assessment of segmental volumes in small animals such as rats and mice, where VLA dimensions are in the order of 4 to 12 mm. Rabbit hearts however are of adequate size to allow measurement of at least 3 discrete segments within the left ventricle through conductance catheter technology, and the multi-segmental approach has been used previously in this species *in vivo* (Pinsky *et al.*, 1996; Royse & Royse, 2005; Solda *et al.*, 1990). Discrete segmental volume estimation within the left ventricle of isolated working rabbit hearts was performed with the use of a 3F 6 – electrode multi-segmental pressure-volume catheter (*Scisense. London, Ontario*). The two outermost electrodes designated the excitation electrodes and were used to generate the electric field within the LV, while four inner electrodes spaced equally apart delineated 3 discrete recording segments 5.5 mm in length. The total recording segment length of the catheter was 16.5 mm with a dead space at the distal portion of the tip measuring 2 mm. Setup and calibration of pressure and volume portions of this catheter was almost identical to that of the *Scisense* VSL catheters. Deviations from the calibration procedure specified earlier in the chapter are described in detail. The catheter was connected to a GX5 pressure-volume control unit and the catheter tip left soaking in 37 ºC Tyrode's solution for 45 minutes prior to use. Output from each recording electrode segment occupied a

single channel on the *PowerLab* A/D board allowing continuous monitoring of individual segment volumes. Pressure and volume calibration within *LabChart* was performed almost identically to that of the VSL catheters, except that each volume segment on the multi-segmental catheter was calibrated separately. The issue of electric field heterogeneity was addressed by taking into consideration recording electrode sensitivity. When exposed to a static volume in a cylindrical well, segments closer to the electric field source electrodes will report a higher voltage than those further away, despite being exposed to the same volume. The *Scisense* multi-segmental system allowed adjustment of individual segment gain and offset values such that each segment displayed the same voltage when exposed to the same volume, compensating for the non-uniform distribution of the electric field. A voltage swing of -2V to +1V was employed, using cylindrical wells of 4 mm and 6 mm radius (276.46 µl and 622.04 µl, respectively when using a recording segment of 5.5 mm) to represent the low and high portions of the voltage span, respectively. An arithmetic channel was created in *LabChart* to display total measured volume, which was defined as the sum of the measured volumes from each recording segment. Catheter insertion and positioning was performed as described in section 2.1.4 and parallel conductance was estimated using the hypertonic saline bolus method. Absolute ventricular volume was calculated as

$$Vol = \frac{1}{\alpha}\left[\left(V_1 + V_2 + V_3\right) - V_P\right] \qquad (8)$$

Where *Vol* is absolute left ventricular volume (ml), α is a dimensionless calibration factor, V_1, V_2 and V_3 are the instantaneous volumes measured by each recording segment (ml), and V_p is the parallel volume (ml).

2.3.7 How are left ventricular pressure-volume relationships obtained?

To obtain load-independent measures of ventricular relaxation in the isolated working heart, loading conditions were altered transiently following a stable steady state period by brief occlusion of the left atrial inflow line. This method was carried out as a surrogate to preload reduction by transient inferior vena caval occlusion, a recommended manoeuvre for determination of pressure-volume relations *in vivo* (Burkhoff *et al.*, 2005; Pacher *et al.*, 2008). Determination of the end diastolic pressure volume relationship is carried out by fitting a mono-exponential relationship to the end diastolic pressure-volume points from the resultant family of loops. This mono-exponential fit describing the end diastolic pressure volume relationship is denoted by

$$EDP = C \exp^{(\beta * EDV)} \quad (9)$$

Where *EDP* is end diastolic pressure (mmHg), *C* is a curve-fitting constant term, β is the diastolic stiffness constant and *EDV* is the end diastolic volume (ml). Pressure-volume loops obtained during a typical atrial inflow occlusion are shown in Figure 2.9A with the red line indicating the mono-exponential curve fit for this example. The diastolic stiffness constant, β could be visualized by plotting chamber stiffness (rate of pressure increase for a given increase in volume, or dP/dV) against pressure and calculating the slope of the resultant linear relationship (Figure 2.9 B). Mean values for the exponential fitting terms are found in Table 2.2.

EDPVR fitting terms - Control group (n = 7)	
β	**R-value**
3.55 ± 0.47	0.99 ± 0.001

Table 2.2 Mean stiffness constant and r-value of EDPVR fit

2.3.8 Data Analysis

All data were recorded as described in section 2.1.4 and analysed offline following the experimental period. An example of typical pressure and volume recordings from the isolated working rabbit heart during a single cardiac cycle is shown in Figure 2.10. A number of functional indices highlighted on the left ventricular pressure and volume traces in the upper panel of Figure 2.10A, were obtained from these individual signals, while Figure 2.10B, shows the pressure-volume loop obtained by plotting pressure as a function of volume for the same cardiac cycle from which stroke volume, stroke work (denoted by the area within the PV loop), and ejection fraction (stroke volume as a % of end diastolic volume) are assessed from steady state pressure volume loops. Steady state values were obtained at pre-defined time points for each set of experiments by analyzing 10 consecutive cardiac cycles and recording the mean values for each measured variable. Indices of steady state ventricular contractility, maximum rate of rise and fall in pressure (dP/dt_{max} and dP/dt_{min}, respectively) were obtained by calculating the first derivative of pressure, as shown in Figure 2.10A. The ventricular relaxation constant τ was calculated from the ventricular pressure trace using *LabChart*'s Blood Pressure Module (described in greater detail in Section 2.3.9. Logistic τ was calculated by fitting a three parametric exponential decay function, starting at the point of maximal rate of fall of the ventricular

pressure trace, dP/dt_{min}, and ending when pressure reaches a value 5 mmHg above the end diastolic pressure of the following beat. This function is of the form

$$P(t) = \left[P(0) - P(\infty)\right]\exp(-t/\tau) + P(\infty) \qquad (10)$$

Where P(t) is the time varying pressure (mmHg), P(0) is the initial pressure at start of fit (mmHg), P(∞) is the asymptotic equilibrium pressure (mmHg), t is time (ms) and τ is a constant describing relaxation (ms) (Langer, 2002).

2.3.9 Analysis programs used

Data were analysed using a number of pressure-volume analysis programs whose calculation methods were confirmed by analysis using *Origin 6.1* and by comparison of results between programs.

(1) LabChart. Many simple calculations could be performed using the *LabChart* interface. Sections of trace could be manually highlighted and a number of simple calculations performed. Mean aortic flow was calculated in this manner by taking the average value over 10 selected beats at predetermined intervals. A low pass digital filter with a cut-off frequency of 50 Hz was applied to remove this noise and ensure more accurate calculation of maximum and minimum volumes by data analysis programs. This filter was sufficient to remove electrical noise without significantly altering the shape of the volume trace. Calculated α and V_p values could be applied to the raw volume trace with the result being displayed in a separate channel.

(2) Blood pressure module. Calculation of parameters associated with the pressure trace were analysed using the blood pressure module (*BPM*) provided with *LabChart*. All steady state parameter calculations, excluding cycle duration, were calculated within a domain known as the cycle region, defined as the period from one end diastolic pressure point to the next. End diastolic pressure was calculated using an algorithm based on the observation that the overall shape of the ventricular pressure waveform will remain consistent despite variation commonly existing around the end diastolic pressure point. A detection algorithm was then applied to the ventricular pressure waveform allowing automated estimation of end diastolic pressure. For each cardiac cycle the blood pressure module was used to calculate end diastolic pressure (mmHg), minimum pressure (mmHg), peak pressure (mmHg), dP/dt_{max} ($mmHg.s^{-1}$), dP/dt_{min} ($mmHg.s^{-1}$), heart rate ($beats.min^{-1}$) and the relaxation constant τ (ms).

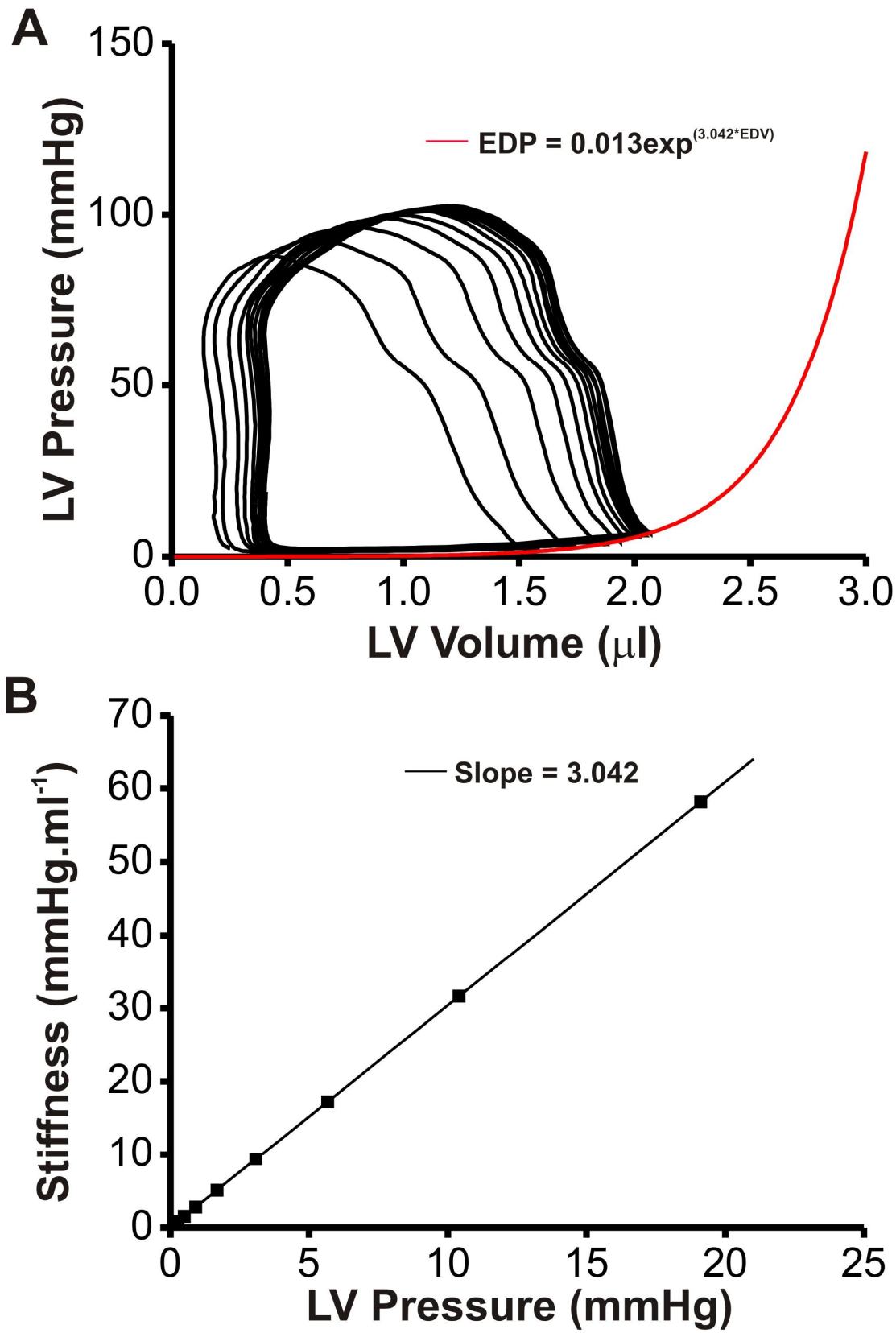

Figure 2.9 Determination of EDPVR. A. Typical family of pressure-volume loops following occlusion. B. Ventricular stiffness (dP/dV) varies linearly with pressure.

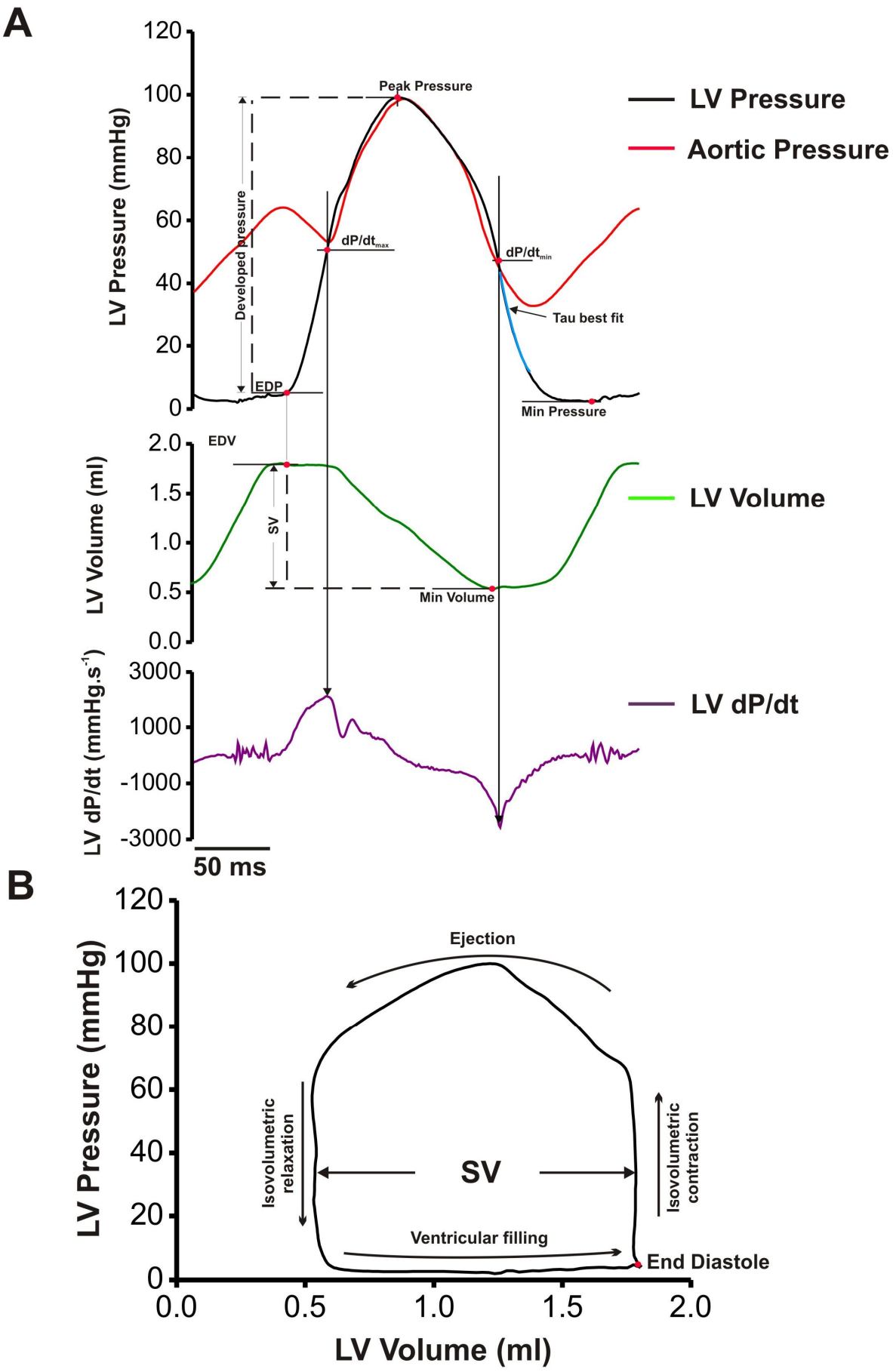

Figure 2.10 Pressure and volume during the cardiac cycle. A. Typical pressure and volume recordings for a single cardiac cycle. B. The pressure-volume loop, illustrating the 4 main phases of the cardiac cycle.

(3) PVAN. The pressure-volume analysis module (*Millar Instruments*) version 3.6 was used to estimate parallel conductance. *PVAN* integrated into *LabChart* allowing recorded data to be imported directly into the program by associating the specific pressure and volume channels with *PVAN*, manually highlighting the selection of trace to be analysed and importing the selection. *PVAN* calculates end diastolic pressure by analyzing the entire pressure trace and assigning a value (for example, x) to each point. The rate of change in pressure is calculated progressively until the rate of change reaches a threshold. *PVAN* assumes the r-wave (the deflection on the ECG associated with ventricular depolarisation) has occurred just before this point and moves back 4 time points, assigning the end diastolic pressure. The parallel conductance is estimated by *PVAN* in exactly the same manner described in section 2.3.3 and a single value for V_p, along with an r-value for the linear fit for the data points are reported.

(4) Labscribe. Data acquisition and analysis software was available through *Labscribe* version 2.0 (*iWorx*; *New Hampshire, US*), which contained built-in modules specifically for analysis of pressure-volume relationships. *Labscribe* was designed specifically for use with *iWorx* A-D boards and as such was not compatible with *PowerLab*. Data could be imported into *Labscribe* from *LabChart* however, by saving selected portions of data as text. *Labscribe* detected a cardiac cycle using a pressure threshold detection method. The pressure trace was then normalized and a pressure volume ratio was calculated by dividing normalized pressure by normalized volume. The end diastolic point was calculated as a point just prior to the minimum of the pressure/volume ratio, while the end systolic point was determined as the point just after the maximum of this ratio. *Labscribe* was used to calculate the EDPVR following atrial inflow line occlusion. The software used the same mono-exponential curve fit described in section 2.3.7, and the accuracy of this fit was confirmed using *Origin 6.1*.

(5) Heart Rate Variability. A final module available within *LabChart* was the heart rate variability (HRV) module, used to calculate mean RR-intervals between successive beats from a selected portion of the pressure trace. R-waves were detected from the pressure trace using a method similar to EDP detection by the blood pressure module. The HRV module allowed user specification of a normal RR interval range, along with calculation of ectopic beats based on this range.

2.3.9.1 Pressure waveform parameters

Pressure variables calculated using the blood pressure module and *Labscribe* were very closely matched, but demonstrated a significant deviation compared with PVAN. This was found to be related to the manner in which *PVAN* calculates end diastolic pressure. In some experiments, a pressure rise associated with atrial contraction would appear on the left ventricular pressure trace. If the slope of the pressure rise associated with this event was of sufficient magnitude *PVAN* would incorrectly determine EDP at this point. The EDP detection algorithms used by *Labscribe* and *BPM* were superior in this respect in that EDP was determined more accurately at a point after this pressure inflection. *Labscribe* determined end-diastolic and end-systolic pressure and volume points by calculating the ratio of instantaneous pressure and volume for each cardiac cycle. End systole was located just after the maximum of the pressure-volume ratio, and end-diastole just before the minimum of the pressure-volume ratio. This method was in consistent agreement with *BPM*. dP/dt_{max} and dP/dt_{min} calculated by *PVAN* also differed significantly from values obtained from *Labscribe* and *BPM*, as well as manual calculation of these parameters using *Origin 6.1*. This occurred because *PVAN* differentiates the pressure signal then applies a smoothing algorithm to the resultant values.

2.3.9.2 Volume signal parameters

End diastolic volume determined manually from the raw volume signal correlated with the values reported by *Labscribe* confirming that this program was appropriate for calculating the end diastolic pressure volume relation. Both *Labscribe* and *PVAN* were capable of estimating V_p by plotting end systolic volume as a function of end diastolic volume, however, due to the shape of the pressure volume loop in the isolated working heart experiments around the point of end systole, neither program would accurately determine V_p using this method. *PVAN* allowed estimation of V_p using maximum and minimum volumes instead, which permitted estimation of V_p for isolated working rabbit heart experiments. All of the above parameters were obtained manually using *Origin 6.1* and compared to the above analysis programs to ensure their accuracy. While it was possible to use solely *Origin 6.1* for most data analysis, this required much more time for manual computation. Once determination of various parameters using the above analysis programs was confirmed to be accurate these were used for the remainder of the study.

2.4 Optimising the isolated working heart preparation

Loading conditions imposed on the isolated working heart are crucial in determining the work performed by the heart, its peak output, and ultimately the longevity of the preparation (Sutherland & Hearse, 2000). Previous studies with the working rabbit heart preparation commonly used an initial preload of 10 to 15 cmH_2O (7.4 - 11 mmHg) (Itoi & Lopaschuk, 1996; Leitch & Patterson, 1994; McCabe *et al.*, 2005; Pye *et al.*, 1996). Afterload pressures utilized in the above studies however were far more variable, ranging from 41 (Leitch & Patterson, 1994) to 105 cmH_2O (Itoi & Lopaschuk, 1996). Perhaps more crucial than the baseline preload settings is the aortic impedance determined by the design of the aortic outflow line. The term impedance describes the interaction between pressure and flow pulses in the aortic outflow tract, which is influenced by the viscoelastic properties inherent to the arterial wall, the fluid moving through the arterial system, and their interaction (Milnor, 1975) Aside from the design of the aortic cannula already discussed, two common factors determining aortic impedance in the isolated working heart are the (i) afterload, and (ii) the volume of air within the compliance chamber providing an aortic Windkessel (Podesser *et al.*, 1993; Van Bilsen *et al.*, 1991). While the isolated working heart is likely to perform stably and consistently over a range of different conditions, no two experimental setups are identical, and it was important to establish the capabilities of the current experimental setup to determine optimal conditions for a prolonged study.

2.4.1 Aortic outflow design and pressure-volume loop shape

Studies investigating instantaneous pressure-volume relations in rodents using conductance catheter technology typically describe either a square or auxotonic configuration of the PV loop (Joho *et al.*, 2007; Pacher *et al.*, 2004; Pacher *et al.*, 2008; Segers *et al.*, 2005) however this is not always reported (Pinsky *et al.*, 1996; Solda *et al.*, 1990). How *et al.* (2005) using an *ex vivo* murine working heart preparation found that PV loop shape was highly influenced by the length of the aortic cannula and the compliance air volume, noting that a longer cannula (positioning the heart further from the compliance chamber) altered the shape of the PV loop such that peak systolic pressure occurred soon after opening of the aortic valves, with pressure falling thereafter throughout ejection (How *et al.*, 2005). Use of a short (3 mm) aortic cannula achieved a rectangular PV loop configuration. Therefore, the effects of a range of compliance air volumes as well as distance from the aortic cannula to the compliance chamber were investigated to determine the optimal

conditions for an isolated working heart preparation. The ultimate aim of this investigation was to define a set of conditions for the isolated working rabbit heart which would produce the greatest mechanical function and cardiac output.

2.4.2 How does compliance volume influence working heart mechanical function?

The volume of air in the compliance bubble trap sufficient to act as an aortic Windkessel in the working rabbit heart has not been well characterized. Van Bilsen *et al*. (1991) attempted to quantify the minimum air volume required in this chamber in a working rat heart system by setting pressure drop (the decrease in pressure from one end of a flow system to the other) of less than 4 kPa as the limiting factor in their calculations (Van Bilsen *et al.*, 1991). Fluid turbulence within the aortic conduit is a major determinant of aortic impedance, and increases as pressure drop increases. Using this they determined a volume of at least 5.5 ml was required. In mouse working hearts volumes quoted are normally significantly smaller, in the order of 1-2 ml (de Windt *et al.*, 1999; How *et al.*, 2005). While very little information is available on the specific compliance chamber volumes used in isolated working rabbit heart preparation, the significantly greater muscle mass and cardiac output of the rabbit heart in comparison to the rat would predict a minimum volume even greater than the 5.5 ml suggested by Van Bilsen and colleagues (Van Bilsen *et al.*, 1991).

2.4.2.1 Experimental protocol for investigation of compliance volume on isolated working heart function

Seven isolated working rabbit hearts were used to study the influence of compliance volume on working heart function in the current experimental setup (Figures 2.11, 2.12 and 2.13). Baseline working heart function was established using a left atrial filling pressure of 7.4 mmHg and an afterload pressure of 60 mmHg. From initial experiments it was found that hearts could not sustain an output in working mode when no air was present. The volume of air in the compliance chamber was initially set at 15 ml of air as this was found to result in a stable steady state function in preliminary experiments. Hearts were paced at 200 beats.min^{-1} throughout the experiment. After establishing baseline left ventricular function, compliance was lowered to a starting value of 5 ml by removal of air with a graduated syringe through a two-way stopcock on top of the compliance chamber. The protocol then involved obtaining steady state functional measurements before increasing compliance volume in 5 ml increments up to 20 ml.

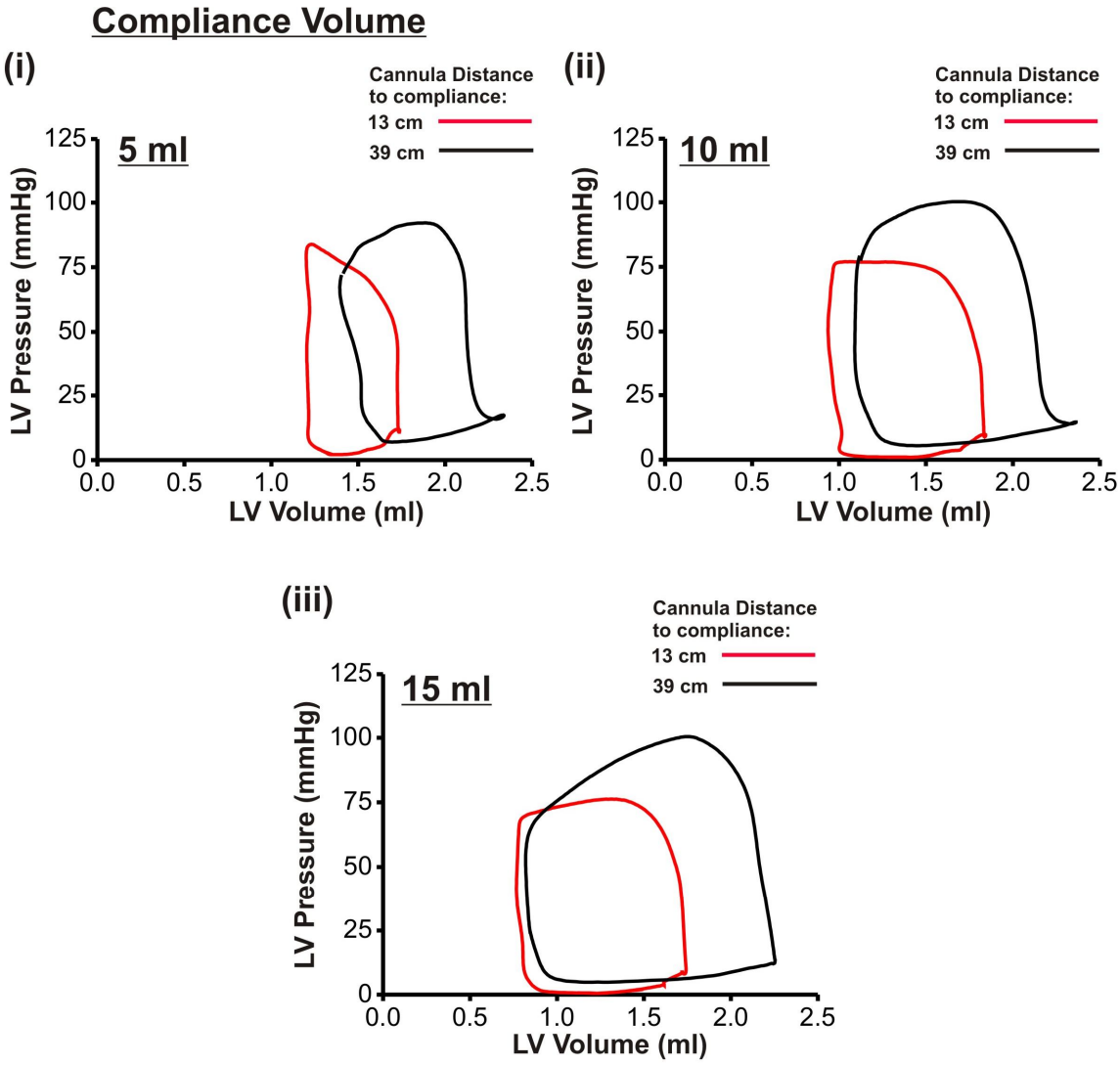

Figure 2.11 Compliance volume and the pressure-volume loop. Typical pressure volume loops from working rabbit hearts using two different compliance chamber positions with compliance air volume set at (i) 5 ml (ii) 10 ml and (iii) 15 ml.

2.4.2.2 Distance from aortic cannula to compliance chamber

The effect of altering the distance between the compliance chamber and aortic cannula on working heart function was also investigated. Constraints in the design of the aortic outflow tract meant that this variable remained fixed during experiments and could not be altered. The experiments were split into 2 groups; in the first, distance from aortic cannula to the compliance chamber was 13 cm (n = 3), the shortest length achievable, while in the second this length was increased to 39 cm (n = 4). Mean values at 5 and 15 ml compliance volumes were compared within groups by repeated measures ANOVA with Tukey's test for multiple comparisons performed as a post test. Mean data between groups at each compliance volume were compared using two-sample student's *t*-test. A *P*-value < 0.05 was considered significant. The diagrams in Figure 2.11 demonstrate the difference in PV

loop shape between the 13 cm and 39 cm configurations, with 13 cm demonstrating a more rectangular shape in comparison. Stroke volume however is larger at all compliance volumes using the 39 cm configuration. Stroke volume in both groups is increased with increasing compliance air volume. No further alterations in the PV loop were apparent at 20 ml compliance volume (data not shown).

2.4.2.3 Effect of compliance on systolic functional parameters

Increasing compliance volume had no effect on peak pressure in either group (Figure 2.12 (i)) however peak pressure was significantly greater in the 39 cm group at 10 and 15 ml compliance volumes by 20.44 and 20.28 % respectively. The maximum rate of rise of pressure (Figure 2.12 (ii)) was 32.98 ± 0.34 % higher at 15 ml compliance vs. 5 ml compliance in the 39 cm group, but there were no differences apparent in the 13 cm group. Additionally, dP/dt_{max} did not significantly differ between groups at any compliance volume.

2.4.2.4 Effect of compliance on diastolic functional parameters

Left ventricular end diastolic pressure was not significantly affected by increasing compliance volume in either group, nor were there any significant differences present between groups (data not shown). The maximum rate of left ventricular pressure fall in the 13 cm group however was significantly increased by 79.58 ± 24.87 % at 15 ml compliance *vs.* 5 ml (Figure 2.12 (iv)). The relaxation time constant τ was also significantly decreased at the higher compliance volume of 15 ml *vs* 5 ml, by 54.43 ± 1.69 % (13 cm group) and 42.92 ± 9.34 % (39 cm group), respectively. There was also a trend for τ to be faster in the 39 cm group at all compliance volumes but this only reached significance at 10 ml compliance volume.

2.4.2.5 Effect of compliance on volume parameters

As can be seen from the representative pressure-volume loops in Figure 2.11 (i-iii) and the mean data in Figure 2.13, increasing compliance had a marked effect on volume parameters of the isolated working heart in both the 13 cm and 39 cm groups. Aortic flow (Figure 2.13 (i)) was significantly increased in both groups between 5 ml compliance and 15 ml compliance (13 cm; 89.60 ± 32.29 %; 39 cm; 120.87 ± 72.58 %) although coronary flow remained unchanged at all compliance volumes (Figure 2.13 (ii)). Additionally, aortic flow was significantly higher in the 39 cm group at 10 (57.35 %) and 15 ml (65.65 %) compliance air volume compared to the 13 cm group. Stroke volume (Figure 2.13 (iii))

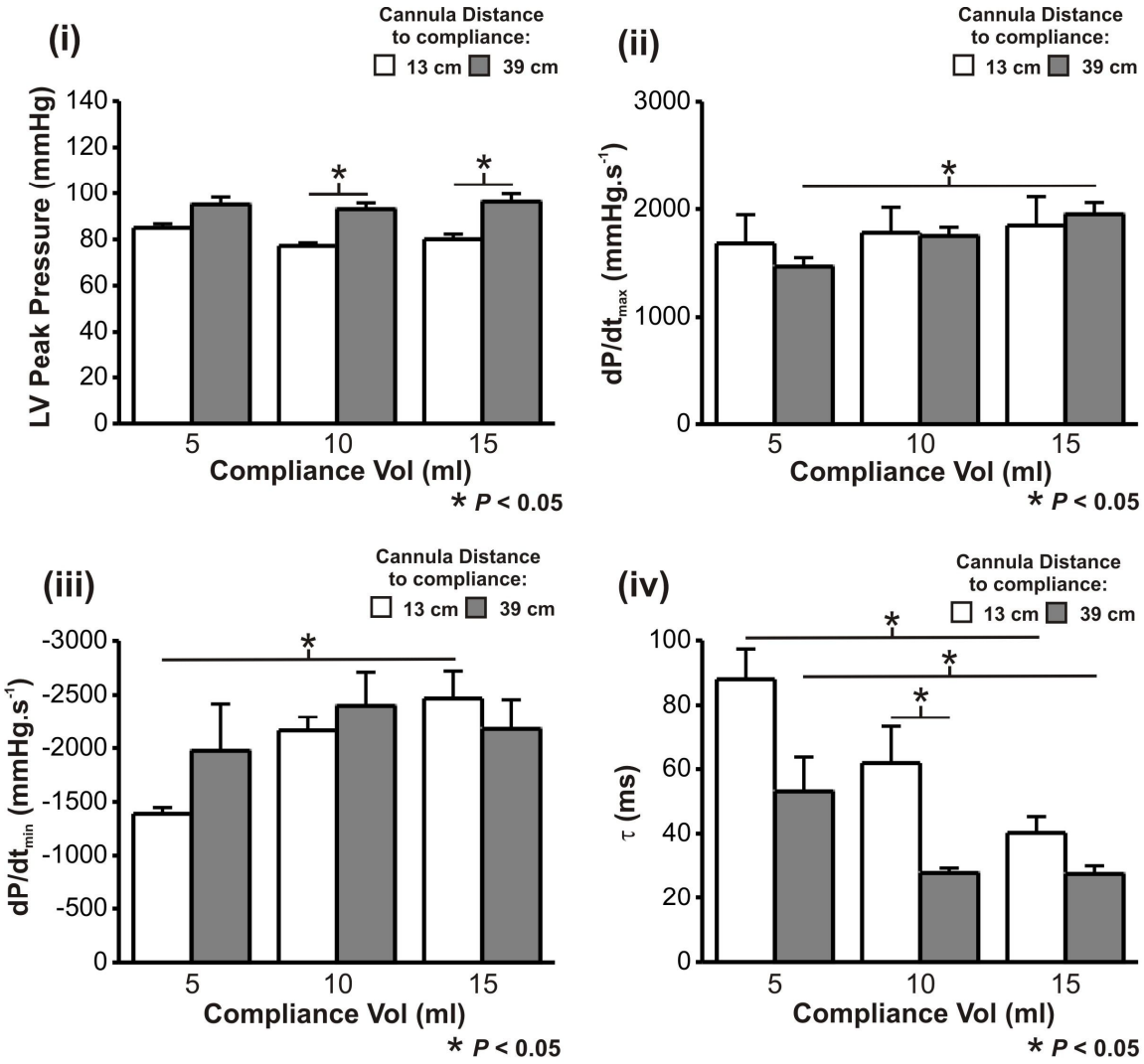

Figure 2.12 Compliance volume and working heart contractility. Influence of compliance distance on indices of contractility under varying compliance volumes in isolated working hearts. Values expressed as mean ± SEM. 13 cm group, n = 2; 39 cm group, n = 4. * $P < 0.05$ 13 cm vs. 39 cm, students unpaired *t*-test; 5 ml vs. 15 ml, repeated measures ANOVA with Tukey-Kramer multiple comparisons test.

as expected followed the same pattern as aortic flow, appearing significantly higher at 15 ml compliance vs. 5 ml compliance in both the 13 cm group (by 63.54 ± 14.82 %) and the 39 cm group (by 84.16 ± 42.14 %). This was due to significantly higher end diastolic volumes in the 39 cm group at all compliance volumes *vs.* the 13 cm group (30.62 % higher at 15 ml compliance - Figure 2.13 (iv)), without a significant difference in end systolic volumes (Figure 2.13 (v)) between groups at any compliance volume. End systolic volume (ESV) was significantly lower in both the 13 cm group and 39 cm group at 15 ml compliance *vs.* 5 ml compliance. Ejection fraction (Figure 2.13 (vi)) was also significantly greater at 15 ml *vs.* 5 ml compliance in the 13 cm (by 67.41 ± 15.28 %) and 39 cm group (by 94.87 ± 47.54 %), owing to a significant reduction in ESV with no change in EDV.

2.4.2.6 Distance from aortic cannula to compliance chamber influences working heart function

Various indices of cardiac function appeared improved when the length of tubing between the aortic cannula and compliance chamber was set to 39 cm, rather than the shortest distance of 13 cm. LV peak pressure (Figure 2.12 (i)), aortic flow and stroke volume (Figure 2.13 (i) and (iii)) were all shown to be elevated in the 39 cm configuration. The increased stroke volume was a consequence of higher end diastolic volumes using the 39 cm configuration (Figure 2.13 (iv)). This may be explained by the trend towards faster relaxation using this configuration, which at a fixed heart rate would allow for more complete filling of the left ventricle during diastole. The PV loops shown in Figure 2.11 demonstrate that a rectangular PV loop configuration could be achieved with the compliance chamber closer to the aortic cannula. Ultimately however a compromise was made between PV loop shape and working heart performance. In order to optimise the function of the working rabbit heart preparation, the 39 cm configuration was chosen.

2.4.2.7 Compliance volume and working heart function

From the data described above, the volume of air within the compliance chamber has a marked influence on cardiac function. As is demonstrated in Figure 2.12, increasing the volume of air in the compliance chamber from 5 ml to 15 ml led to a significant improvement in the maximum rate of ventricular pressure rise and decreased the relaxation constant τ. Aortic flow, stroke volume and ejection fraction (Figure 2.13) were also significantly elevated with 15 ml compliance volume in comparison to 5 ml. A compliance volume of 5 ml air was therefore considered unsuitable for working rabbit heart experiments as function could be vastly improved with the use of 15 ml air. It was found that increasing compliance volume to 20 ml induced no further changes in ventricular performance (data not shown). One possible explanation for the relatively poor function observed using 5 ml air as compliance volume is elevation of arterial impedance. Impedance is determined *in vivo* by the compliance of the arterial system and the resistance of the systemic vascular bed (Urschel *et al.*, 1968). Urschel *et al.* (1968) increased compliance in the aorta of unconscious dogs by directing aortic blood flow through a stiff glass bypass (Urschel *et al.*, 1968). When alterations in preload were controlled for an increase in aortic impedance and a decline in

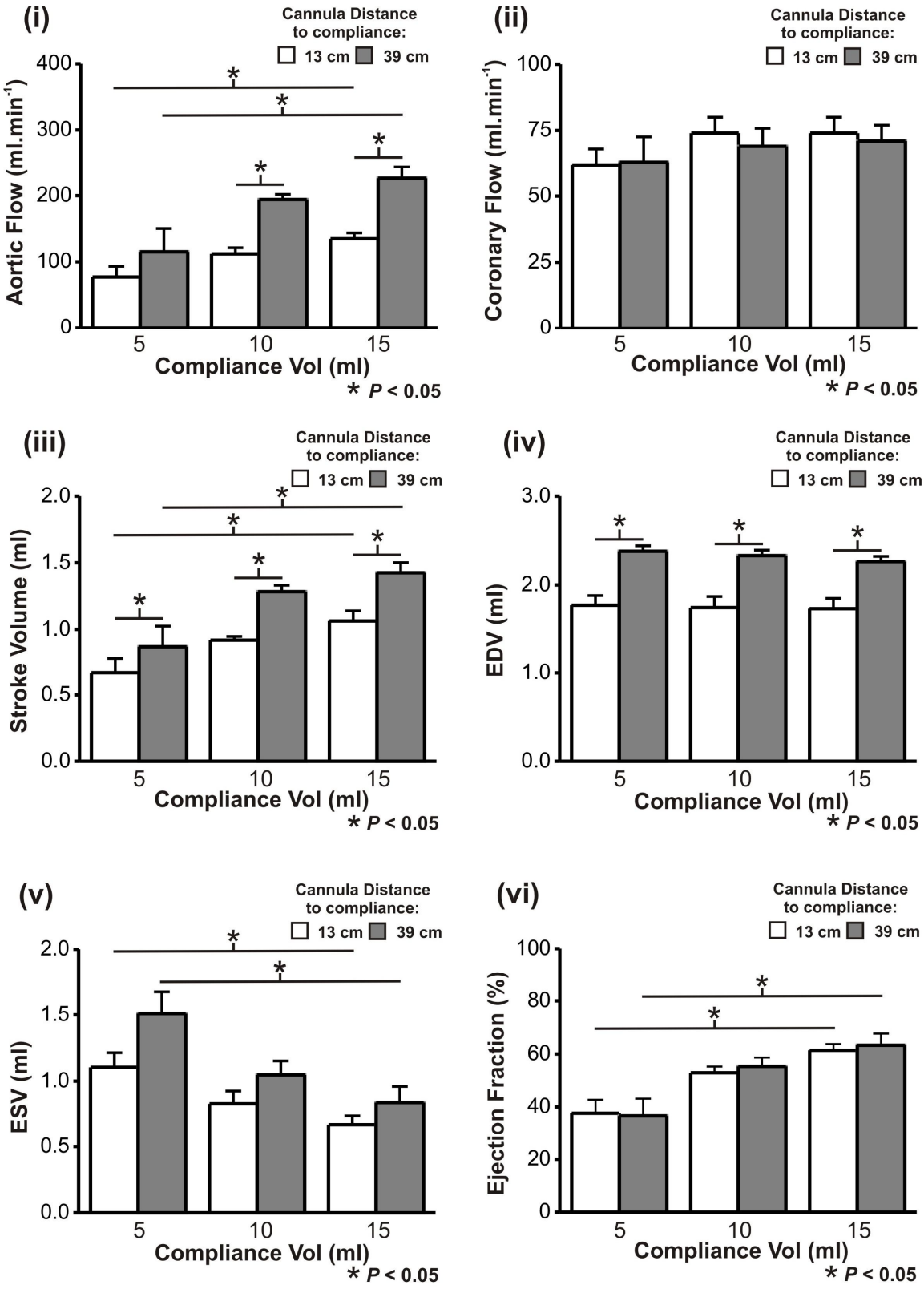

Figure 2.13 Compliance volume and working heart volume parameters.

Influence of compliance distance on volume and flow measurements under varying compliance volumes in isolated working hearts. * $P < 0.05$ 13 cm vs. 39 cm, students unpaired *t*-test; 5 ml *vs.* 15 ml, repeated measures ANOVA with Tukey-Kramer multiple comparisons test. Values expressed as mean ± SEM.

stroke volume was found to occur, suggesting a decline in compliance can significantly reduce output. Leite-Moreira and Gillebert (1994) demonstrated that large increases in afterload, induced by clamping the aorta in early systole, significantly slowed left ventricular pressure fall (Leite-Moreira & Gillebert, 1994). Relatively large increases in afterload induced by aortic clamping have also been shown to elevate end diastolic pressures, potentially impairing left ventricular filling (Leite-Moreira *et al.*, 1999). The authors explained this phenomenon in terms of 'relative load' (the ratio of baseline systolic pressure to isovolumic pressure) demonstrating that hearts under a high relative load experience a decline in the rate of left ventricular pressure fall when exposed to elevations in systolic pressure (Gillebert *et al.*, 1997; Leite-Moreira *et al.*, 1999). Although there were no significant differences between 10 and 15 ml of air, 15 ml tended to show the highest mean values for dP/dt_{max}, aortic flow, stroke volume and ejection fraction. The remainder of isolated working heart experiments therefore used a compliance volume of 15 ml.

2.4.3 How does afterload pressure affect working heart mechanical function?

The influence of afterload pressure on working rabbit heart mechanical function was evaluated by exposing isolated working rabbit hearts to stepwise increases in afterload pressure from 50 mmHg to 80 mmHg in 10 mmHg increments. These experiments were used to establish optimal loading conditions for the isolated working heart in terms of stroke volume and coronary flow reserve using the current setup. Crystalloid perfusates such as Krebs-Henseleit and Tyrode's solution have been shown to have poor oxygen-carrying capacity compared to blood (Masuda *et al.*, 1994; Sutherland & Hearse, 2000). Furthermore use of such solutions has been shown to limit coronary reserve in isolated working heart preparations (Masuda *et al.*, 1994). Therefore the ability to increase coronary flow with increasing afterload was also investigated. The protocol was completed using the hearts from the 39 cm group reported above. Following the completion of the compliance alterations, compliance volume was once again set to 15 ml of air to ensure steady state values returned to baseline and the preparation was stable. Preload remained at 7.4 mmHg and hearts were paced at 200 $beats.min^{-1}$ throughout. Mean values of measured functional parameters at 50 and 80 mmHg afterload were compared within groups by repeated measures ANOVA with Tukey's test for multiple comparisons performed as a post test. A P-value < 0.05 was considered significant.

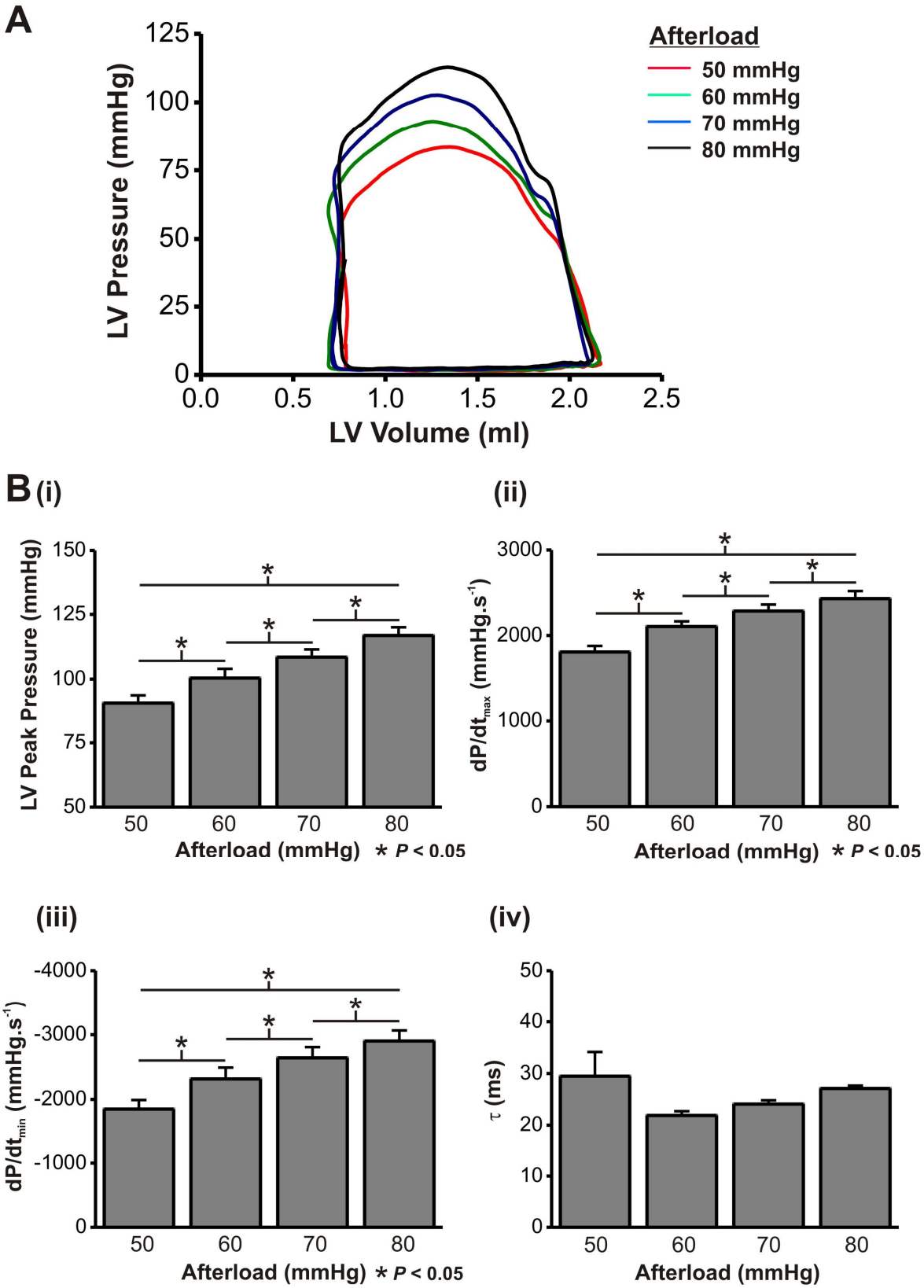

Figure 2.14 Influence of afterload on working heart contractile function. A. Representative PV loops at increasing afterload pressures. B(i – iv) Effect of increasing afterload on isolated working heart contractile and relaxation parameters (n=4). All values expressed as mean ± SEM.

2.4.3.1 Afterload and systolic functional parameters

As can be seen from the representative pressure-volume loops in Figure 2.14A, elevation of afterload in a stepwise manner between 50 and 80 mmHg led to incremental elevation of peak systolic pressure with little change in stroke volume over the range. Peak pressure (Figure 2.14 B(i)) significantly increased by 28.56 ± 2.55 % between 50 and 80 mmHg, and was significantly elevated with each afterload increment. Similarly, dP/dt_{max} (Figure 2.14 B(ii)) was 33.16 ± 5.39 % higher at 80 mmHg compared with 50, and each step increase in afterload led to a significant increase in dP/dt_{max}.

2.4.3.2 Afterload and diastolic functional parameters

Maximum rate of ventricular pressure fall (dP/dt_{min} - Figure 2.14 B(iii)) was significantly increased between 50 and 80 mmHg by 55.93 ± 4.37 %, with each elevation of afterload inducing a significant increase. The relaxation constant τ (Figure 2.14 B(iv)) however did not change significantly within the range of afterload pressures investigated, although there was a trend for τ to be fastest at 60 mmHg. Increasing afterload between 50 and 80 mmHg had no effect on end diastolic pressures.

2.4.3.3 Afterload and volume parameters

Aortic flow (Figure 2.15 (i)) was not significantly altered with each afterload increment within the range studied, but a significant reduction of 11.55 ± 5.31 % was evident at 80 mmHg vs, 50 mmHg. Aortic flow also fell significantly between 80 and 60 mmHg (not shown on graph). Coronary flow however had a tendency to increase with increasing afterload pressure but this was only significant between 50 vs. 60 mmHg (23.72 ± 4.42 % increase), and 50 vs. 80 mmHg (31.04 ± 7.58 %). The combination of increasing coronary flow with decreasing aortic flow at higher afterload pressures resulted in no significant changes evident in stroke volume (Figure 2.15 (iii)). End diastolic and end systolic volumes were not different between any of the afterload settings investigated (data not shown). Ejection fraction (Figure 2.15 (vi)) tended to be greatest at 60 mmHg also, but no significant differences were observed.

2.4.3.4 Afterload pressure influences myocardial contractility and coronary flow

Optimal afterload pressure for the current isolated working heart set up was studied by varying afterload between 50 and 80 mmHg, with the aim of selecting an afterload which produced maximal cardiac output and working heart performance. In addition, it was

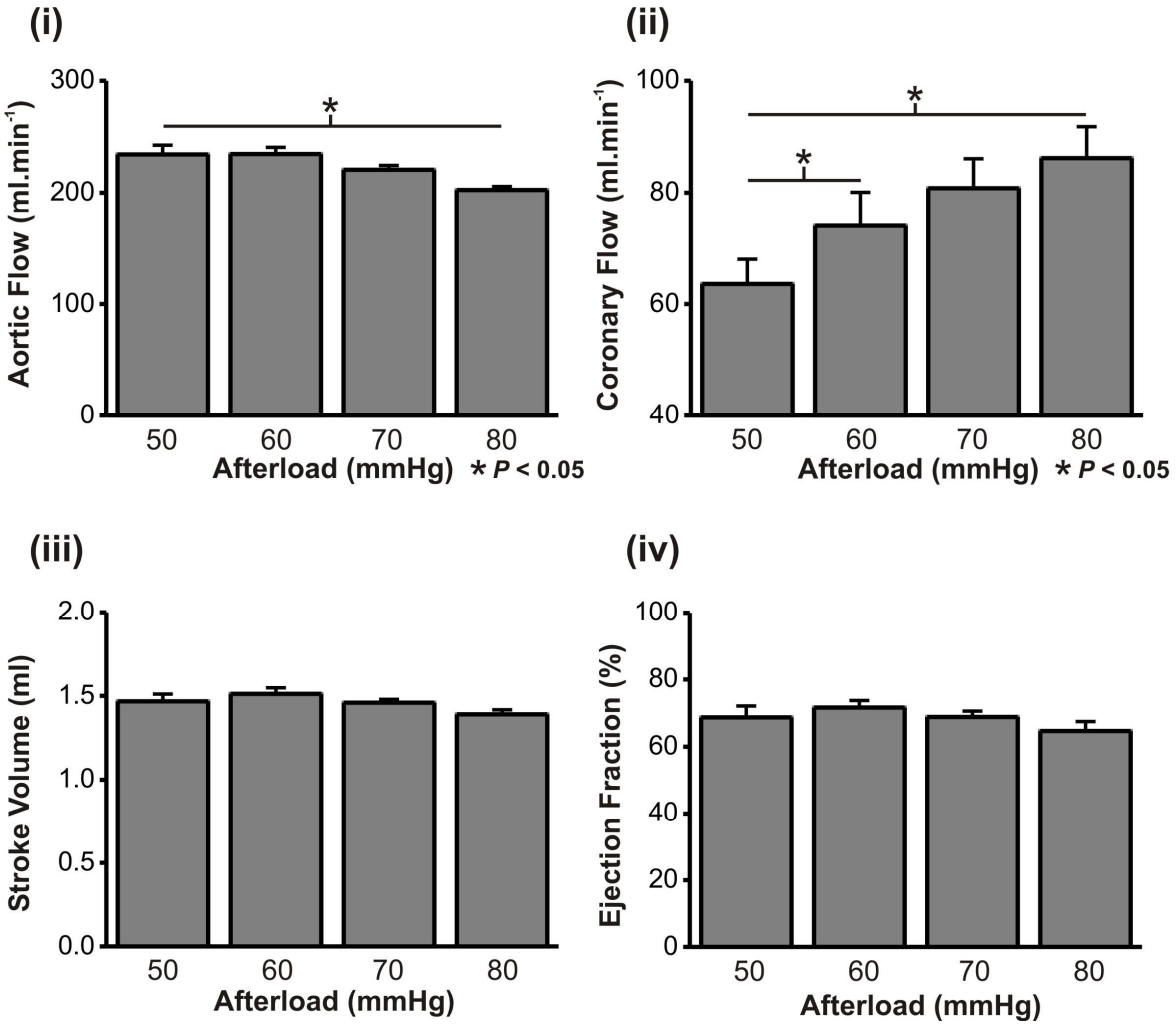

Figure 2.15 Influence of afterload pressure on working heart volume parameters. (i-v) Volume and flow parameters at varying afterload pressures (n=4). All values expressed as mean ± SEM.

hoped that some coronary flow reserve would still be evident and that coronary flow could increase if work demand (load) was increased. As shown in Figure 2.14 increasing afterload pressure in the current study led to stepwise elevations in peak systolic pressure, dP/dt_{max} and dP/dt_{min}. The relaxation constant τ was not significantly altered between any of the afterload pressures investigated, although relaxation tended to be fastest at 60 mmHg. In terms of systolic pressure parameters 80 mmHg provided the greatest level of performance, however it was found that aortic flow began to decline significantly at this afterload pressure in comparison to 50 and 60 mmHg (Figure 2.15 (i)). This was offset by an increased coronary flow *vs.* 50 mmHg, but not *vs.* 60 mmHg. Selection of optimal afterload was a compromise between peak cardiac output and maximal systolic parameters. In terms of cardiac output (sum of aortic flow and coronary flow), stroke volume and ejection fraction 60 mmHg tended to show the greatest performance (Figure 2.15). In addition relaxation also tended to be quickest at 60 mmHg. The afterload pressures achievable by the perfusion apparatus were restricted by height limitations within the

laboratory, such that the system was working close to its limit at 80 mmHg. The *in vivo* afterload of healthy mature rabbits has been reported by Baker *et al*. (1988) as 86 ± 14 mmHg (Baker *et al.*, 1988) which would suggest 80 mmHg as the most appropriate choice. Preliminary longevity studies with 80 mmHg afterload however (data not shown) suggested that functional decline after 60 min was ≅ 10 % which is generally what is accepted in isolated working heart studies ((Sutherland & Hearse, 2000), see also section 2.4.3.1 below). For these reasons 60 mmHg was chosen as afterload perfusion pressure for the remainder of the investigation.

2.4.3.5 Increased contractility with increasing afterload may be explained by Gregg's phenomenon

The initial response of the heart to acute increases in arterial resistance (and hence afterload) *in vivo* is elevation of peak ventricular and aortic pressures with a concomitant decline in stroke volume (Milnor, 1975). The relationship between ventricular wall stress and the contractile element velocity (the force-velocity curve) is altered following a change in arterial resistance in favour of increased force production at any given velocity (Bove & Lynch, 1970; Milnor, 1975). Changes that occur upon increasing afterload in isolated heart preparations result in an increase in contractility through several recognized regulatory effects, though their relevance to contractile regulation *in vivo* remains unclear. One such effect is known as Gregg's phenomenon, where changes in coronary perfusion (elicited by alteration of afterload) alter contractile strength and myocardial oxygen consumption (Feigl, 1983) While several mechanisms have been proposed to try and explain this effect it is still not clear which is responsible. One such mechanism, proposed by Arnold *et al*. (1968) known as the 'garden-hose' effect suggests that the increase in transmural pressure causes distension of the coronary vessels leading to increased stretch of the myocardial fibers which could increase contraction by the Frank-Starling mechanism (increased fibre length) (Arnold *et al.*, 1968). Evidence to support this comes from studies which demonstrate that increasing coronary distension while keeping coronary flow constant can elicit this effect (Feigl, 1983). Abel and Reis (1970) however, reported that coronary flow was more important than coronary distension pressure for dictating this effect (Abel & Reis, 1970). Using isovolumically contracting canine hearts, they found that the maximum velocity of contractile element shortening (V_{ce}) could be increased by increasing flow at a constant pressure, but that altering pressure while keeping flow constant would have no effect on contractility (Abel & Reis, 1970). In line with previous investigations, perfusion pressure had a marked influence on contractility and

coronary flow in the present study that may be attributable to this phenomenon (Masuda *et al.*, 1994).

2.4.4 Isolated working heart longevity

Of critical importance to the validity of any results obtained from the isolated working heart is the stability of the preparation over time. To assess this using the optimized working heart setup, the mechanical performance of 7 isolated working rabbit hearts was recorded over a period of 90 min. Preload was set to 7.4 mmHg and afterload to 60 mmHg. Compliance volume was held constant at 15 ml air. Settings were chosen based on the data shown in sections 2.4.2 and 2.4.3 above. Hearts were paced at constant rate, as close to 200 beats.min^{-1} as possible (average = 204.10 ± 3.81 beats.min^{-1}). Following establishment of steady state baseline function, hearts were given a period of 5 minutes to stabilize before the experiment commenced. Data at predefined intervals throughout the 90 minute perfusion protocol were compared to control values (mean values at 0 min) using a paired student's *t*-test. *P*-values of < 0.05 were considered significant.

2.4.4.1 Stability of working heart contractile parameters during prolonged perfusion

Over the 90 min perfusion period in working heart mode, left ventricular peak pressure (Figure 2.16 (i & ii)) and the maximum rate of left ventricular pressure rise (Figure 2.16 (iii & iv)) remained stable. There was a tendency for both parameters to increase over the first 30 min relative to baseline but this did not reach significance. Cardiac output (Figure 2.16 (v & vi)) was also stable over the 90 min, falling by 3.14 ± 2.24 % (not significant). End diastolic pressure (Figure 2.17 (i & ii)) was stable over the first 60 min of perfusion but became significantly elevated by 90 min (27.15 ± 13.27 % above baseline). While the maximum rate of left ventricular pressure fall did not significantly differ from baseline after 90 min (Figure 2.17 (iii & iv)), the relaxation constant τ (Figure 2.17 (v & vi)) was significantly prolonged after this time, increasing by 26.22 ± 10.44. Coronary flow was not significantly different from baseline at any point.

2.4.4.2 Expected longevity of the isolated working heart preparation

Long term stability of an *ex vivo* working heart preparation is dependent on a number of factors, including composition of the perfusion medium, work load imposed on the heart,

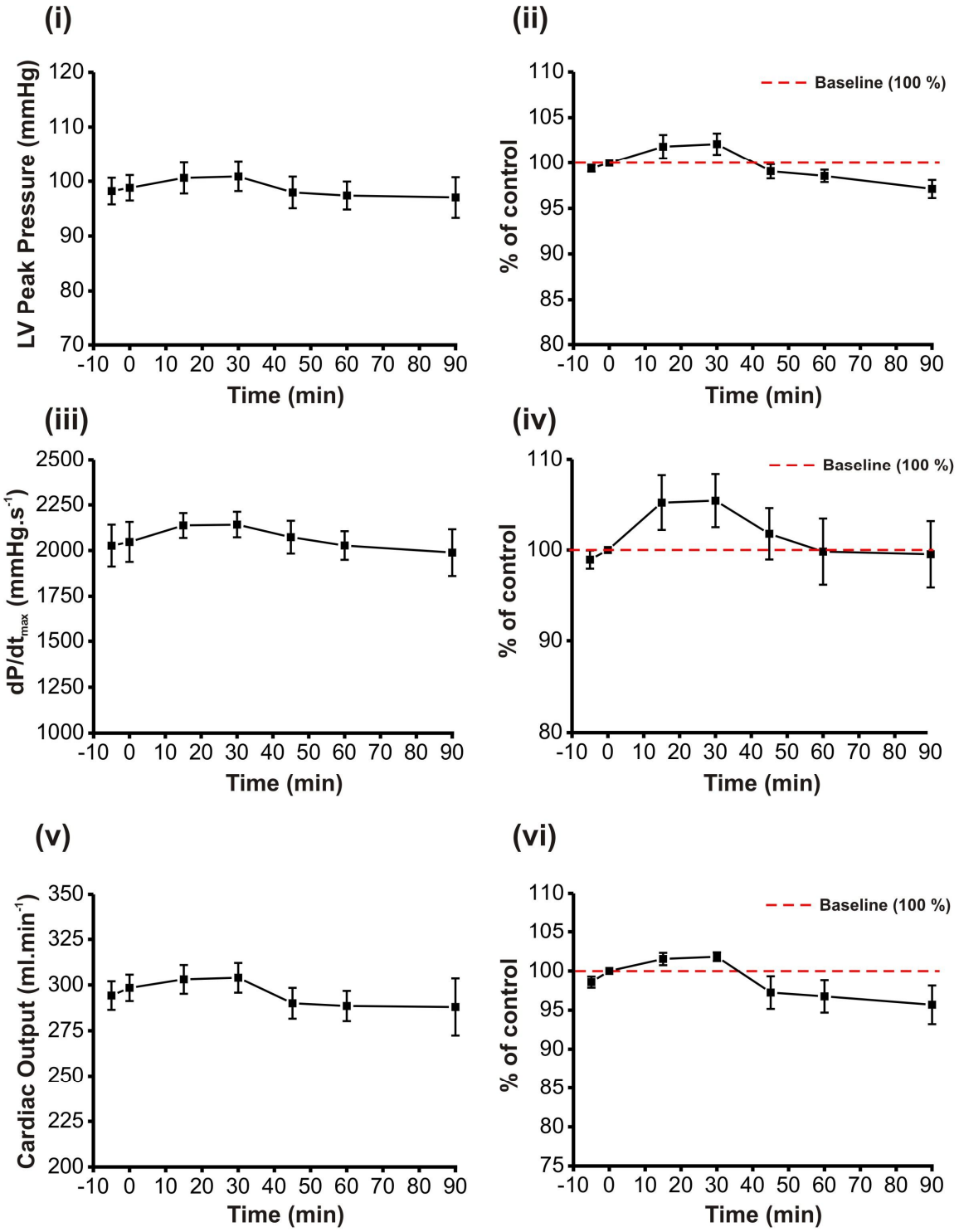

Figure 2.16 Systolic function of the working heart during prolonged perfusion. Left ventricular peak pressure, dP/dt_{max} and cardiac output during 90 min of working heart perfusion (n=7). Panels on left indicate mean ± SEM values, panels on right indicate values as % of control (0 min)

and the presence of exogenous drugs or compounds (Sutherland & Hearse, 2000). In addition, the specific design of the aortic outflow tract may significantly influence the stability of working heart preparations over time (Van Bilsen *et al.*, 1991). Values for functional decline over prolonged periods have been suggested to be around 5 – 10 % per

hour (Sutherland & Hearse, 2000) using left ventricular developed pressure or cardiac output as the comparative functional index. In agreement with this, Lewandowski *et al.* (1987) reported a 5 % drop in cardiac output of isolated working rabbit hearts 65 min after recording of baseline measurements, widening to 14.1 % after 79 min (calculated from mean reported values) (Lewandowski *et al.*, 1987). DeWindt *et al.* (1999) reported a non-significant decline in isolated murine heart cardiac output of 8 ± 10% after 100 min antegrade (working heart) perfusion compared with 20 min after initiation of working heart (de Windt *et al.*, 1999). Chemnitius and colleagues (1985) reported that cardiac outputs of a rabbit working heart preparation increased (non-significantly) by 6.4 % between initial control values and following 60 min, however it should be noted that an equilibration period of 2-3 min was reported following initiation of working heart perfusion compared with 30 min in the present study (Chemnitius *et al.*, 1985). A non-significant decrease in cardiac output was found in the current investigation following 90 min of perfusion in isolated working rabbit hearts, in good agreement with previously reported values for isolated working heart preparations following 60 min of perfusion with crystalloid perfusion media. Although end diastolic pressure (Figure 2.17 (i & ii)) and τ (Figure 2.17 (v & vi)) were significantly elevated after 90 min of perfusion in the current study, no significant differences were apparent after 60 min of perfusion.

2.4.4.3 Improving stability of the isolated working heart preparation

The isolated working heart setup described in this chapter was used in conjunction with a crystalloid perfusion medium. While this is the most commonly used perfusate for isolated heart studies (Podesser *et al.*, 1999) the oxygen carrying capacity of such solutions is much lower than that of blood (Sutherland & Hearse, 2000). In addition, prolonged perfusion periods are associated with increasing levels of oedema and tissue swelling which may adversely affect coronary perfusion by inducing compression of the microvasculature (Segel & Ensunsa, 1988). In the current study it may have been possible to improve stability even further with the addition of exogenous substrates to the perfusion medium. Increased tissue water content has been demonstrated to be reduced in isolated, non-ejecting rabbit hearts by addition of bovine serum albumin to the perfusion medium (Mann, 1981). Addition of albumin is also associated with preserved coronary vascular resistance and reduced leakage of creatine kinase in working rabbit hearts perfused with a perfluorochemical-based buffer (Segel & Ensunsa, 1988). Inclusion of albumin to the perfusion medium in the present study may have helped to improve longevity, although the

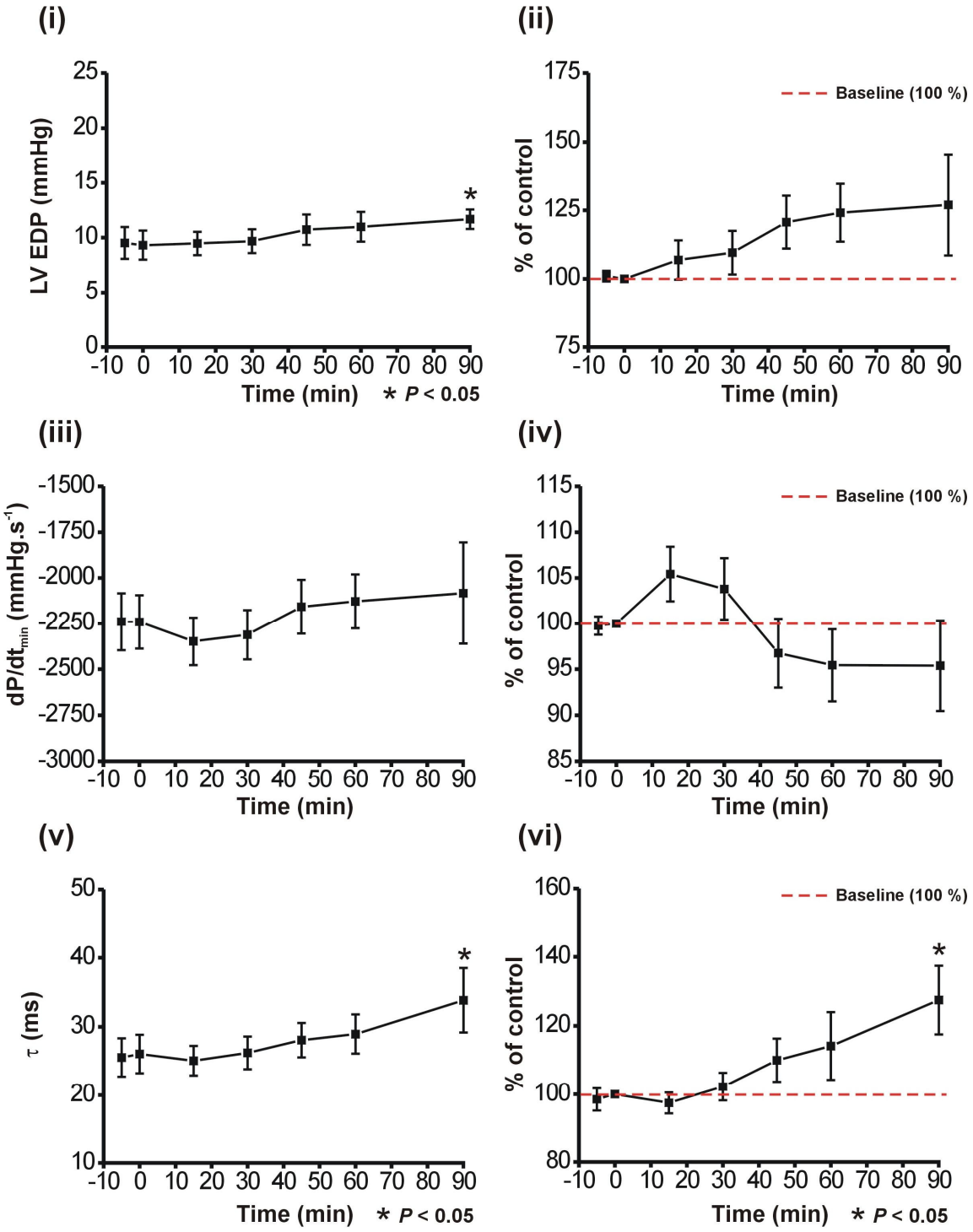

Figure 2.17 Diastolic functional parameters of the working heart during prolonged perfusion. End diastolic pressure (LVEDP), dP/dt_{min} and τ during 90 min perfusion in working heart mode. Panels on left indicate mean ± SEM values, panels on right indicate values as % of control (0 min)

method of perfusate oxygenation would have to be altered to accommodate this, as direct gas bubbling of solutions containing free fatty acids results in significant foaming (Sutherland & Hearse, 2000). Pyruvate is another metabolic substrate that is commonly included in crystalloid buffer solutions alongside glucose (de Windt *et al.*, 1999; Gillis *et*

al., 1996; Schmidt, 2001; Van Bilsen *et al.*, 1991). Pyruvate has been demonstrated to influence intracellular Ca^{2+} cycling, SR Ca^{2+} load and myofilament Ca^{2+} sensitivity (Hasenfuss & Pieske, 2002; Hermann *et al.*, 2000a). Hermann *et al.* (2000) demonstrated that pyruvate potentiated the increased force development induced by isoproterenol in isolated ventricular muscle preparations (Hermann *et al.*, 2000b). Pyruvate also increased SR Ca^{2+} load, time to peak developed tension, and time from peak tension to half-maximal relaxation, an observation the authors suggested was indicative of an alteration in Ca^{2+} cycling and/or myofilament cross-bridge kinetics. In ventricular myocardium from failing human hearts pyruvate led to an increase in systolic force and a decrease in diastolic force, attributable to i) increased SR Ca^{2+} cycling and ii) elevated pH_i effecting an increase in myofilament Ca^{2+} sensitivity. As the main focus of this thesis is Ca^{2+} cycling with respect to SR function the decision was made not to include pyruvate as a metabolic substrate to avoid complication of subsequent results.

2.4.4.4 Alternative perfusion media

Crystalloid perfusion solutions are the most frequently used for isolated working heart experiments, however other possibilities exist for perfusion of the isolated heart, including perfluorochemical emulsion (Chemnitius *et al.*, 1985) and erythrocyte-washed solutions (Chen *et al.*, 1987; Gillis *et al.*, 1996; Masuda *et al.*, 1994; Podesser *et al.*, 1999). Both have superior oxygen carrying capacity in comparison to crystalloid perfusates and have been demonstrated to improve contractile performance (elevated dP/dt_{max} and dP/dt_{min}) and reduce the loss of high energy phosphates over time in the working rabbit heart (Chemnitius *et al.*, 1985; Chen *et al.*, 1987; Podesser *et al.*, 1999). Significantly greater contractile reserve, measured by assessment of reactive hyperaemia after transient ischaemia, is also evident when using perfluorochemical emulsion (Chemnitius *et al.*, 1985) or erythrocyte-enriched solutions (Masuda *et al.*, 1994) in comparison to crystalloid perfusion solutions. For these reasons such preparations are recommended over crystalloid perfusates in studies of ischaemia and reperfusion injury. A compromise must be made with regard to cost and preparation time however, especially with erythrocyte enhanced solutions. Membrane oxygenation is a requirement for any perfusion solution containing erythrocytes as directly gassing the solution with a glass bubbler results in significant foaming. In addition, recirculation of solution through the system via peristaltic pump motion is associated with erythrocyte haemolysis and subsequent accumulation of free haemoglobin (Podesser *et al.*, 1999). In the present study, a crystalloid perfusion medium (modified Tyrode's solution) was adequate for sustaining working heart function over a

prolonged period with only minimal decline in contractile and relaxation parameters. Solution preparation was relatively swift and large quantities (15-20 L) could be made at little cost. Had preparation longevity been in doubt, perfluorochemical emulsion or erythrocyte-enriched perfusion solutions may have been investigated, however the ease of preparation in addition to the above data regarding longevity meant that in the current study modified Tyrode's solution was an adequate choice for working heart perfusion.

3 The effects of K201 (JTV-519) on left ventricular mechanical function in the isolated working rabbit heart

3.1 Introduction

Coordinated regulation of Ca^{2+} release from the sarcoplasmic reticulum (SR) is critical to normal cardiomyocyte function. In the ventricular myocyte, SR Ca^{2+} release is visualised as unitary local release events known as Ca^{2+} sparks, which represent activation of a cluster of ryanodine receptors (RyR2s) opening in concert to release Ca^{2+} (Cheng *et al.*, 1993). These events occur at a low frequency (~100 s^{-1}) and do not necessarily require a triggering influx of Ca^{2+} to occur (Bers, 2002; Cheng *et al.*, 1993). Under normal conditions, synchronised SR Ca^{2+} release via the cardiac ryanodine receptor (RyR2) is triggered by the inward Ca^{2+} current, and the rising phase of the intracellular Ca^{2+} transient is believed to reflect the temporal and spatial summation of thousands of Ca^{2+} sparks (Bers, 2002). Excessive spontaneous SR-mediated Ca^{2+} release during diastole however, has been demonstrated to occur in situations where RyR2 function is altered. Mutations in the RyR2 channels (Liu *et al.*, 2008) as well as changes in channel function evident in various disease states such as congestive heart failure (Tateishi *et al.*, 2009) have been shown to result in an increased frequency of Ca^{2+} release during the diastolic period. Excessive spontaneous Ca^{2+} release during diastole has been identified as a potential mechanism in the genesis of triggered arrhythmias (Bers *et al.*, 2006; Hove-Madsen *et al.*, 2004). Moreover, diastolic Ca^{2+} leak has also been proposed to lead to increased diastolic tone and incomplete relaxation, as well as potentially contributing to decreased SR content (Shannon *et al.*, 2003). In the search for potential therapeutic strategies, attention has focused on agents or treatments which can specifically target the RyR2 and restore normal function. One such drug which has emerged in the literature in recent years is K201 (JTV-519). First described for its cardioprotective properties against myocardial over-contraction and necrosis (Kaneko, 1994), K201 has since been shown to possess potential as both a cardioprotective and anti-arrhythmic agent (Hasumi *et al.*, 2007; Inagaki *et al.*, 2000b). Most recently, it has been demonstrated using a mouse myocardial infarction model (Wehrens *et al.*, 2005), as well as a canine model of pacing induced heart failure (Yano *et al.*, 2003) that K201 is able to significantly attenuate development of cardiac dysfunction and ventricular remodelling. In these models, K201 was proposed to stabilise the RyR2 in the closed state, preventing SR Ca^{2+} leak and potentially arrhythmogenic events from occurring (Tateishi *et al.*, 2009; Wehrens *et al.*, 2005; Yano *et al.*, 2003).

3.1.1 Initial investigations with K201 and myocardial preservation

The chemical formation of K201 is depicted in Figure 3.1. K201 is a 1, 4-benzothiazepine derivative, initially developed as a cardioprotective agent to inhibit cellular damage and myocardial over-contraction associated with ischaemia-reperfusion injury and myocardial

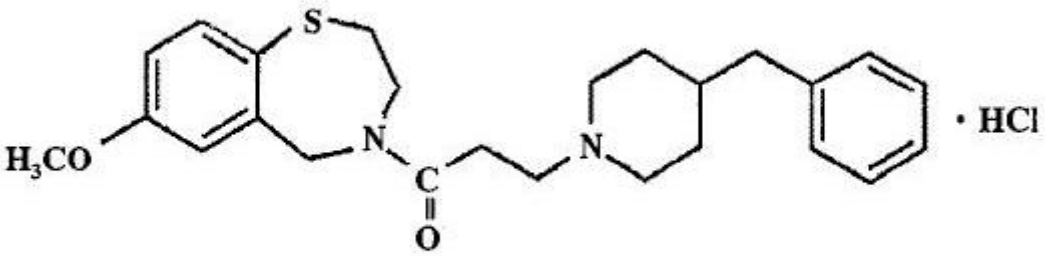

Figure 3.1 Chemical structure of K201. 4-[3-{1-(4-benzyl) piperidinyl}propionyl]-7-methoxy-2,3,4,5-tetrahydro-1,4-benzothiazepine. From Inagaki *et al.* (2000)

infarction (Kaneko, 1994). At concentrations of 1.0 μM and above the compound was shown to significantly suppress cellular necrosis and myocardial over-contraction in a rat Langendorff model induced by perfusion of epinephrine (0.1 mg, administered as 546 μM bolus) and/or caffeine (10 mg, administered as 52 mM bolus) (Kaneko, 1994). K201 was also shown to inhibit the binding of F-actin to the calcium binding protein Annexin V, however this was only achievable using a minimum concentration of 10 μM. Further detailing of K201's cardioprotective effects were made using experimental models of ischaemia-reperfusion injury (Hachida *et al.*, 1999; Inagaki *et al.*, 2000a; Inagaki *et al.*, 2000b; Kawabata *et al.*, 2000).

3.1.1.1 K201 influences recovery of mechanical function in models of ischaemia-reperfusion and prolonged myocardial preservation

Hachida and colleagues (1999) studied K201's cardioprotective effects in the setting of prolonged myocardial preservation with Bretschneider's histidine-tryptophan-ketoglutarate (HTK) cardioplegic solution (Hachida *et al.*, 1999). Rat hearts preserved for 6 hours with an HTK solution containing 10 μM K201 demonstrated a significantly greater recovery of left ventricular developed pressure and coronary blood flow following normothermic perfusion in comparison with untreated controls. Elevation of $[Ca^{2+}]_i$, as assessed by the

Ca^{2+}-sensitive dye Fura-2/AM, was also significantly attenuated in hearts perfused with K201 (Hachida *et al.*, 1999). Inagaki *et al*. (2000) assessed contractile function of the isolated rat heart following 30 min of global ischaemia and 30 min reperfusion (Inagaki *et al.*, 2000a). They discovered that a 5 min perfusion period with K201 (0.3, 1.0 or 3.0 μM) prior to 30 min global ischaemia led to a reduction in the level of myocardial stunning in comparison to untreated control hearts, as evidenced by left ventricular developed pressure recovering to levels significantly greater than controls 30 min after reperfusion. No significant differences were seen in left ventricular end diastolic pressure (LVEDP) between K201 treated and control hearts. This protective effect was also observed when 1.0 μM K201 was perfused either prior to the ischaemic period, or during the initial 5 min of the reperfusion phase. The authors concluded that this effect was mediated by activation of PKC-δ, as the protective effect was abolished in the K201 groups by treatment with the PKC inhibitor GF109203X (Inagaki *et al.*, 2000a). In a follow up study by the same group, hearts were loaded with the fluorescent Ca^{2+} indicator Indo-1, allowing the authors to determine that prolonged (> 10 min) ischaemia and subsequent reperfusion was associated with an increase in $[Ca^{2+}]_i$ (Inagaki *et al.*, 2000b). This rise in $[Ca^{2+}]_i$ was significantly attenuated by K201 at 1.0 μM and above, while preservation of myocardial contractile function could be achieved using even lower concentrations (0.3 μM) (Inagaki *et al.*, 2000b). Kawabata *et al*. (2002) investigated the role of nitric oxide (NO) in the protective action of K201 following ischaemia and reperfusion by simultaneously perfusing hearts with K201 and the NO synthase inhibitor N^G-nitro-$_L$-arginine methyl ester (L-NAME) for 40 min prior to 20 min global ischaemia (Kawabata *et al.*, 2002) Ischaemia induced a rise in diastolic tension (assessed from LVEDP) in untreated control hearts which was significantly inhibited by pre-treatment with 1.0 μM K201. NO synthase inhibition had little effect on the ability of K201 to inhibit elevation in diastolic tension during the ischaemic period suggesting increased cytosolic calcium levels associated with ischaemic contracture are more effectively impeded by K201 than by NO synthase alone. Interestingly in this investigation neither LVEDP or developed pressure in the K201 groups were significantly different from control following the 30 min reperfusion period, contrary to the findings of Inagaki and colleagues in the rat heart, who reported a significant recovery of developed pressure 30 min after reperfusion (Inagaki *et al.*, 2000a).

3.1.1.2 K201 preserves high energy phosphates in ischaemia-reperfusion models

Inagaki *et al.* (2000) determined efflux of creatine phosphokinase (CPK) and lactate dehydrogenase (LDH) by measuring levels of each in coronary effluent samples of rats following ischaemia and subsequent reperfusion (Inagaki *et al.*, 2000a). Perfusion of K201 prior to ischaemia resulted in a significant reduction in the levels of both CPK and LDH present in coronary effluent samples at 30 min of reperfusion in comparison to samples from untreated control hearts. Beneficial metabolic effects of K201 were also reported by Kawabata *et al.* (2000) following 20 min ischaemia then reperfusion in the isolated rabbit heart (Kawabata *et al.*, 2000). The investigators found that while ischaemia resulted in a decline in ATP and increase in inorganic phosphate (P_i) in control hearts, pre-perfusion with K201 significantly attenuated both of these effects. In a follow-up investigation, simultaneous pre-perfusion with K201 and the NO synthase inhibitor L-NAME abolished the influence of K201 on ATP and P_i levels during ischaemia and reperfusion (Kawabata *et al.*, 2002). Thus K201 appears to preserve high energy phosphate levels following myocardial ischaemia and reperfusion injury, with evidence suggesting this effect may be mediated in part by stimulation of NO synthase.

3.1.2 Effect of K201 on membrane currents and its anti-arrhythmic potential

A number of investigations have reported on the potential of K201 as an anti-arrhythmic agent, ascribed mainly to its inhibitory actions on a number of ionic currents (Kumagai *et al.*, 2003; Nakaya *et al.*, 2000). From the work of Kimura and colleagues (1999) using guinea pig ventricular myocytes it was established that K201 possessed an inhibitory effect on several ionic currents, including the inward sodium current, I_{Na}, the inward calcium current, I_{Ca}, and the inwardly rectifying potassium current I_{K1}. The action potential duration was significantly shortened in the presence of concentrations as low as 1.0 μM, an effect that could not be explained by inhibition of these three ionic currents alone (Kimura *et al.*, 1999). Further investigation of K201's channel blocking action was carried out using guinea pig atrial cells (Nakaya *et al.*, 2000). Both $I_{K\text{-}ACh}$ and I_{Kr} were potently suppressed by K201, with an IC_{50} of 2.29 μM and 2.42 μM respectively. As current pharmacological treatments for AF possess similar channel blocking actions (Wettwer *et al.*, 2007), it was postulated that K201 may possess anti-arrhythmic properties in such a setting. Indeed, in a guinea-pig Langendorff model of AF, 1.0 μM K201 led to a reversal of the reduction in monophasic action potential (MAP_{90}) and effective refractory period

(ERP) durations induced by carbachol chloride (CCh), and completely prevented AF induction by a train of stimuli, despite the presence of CCh (Nakaya *et al.*, 2000). Sole application of K201 (0.3 and 1.0 μM) to atrial myocytes did not significantly alter APD, in contrast to the significant shortening reported by Kimura *et al*. (Kimura *et al.*, 1999). K201 was also shown to be effective in preventing AF using the canine sterile pericarditis model (Kumagai *et al.*, 2003). Treatment with K201 completely prevented induction of AF by rapid atrial pacing in this model, and while it was still possible to generate sustained atrial flutter, the number and duration of these episodes was significantly reduced. Atrial effective refractory period for any given cycle length was also significantly prolonged by K201, although conduction time within the right atrium itself was not significantly altered (Kumagai *et al.*, 2003). Hasumi *et al.* (2007) studied the anti-arrhythmic potential of K201 in the setting of pharmacologically-induced ventricular Torsades de Pointes (Hasumi *et al.*, 2007). Treatment with clofilium in the presence of α_1-adrenoceptor blockade led to induction of Torsades de Pointes, an effect which was completely blocked by administration of 400 $\mu g.kg^{-1}$ K201 (~12.85 μM) (Hasumi *et al.*, 2007).

3.1.3 K201 and the cardiac ryanodine receptor

Since the discovery of the binding protein FKBP12.6 (calstabin2) and its relationship with the cardiac ryanodine receptor (Lam *et al.*, 1995; Timerman *et al.*, 1996), attempts have been made to characterise this relationship in various cardiac disease states, including heart failure. It has been reported that the stoichiometry of FKBP12.6 binding to RyR2 is significantly reduced in ventricular tissue from failing hearts (Marx *et al.*, 2000; Ono *et al.*, 2000; Yano *et al.*, 2000) which has been proposed to occur as a direct consequence of 'hyperphosphorylation' of RyR2 by protein kinase A (PKA) in heart failure (Marx *et al.*, 2000; Reiken *et al.*, 2003). Yano and colleagues (2003) demonstrated that a canine chronic right ventricular pacing model of heart failure was associated with increased PKA phosphorylation of RyR2, dissociation of FKBP12.6 from the channel and an apparent increase in diastolic calcium leak (Yano *et al.*, 2003). Treatment with K201 throughout the period of chronic pacing significantly attenuated the decline in systolic and diastolic function and prevented remodelling of the left ventricle. These effects were attributed to the ability of K201 to restore normal FKBP12.6-RyR2 stoichiometry and inhibit diastolic Ca^{2+} leak (Yano *et al.*, 2003). In normal SR vesicles prepared from canine left ventricular homogenates, treatment with FK506 (dissociating FKBP12.6 from RyR2) led to a decline in the rate and magnitude of Ca^{2+} release to levels comparable with failing SR vesicles. In normal and failing SR vesicles both parameters could be restored towards control levels

using 1 μM K201 (Kohno *et al.*, 2003). K201 treatment was also effective in preventing exercise-induced arrhythmias in FKBP12.6 $^{+/-}$ mice, although this was not the case in FKBP12.6 $^{-/-}$ mice, suggesting that FKBP12.6 is a prerequisite for K201's antiarrhythmic action in this setting (Wehrens *et al.*, 2004).

3.1.4 Is FKBP12.6 the critical mediator of K201 RyR2 channel stabilisation?

While some studies have shown that K201's actions are mediated via the RyR2 to some extent, investigators have challenged a number of observations regarding the action of the drug. It has been suggested that the initial trigger for dissociation of FKBP12.6 from RyR2 occurs as the result of disruption of normal receptor interdomain interaction (Oda *et al.*, 2005). Through the use of peptide constructs that correspond to subdomains of the RyR2 previously shown to harbour mutations in CPVT, unzipping of the N-terminal/Central domain interactions led to cAMP-dependent hyperphosphorylation of RyR2, dissociation of FKBP12.6 from the channel complex and Ca^{2+} leak. Of note was that domain unzipping was already present in failing hearts. The specific binding site of K201 was identified by Yamamoto *et al*. (2008) using synthetic peptides corresponding to specific regions of RyR2 (Yamamoto *et al.*, 2008). They identified an amino acid sequence in the RyR2 that shared sequence homology with Annexin V, a protein known to bind with K201 (Kaneko *et al.*, 1997). This region, known as domain$^{2059\text{-}2156}$, included a smaller domain (domain$^{2114\text{-}2149}$). The domain peptide$^{2114\text{-}2149}$ (DP$^{2114\text{-}2149}$) was synthesised by the group and found to bind K201. Inclusion of larger RyR2 fragments in the search revealed that K201 did not bind fragments that contained no sequence homology with DP$^{2114\text{-}2149}$. DP$^{2114\text{-}2149}$ was shown to interact with the RyR2 in SR vesicles and prevent Ca^{2+} leak induced by application of FK506. This effect could be achieved in the presence of 30 μM FK506 which binds FKBP12.6 completely, suggesting that stabilisation can occur without re-association of FKBP12.6 to the channel complex (Yamamoto *et al.*, 2008). Investigations by Hunt *et al* (2007) led to the conclusion that FKBP12.6 was not essential for suppression of SR Ca^{2+} leak in cells exhibiting spontaneous SR Ca^{2+} release (termed store overload induced Ca^{2+} release, or SOICR) from the following observations; (a) K201 suppressed spontaneous release events in intact ventricular myocytes to the same degree, regardless of the presence or absence of 2 μM FK506, (b) the level of K201's inhibition of spontaneous Ca^{2+} release from human embryonic kidney (HEK-293) cells co-expressing RyR2 and FKBP12.6 were the same as HEK-293 cells expressing RyR2 alone (Hunt *et al.*, 2007). Evidence is therefore accumulating which suggests FKBP12.6 is not a

requirement for restoration of normal RyR2 gating function in the presence of K201, although this issue remains to be fully resolved.

3.1.5 What is the effect of K201 on E-C coupling in normal cardiac preparations?

The beneficial effects of K201 in the setting of ischaemia-reperfusion injury, experimental heart failure, as well as in various models of atrial fibrillation have all been well documented. Little effort however has been made to characterise the influence of K201 on normal cardiac function with regards to excitation-contraction coupling. From the work of Kimura and colleagues (1999) it is clear that K201 treatment leads to a concentration dependent suppression of $I_{Ca,L}$, I_{Na} and I_{K1} in guinea pig ventricular myocytes (Kimura *et al.*, 1999). Inagaki *et al.* (2000) noted depression of L-type Ca^{2+} current in isolated rat ventricular myocytes using 1.0 μM (by 22 %) and 3.0 μM (by 59.6 %) K201 but concluded that interaction with the L-type Ca^{2+} channel did not play a significant role in the cardioprotective effect of K201, as the concentration of K201 required to elicit protection against ischaemia-reperfusion injury (0.3 μM) did not significantly inhibit $I_{Ca,L}$ (Inagaki *et al.*, 2000b). Furthermore, although $I_{Ca,L}$ was significantly inhibited at both 1.0 and 3.0 μM K201, only 3.0 μM demonstrated a significant depression of left ventricular developed pressure prior to onset of ischaemia. More recently, Loughrey *et al.* (2007) explored in depth K201's influence on E-C coupling mechanisms in rabbit cardiomyocytes. K201 at 1.0 μM was shown to significantly reduce Ca^{2+} leak from the SR without altering SR Ca^{2+} content, and at this concentration diastolic Ca^{2+} waves induced by Ca^{2+} overload were significantly attenuated (Loughrey *et al.*, 2007). Application of 3.0 μM K201 effectively abolished Ca^{2+} waves however this was also associated with a reduction in SR content (Loughrey *et al.*, 2007). They also found that, in contrast to previous findings, $I_{Ca,L}$ was inhibited at 3.0 μM but not 1.0 μM K201, and that the maximal rate of SR Ca^{2+} uptake by SERCA (V_{max}) was significantly reduced to 88 % and 77 % of control values using 1.0 and 3.0 μM respectively, an observation in disagreement with those of Yano *et al.*, who reported that SR Ca^{2+} uptake was not altered by K201 (Yano *et al.*, 2003). Taken together, the results of these previous studies suggest that there are marked alterations in E-C coupling mechanisms in the presence of 3.0 μM K201 that would favour a depression of cardiac inotropy in normally functioning hearts (decreased $I_{Ca,L}$, RyR2 open probability and SR Ca^{2+} uptake), but the implications for 1.0 μM K201 are not so clear due to the aforementioned disparities between results of individual investigations.

3.1.6 Aims

The aim of the work described in this chapter was to establish the effects of different concentrations of K201 on cardiac inotropy and mechanical function in an isolated working rabbit heart preparation. Contractile function in the isolated working heart preparation is more physiological than that measured in previous Langendorff-based investigations, allowing more thorough characterisation of mechanical function, including assessment of ventricular volumes. Based on the results of previous studies looking at the actions of this drug on EC coupling, it was hypothesised that K201 would demonstrate a depressive effect on contractile function in the isolated working heart that would become apparent at concentrations of 3.0 μM and above.

3.2 Methods

3.2.1 Isolated working heart setup

Hearts from 8 male New Zealand White rabbits were excised and perfused initially in Langendorff mode on the isolated working heart apparatus as described in the General Methods chapter section 2.1.3. After cannulation of the left atrium and initiation of working heart mode, perfusate solution was recirculated to establish working heart recirculating mode with a fixed volume of 540 ml. Preload was set at 7.4 mmHg and afterload set to 60 mmHg. These settings remained constant throughout the experimental protocol.

3.2.2 Left ventricular function by pressure-volume catheterisation

A 3F *Scisense* VSL catheter with a recording electrode segment of 19 mm was advanced slowly past the aortic valves into the left ventricle to obtain pressure-volume measurements throughout the experimental protocol. Estimation of V_p was made by injection of a 20 % hypertonic saline bolus into the left atrial inflow line 5 min prior to the beginning of the protocol.

3.2.3 Solutions

Perfusion of the isolated working heart was performed using Tyrode's solution, the composition of which is described in General Methods section 2.1.3. K201 was created by dissolving K201 (molecular weight 461 $g.mol^{-1}$) in a 10% dimethyl sulfoxide (DMSO)

solution to yield a stock K201 concentration of 1 mM. The 10% DMSO acted as vehicle solution in control experiments

3.2.4 Experimental Protocol

The effect of increasing concentrations of K201 on mechanical function was investigated in 8 isolated working rabbit hearts. After recording of baseline function 162 µl of a 1 mM K201 stock were added to the recirculating perfusate via the recirculation reservoir, yielding a final concentration of 0.3 µM K201. The concentration of K201 was increased to 1.0 µM 4 min after this point by addition of 378 µl, with a final increase in concentration to 3.0 µM performed once again 4 min later by addition of 1080 µl. Hearts were not paced throughout the protocol.

3.2.5 Data Recording and statistical analysis

All data were recorded on a *Dell* PC using *LabChart* software version 5.5.6 at a sampling rate of 1000 Hz, and analysed offline using *LabChart*'s Blood Pressure Module and *LabScribe2.0* software. V_p estimation was performed offline using *PVAN*. Student's *t*-test or Repeated Measures ANOVA and Tukey-Kramer multiple comparisons test were used to compare the effect of each addition of K201 on a number of functional parameters. A *P*-value of < 0.05 was considered statistically significant.

3.3 Results

The protocol for incremental addition of K201 to the isolated working heart perfusate is shown in Figure 3.2A. Arrows along the top represent the point where the drug was added to the perfusion reservoir, with labeled bars showing the concentration of drug perfusing the heart. Time delay between addition of drug to the reservoir and the drug reaching the heart was estimated based on the preliminary calculations discussed in General Methods Chapter section 2.1.1. Before 4 min of perfusion with 3.0 µM K201, 3 of the 8 hearts were no longer able to maintain a cardiac output sufficient to sustain working heart function and did not last the full 4 min at this concentration. For this reason, subsequent functional mean data comparisons were therefore made at 90 s after addition of 3.0 µM to the perfusate when all hearts produced a measurable aortic flow. Left intra-ventricular (LV) pressure and volume recordings at each concentration of K201 are depicted in Figure 3.2B (i–iv) and corresponding pressure volume loops in Figure 3.2C. Whilst 0.3 µM K201 did not affect heart rate (HR), 1.0 and 3.0 µM K201 induced a concentration-dependent

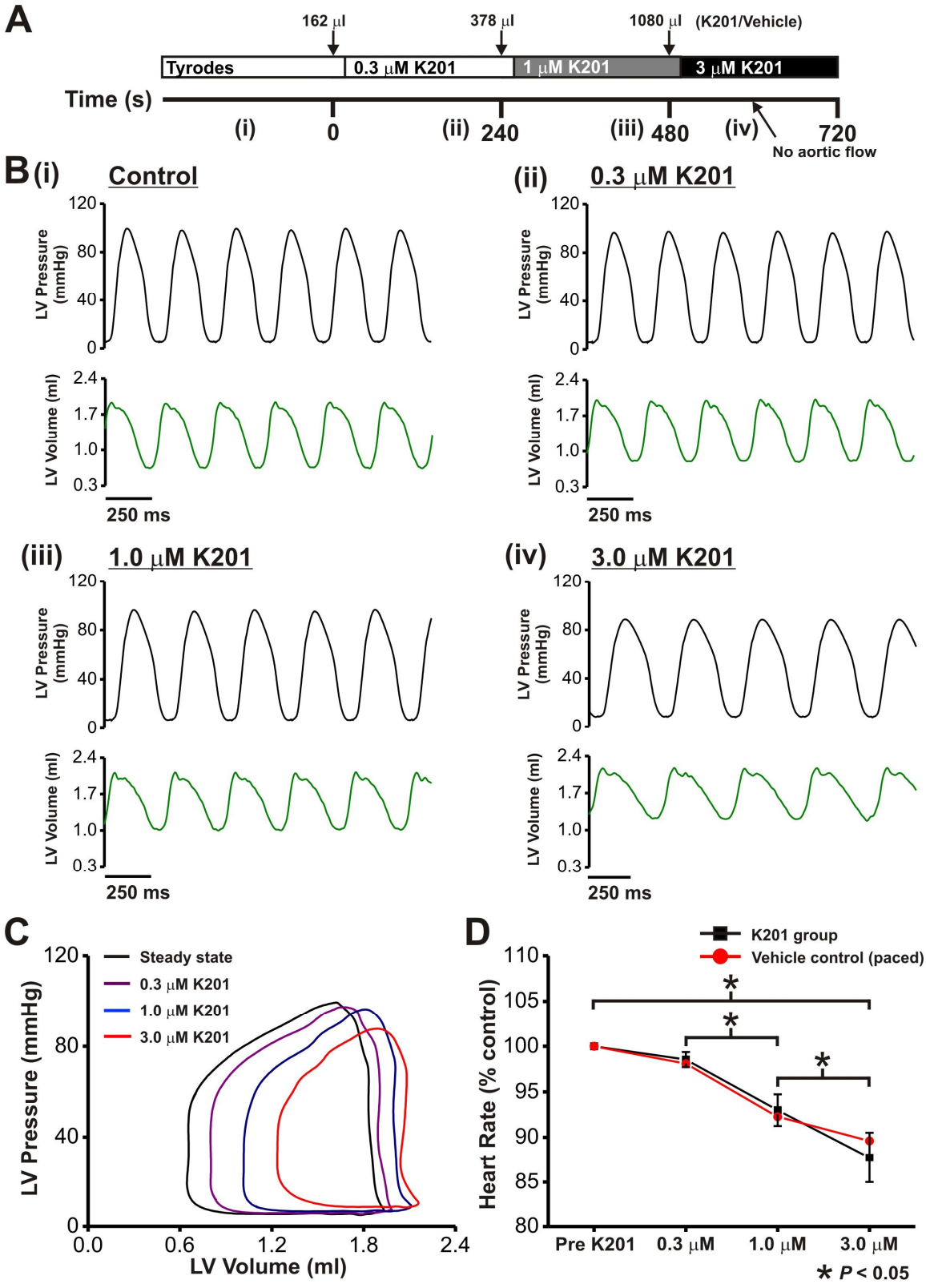

Figure 3.2 K201 concentration response. A. Diagram of the experimental protocol. B(i–iv). Representative pressure and volume traces taken from points denoted in A. C. Representative pressure-volume loops at each of the time points indicated in A. D. Heart rate in K201 (n=8) and paced vehicle control (n=4) groups, expressed as a % of control.

reduction in HR (to 92.99 ± 1.74 % and 87.75 ± 1.74 % of pre-K201 value (204.58 ± 3.19 beats.min-1) - Figure 1D). This reduction in HR did not occur in the vehicle control (198.4 ± 6.6 beats.min^{-1} (steady state) vs. 200.2 ± 6.4 beats.min^{-1} (90 s post-1080 µl vehicle); n=3). Therefore, to enable assessment of cardiac functional parameters at equivalent heart rates with timed controls, a subset of hearts were perfused with the corresponding concentration of vehicle and paced at rates equivalent to the mean values achieved with each concentration of K201 (Figure 3.2D).

Table 1	Left Ventricular Functional Indices from Isolated Working Rabbit Hearts			
	Pre-K201	0.3 µM K201	1.0 µM K201	3.0 µM K201
Parameter				
HR (beats.min^{-1})	203.72 ± 3.17	200.79 ± 3.85	189.58 ± 5.36	177.29 ± 7.54
AF (ml.min^{-1})	177.06 ± 13.87	166.04 ± 15.63	135.35 ± 20.79*	99.57 ± 23.71*
CF (ml.min^{-1})	67.50 ± 4.50	67.75 ± 4.64	67.88 ± 4.63	67.75 ± 4.71
SV (ml)	1242.92 ± 92.45	1192.31 ± 96.64	1079.60 ± 122.92*	921.84 ± 121.72*
Systolic				
PSP (mmHg)	98.11 ± 1.45	97.28 ± 2.09	93.35 ± 2.19*	89.37 ± 1.89*
dP/dt_{max} (mmHg.s^{-1})	1916.10 ± 72.67	1830.76 ± 109.58	1501.20 ± 114.81*	1276.68 ± 93.12*
ESV (ml)	632.33 ± 68.33	686.06 ± 76.05	865.24 ± 127.30	1055.54 ± 140.00
EF (%)	66.27 ± 3.28	63.47 ± 3.48	56.27 ± 5.08*	46.78 ± 4.85*
Diastolic				
EDP (mmHg)	8.15 ± 1.38	9.12 ± 1.50	9.83 ± 1.62	10.15 ± 1.45
dP/dt_{min} (mmHg.s^{-1})	-2077.03 ± 144.54	-1986.55 ± 145.67	-1787.33 ± 137.12	-1522.80 ± 149.91
EDV (ml)	1875.24 ± 102.78	1878.37 ± 108.91	1944.84 ± 135.71	1977.38 ± 155.61
Tau (ms)	27.38 ± 2.77	29.03 ± 3.06	37.68 ± 4.56*	49.11 ± 7.05*

Table 3.1 Effect of K201 on haemodynamic parameters of the isolated working rabbit heart. HR, heart rate; PSP, LV peak systolic pressure; EDP, end diastolic pressure; ESV, end systolic volume; EDV, end diastolic volume; SV, stroke volume; AF, aortic flow; CF, coronary flow; EF, ejection fraction. Values expressed as mean ± SEM. * $P < 0.05$ vs. previous K201 concentration.

3.3.1 Effect of K201 on systolic functional parameters in the isolated working rabbit heart

Mean functional parameters from hearts perfused with K201 are shown in Table 3.1. As demonstrated by the representative trace and PV loop in Figure 3.2B(ii) and 3.2C, respectively, application of 0.3 µM K201 did not significantly effect any systolic functional parameter measured (Table 3.1 & Figure 3.3). However, as can be seen from example traces in Figure 3.2B, and PV loops in Figure 3.2C, 1.0 and 3.0 µM K201 led to a significant concentration dependent reduction in LV peak systolic pressure (PSP) which when normalised for the negative chronotropic effect and DMSO decreased to 92.16 and

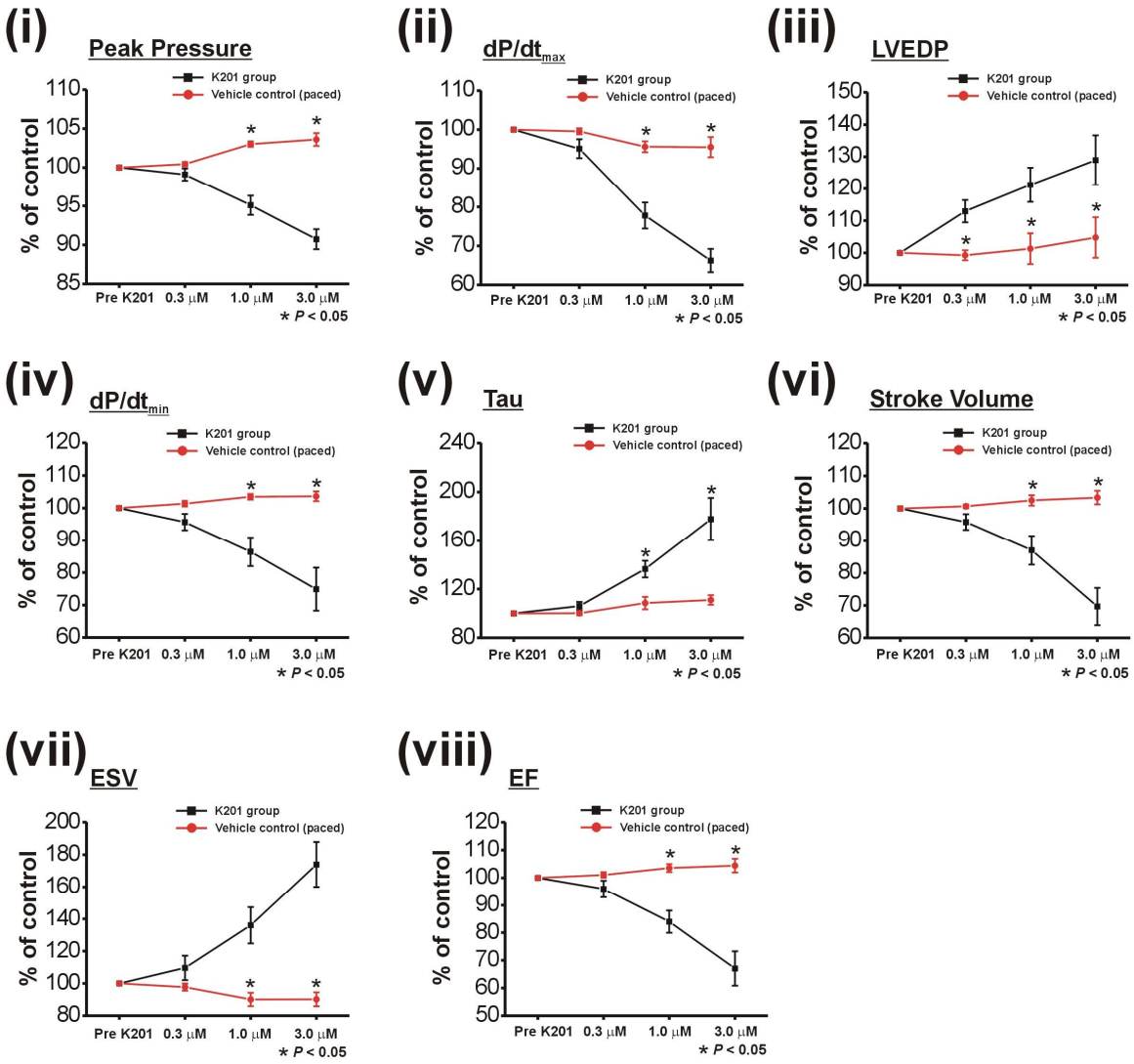

Figure 3.3 Influence of K201 on working heart function. (i-iiiv). Effect of K201 on functional parameters of unpaced isolated working hearts (black squares, n=8) in comparison to paced vehicle controls (red circles, n=4). All values are non-normalised and expressed as % of pre-K201 values.

87.78% of control values, respectively (Figure 3.3(i)). Similarly, the maximum rate of rise of intra-ventricular pressure was significantly reduced to 80.93 and 69.11% of control respectively (Figure 3.3(ii)).

3.3.2 Effects of K201 on diastolic functional parameters in the isolated working rabbit heart

Normalising for the effect of negative inotropy and DMSO, the relaxation of the myocardium was also impaired by 0.3, 1.0 and 3.0 μM K201 as assessed by the end diastolic pressure (EDP) which was significantly increased to 113.79, 119.68 and 123.10% of control values (Figure 3.3(iii)). Similarly, 1.0 and 3.0 μM K201 decreased the maximum rate of LV pressure fall (dP/dt_{min} – Figure 3.3(iv)) to 83.45 and 71.64% of the

control value and increased the time for the relaxation constant (τ) to 125.19 and 158.58% of the control value (Figure 3.3(v)).

3.3.3 Effects of K201 on volume parameters in the isolated working rabbit heart

As can be observed in the PV loops shown in Figure 3.2C and mean data in Table 3.1 and Figure 3.3(vi), 1.0 and 3.0 μM K201 led to a decline in stroke volume (SV) to 83.62 and 70.18% of control values. This was due to an increase in end-systolic volume (ESV) to 150.71 and 185.56 % of control, shown in Figure 3.3(vii) as opposed to the any significant alteration in end-diastolic volume (mean data in Table 3.1, percentage data not shown). As a result of these volume changes the ejection fraction was reduced by 1.0 and 3.0 μM K201 to 80.44 and 66.63% of control values (Figure 3.3(viii)). K201 did not alter coronary flow which at steady state was 67.50 ± 4.50 $ml.min^{-1}$.

3.3.4 Comparison of the effects of K201 in paced *vs*. non-paced hearts

Due to the negative chronotropy induced by K201 the control hearts had to be paced at equivalent heart rates. This led to a situation where the control hearts were paced but the hearts exposed to K201 were not paced. It is possible that the pacing in control hearts had altered the electrical activation pattern and therefore the subsequent mechanical function therefore making direct comparison complex. To ensure that the effect of K201 on systolic, diastolic and volume parameters is the same between paced and non-paced hearts a subset of hearts were paced at a set rate (201.98 ± 2.26 bpm) and then perfused with 1.0 μM K201 during continued pacing. Figure 3.3B compares the effects of a 4 min period of K201 perfusion in paced and non-paced hearts. The non-paced hearts were comprised of the same group as shown in Figure 3.3A and table 3.1, however pre-1.0 μM values were expressed as a % of values 4 min after perfusion with 0.3 μM K201, as this allowed for direct comparison of the same time period in 1.0 μM K201 for both groups. As can be seen from Figure 3.4(i) & (ii), all parameters measured, with the exception of the relaxation constant were altered significantly in the same direction as when not paced demonstrating that the mechanical effects of K201 on the normal heart is due to a direct effect of K201 rather than any pacing induced modulation.

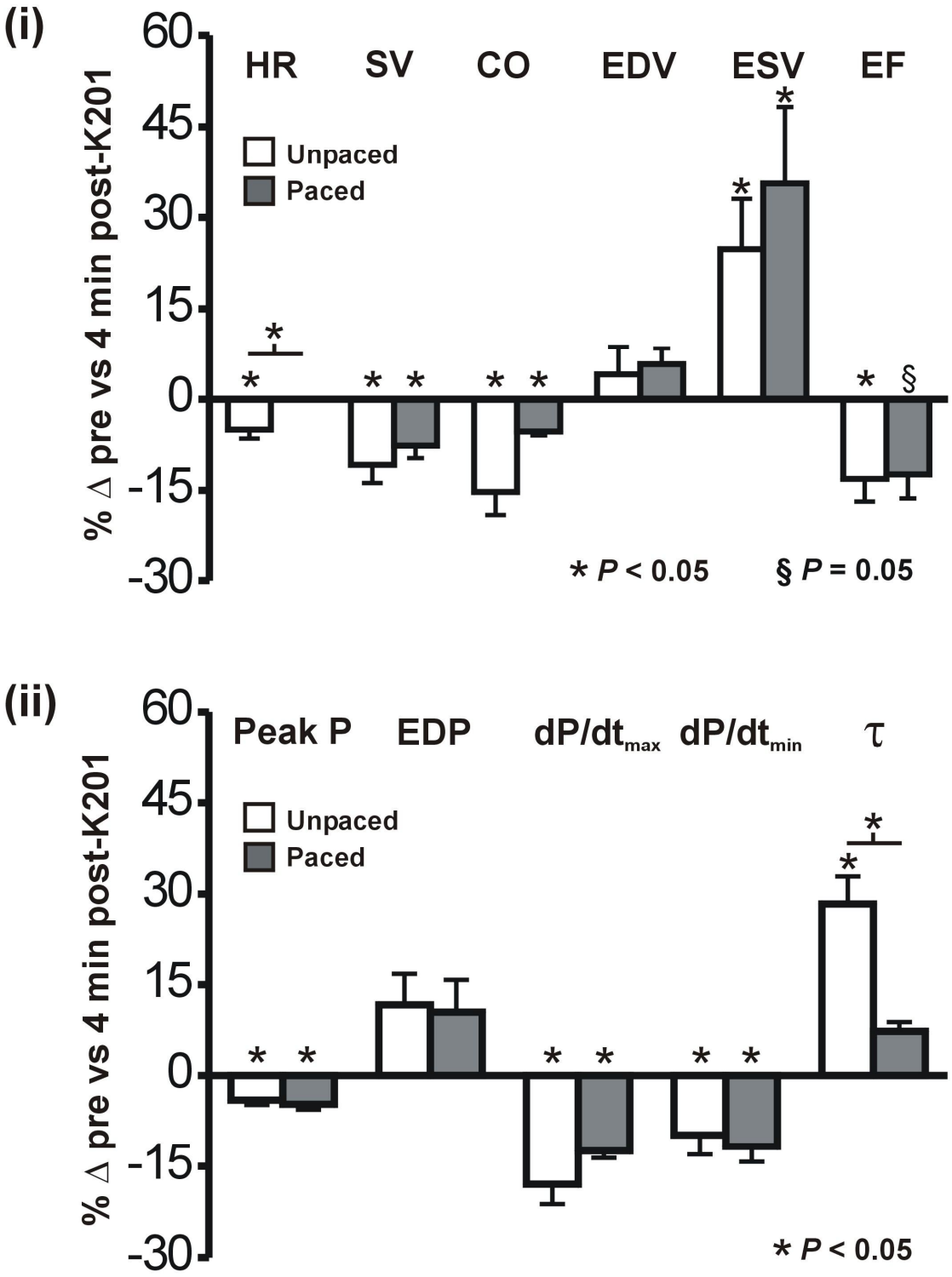

Figure 3.4 Influence of K201 on working heart function. (i-ii). % change in functional parameters of unpaced (white bars, n=8) and paced (grey bars, n=4) hearts exposed to 1.0 μM K201 for 4 min. Paced hearts expressed as a % of pre-K201 values. Non-paced hearts expressed as a % of post-4min 0.3 μM K201 values to compare identical perfusion times in 1.0 μM K201 for both groups

3.4 Discussion

3.4.1 K201 has a negative inotropic effect on the intact isolated ejecting heart

The potential cardioprotective effects of K201 have been demonstrated in a number of investigations utilizing different stress-inducing protocols. Kaneko *et al.* (1994) demonstrated that K201 could protect against myocardial over-contraction and cell necrosis following administration of epinephrine and/or caffeine (Kaneko, 1994), while preservation of left ventricular function was achieved in ischaemia-reperfusion studies when K201 was perfused both before the onset of ischaemia (Ito *et al.*, 2000) and during reperfusion (Inagaki *et al.*, 2000b). Little is known however about the effects of K201 on contractile function in the normally functioning heart. The results from this investigation demonstrate that K201 has a negative inotropic effect on the isolated working heart at concentrations of 1.0 μM and above. These results may have implications for the use of K201 as a therapeutic treatment in various cardiac disease states, as the dosage required to effectively treat such conditions may alter heart function. Aside from LVEDP none of the parameters measured during this study were significantly altered at a concentration of 0.3 μM, but depression of a number of contractile indices, including dP/dt_{max}, left ventricular developed pressure, stroke volume and ejection fraction, became apparent at 1.0 μM. At a concentration of 3.0 μM K201 proved to be particularly cardio-depressive and indeed 3 of the 8 hearts used during this investigation were not able to sustain aortic flow after several minutes of perfusion with this concentration, leading to a drop in perfusion pressure and a decline in left ventricular contractility. These findings suggest K201 may possess a narrow therapeutic window.

3.4.2 The influence of heart rate on the negative inotropic effect of K201

Increasing stimulation rate is well known to influence myocardial contractility (by the so-called force-frequency relationship (Endoh, 2004; KOCH-WESER & BLINKS, 1963)). A positive force-frequency relationship has been demonstrated in mammalian ventricular myocytes from a number of species including the rabbit, and is explained by a) elevated SR Ca^{2+} content at higher stimulation frequencies and b) an increase in $[Na]_i$ causing a shift in the SR Ca^{2+} uptake/Ca^{2+} extrusion balance by favouring reduced Ca^{2+} efflux via the Na^{+}/Ca^{2+} exchange (NCX) (Maier *et al.*, 2000). The observation that SR Ca^{2+} content is

not appreciably altered with increasing stimulation frequency in rat cardiac myocytes explains the negative force-frequency relationship in this species, where the dominant effect of increased stimulation frequency is the time encroachment on full restitution of EC coupling mechanisms (Maier *et al.*, 2000). In the isolated working rabbit heart therefore, a decrease in heart rate may be expected to have a negative influence on left ventricular inotropy and in part explain the effects of K201. Using hearts from a subset of experiments where heart rate was fixed throughout the protocol, the % change from baseline in a number of functional indices after 4 min of perfusion with 1.0 μM K201 was compared with the equivalent perfusion period used in the initial protocol where heart rate declined (mean HR values are displayed in Table 3.1). From this it was possible to assess the effects of heart rate on left ventricular inotropy in the isolated working heart during perfusion with K201. As shown in Figure 3.4, in both sets of hearts the direction of the change in every parameter was the same, and aside from the relaxation constant τ there were no significant differences in the magnitude of change in any parameter between groups. This suggests that the decline in heart rate caused by K201 does not explain the drugs' negative inotropic action at 1.0 μM.

3.4.3 What are the main factors contributing to the negative inotropic effect of K201?

Previous investigations looking at the mechanisms of K201's actions in normally functioning heart preparations are somewhat limited. Kaneko (1994) found that K201 inhibited the Ca^{2+}-dependent binding of Annexin-V to F-actin, a protein which comprises the microfilaments of the cytoskeleton. This effect however required concentrations of 10 μM or higher (Kaneko, 1994; Kaneko *et al.*, 1997). Kimura *et al.* (1999) using guinea pig ventricular myocytes, found that K201 inhibited $I_{Ca,L}$ by 20% and 50% using 1.0 and 3.0 μM respectively (Kimura *et al.*, 1999). A similar result was also reported by Inagaki *et al.* (2000) who demonstrated 1.0 and 3.0 μM led to a 22 % and 59 % inhibition of $I_{Ca,L}$ respectively in rat ventricular myocytes (Inagaki *et al.*, 2000b). They also reported that left ventricular developed pressure in the rat Langendorff setup was significantly depressed after administration of 3.0, but not 1.0 μM K201 prior to ischaemia (Inagaki *et al.*, 2000a). Loughrey *et al.* (2007) found that 1.0 μM K201 decreased the Ca^{2+} transient in normal rabbit ventricular myocytes by 17 % and inhibited SR Ca^{2+} uptake by SERCA but that concentrations of 3.0 μM were required to inhibit $I_{Ca,L}$ amplitude significantly (Loughrey *et al.*, 2007). The negative inotropic action of K201 could most likely be explained by the above observations of K201's action on intracellular Ca^{2+} handling. The reduction in $I_{Ca,L}$

amplitude at 3.0 μM coupled with a reduction in SR Ca^{2+} uptake, and subsequent reduction in SR Ca^{2+} content would be expected to significantly reduce cardiomyocyte inotropy. Our results suggest 1.0 μM K201 is enough to significantly inhibit contractile function in the working heart, albeit by a small amount. This effect cannot be explained by a significant reduction in L-type Ca^{2+} current which was found to be unaltered by 1.0 μM in isolated rabbit ventricular myocytes (Loughrey *et al.*, 2007).

Several studies have shown that K201 restores normal channel function to RyR2s from failing hearts by reducing channel P_o and inhibiting Ca^{2+} leak from the channel (Kohno *et al.*, 2003; Wehrens *et al.*, 2005; Yano *et al.*, 2003). In addition, increased spontaneous SR Ca^{2+} release events in intact ventricular myocytes evoked by elevated $[Ca^{2+}]_o$ are significantly attenuated in the presence of 1.0 μM K201 (Hunt *et al.*, 2007; Loughrey *et al.*, 2007). Loughrey *et al*. (2007) made several observations regarding the action of 1.0 μM K201 on Ca^{2+} release characteristics in rabbit ventricular myocytes; 1) Application of 1.0 μM to permeabilised rabbit ventricular myocytes resulted in a significant decline in Ca^{2+} spark duration (to 82% of control) and Ca^{2+} spark frequency (to 63% of control) without altering spark amplitude or width, and 2) the rate of Ca^{2+} leak from the SR of permeabilised myocytes was significantly reduced to 84% of control in the presence of 1.0 μM K201. Inhibition of RyR2 alone however would not be expected to result in steady state alteration of contractility and by itself is unlikely to explain the negative inotropic effects of K201. Addition of agents such as caffeine or BDM to enhance CICR only result in transient changes in the systolic Ca^{2+} transient and do not result in a sustained increase in contractility (Trafford *et al.*, 1998). While decreasing RyR2 sensitivity to activation by Ca^{2+} would be predicted to increase SR Ca^{2+} content, similar to the effect seen with application of tetracaine (Overend *et al.*, 1997), this was not shown to occur with 1.0 or 3.0 μM K201, indicating the presence of alternative mechanisms of K201's actions at these concentrations. This was confirmed by the observation that K201 also leads to inhibition of SR Ca^{2+} uptake via SERCA at 1.0 μM and above (Loughrey *et al.*, 2007). The combination of RyR2 and SERCA inhibition at 1.0 μM significantly inhibited the ability for Ca^{2+} waves to propagate, decreases Ca^{2+} spark duration and frequency, and together could potentially explain some of the negative inotropic action of K201 at this concentration.

3.4.4 The influence of ion current inhibition by K201 on cardiac inotropy

Inhibition of ion currents critical to maintenance of resting membrane potential (E_m) and action potential characteristics may influence contractile function and cardiac inotropy. I_{Na} inhibition with anti-arrhythmic agents such as lidocaine has been shown to shorten the action potential duration (APD), which leads to a reduction in the duration of Na^+ and Ca^{2+} influx during the action potential and ultimately a reduction in Ca^{2+} transient amplitude (Pankucsi *et al.*, 1996; Sheu & Lederer, 1985). While K201 has been shown to inhibit fast I_{Na} current (Kimura *et al.*, 1999) and shorten APD (Kimura *et al.*, 1999; Kiriyama *et al.*, 2000) in isolated guinea pig ventricular myocytes, slow inward Na^+ current was not found to be inhibited by K201 (Kimura *et al.*, 1999). In addition, E_m was not significantly different between K201 treated cells and untreated control myocytes. Kiriyama *et al.* (2000) found that application of 1.0 μM K201 significantly inhibited the delayed rectifier K^+ current, I_{Kr} in isolated guinea-pig ventricular myocytes. Kimura also reported that in addition to its inhibitory action on I_{Na} and $I_{Ca.L}$, K201 irreversibly inhibited I_{K1} (to approximately 70% of control values at 1.0 μM). Inhibition of repolarising K^+ currents would be expected to result in prolongation of the action potential and induce a positive inotropic effect, which is believed to be mediated by a net increase in Ca^{2+} influx via the L-type Ca^{2+} channel (Bouchard *et al.*, 1995). Kaprielian *et al.* (1999) found that APD was significantly prolonged in right ventricular myocytes from rats that had undergone coronary artery ligation 8 weeks previously in comparison to myocytes from sham operated controls (Kaprielian *et al.*, 1999). This was attributed to a reduction in repolarising K^+ current density, specifically I_{TO} and I_{K1}. Stimulating sham ventricular myocytes with MI-derived action potentials resulted in a significantly increased [Ca^{2+}] transient amplitude with no change in diastolic $[Ca^{2+}]_i$. While peak $I_{Ca.L}$ was reduced by stimulating sham myocytes with the post-MI waveform, the net Ca^{2+} influx through L-type Ca^{2+} channels was significantly increased (Kaprielian *et al.*, 1999).

From the results of studies on isolated guinea-pig ventricular myocytes the overall effect of K201 is a significant shortening of the ventricular action potential despite inhibition of the repolarising K^+ currents I_{Kr} and I_{K1} (Kimura *et al.*, 1999; Kiriyama *et al.*, 2000). A significant contributor to the shortened APD is undoubtedly inhibition of I_{Na}, however the degree of inhibition demonstrated may not be enough to account for the degree of APD shortening and modulation of ion currents as yet unreported may contribute (Kimura *et al.*, 1999). In addition, the influence of K201 on APD in rabbit ventricular myocytes has not

been investigated, and in order to fully elucidate the mechanisms contributing to the negative inotropic effect of K201 in the current investigation further study is warranted.

3.4.5 Implications for use in therapeutic treatment strategies

In order to work as a potentially viable treatment for conditions such as heart failure or atrial fibrillation an optimal range of concentrations in which K201 is effective must be established. In light of the results of this study, due caution may have to be paid to the concentration of K201 used due to its negative inotropic influence. Both Inagaki *et al.* (2000) and Ito *et al.* (2000) found that 0.3 μM K201 was sufficient to elicit a protective effect on left ventricular mechanical function in ischaemia-reperfusion injury models, with no further preservation of function evident using 1.0 μM (Inagaki *et al.*, 2000b; Ito *et al.*, 2000). Loughrey *et al.* (2007) reported that 1.0 μM suppressed spontaneous Ca^{2+} waves in permeabilised rabbit ventricular myocytes but 3.0 μM was able to abolish them completely (Loughrey *et al.*, 2007). Store overload-induced Ca^{2+} release (SOICR) in rat ventricular myocytes was also significantly attenuated using 3.0 μM K01 and eliminated at higher concentrations (Hunt *et al.*, 2007). The concentration of K201 required to confer a beneficial response appears therefore to be dependent on the experimental conditions in which the drug is used, as well as the species investigated. While in the above examples higher concentrations of K201 were more effective in abolishing spontaneous Ca^{2+} release events, results from this investigation suggest that significant depression of cardiac mechanical function may occur at such concentrations. The importance of such knowledge to the therapeutic potential of K201 was highlighted in a recent publication by Toischer *et al.* (2009) who investigated the influence of K201 on contractile performance of isolated muscle preparations from end-stage heart failure patients (Toischer *et al.*, 2009). While K201 was shown to confer some beneficial effects on post-rest potentiation and frequency-dependent changes in systolic and diastolic tension (force-frequency relations) at a concentration of 0.3 μM under conditions believed to promote increased SR Ca^{2+} leak (5 mM $[Ca^{2+}]_o$), 1.0 and 3.0 μM were not acutely beneficial to systolic contractile function, and indeed at 1.0 μM inhibited developed tension by 9.8 % in comparison to control. The authors concluded that initial investigations with K201 in human patients should begin using sub-micromolar concentrations of the drug to avoid potentially adverse effects of further depressed contractile function in heart failure patients.

3.5 Summary

The data presented in this chapter demonstrate that perfusion of the isolated working rabbit heart with K201 leads to a concentration-dependent depression of heart rate and left ventricular function that becomes prominent at 1.0 and 3.0 μM. The negative inotropic effects may be explained by previously documented action of K201 on excitation-contraction coupling and intracellular Ca^{2+} handling mechanisms which promotes a concentration-dependent reduction in L-type Ca^{2+} current amplitude (at 3.0 μM in rabbit ventricular myocytes), SR Ca^{2+} uptake (via SERCA) and consequently SR Ca^{2+} content, and an inhibition of the SR Ca^{2+} release channel, RyR2. In addition, previous findings describing shortening of the ventricular action potential due in part to inhibition of I_{Na} may also explain a portion of the negative inotropic effects of this compound in isolated working rabbit hearts, although the contribution of this mechanism in rabbit myocardium requires further investigation. A reduction in intrinsic heart rate was also shown to occur but the contribution to the overall negative inotropic effects of K201 appear to be small. Given that cardioprotection in previous studies requires concentrations of up to 1.0 μM yet 3.0 μM significantly depresses left ventricular function, K201 appears to have a very narrow therapeutic window.

4 Calcium loading and β-adrenergic stimulation: Influence on left ventricular mechanical function in the isolated working rabbit heart

4.1 Introduction

Cardiac inotropy and lusitropy is influenced on a beat-to-beat basis by a large number of factors, including loading conditions imposed on the heart, myofilament Ca^{2+} sensitivity, energy availability and intracellular Ca^{2+} fluxes. Interventions which increase the available levels of Ca^{2+} within the cell will, initially, lead to an increase in cardiac inotropy (Scholz, 1983). In physiological situations, activation of the β-adrenergic system (via sympathetic stimulation) permits control of the inotropic state of the heart. Many inotropic agents work by increasing intracellular Ca^{2+} levels, either directly by stimulating an increase in intracellular Ca^{2+} levels (in this way Ca^{2+} itself can be considered an inotropic agent as increasing $[Ca]_o$ elicits a positive inotropic response) (Scholz, 1983), or indirectly as in the case of phosphodiesterase inhibitors such as milrinone, which prevent the enzymatic inactivation of cyclic adenosine monophosphate (cAMP) allowing a more sustained β-adrenergic response (Alousi & Johnson, 1986). While increasing intracellular Ca^{2+} load is essential in regulation of physiological positive inotropic responses, such as in exercise or during the so-called 'fight or flight' response, an increase beyond threshold levels eventually leads to a decline in cardiac inotropy and the development of mechanical and electrical abnormalities, also known as Ca^{2+} overload (Vassalle & Lin, 2004).

4.1.1 Catecholamine excess causes Ca^{2+} overload and myocardial damage

Activation of β_1-adrenergic receptors by endogenous catecholamines results in stimulation of an intracellular signaling cascade resulting in the phosphorylation of a number of intracellular proteins involved in Ca^{2+} regulation within the cardiomyocyte. Initiation of the β_1-adrenergic receptor pathway results in a stimulatory protein, G_s, activating Adenylyl Cyclase which in turn increases production of cAMP. This results in stimulation of cAMP-dependent protein kinase A (PKA) which phosphorylates a number of intracellular targets, including L-type Ca^{2+} channels, the cardiac ryanodine receptor (RyR2), the SR Ca^{2+} uptake inhibitory protein phospholamban and cardiac troponin I (Bers, 2002). The net effect is a significant enhancement of cardiac inotropy and lusitropy. While these effects are of importance in the physiological regulation of cardiac inotropy, it has been suggested that excessive stimulation of the β_1-adrenergic receptor pathway is detrimental for cardiac function, leading to Ca^{2+} overload and the formation of myocardial lesions in conjunction with depletion of high energy phosphate reserves (Fleckenstein *et al.*, 1983; Rona, 1985). It has been hypothesized that Ca^{2+} homeostasis during β-adrenergic

stimulation involves a preferential reliance on glycolysis rather than oxidative phosphorylation. Nakamura and colleagues (1993) tested this hypothesis by inhibiting glycolysis in isolated rabbit hearts exposed to isoproterenol (ISO) (Nakamura *et al.*, 1993). Treatment with iodoacetate (IAA) to inhibit glycolysis produced no depression in cardiac function and had little effect on overall ATP or phosphocreatine (PCr) levels. Subsequent addition of ISO however resulted in a marked depression of function (lower systolic pressure, elevated end diastolic pressure) and high energy phosphate levels. This effect was attributed to accumulation of intracellular Ca^{2+} and Ca^{2+} overload as exposure to low $[Ca^{2+}]_o$ (0.6 mM) resulted in prevention of ATP depletion and decline of contractile function (Nakamura *et al.*, 1993). Excessive β-adrenergic stimulation is known to be cardiotoxic, leading to the formation of myocardial lesions and tissue damage (Goldspink *et al.*, 2004; Haft, 1974; Mann *et al.*, 1992; Rona, 1985). Studies by Mann *et al*. (1992) showed that in isolated ventricular myocytes from dogs, cats and rats, continuous exposure to > 10 nM norepinephrine led to a marked increase in spontaneous contractile behaviour and eventually (> 24hrs) irreversible hypercontracture of cells, both of which could be inhibited by treatment with the β-antagonist propanolol (1 μM) (Mann *et al.*, 1992). 48-72 hrs exposure to 0.1 μM isoproterenol resulted in an almost identical decline in the % of viable rod-shaped cardiomyocytes to that achieved with 1 μM norepinephrine. The investigators found that these effects were a direct result of cAMP-mediated $[Ca^{2+}]_i$ overload, as evidenced by both specific upregulation of cAMP inducing spontaneous contraction and hypercontracture, and pretreatment with the L-type Ca^{2+} channel blocker verapamil prevented these effects.

4.1.2 Ca^{2+} overload may be ameliorated by K201

Ca^{2+} overload represents a dysfunction in intracellular Ca^{2+} handling that results in decreased inotropy and an increased propensity for triggered arrhythmias. Pharmacological interventions which target specific intracellular Ca^{2+} handling components, in particular those associated with the sarcoplasmic reticulum may therefore prove beneficial in alleviating the detrimental effects of Ca^{2+} overload. The cardioprotective effects of K201 have already been discussed in the previous chapter. A number of studies utilizing different species have demonstrated that K201 appears to have a protective effect in ischaemia-reperfusion injury (Inagaki *et al.*, 2000b; Ito *et al.*, 2000; Kawabata *et al.*, 2000). Inagaki *et al.*, (2000) concluded that K201 reduced the levels of Ca^{2+} overload associated with ischaemia-reperfusion, as evidenced by a significantly reduced systolic and diastolic Indo-1 fluorescence (indicative of $[Ca^{2+}]_i$) during reperfusion

in K201 treated hearts compared to controls (Inagaki *et al.*, 2000b). K201 was shown also to inhibit apoptosis and necrosis induced by single injections of isoproterenol in rats, an effect the authors attributed to the inhibition of diastolic Ca^{2+} leak mediated by hyperphosphorylation of RyR2 (Ellison *et al.*, 2007). Spontaneous SR-mediated release events induced by elevation of extracellular Ca^{2+} levels have also been shown to be inhibited in single cell studies with K201, using both rat (Hunt *et al.*, 2007) and rabbit (Loughrey *et al.*, 2007) ventricular myocytes loaded with Ca^{2+}-sensitive fluorescent probes. Recently, Elliott *et al*. (2008) investigated the effect of K201 on diastolic SR Ca^{2+} release in intact field-stimulated rat ventricular myocytes in the presence of elevated $[Ca^{2+}]_o$ and the β-agonist isoproterenol (Elliott *et al.*, 2008). The diastolic Ca^{2+} release events, and subsequent contractile activation associated with β-adrenergic stimulation were significantly inhibited using 1.0 μM K201. How such results translate to the overall mechanical function of the whole heart however is still not clear. Kaneko and colleagues (2006) attempted to address this question using a Ca^{2+}-loading protocol (elevated $[Ca^{2+}]_o$ + norepinephrine administration) in an *in vivo* rat model (Kaneko *et al.*, 2006). While elevated $[Ca^{2+}]_o$ alone did not induce any abnormalities in left ventricular pressure, simultaneous infusion of Ca^{2+} (12 $mg.kg.min^{-1}$) and norepinephrine (30 $\mu g.kg.min^{-1}$) resulted in elevated left ventricular end diastolic pressures and the appearance of diastolic contractures which, when of sufficient magnitude exceeded aortic pressure and induced aortic valve opening during diastole. Pre-infusion of K201 prior to administration of norepinephrine significantly attenuated the rise in EDP, prevented diastolic aortic valve opening and improved mortality, effects that were not observed with diltiazem (Kaneko *et al.*, 2006). From these investigations it is clear that K201 possesses the potential to prevent the deleterious effects of Ca^{2+} overload (contractile dysfunction, apoptosis and necrosis, electrical abnormalities) which may be mediated, at least in part, by its ability to prevent diastolic Ca^{2+} release in conditions of elevated $[Ca^{2+}]_i$ and β-adrenergic stimulation. The exact mechanism of action under such conditions however is still unclear.

4.1.3 Non cardiac-specific effects of K201

The action of K201 on cardiac function in the above study by Kaneko *et al*. (2006) may be mediated in part by systemic effects of the drug. Lisy & Burnett. (2006) reported that administration of K201 in healthy anaesthetized dogs resulted in enhancement of renal haemodynamics, glomerular filtration rate and urinary sodium excretion (Lisy & Burnett, Jr., 2006). A mild reduction in mean arterial pressure was also observed. It is possible that additional vascular effects *in vivo* may play a role in the protective action of K201.

4.1.4 Aims

The aims of the work described in this chapter were to investigate the functional consequences of combined elevation in Ca^{2+} loading and β-adrenergic stimulation in the isolated working rabbit heart, and further, to examine how addition of K201 alters the contractile profile of isolated working hearts exposed to these conditions. The isolated working heart provides a model for examining the direct actions of K201 on cardiac function in the face of a pathological situation simulated using elevated [Ca^{2+}] and β-adrenergic stimulation, allowing determination of the direct effects of K201 on whole heart function without the confounding influence of systemic variables. It was hypothesized that the combination of Ca^{2+} loading and β-adrenergic stimulation would result in a decline in contractile performance ultimately detrimental to working heart function, and that application of 1.0 μM K201 would result in a rescue of contractile function as a result of its direct influence on the myocardium.

4.2 Methods

4.2.1 Isolated working heart setup

Hearts from 20 male New Zealand White rabbits were excised and perfused initially in Langendorff mode on the isolated working heart apparatus as described in the General Methods chapter section 2.1.3. After cannulation of the left atrium working heart mode was initiated. Preload was set at 7.4 mmHg and afterload set to 60 mmHg. These settings remained constant throughout the experimental protocol. Hearts were not paced and were allowed to beat spontaneously throughout the experiment.

4.2.2 Left ventricular function by pressure-volume catheterisation

A 3F *Scisense* VSL catheter with a recording electrode segment of 19 mm was advanced slowly past the aortic valves into the left ventricle to obtain pressure-volume measurements throughout the experimental protocol.

4.2.3 Solutions

Perfusion of the isolated working heart was performed using Tyrode's solution, the composition of which is described in General Methods section 2.1.3. Drugs were made 10 minutes prior to the beginning of each experiment and stored in light-shielded containers. Stock K201 solution was created by dissolving K201 in a 10% dimethyl sulfoxide (DMSO) solution to yield a concentration of 1 mM. Isoproterenol hydrochloride was dissolved in de-ionized water and diluted to yield a stock concentration of 1 mM.

4.2.4 Experimental Protocol

The protocol used was similar to that described by Kaneko *et al* (2006) in an *in vivo* rat model (Kaneko *et al.*, 2006). All hearts perfused in working heart mode underwent a protocol involving an increase in extracellular calcium concentration from 2.5 mM to 4.5 mM by addition of $CaCl_2$ to the perfusate. 5 min later hearts were then additionally perfused with 150 nM isoproterenol (ISO), a β-adrenergic agonist. Hearts were then split into two groups; the first received no further intervention (4.5 mM $[Ca^{2+}]$/ISO) whilst the second group were perfused with 1.0 μM K201 30 s after addition of ISO (4.5 mM $[Ca^{2+}]$/ISO + K201). The end of the experiment was reached when hearts were no longer

able to produce an aortic flow, resulting in a decline in coronary perfusion pressure and a precipitous decline in mechanical function as a direct result.

4.2.5 Measurement of lactate release from the isolated working heart

In a subset of hearts from each group (4.5 mM $[Ca^{2+}]$/ISO; n = 5. 4.5 mM $[Ca^{2+}]$/ISO + K201; n =3) coronary effluent samples were collected in duplicate from hearts for assessment of lactate levels. Samples were collected prior to perfusion with elevated extracellular Ca^{2+}, during the 5 minute period of perfusion with 4.5 mM $[Ca^{2+}]_o$, and at 1 minute intervals for 10 minutes following addition of ISO. All samples were collected in numbered 1.5 ml *Eppendorff* tubes, which were immediately sealed and snap frozen in liquid nitrogen. At the end of each experiment, samples were stored at -80 ºC. Lactate levels were assessed spectrophotometrically based on the method of Maughan (1982) (Maughan, 1982). Briefly, coronary effluent samples were thawed on the day of analysis and 20 µl of each sample diluted in 200 µl of 0.4 mM perchloric acid (PCA) to de-proteinize the sample. 1.1 M hydrazine buffer was prepared the day before using 1.3 g hydrazine sulphate, 5.0 g hydrazine hydrate and 0.2 g EDTA dissolved in 100 ml double distilled water, pH 9.0. The reaction mixture was prepared prior to each experiment using a combination of 10 ml hydrazine buffer, 0.5 ml NAD^+ (final concentration 5.0 mM) and 0.1 ml lactate dehydrogenase (LDH). Lactate standards of the following concentrations were prepared by dilution of an 8 mM L-lactate standard calibration solution; 0.25 mM, 1.0 mM, 2.0 mM and 3.0 mM. All standards were diluted in PCA to yield the same 1/11 dilution factor as the coronary effluent samples. 20 µl of each sample, in duplicate, was added to a 96-well plate, along with duplicates of each standard, a blank sample, and a control sample (3 mM L-lactate). 200 µl of reagent was then added to each of the wells containing a sample, and the plate was loaded into a *SPECTRAmax M2e (Molecular Devices, US)* for spectrophotometric measurement of L-lactate levels using light absorbance at 340 nm wavelength. The principle is based on the notion that conversion of L-lactate to pyruvate is linked to NAD^+ by the following reaction:

$$L-lactate + NAD^+ \xleftrightarrow{LDH} pyruvate + NADH + H^+$$

Inclusion of hydrazine in the mixture ensures the ketone (pyruvate) is removed from the reaction. By addition of excess NAD^+ the reaction can proceed to completion (from left to right). The level of NADH assessed by absorbance at 340 nm is directly proportional to

the L-lactate levels in each sample. The *SPECTRAmax M2e* created a linear calibration curve between the known lactate concentrations, with the lactate concentration of each standard calculated by the *SPECTRAmax* using the measured absorbance values of NADH at 340 nm. Values from all samples were calculated relative to the linear calibration established from the lactate standards. Samples were analysed in duplicate with the mean value of the two samples reported.

4.2.6 Determination of arrhythmogenicity

Arrythmogenicity in isolated working hearts was assessed by analysis of the ventricular pressure trace using the Heart Rate Variability (HRV) module in *LabChart* 5.5.6. HRV was set to detect a peak in the pressure trace greater than 30 mmHg as the occurrence of an electrical event synonymous with R-wave detection. Arrhythmogenicity was assessed by calculating the mean interval between successive pressure peaks (mean inter-peak interval) as well as the standard deviation of the mean interval (SD of mean inter-peak interval) from a selection of 10 consecutive pressure peaks 0, 10, 20, 50 and 200s after perfusion with isoproterenol, then at 100s intervals after this up to 600s.

4.2.7 Data recording and statistical analysis

All working heart functional data were recorded on a *Dell* PC using *LabChart* software version 5.5.6 at a sampling rate of 1000 Hz, and analysed offline using *LabChart*'s Blood Pressure Module and *LabScribe2.0* software. Quantification of ectopic electrical activity and arrythmogenicity was performed using the HRV module in *LabChart*. Coronary effluent samples were assessed for L-lactate using *SoftMax Pro* software version 5.3. All results were saved to an external hard drive. Two-sample Student's *t*-test was used to compare values between groups on a number of functional parameters. A *P*-value of < 0.05 was considered statistically significant.

4.3 Results

4.3.1 Transient effects of elevated $[Ca^{2+}]_o$ and isoproterenol

A schematic of the experimental protocol is depicted in Figure 4.1A. Figure 4.1 shows typical traces and PV loops demonstrating the transition from 2.5 mM to 4.5 mM $[Ca^{2+}]_o$ (Figure 4.1B(i) & (ii)) and addition of ISO (Figure 4.1C(i) & (ii)). Elevation of $[Ca^{2+}]_o$ from 2.5 mM to 4.5 mM (Figure 4.1B) was associated with an increase in both developed

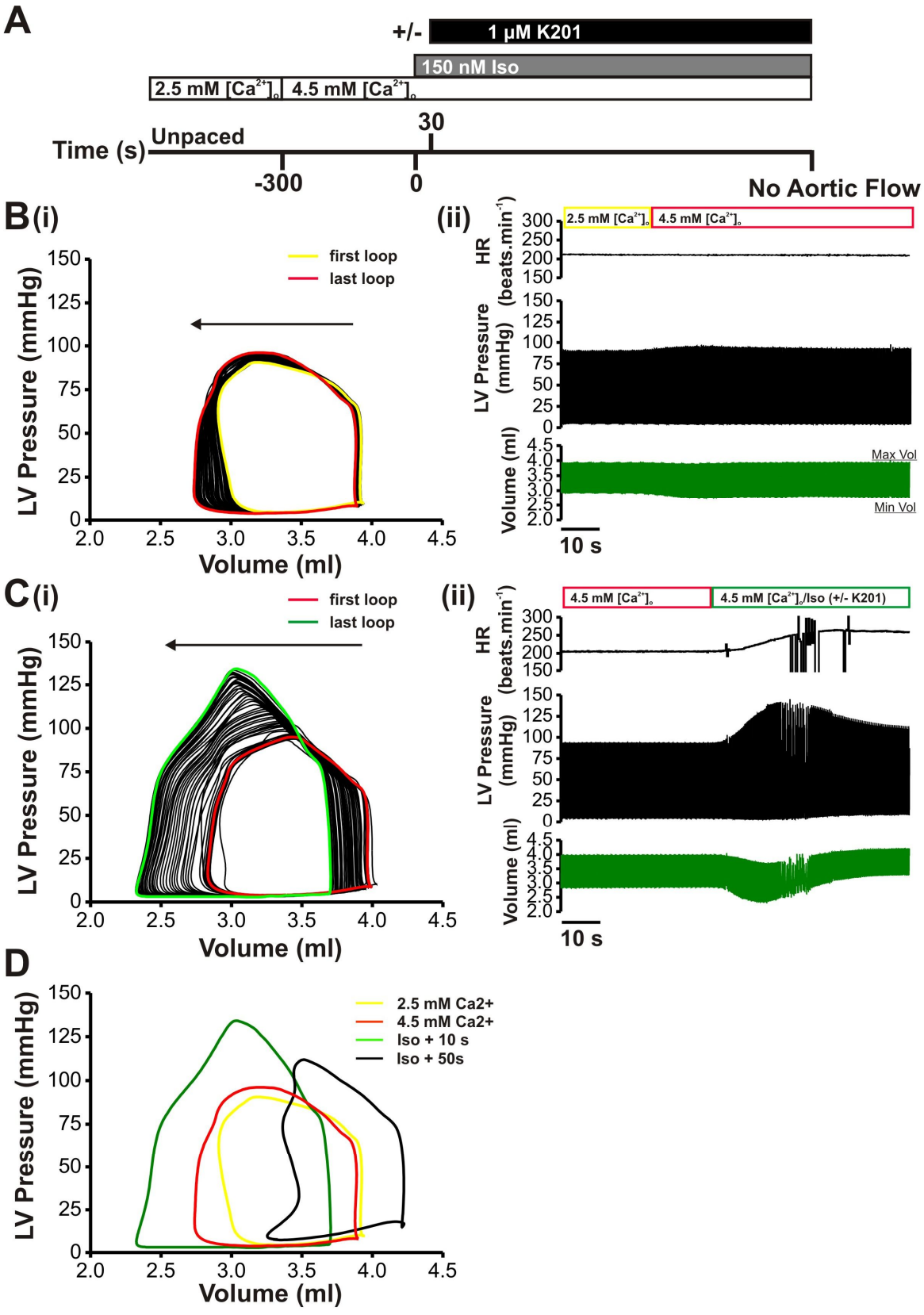

Figure 4.1 Pressure-volume traces during elevated $[Ca^{2+}]_o$ and β-adrenergic stimulation. A. Protocol diagram. Arrows on both diagrams represent the direction of change, with first and last loop in sequence colour-highlighted. B(ii) & C (ii). Representative pressure, volume and heart rate traces following elevation of $[Ca^{2+}]_o$ and addition of ISO, respectively. D. Representative steady state PV loops in 2.5 mM $[Ca^{2+}]_o$ (yellow trace), 4.5 mM $[Ca^{2+}]_o$ (red trace) and 4.5 mM $[Ca^{2+}]_o$ plus 150 nM ISO (10 s (green trace) and 50 s (black trace) after addition). Volume values were not corrected for parallel volume offset (V_p).

pressure and stroke volume. The effect was biphasic, with developed pressure rising to a peak before dropping slightly to reach a new steady state value greater than the steady state in 2.5 mM $[Ca^{2+}]_o$. Similarly addition of 150 nM ISO (Figure 4.1C) resulted in a positive inotropic response albeit of greater magnitude in comparison to that exhibited by the increased $[Ca^{2+}]_o$. Elevated $[Ca^{2+}]_o$ had no effect on heart rate (Figure 4.1B(ii); top panel) however addition of ISO was associated with an immediate increase in heart rate (Figure 4.1C(ii); top panel, mean values in Figure 4.5B(i & ii)). Representative PV loops from the steady state, elevated $[Ca^{2+}]_o$ perfusion, 10s and 50s after ISO perfusion are shown in Figure 4.1D. Mean data for contractile indices before and up to 50s after ISO perfusion are shown in the left hand panels of Figures 4.3B and 4.4A.

4.3.2 Effect of elevated extracellular calcium on systolic functional parameters

As shown from the example traces in Figure 4.1B(i) & (ii) and the mean data in Figure 4.2, increasing extracellular Ca^{2+} from 2.5 mM to 4.5 mM initially led to a transient increase in left ventricular functional parameters. LV peak pressure (Figure 4.2(i)) rose significantly by 10.69 ± 2.09 % shortly after increasing $[Ca^{2+}]_o$ before settling to a new steady state that was significantly higher than steady state peak pressure in 2.5 mM $[Ca^{2+}]_o$ (by 4.39 ± 1.88 %). Similarly, the maximum rate of rise of LV pressure was significantly increased by 23.55 ± 4.22 %, and remained significantly elevated by 20.12 ± 3.89 % in steady state *vs.* 2.5 mM $[Ca^{2+}]_o$ steady state (Figure 4.2(ii)). Heart rate was not significantly altered after elevation of $[Ca^{2+}]_o$ (data not shown).

4.3.3 Effect of elevated extracellular calcium on diastolic functional parameters

LV end diastolic pressure (LVEDP – Figure 4.2(iii)) was significantly reduced by 14.11 ± 2.84 % initially after increasing $[Ca^{2+}]_o$ but was not significantly different at higher $[Ca^{2+}]_o$ in steady state. Similarly, in comparison to steady state 2.5 mM $[Ca^{2+}]_o$, the maximum rate of LV pressure fall was significantly increased initially by 16.98 ± 6.13 % but declined back to levels comparable to 2.5 mM $[Ca^{2+}]_o$. Ventricular relaxation therefore was not significantly different once steady state was achieved.

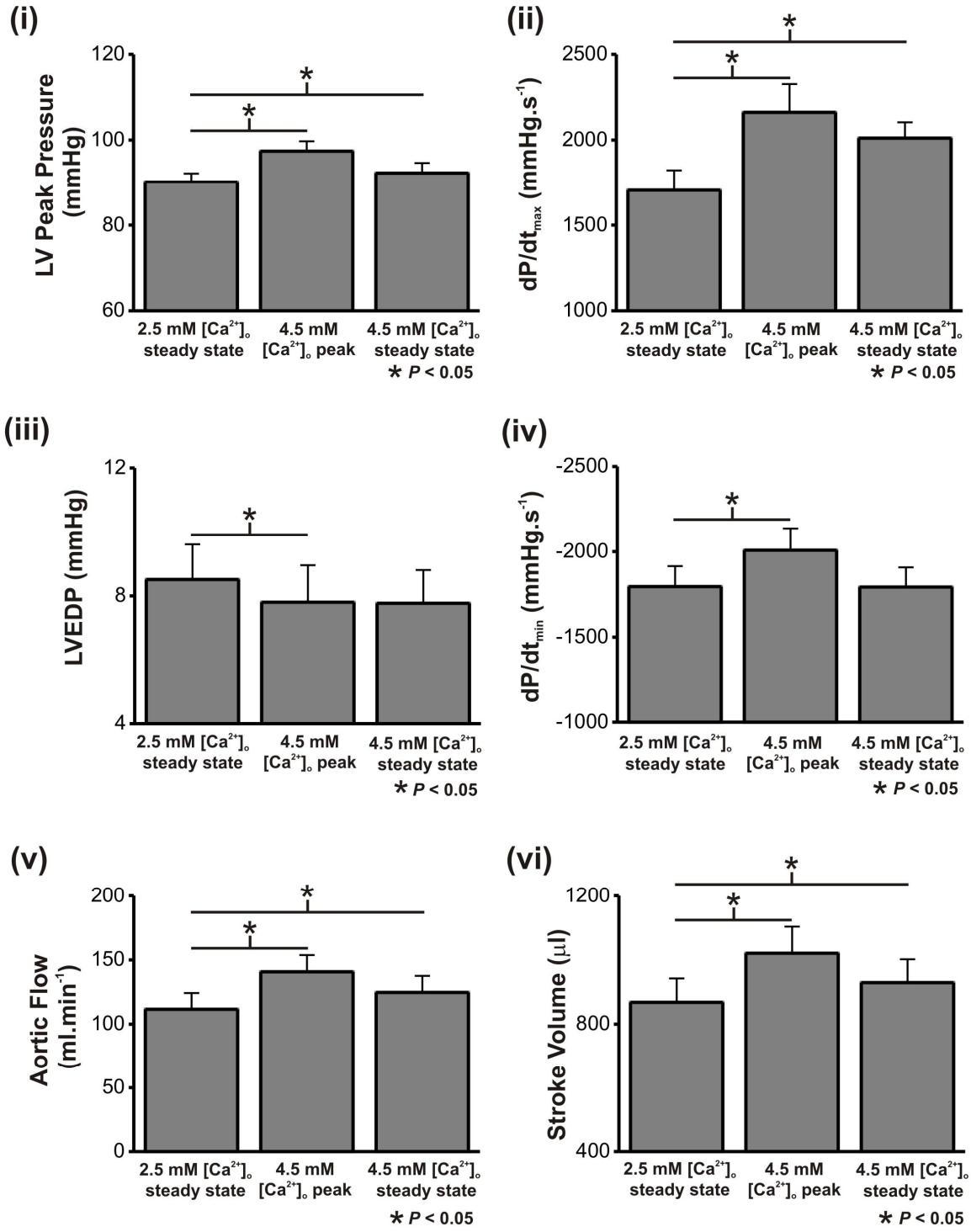

Figure 4.2 Elevation of $[Ca^{2+}]_o$ and working heart mechanical function. Indices of mechanical function during steady state 2.5 mM $[Ca^{2+}]_o$ perfusion (left bar), at peak developed pressure during the transient increase in left ventricular function following 4.5 mM $[Ca^{2+}]_o$ perfusion (middle bar), and in steady state 4.5 mM $[Ca^{2+}]_o$ (right bar). All values expressed as mean ± SEM. Significance evaluated using paired Student's *t*-test.

4.3.4 Effect of elevated extracellular calcium on volume parameters

Aortic flow (Figure 4.2(v)) was increased significantly by 28.55 ± 5.32 % in the initial period following elevation of $[Ca^{2+}]_o$ and remained significantly elevated in steady state by 13.43 ± 4.75 %. As coronary flow did not change in response to elevated $[Ca^{2+}]_o$ (data not shown), stroke volume mirrored the response of aortic flow, increasing both in the initial phase after elevation of $[Ca^{2+}]_o$ (by 18.31 ± 3.46 %) and in steady state (by 8.24 ± 3.24 %) in comparison to steady state 2.5 mM $[Ca^{2+}]_o$.

4.3.5 The effect of prolonged β-adrenergic stimulation and elevated $[Ca^{2+}]_o$ on mechanical function, and the influence of K201

Changes in the mean functional indices in the subsequent sections are expressed relative to values 50s after addition of ISO when the transient phase of the ISO perfusion has passed. The data shown only includes surviving hearts still producing an aortic flow. The number of hearts still producing an aortic flow is shown in Figure 4.3A(i) and expressed as a function of time post-ISO perfusion.

While the addition of ISO produced a transient increase in cardiac performance (Figure 4.3B(i-iv), left hand panels) that was similar in both groups, the net effect of ISO perfusion alone was an impaired cardiac function with only 5 out of 11 hearts still producing an aortic outflow within the first 600 s (Figure 4.3A(i)). In contrast, addition of 1.0 μM K201 led to all hearts sustaining an aortic flow within the first 600 s and prolonged the time before aortic flow ceased by 317.63 % (Figure 4.3A(ii)).

4.3.5.1 The effect of K201 on systolic and diastolic parameters following elevated $[Ca^{2+}]_o$ and β-adrenergic stimulation

Hearts perfused solely with elevated $[Ca^{2+}]_o$ and ISO demonstrated a decline in peak pressure and dP/dt_{max} relative to function at 50s post-ISO (Figures 4.3B(i) & (ii)). K201 prevented the subsequent decline in function in both parameters measured at 600s post-ISO (87.39 % vs. 66.48 %; with (n=9) *vs.* without K201 (n=5) and 97.37 % *vs.* 68.27 %; with *vs.* without K201 respectively, $P<0.05$). The protocol did not result in a significant change in EDP (Figure 4.3B(iii)) but K201 improved relaxation as measured by dP/dt_{min} (Figure

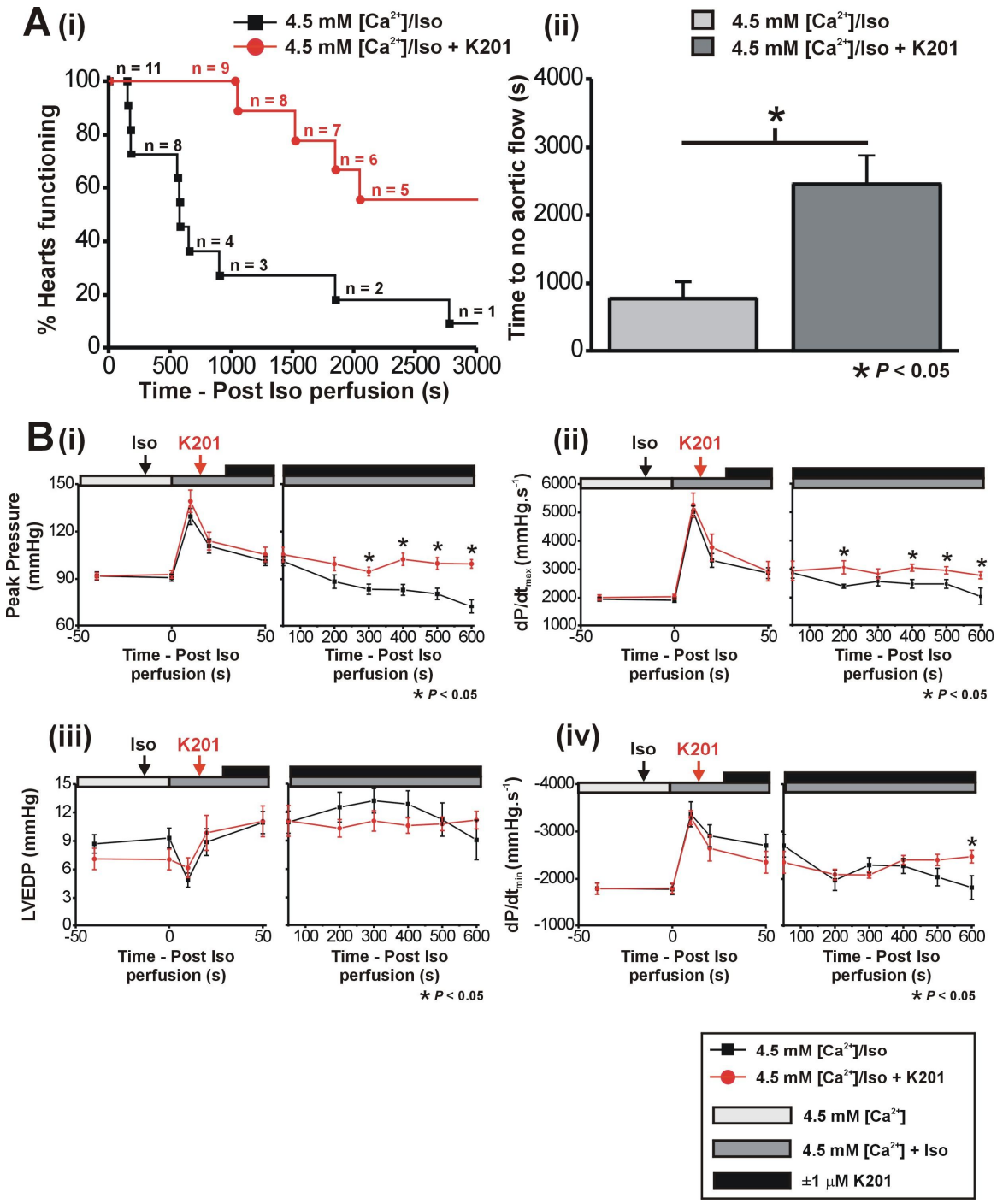

Figure 4.3 Mechanical function during 600 s of elevated $[Ca^{2+}]_o$ and ISO perfusion (± K201). A(i). Survival plot showing % of hearts functioning in each group during 3000 s (50 min) of ISO perfusion with n-value at each stage of protocol indicated. (ii) Mean functional time during ISO perfusion in both groups. B(i-iv); Systolic and diastolic functional parameters 50s before and after perfusion with ISO (left panels) and up to 600s after perfusion with ISO (right panels). Hearts without K201 = black squares; with K201 = red circles. All values expressed as mean ± SEM. Significance between groups evaluated with unpaired Student's *t*-test.

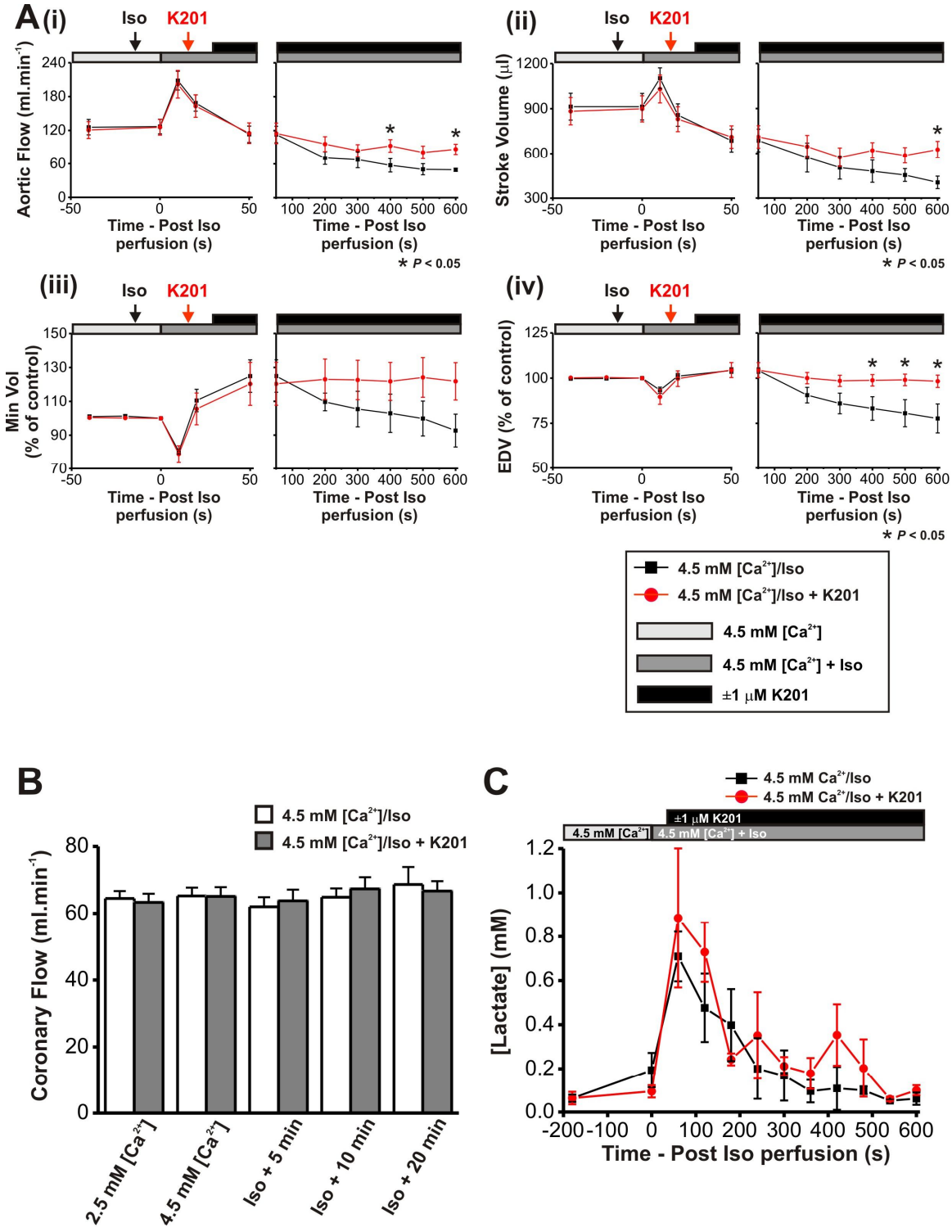

Figure 4.4 Volume indices during 600s of elevated $[Ca^{2+}]_o$ and ISO perfusion (± K201). A(i-iv); Volume parameters 50 s before and after perfusion with ISO (i) and up to 600s after perfusion with ISO (ii). B. Coronary flow at several stages throughout the protocol. C. Lactate concentration measured from coronary effluent samples. All values expressed as mean ± SEM. Significance between groups evaluated with unpaired Student's *t*-test.

4.3B(iv)) thus preventing a decline in dP/dt_{min} at 600s post-ISO (105.27 % vs. 64.97 %; with (n=9) *vs.* without K201 (n=5), $P<0.05$).

4.3.5.2 The effect of K201 on volume parameters during β-adrenergic stimulation and elevated $[Ca^{2+}]_o$

Subsequent to a transient rise 15s post-ISO, aortic flow (Figure 4.4A(i)) decreased 600s post-ISO, however, K201 limited the degree to which aortic flow declined at 600s post-ISO (78.61 % vs. 37.52%; with (n=9) *vs.* without K201 (n=5), $P<0.05$). This pattern was similar to the assessment of stroke volume (Figure 4.4A(ii)) 600s post-ISO (93.55 % vs. 60.62%; with (n=9) *vs.* without K201 (n=5), $P<0.05$). Coronary flow (Figure 4.4B) was not significantly different between groups at 600s post-ISO (66.67 ± 2.96 *vs.* 68.67 ± 5.21 $ml.min^{-1}$). Similarly lactate concentrations (Figure 4.4C) measured from the coronary perfusate were not significantly different between groups 600s post-ISO (0.100 ± 0.023 mM vs. 0.061 ± 0.028 mM; with (n=3) vs. without K201 (n=3).

4.3.6 Arrythmicity following elevated extracellular Ca^{2+} and β-adrenergic stimulation, and the influence of K201

Prior to ISO perfusion, contraction appeared regular under sinus rhythm (Figure 4.5A(i)) and inter-peak interval variability was low. At 600s post-ISO irregular contractile function was present (Figure 4.5A(ii)) which was reduced in K201 (Figure 4.5A(iii)). There were no significant differences in mean inter-peak interval between groups at any point in the protocol (Figure 4.5B(i) & (ii)). The standard deviation of the mean inter-peak interval (Figure 4.5C) was however significantly lower at 600s post-ISO in hearts perfused with K201 (27.29 ± 7.91 ms vs. 66.07 ± 17.91 ms; with (n=9) *vs.* without K201 (n=5); $P < 0.05$). This result suggests that K201 was able to partially reduce the increase in mean inter-peak interval variability.

4.3.7 Investigating the difference in the timing of addition of K201 on cardiac function

In a separate subset of hearts, K201 was applied at a later time point during the protocol (300s *vs.* 30s post-ISO). This was performed in order to establish whether K201 prevented deterioration of cardiac functional parameters if applied at a later stage of the protocol where decline in cardiac function had already begun. Similar to application of K201 at 30s

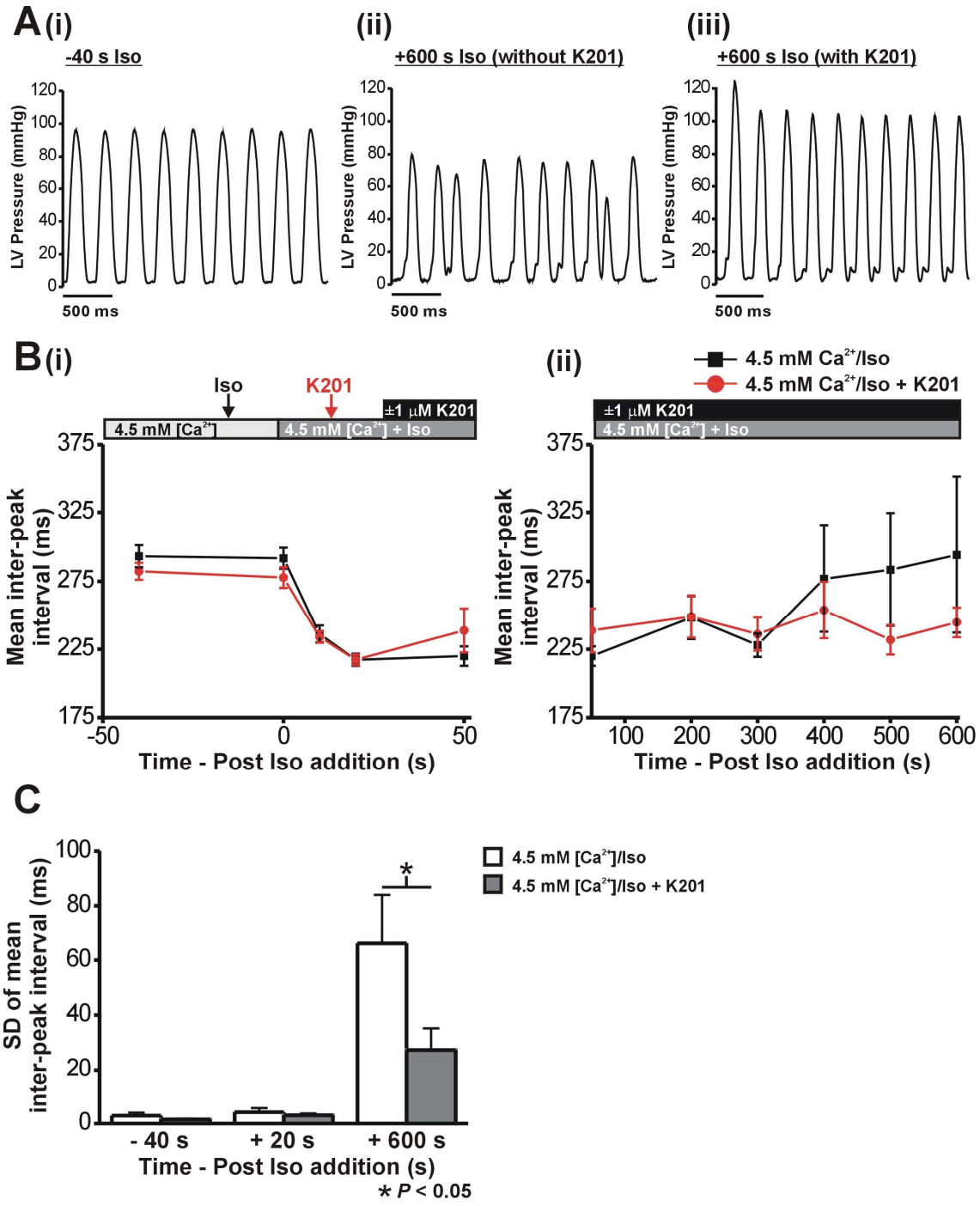

Figure 4.5 Arrhythmicity following perfusion with elevated $[Ca^{2+}]_o$ and β-adrenergic stimulation. A. Representative pressure recordings 40s prior to ISO perfusion (i), 600s after ISO perfusion without (ii) and with K201 (iii). B. Mean inter-beat interval during the 600s of ISO perfusion in K201 treated *vs.* untreated hearts. C. Standard deviation of the mean inter-peak interval in K201 treated *vs.* untreated hearts. All data expressed as mean ± SEM. Significance between groups evaluated with unpaired Student's *t*-test.

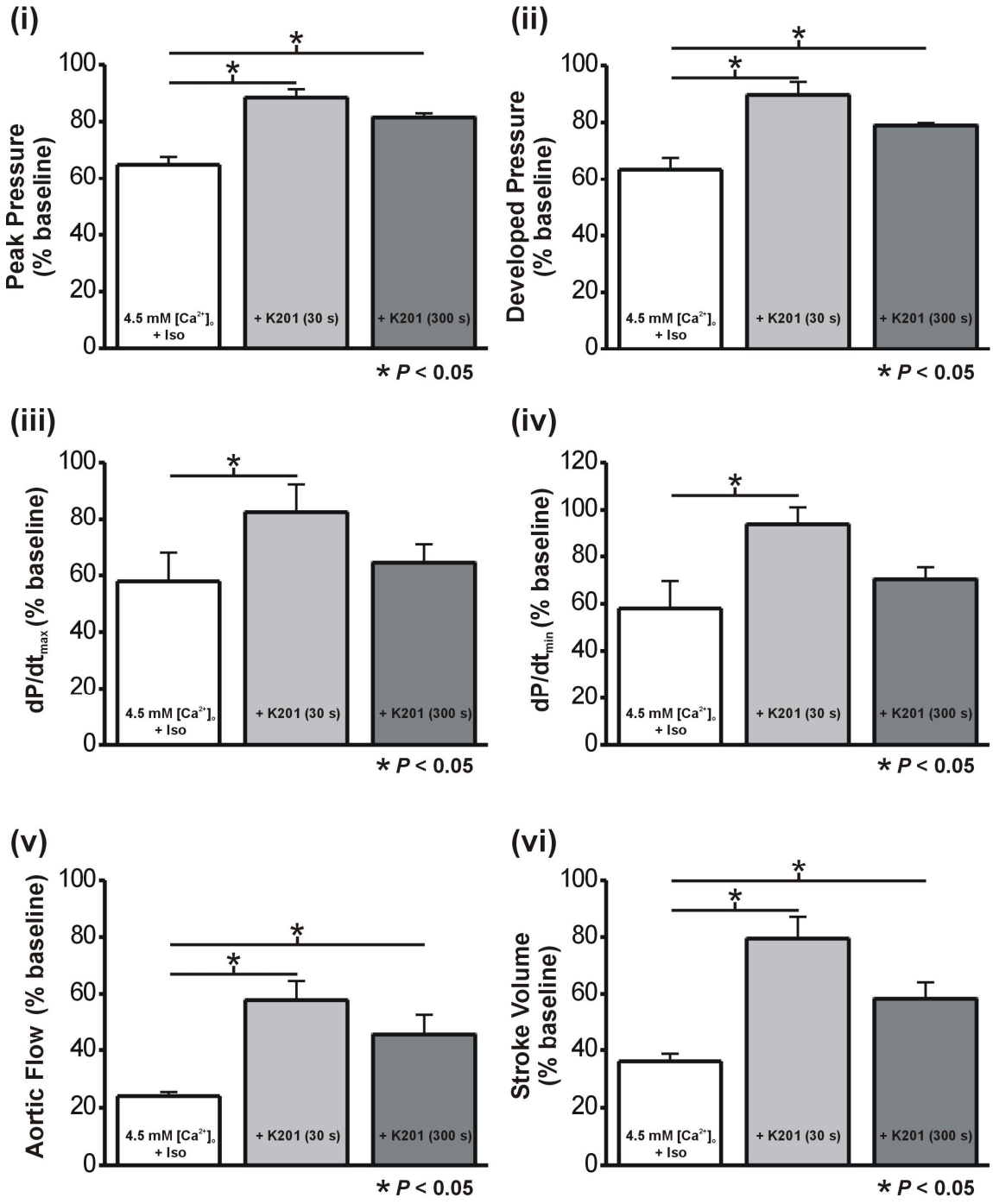

Figure 4.6 Cardioprotection Preservation of mechanical function after perfusion with K201 at 30s or 300s. Mechanical function and volumes after 600s ISO perfusion expressed as % of values following 20s ISO perfusion. 4.5 mM $[Ca^{2+}]_o$ + ISO; n=4; + K201 (30s); n=9; + K201 (300s); n=3. All values expressed as mean ± SEM. Significance between groups evaluated with unpaired Student's *t*-test.

post-ISO, application of K201 at 300s post-ISO significantly limited the decline in peak pressure, aortic flow and SV when compared to hearts without K201 (81.49 ± 1.48 % vs. 64.53 ± 4.20 %, 45.67 ± 5.97 % vs. 25.10 ± 2.49 %, and 58.29 ± 3.79 % vs. 40.29 ± 4.72 %; $P<0.05$, Figure 4.6) but had no effect on the decline in dP/dt_{max} or dP/dt_{min} induced by the protocol.

4.4 Discussion

4.4.1 K201 attenuates the negative inotropic effects associated with elevated $[Ca^{2+}]_o$ and simultaneous β-adrenergic stimulation

The present study aimed to assess the ability of K201 to preserve contractile function in a whole heart model of left ventricular dysfunction induced by elevated $[Ca^{2+}]_o$ with β-adrenergic stimulation. The use of an isolated working heart model allowed the assessment of ventricular mechanical function without the possibility of confounding systemic effects of any of the compounds used. Increasing perfusate $[Ca^{2+}]_o$ from 2.5 mM to 4.5 mM led to a steady state increase in a number of functional parameters in the isolated working heart, including left ventricular peak pressure, dP/dt_{max} and stroke volume (Figure 4.2), and by itself improved left ventricular function. Administration of isoproterenol in the isolated working rabbit heart following 5 min of increased $[Ca^{2+}]_o$ perfusion in the present study initially caused a transient positive inotropic effect with a concomitant increase in cardiac output. Following this initial (10-15s) phase, function declined quickly such that after 600s (10 min) of isoproterenol perfusion only 5 of the 11 hearts perfused with elevated Ca^{2+} and ISO alone were able to sustain an aortic flow sufficient to maintain coronary perfusion pressure at 60 mmHg. As shown in Figures 4.3 and 4.4 however, in hearts perfused with K201 30s after ISO perfusion functional decline was significantly attenuated, allowing hearts to maintain aortic flow for a significantly longer period of time.

4.4.2 Possible mechanisms of action of K201 following elevated $[Ca^{2+}]_o$ with β-adrenergic stimulation

There are a number of possible mechanisms by which K201 may have elicited its cardioprotective effects in the setting of elevated $[Ca^{2+}]_o$ and β-adrenergic stimulation. K201 has been shown to attenuate the formation of myocardial lesions and development of contracture induced by administration of epinephrine or caffeine in a whole heart rat Langendorff preparation (Kaneko, 1994). The use of Ca^{2+}-sensitive fluorophores in isolated whole heart models of ischaemia-reperfusion injury and prolonged myocardial preservation indicated that K201 significantly attenuated the rise in $[Ca^{2+}]_i$ associated with reperfusion (Hachida *et al.*, 1999; Inagaki *et al.*, 2000b). K201 has also been shown to limit spontaneous SR-mediated Ca^{2+} release events in isolated myocytes from both rat and

rabbit left ventricle (Hunt *et al.*, 2007; Loughrey *et al.*, 2007), as well as eliciting significant attenuation of diastolic Ca^{2+} release events in field-stimulated rat myocytes subjected to perfusion with 4.5 mM $[Ca^{2+}]_o$ and β-adrenergic stimulation (Elliott *et al.*, 2008). Given that K201 has been demonstrated to have such potent effects in experimental models associated with elevation of $[Ca^{2+}]_i$ it is likely that some of its cardioprotective effects in the current study may be attributed to a reduction in cellular Ca^{2+} overload. Consistent with this, K201 has been shown to target a number of intracellular Ca^{2+} handling components. 1.0 μM K201 significantly inhibits I_{CaL} in guinea pig and rat ventricular myocytes by 20 and 22 % respectively (Inagaki *et al.*, 2000b; Kimura *et al.*, 1999) and in rabbit pulmonary vein cardiomyocytes by 38 % (Chen *et al.*, 2008), although in rabbit ventricular myocytes a significant inhibition was reported at 3.0 μM but not 1.0 μM (Loughrey *et al.*, 2007). Loughrey *et al*. (2007) also demonstrated a significant inhibition of SR Ca^{2+} uptake via SERCA2a in rabbit ventricular myocytes at 1.0 μM (V_{max} reduced to 88 % of control) although at this concentration SR Ca^{2+} content was not altered (Loughrey *et al.*, 2007). While the possibility exists that K201 interacts directly with the β-adrenergic receptor to inhibit the action of isoproterenol the findings of Ellison *et al*. (2007) would suggest this is not the case as 1.0 μM K201 was demonstrated to prevent cell apoptosis and necrosis in adult rat ventricular myocytes exposed to 10 μM ISO without significantly altering the ISO-induced activation of protein kinase A (Ellison *et al.*, 2007).

4.4.2.1 Stabilisation of the cardiac Ryanodine receptor by K201 may underlie the protective effect following elevated $[Ca^{2+}]_o$ and β-adrenergic stimulation

With respect to intracellular Ca^{2+} handling, one of the most widely documented effects of K201 is its ability to stabilize the cardiac ryanodine receptor (RyR2) in its closed state, thereby inhibiting potentially arrhythmogenic Ca^{2+} release from the SR (Chen *et al.*, 2008; Kohno *et al.*, 2003; Wehrens *et al.*, 2004; Yano *et al.*, 2003). Increased spontaneous Ca^{2+} release during the diastolic period may produce heterogenous myocyte contraction, reducing the number of myocytes available for recruitment during the next stimulated beat and decrease the amplitude of contraction (Stern *et al.*, 1988). An increase in diastolic $[Ca^{2+}]_i$ levels would also be expected, which may also result in an increased diastolic tone. Reduction of RyR2 open probability has been proposed as a mechanism for the prevention of diastolic Ca^{2+} release and the potentiation of systolic release (Venetucci *et al.*, 2006). Venetucci *et al*. (2006) demonstrated that application of 1 μM ISO in rat ventricular myocytes was sufficient to cause spontaneous Ca^{2+} waves in steady state. Stimulated Ca^{2+}

transients immediately proceeding a Ca^{2+} wave were significantly reduced in amplitude and decreasing RyR2 open probability (P_o) with the pharmacological agent tetracaine (50 μM) during ISO stimulation not only significantly attenuated Ca^{2+} waves but also increased the systolic Ca^{2+} transient (Venetucci *et al.*, 2006). Ellison *et al.* (2007) noted that hyperphosphorylation of the RyR2 appeared critical to the induction of apoptosis mediated by a single dose of isoproterenol (5 $mg.kg^{-1}$, ~ 370 μM) in rat hearts (Ellison *et al.*, 2007). Treatment with 1.0 μM K201 led to a reduction in PKA and CaMKII phosphorylation of the RyR2 and a reduction in ISO-induced apoptosis. Elliott *et al.* (2008) also demonstrated that a similar Ca^{2+} loading protocol to that used in the current investigation led to the appearance of Ca^{2+} waves and after-contractions in intact field-stimulated rat cardiomyocytes which were significantly attenuated upon application of 1.0 μM K201 (Elliott *et al.*, 2008). Taken together, the net effect of K201 in the present study may involve reduction of $[Ca^{2+}]_{i,}$ and an inhibition of the negative inotropic effects associated with excessive $[Ca^{2+}]_i$ loading. In the present study elevated $[Ca^{2+}]_o$ and β-adrenergic stimulation led to the appearance of ventricular ectopic beats. Application of K201 in this model resulted in a reduction in the mean inter-peak interval variability, as assessed by standard deviation of the mean inter-peak interval.

4.4.2.2 Effects of late versus early K201 perfusion on cardioprotection

In the current study, K201 was able to exert a cardioprotective effect when administered shortly (30s) after addition of isoproterenol, however it was unclear whether or not the predominant mechanism for the reduction in inotropy induced by elevated $[Ca^{2+}]_o$ and ISO was due to the inhibition of reversible events such as Ca^{2+} wave production, or the result of irreversible cellular damage. This was tested by administration of K201 in a subset of hearts already exposed to 5 minutes (300s) of ISO perfusion. It was found that K201 administered at this time point resulted in a significant rescue in some of the measured parameters including peak pressure and stroke volume. Recovery of function was not significant in the rates of change in left ventricular pressure, indicating that cardioprotection was not as effective as it was in hearts perfused with K201 30 s after ISO addition. Taken together this demonstrates that K201 was able to reverse some of the cellular dysfunction induced by elevated $[Ca^{2+}]_o$ and ISO, suggesting that, up until 5 minutes after perfusion of ISO at least, that irreversible cellular damage (mitochondrial membrane permeability transition, cellular apoptosis, cellular necrosis) was not the primary mechanism of left ventricular dysfunction.

4.4.3 Detrimental effects of isoproterenol administration include mechanisms independent of Ca^{2+} overload

Ca^{2+} overload has been shown to be critical to the detrimental effects of excessive β-adrenergic stimulation by catecholamines, as well as sympathomimetics such as isoproterenol (Fleckenstein *et al.*, 1983; Mann *et al.*, 1992; Rona, 1985). Accompanying the negative inotropic effects of catecholamine-induced Ca^{2+} overload however is the development of myocardial lesions, cellular necrosis (Fleckenstein *et al.*, 1983) and apoptosis (Shizukuda *et al.*, 1998). Studies of excessive β-adrenergic stimulation on isolated cultured myocytes and in whole heart preparations have revealed additional effects of excessive β-adrenergic stimulation that may contribute to myocardial injury (and ultimately loss of inotropy) independent of Ca^{2+} overload (Bloom & Davis, 1972; Dhalla *et al.*, 1978; Mohan & Bloom, 1999; Ramos *et al.*, 1984; Somani *et al.*, 1970; Yates *et al.*, 1981).

4.4.3.1 Hypoperfusion of the ventricular myocardium following isoproterenol treatment

Somani *et al*. (1970) investigated the influence of ISO perfusion on capillary blood flow using an isolated supported canine heart preparation, in which an *ex vivo* heart is supplied with blood and nutrients from an anaesthetized support animal. The extraction of the radio-labeled isotope Rubidium-86 from the blood was used as a marker for determining the proportion of total coronary blood flow that reaches the capillary beds. The investigation demonstrated that ISO administration (0.05-0.1 $\mu g.min^{-1}$) led to a drop in coronary artery perfusion pressure and a reduction in the extraction of Rubidium-86 from the coronary blood irrespective of total coronary blood flow (Somani *et al.*, 1970). This effect was attributable in part to the increase in heart rate and to a lesser extent the increase in left ventricular systolic pressure following ISO administration. Because the inner layers of the myocardium are perfused primarily during diastole, decreasing the diastolic interval may reduce the total blood flow through these areas of the heart. In addition, the authors suggested that the increase in left ventricular systolic pressure and heart rate increases extravascular resistance, leading to a redistribution of coronary blood flow to the detriment of the endocardial and sub-endocardial layers. No alterations in global coronary flow were noted in the current study however this does not eliminate the possibility of inner myocardial layers becoming hypoperfused.

4.4.3.2 Oxidation of isoproterenol and free-radical damage

Negative inotropic and necrotic effects of endogenous catecholamines, as well as isoproterenol have also been attributed to the formation of oxidation products (Rona, 1985; Yates *et al.*, 1981). Catecholamine's (epinephrine, norepinephrine) as well as isoproterenol have the ability to oxidize to *o*-quinones in the presence of oxidizing agents or alkalis (Bindoli *et al.*, 1989; Remiao *et al.*, 2002). These intermediary products undergo an irreversible cyclisation reaction with the resultant leukoadrenochrome being further oxidized either by oxidizing agents or other *o*-quinones to form adrenochrome (Bindoli *et al.*, 1989). Dhalla *et al.* (1978) demonstrated that spontaneously oxidized isoproterenol caused myocardial lesion formation and contractile dysfunction, the extent of which was exacerbated in a dose-dependent manner (Dhalla *et al.*, 1978). Ramos *et al.* (1984) found that toxic concentrations of ISO (> 24 μM) induced a biphasic increase in Ca^{2+} uptake in cultured rat cardiomyocytes, the secondary phase of which occurred between 7 and 10 min post-ISO addition (absent with treatment of 240 nM) and was attenuated by antioxidant treatment (ascorbic acid and sodium bisulfite) but not by propanolol or verapamil (Ramos *et al.*, 1984). Persoon-Rothert *et al.* (1989) demonstrated that isoproterenol-induced myocardial necrosis following 6 hour incubation with 0.5-2.5 mM isoproterenol in cultured neonatal rat cardiomyocytes, assessed by measurement of α-hydroxybutyrate dehydrogenase (α-HBDH) release from the cytoplasm, could be significantly attenuated with the use of free-radical scavengers and substances which inhibit isoproterenol oxidation (Persoon-Rothert *et al.*, 1989). Furthermore, β-adrenoceptor antagonism with propanolol did not reduce the levels of α-HBDH release, while exposure of cells to the non-oxidising β-adrenoceptor agonist fenoterol did not significantly alter α-HBDH release in comparison to control myocytes. It is unclear to what extent this mechanism contributes to the contractile dysfunction seen in the current study. In general studies investigating isoproterenol-induced myocardial injury have used single injections or continuous doses that are several orders of magnitude greater than those used in the current investigation (Bloom & Davis, 1972; Dhalla *et al.*, 1978; Mohan & Bloom, 1999) and as such may not be expected to induce a significant level of oxidative stress through this mechanism. In addition, studies such as those conducted by Persoon-Rothert *et al.* (1989) involve incubation periods of several hours, and are unlikely to account for the decline in mechanical function seen within a 10 min period in the current investigation. This could have been investigated in the current experimental protocol by using agents which prevent oxidation of ISO and comparing functional indices against the heart treated with elevated [Ca^{2+}] and ISO only.

4.4.4 Metabolism and mitochondrial function during Ca^{2+} loading and β-adrenergic stimulation – Influence of K201

The mitochondria have been demonstrated to be susceptible to Ca^{2+} overload, resulting in a reduction in high energy phosphate production, intracellular ATP levels and exhaustion of intracellular energy stores (Fleckenstein *et al.*, 1983; Miyata *et al.*, 1992). Moreover, mitochondrial Ca^{2+} overload occurring during ischaemia and reperfusion has been implicated in opening of the membrane permeability transition pore and the subsequent signaling cascade that leads to triggered cell death (apoptosis) and necrosis (Toda *et al.*, 2007). In the current study lactate release from the isolated working heart was used as a measure of anaerobic respiration before and after the addition of isoproterenol. It was found that lactate concentration increased in the initial 60 -120s following ISO perfusion, but that lactate release declined beyond this point back to pre-ISO levels in both groups, with no detectable difference between groups. It is possible that lactate release was too indirect a measure of the respiratory state of the muscle and that other marker's of energy metabolism may have revealed a difference between the groups. Kawabata *et al*. (2000) measured changes in ATP, inorganic phosphate (P_i) and phosphocreatine (PCr) levels during ischaemia and reperfusion in the isolated rabbit heart by ^{31}P-NMR spectrometry, revealing a preservation of ATP levels during ischaemia and reperfusion, as well as an attenuation of rising P_i during ischaemia following application of 1.0 μM K201 (Kawabata *et al.*, 2000). Direct measurement of ATP levels in the isolated working rabbit heart therefore may have revealed a significant effect of K201 on myocardial metabolism. K201 has been shown to exhibit cardioprotective properties in ischaemia-reperfusion studies, and this protective effect has been associated with an attenuation of intracellular Ca^{2+} overload (Inagaki *et al.*, 2000b) as well as activation of protein kinase C (PKC) (Inagaki *et al.*, 2000a; Ito *et al.*, 2000). PKC has been implicated in the signaling cascade involved in ischaemic preconditioning (Ytrehus *et al.*, 1994), and this may be related to the activation of mitochondrial ATP-sensitive K^+ channels (K_{ATP}) (Korge *et al.*, 2002; Liu *et al.*, 1999). Ito *et al*. (2000) demonstrated that the cardioprotective effect of K201 could be significantly attenuated by application of the PKC inhibitor chelerythrine, or by selective blockade of mitochondrial K_{ATP} channels with 5-hydroxydecanoic acid (5-HD) (Ito *et al.*, 2000). Inagaki *et al*. (2000) noted that translocation of PKC-δ to the plasma membrane was key to K201's cardioprotective effect in a rat model of ischaemia reperfusion injury as selective blockade of this isoform prevented any myocardial protection by K201 (Inagaki *et al.*, 2000a). PKC was not investigated in the current study but provides a potential mechanism for future investigations using this protocol. A number of inhibitors of PKC

(chelerythrine, GF109203X) previously used in isolated Langendorff-perfused heart preparations are available that could be applied to the isolated working rabbit heart to further investigate this potential mechanism. K201 therefore may well exert at least an indirect protective effect on the mitochondria through activation of a specific PKC isoform however this was not investigated in the current study, and warrants further investigation.

4.5 Summary

Perfusion of isolated working rabbit hearts with high $[Ca^{2+}]_o$ and the β-adrenergic agonist isoproterenol led to a decline in left ventricular contractility and cardiac output such that the majority of hearts could not maintain sufficient output to sustain function beyond 600s of ISO perfusion. Application of K201 shortly after ISO perfusion (30s) led to a significant preservation of mechanical function and cardiac output allowing hearts to function for a significantly longer period of time. Application of K201 at a later time in the protocol (300s) led to a significant rescue of function, indicating a reversible disruption of intracellular function was mainly responsible for the decline in inotropy. From the effects of K201 documented in the literature an attenuation of cellular Ca^{2+} overload is one likely mechanism for this cardioprotective response, although the influence of mitochondria-specific effects have not been fully elucidated and may play a role.

5 Acute effects of K201 on cardiac function in a rabbit model of left ventricular dysfunction following coronary artery ligation

5.1 Introduction

Current definitions of heart failure describe the condition as an impairment of cardiac function resulting in an inability of the heart to maintain a cardiac output sufficient to meet the metabolic demands of the body (Braunwald E, 2008; Ritter & Neyses, 2003). Abnormalities in Ca^{2+} handling and E-C coupling mechanisms are a common finding in cardiac disease states, with key alterations in heart failure including a reduction in SR Ca^{2+} uptake (Beuckelmann *et al.*, 1995; Hasenfuss & Pieske, 2002), upregulation of NCX (Pogwizd *et al.*, 1999a), and altered RyR2 function (Yano *et al.*, 2003), all of which are thought to contribute to a reduced SR Ca^{2+} content and a reduction in the size of the systolic Ca^{2+} transient (Bers *et al.*, 2003; Houser *et al.*, 2000). Recently a great deal of attention has been focused on the concept of altered RyR2 function, and the enhancement of diastolic Ca^{2+} leak from the SR in heart failure although the contribution of this mechanism to the overall contractile dysfunction in heart failure remains controversial (Belevych *et al.*, 2007; Bers *et al.*, 2003; George, 2008; Tateishi *et al.*, 2009). The 1, 4-benzothiazepine derivative K201 has, in a number of studies, been demonstrated to reduce RyR2-mediated SR Ca^{2+} leak and spontaneous SR-mediated triggered activity in ventricular myocytes (Hunt *et al.*, 2007; Loughrey *et al.*, 2007; Yano *et al.*, 2003) and may therefore prove beneficial as part of therapeutic treatment strategies for heart failure.

5.1.1 Beneficial effects of K201 in animal models of heart failure

Several investigations have reported on the beneficial effects of K201 in animal models of heart failure (Kohno *et al.*, 2003; Wehrens *et al.*, 2005; Yano *et al.*, 2003). In a canine pacing-induced heart failure model, K201 was shown to be effective in preventing the development of left ventricular remodeling following a 4 week period of chronic right ventricular pacing, resulting in significantly improved left ventricular function compared to untreated, paced animals (Yano *et al.*, 2003). The study identified several critical elements of K201's protective effects in this particular heart failure model; the pacing induced model of heart failure resulted in a dissociation of FKBP12.6 from the RyR2, leading to an increase in Ca^{2+} leak through the channel. K201, by restoring the binding of FKBP12.6 to the RyR2 led to a reduction in the Ca^{2+} leak from failing SR vesicles. In SR vesicles from failing hearts not treated with K201, there was an upregulation of RyR phosphorylation by PKA in comparison to unpaced controls. In K201 treated SR vesicles from failing hearts however this 'hyperphosphorylated' state was reversed. The study also found that while K201 had no effect on Ca^{2+} uptake in normal or failing SR vesicles when applied acutely,

SR vesicles from animals treated throughout the 4 week pacing period demonstrated a significantly greater level of SR Ca^{2+} uptake, as well as higher SERCA2a protein expression compared to those from untreated heart failure animals (Yano *et al.*, 2003). The finding that K201 has no effect on SR Ca^{2+} uptake is in contrast to a recent report by Loughrey *et al.*, (2007) who demonstrated a reduction in maximal SR Ca^{2+} uptake rate (V_{max}) to 88 % of control at 1.0 μM K201 using rabbit ventricular myocytes (Loughrey *et al.*, 2007). Kohno *et al.* (2003) also found that in SR vesicles from failing hearts, as well as from normal control hearts treated with 30 μM FK506 (to dissociate FKBP12.6 from the RyR2), the rate of Ca^{2+} release induced by polylysine was significantly reduced compared to untreated controls (Kohno *et al.*, 2003). Treatment with K201 in both instances led to a restoration of Ca^{2+} release kinetics towards control values. Increased Ca^{2+} spark frequency in SR vesicles from pacing-induced heart failure dogs in comparison to controls has been demonstrated by Tateishi *et al.* (2009) (Tateishi *et al.*, 2009). Application of 0.3 μM K201 significantly reduced Ca^{2+} spark frequency and led to an increase in Ca^{2+} spark amplitude. The investigators concluded that this may be a crucial factor in the action of K201 to improve contractile function in the failing heart. Boyden *et al.*, (2004) reported that K201 was effective in limiting the appearance of arrhythmogenic micro Ca^{2+} waves in Purkinje fibres from canine hearts 48 hours after myocardial infarction (MI) (Boyden *et al.*, 2004). The effects of K201 on murine cardiac function were also investigated using a ligation induced myocardial infarction model (Wehrens *et al.*, 2005). Cardiac function in wild-type (WT) mice 4 weeks after MI was significantly improved following continuous infusion of K201 (0.5 $mg.kg^{-1}.h^{-1}$) compared to untreated WT MI mice. In FKBP12.6 $(calstabin2)^{-/-}$ mice however K201 did not demonstrate any significant influence on left ventricular haemodynamics, with post-MI function in FKBP12.6$^{-/-}$ mice unchanged in comparison to WT MI mice. The authors attributed this effect to stabilization of the RyR2 by K201 which led to a reduced open probability and abolition of channel subconductance state. Additionally, as these effects were not observed in FKBP12.6$^{-/-}$ mice it was concluded that re-association of FKBP12.6 with the RyR2 is a prerequisite for the normal action of K201. To date no reports have been published describing the influence of K201 on cardiac function in healthy animals.

5.1.2 Non-cardiac specific effects of K201

K201 has been shown to affect function of non-cardiac tissues including skeletal muscle and in the kidney (Almassy *et al.*, 2008; Lisy & Burnett, Jr., 2006; Wehrens *et al.*, 2005). Wehrens *et al.* (2005) reported an improvement in skeletal muscle function (as assessed by

reduced rate of fatigue) in both wild-type and FKBP12.6$^{-/-}$ mice 4 weeks following MI, suggesting that K201 elicited a beneficial effect on skeletal muscle function independent of an improvement in cardiac function (Wehrens *et al.*, 2005). This study however did not address the influence of K201 treatment on cardiac function in non-failing wild type mice. The effects of K201 on RyRs in the kidney and renal function was investigated by Lisy & Burnett (2006) (Lisy & Burnett, Jr., 2006). At the largest dose used in the investigation (0.5 mg.kg^{-1}.min^{-1}, approximately 13.5 μM) K201 led to a significant enhancement of glomerular filtration rate and renal blood flow. These changes could not be attributed to an increase in cardiac output, as K201 at this dose significantly lowered cardiac output by ~26% (Lisy & Burnett, Jr., 2006). K201 was also found to be natriuretic and diuretic, leading to an increased urinary volume and sodium excretion. The authors suggested the combination of these effects may prove beneficial in the setting of congestive heart failure by limiting fluid retention and improving renal function, however this observation would seem counter-intuitive as doses required to illicit an acute response led to significant depression of cardiac output (Lisy & Burnett, Jr., 2006). In this regard further investigation is warranted in order to clarify any long term benefit therapeutic doses of K201 may have on renal function, especially in the setting of congestive heart failure. The effects of K201 therefore are not limited merely to the drugs' previously reported actions on cardiac tissue. Moreover, in the setting of heart failure K201 may indirectly improve cardiac function via its effects on other tissues in the intact animal. Isolating the influence of K201 on whole heart mechanical function after MI, independent of systemic effects has not been attempted to date. In addition, studies where K201 has been shown to improve cardiac function in models of heart failure have involved chronic administration of the drug at or close to the start of treatment to induce heart failure (Wehrens *et al.*, 2005; Yano *et al.*, 2003). Therefore, there is currently no information available on the acute effects of K201 administration on ventricular mechanical function in an MI model of left ventricular dysfunction.

5.1.3 Aims

The aims of the work described in this chapter were to characterize pressure-volume work of the isolated working rabbit heart 8 weeks after induction of an ischaemic myocardial insult, and following this to determine the effects of acute administration of K201 on left ventricular contractile function. Results from the previous chapters highlight a dichotomy regarding the actions of K201. Despite application of K201 in hearts from healthy animals causing a decline in mechanical function, in the setting of elevated Ca^{2+} and β-adrenergic

stimulation which induced contractile dysfunction K201 proved to be beneficial. Therefore, based on the results presented in Chapter 3 it was hypothesized that application of K201 to hearts exposed to chronic myocardial infarction 8 weeks previous would result in a decrease in contractile performance.

5.2 Methods

5.2.1 Coronary artery ligation model of myocardial infarction

The rabbit myocardial infarct model by ligation of the circumflex branch of the left coronary artery was employed for this study. This model has been described in detail previously (Pye *et al.*, 1996). All procedures were carried out in accordance with The Animals (Scientific Procedures) Act 1986, and were approved by the University of Glasgow's ethics committee.

All surgical procedures were performed by Michael Dunne. Briefly, adult New Zealand White rabbits (2.5 – 3.5 kg) were pre-medicated with intramuscular fentanyl/fluanizone 0.3 $ml.kg^{-1}$ (*Hypnorm, Jansen Pharmaceuticals*). Anaesthesia was induced with midazolam (1 – 2 $mg.kg^{-1}$) administered in the marginal ear vein via an indwelling cannula. Rabbits were intubated and ventilated, with anaesthesia maintained using a 1:1 mixture nitrous oxide and oxygen containing 1 % halothane. A left thoracotomy was performed through the 4^{th} intercostal space to gain access to the left coronary artery. 10 $mg.kg^{-1}$ Quinidine hydrochloride (*Sigma Pharmaceuticals*) was intravenously administered immediately prior to coronary artery ligation to reduce the incidence of ventricular fibrillation during the procedure. A ligation was made in the major ventricular branch of the left coronary artery halfway between its origin and the apex of the heart, quickly resulting in the appearance of an ischaemic area of myocardium. Animals were allowed to stabilise for a period of 10-15 minutes before the wound was closed and saline administered to replace fluids lost during the procedure. Post-operative analgesia (buprenorphine, 0.05 $mg.kg^{-1}$) was provided every 8 hrs for 3-4 days. Animals were kept in a warm, clean environment and checked regularly for signs of distress in order to aid convalescence. Ligation resulted in an infarct accounting for 20-30% of the left ventricle following 8 weeks of recovery, at which point animals underwent haemodynamic assessment. The same surgical procedure was carried out in a second population of animals with the exception of the coronary artery ligation. This group of animals acted as sham-operated controls.

5.2.2 Isolated working heart setup

Hearts from 8 male New Zealand White rabbits that had undergone surgery 8 weeks previously (myocardial infarct; n = 4; sham control; n = 4) were excised and perfused initially in Langendorff mode on the isolated working heart apparatus as described in the

General Methods chapter section 2.1.3. After cannulation of the left atrium working heart mode was initiated and solution was recirculated to perfuse hearts from a fixed volume of 540 ml. Preload was set at 7.4 mmHg and afterload set to 60 mmHg. These settings remained constant throughout the experimental protocol. A pair of platinum subdermal needle electrodes connected to a constant voltage isolated stimulator and train generator were attached to the right atrial tissue and hearts were paced at 200 beats.min^{-1} throughout the protocol.

5.2.3 Left ventricular function by pressure-volume catheterisation

A 3F *Scisense* multi-segmental catheter with three recording electrode segments of 5.5 mm each was advanced slowly past the aortic valves and into the left ventricle to obtain pressure-volume measurements throughout the experimental protocol. Recording software was set to display volume signals from each individual segment in separate channels, with the total volume signal achieved by summation of all three segments. The individual segments delineated 3 discrete regions within the left ventricular chamber, denoted Apex, Mid and Base, respectively, from which regional stroke volume and stroke work was assessed.

5.2.4 Solutions

Perfusion of the isolated working heart was performed using Tyrode's solution, the composition of which is described in General Methods section 2.1.3. K201 stock solution was created by dissolving K201 in a 10% DMSO solution to yield a stock concentration of 1 mM. K201 was prepared 10 min prior to the beginning of each experiment and stored in a light-shielded container.

5.2.5 Experimental Protocol

After initiation of working heart perfusion, the multi-segmental catheter was slowly advanced through the aortic valves into the LV chamber. The catheter was positioned such that recording segment 1 (denoted Apex) was as close to the apex of the heart as possible without interfering with regular heart rhythm and contractile function. Following assessment of parallel conductance with saline bolus injection, hearts were allowed to stabilize before performing a transient occlusion of the left atrial inflow line to assess end diastolic pressure-volume relationships. Afterwards, 540 µL of K201 stock (1.0 mM) was added to the recirculating reservoir to yield a final concentration of 1.0 µM K201. Hearts

were perfused with K201 for a total of 9 min, with continuous pressure-volume measurements recorded throughout for assessment of the acute effects of the drug.

5.2.6 Data recording and statistical analysis

All working heart functional data were recorded on a *Dell* PC using *LabChart* software version 5.5.6 at a sampling rate of 1000 Hz, and analysed offline using *LabChart*'s Blood Pressure Module and *LabScribe2.0* software. Assessment of end diastolic pressure-volume relationships was performed by fitting a mono-exponential relationship to the end diastolic pressure-volume points obtained during transient occlusion of the left atrial inflow line. This mono-exponential relationship was of the form $EDP = Cexp(^{\beta * EDV})$, where *EDP* is the end diastolic pressure, *C* is a curve fitting constant, β is the diastolic stiffness constant and *EDV* is the end diastolic volume (See General Methods section 2.3.7). All results were saved to an external hard drive. Two-sample Student's *t*-test was used to compare values between groups on a number of functional parameters. A *P*-value of < 0.05 was considered statistically significant.

5.3 Results

5.3.1 Baseline haemodynamic function of 8 week ligation *vs*. sham

Baseline haemodynamic function was assessed prior to addition of 1.0 μM K201 with the multi-segmental pressure volume catheter. This catheter was not available for 1 of the 4 sham control experiments, and pressure-volume work was instead assessed with a 3F VSL catheter (19 mm electrode spacing). Data from this heart was not included in the subsequent assessment of regional function (see section 5.3.3).

5.3.1.1 Load-independent left ventricular function

As can be seen in Figure 5.1A, PV loops from 8 week ligation hearts appear shifted to the right in comparison to those from sham controls. Representative families of PV loops obtained using transient atrial inflow line occlusion are plotted in Figure 5.1B(i = sham, ii = 8 week ligation). Mean diastolic stiffness constant values (Figure 5.1C(ii)) were not significantly different between groups. Therefore despite the presence of an apical infarct, by 8 weeks post ligation the diastolic stiffness constant was not significantly altered.

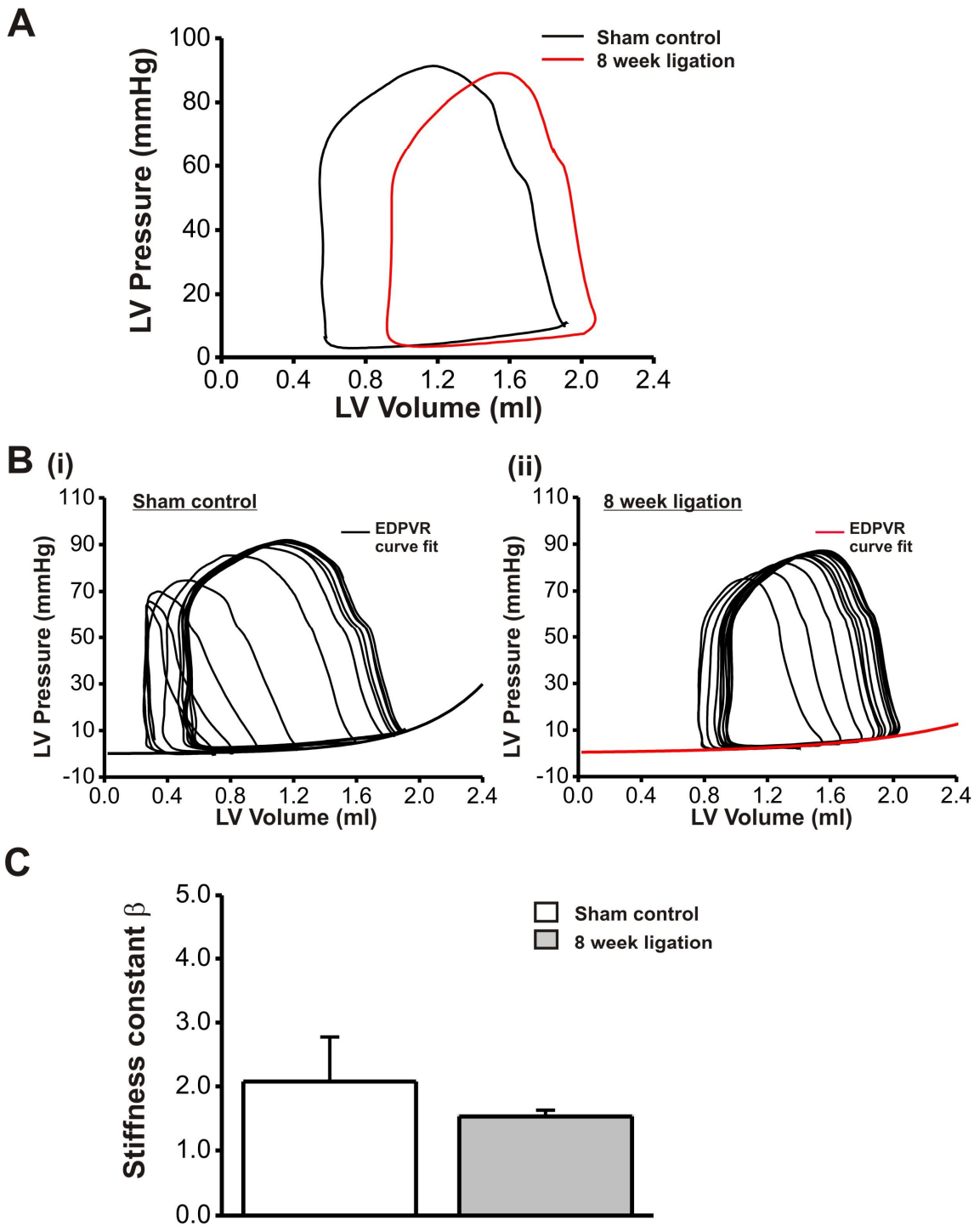

Figure 5.1 Pressure-volume relationships: 8 week ligation vs. sham control. A. Representative steady state pressure-volume loops from sham (black line) and 8 week ligation (red line) hearts. B. Families of PV loops obtained by transient occlusion of the left atrial inflow line in sham (i) and 8 week ligation (ii) hearts. The EDPVR curve fit for these individual hearts is shown on the graph. C. Mean diastolic stiffness constants (β) are shown for each group. Sham control, n = 4; 8 week ligation, n = 4. Mean stiffness constants compared using unpaired student's *t*-test.

5.3.1.2 Baseline systolic and diastolic function of 8 week ligation hearts vs. sham controls

Mean values for contractile and relaxation indices are shown in the top panels of Figure 5.2 with values up to and including time 0 indicating baseline function prior to addition of K201. There was a tendency for left ventricular peak pressure (Figure 5.2(i)) to be higher in the sham operated hearts, but this did not reach significance. Contractility, as assessed by dP/dt_{max} (Figure 5.2(ii)) was not significantly different between the two groups at baseline. End diastolic pressure (Figure 5.2(iii)) was not significantly different between the two groups, however dP/dt_{min} (Figure 5.2(iv), an index of ventricular relaxation was significantly lower in 8 week ligation hearts [-1675.72 ± 55.05 $mmHg.s^{-1}$ (8 week ligation) *vs.* -2175.69 ± 137.59 $mmHg.s^{-1}$ (sham control); $P < 0.05$]. There were no differences in the relaxation constant τ (Figure 5.2(v)) between groups.

5.3.1.3 Baseline volume parameters of 8 week ligation hearts vs. sham controls

Aortic flow (Figure 5.3 A(i)) and stroke volume (Figure 5.3 A(ii)) both tended to be higher in the sham operated hearts compared to the 8 week ligation, but this did not reach significance in either parameter. There was no significant difference in end diastolic volume (EDV – Figure 5.3 A(iii)) between groups at baseline, though this tended to be higher in the 8 week ligation hearts. End systolic volume (ESV – Figure 5.3 A(iv)) however, was significantly higher at baseline in the ligation hearts [1069.78 ± 56.87 µl (8 week ligation) *vs.* 643.36 ± 56.70 µl (sham control); $P < 0.01$]. Ejection fraction (Figure 5.3A(v)) was also found to be significantly lower in the 8 week ligation group compared to the sham operated hearts [51.83 ± 4.09 % (8 week ligation) *vs.* 68.74 ± 1.38 % (sham control); $P < 0.05$]. Coronary flow (Figure 5.3B) was not significantly different between groups. Baseline functional data demonstrate that some degree of functional impairment was apparent 8 weeks after coronary artery occlusion resulting in a significantly reduced ejection fraction and higher end systolic volume compared with sham operated controls.

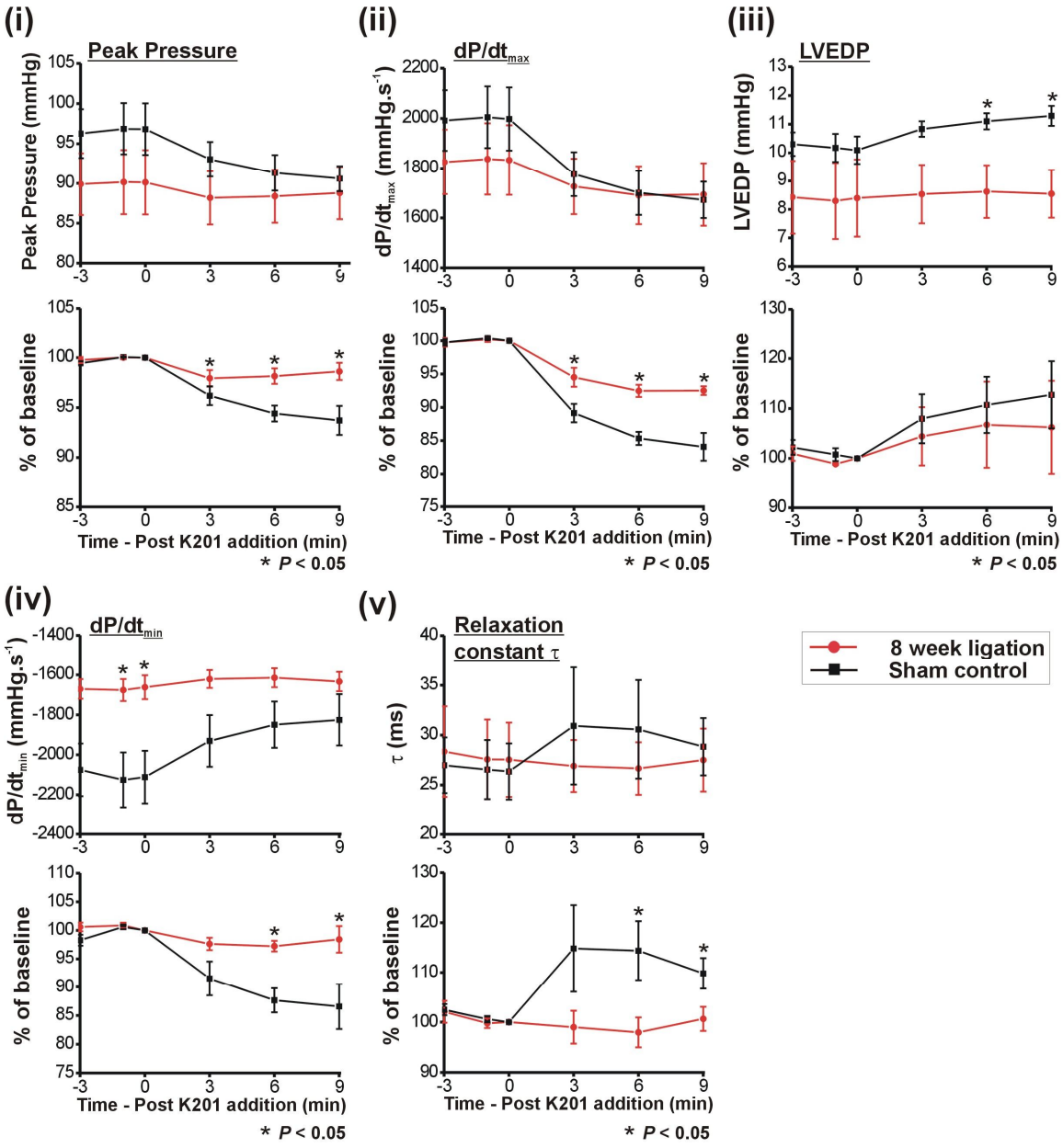

Figure 5.2 Pressure, contractility and relaxation following addition of 1.0 µM K201. (i-v). Indices of LV mechanical function during the K201 perfusion protocol. Top panels; mean ± SEM for each parameter in sham (black squares, n = 4) and 8 week ligation (red circles, n = 4) hearts; Bottom panels; mean values expressed as % of baseline (0 min). Statistical significance between groups tested using unpaired student's *t*-test.

5.3.2 Acute effects of K201 on mechanical function of 8 week ligation hearts

5.3.2.1 Systolic and diastolic functional parameters

In hearts from the sham operated animals peak systolic pressure (Figure 5.2A(i)) fell to 93.72 ± 1.45 % of baseline (value at time 0) after 9 minutes of K201 perfusion, dropping

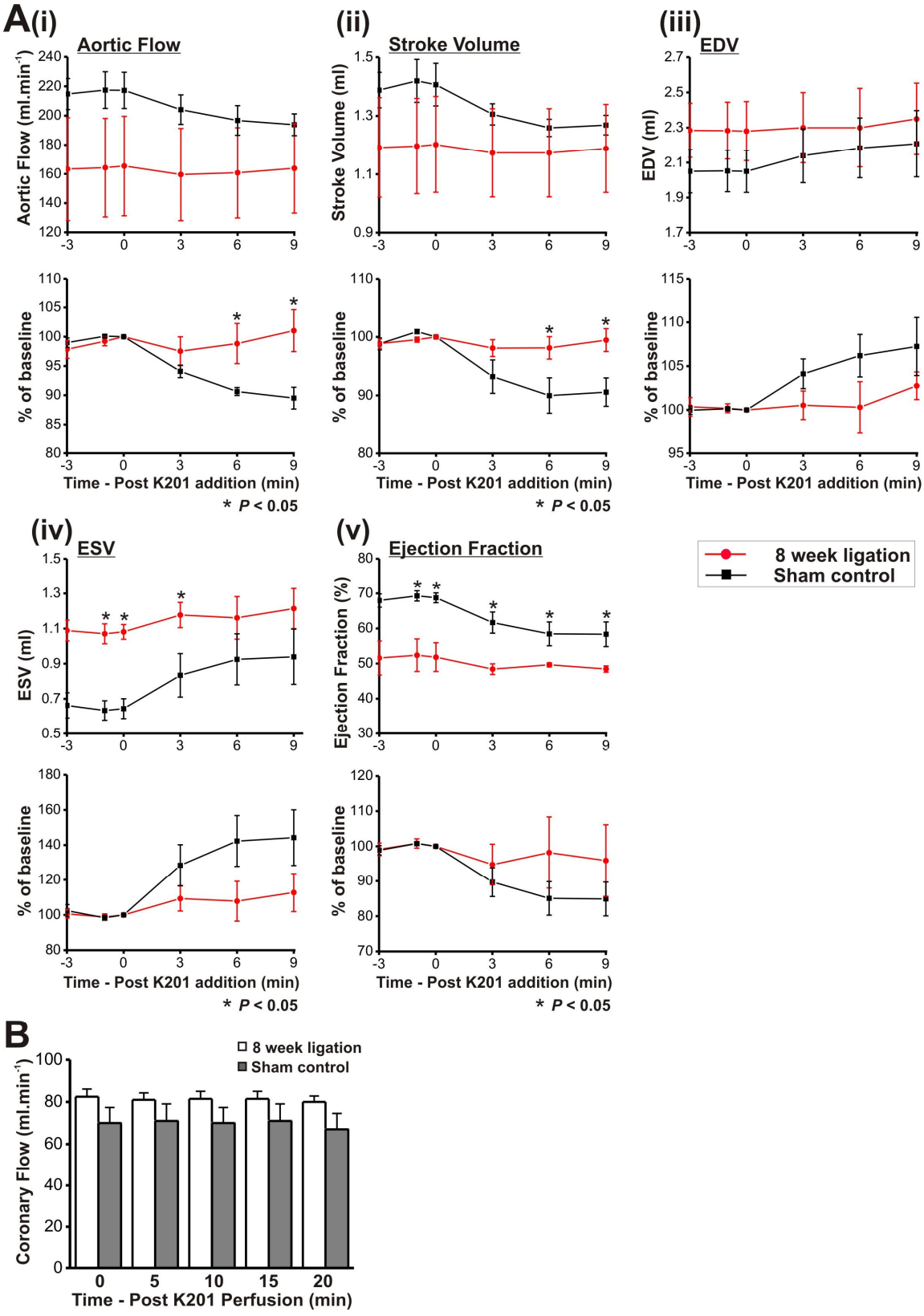

Figure 5.3 Volume and flow data following addition of 1.0 µM K201. A(i-v). Volume indices and flow measurements obtained before and during perfusion with K201. Top panels; mean data from sham (black squares, n = 4) and 8 week ligation (red circles, n = 4) hearts; bottom panels; mean values expressed as % of baseline (0 min). B. Mean coronary flow measured at 5 min intervals during the protocol. All values expressed as mean ± SEM. Statistical significance between groups tested with unpaired student's *t*-test.

significantly further than the 8 week ligation hearts (98.62 ± 0.86 % of baseline). Similarly, contractility (assessed by dP/dt_{max} – Figure 5.2(ii)) was significantly more depressed in the sham control group (84.07 ± 2.09 %) *vs.* the 8 week ligation (92.51 ± 0.65 %; $P < 0.01$) after 9 min of K201 perfusion, although it should be noted that dP/dt_{max} was significantly reduced relative to baseline in the 8 week ligation hearts by 9 min post-K201 perfusion (100.00% vs. 92.51 ± 0.65%; $P < 0.01$, not indicated on graph). LVEDP (Figure 5.2(iii)) was significantly elevated in sham control (11.10 ± 0.28 mmHg) *vs.* 8 week ligation hearts (8.63 ± 0.93 mmHg; $P < 0.05$) following 9 min of K201 perfusion, however, as can be seen from Figure 5.2(iv) the % change from baseline was not significantly different between groups. 1.0 μM K201 led to a significantly greater fall in dP/dt_{min} in the sham control hearts (86.59 ± 3.94 %) *vs.* 8 week ligation hearts (98.42 ± 2.34 %) after 9 min of perfusion. In addition, the relaxation constant τ (Figure 5.2(v)) increased significantly more in the sham controls (109.80 ± 3.10 %) *vs.* 8 week ligation hearts (100.66 ± 2.40 %; $P < 0.05$) after 9 min of K201 perfusion.

5.3.2.2 Volume parameters

Aortic flow (Figure 5.3A(i)) fell from baseline by a significantly greater degree in sham control hearts (89.51 ± 1.86 %) *vs.* 8 week ligation (101.04 ± 3.59; $P < 0.05$) after 9 min in 1.0 μM K201, as did stroke volume (Figure 5.3A(ii)) [92.07 ± 1.38 (sham control) *vs.* 99.46 ± 1.95 (8 week ligation); $P < 0.05$]. As shown in Figure 5.3A(iii) & (iv), the % change from baseline in end diastolic volume and end systolic volume was not significantly different between groups at any point, although tended to be greater in the sham controls. The % change in ejection fraction from baseline was not significantly different between groups after addition of K201, although sham controls tended to show a greater degree of change. K201 did not significantly alter coronary flow at any stage however (Figure 5.3B). In sham control hearts therefore, 1.0 μM K201 had a negative inotropic effect, but this was significantly reduced in hearts that had undergone coronary artery ligation 8 weeks previously.

5.3.3 Regional function in the isolated working heart

Use of the 3 segment, multi-segmental pressure-volume catheter permitted comparative assessment of regional stroke volume and stroke work in the 8 week ligation and sham control hearts. Figure 5.4A shows representative pictures of an isolated heart from an 8 week ligation animal, with the right hand panel demonstrating the relative positions of each volume segment. Segment 1 was positioned closest to the area of infarction, with the

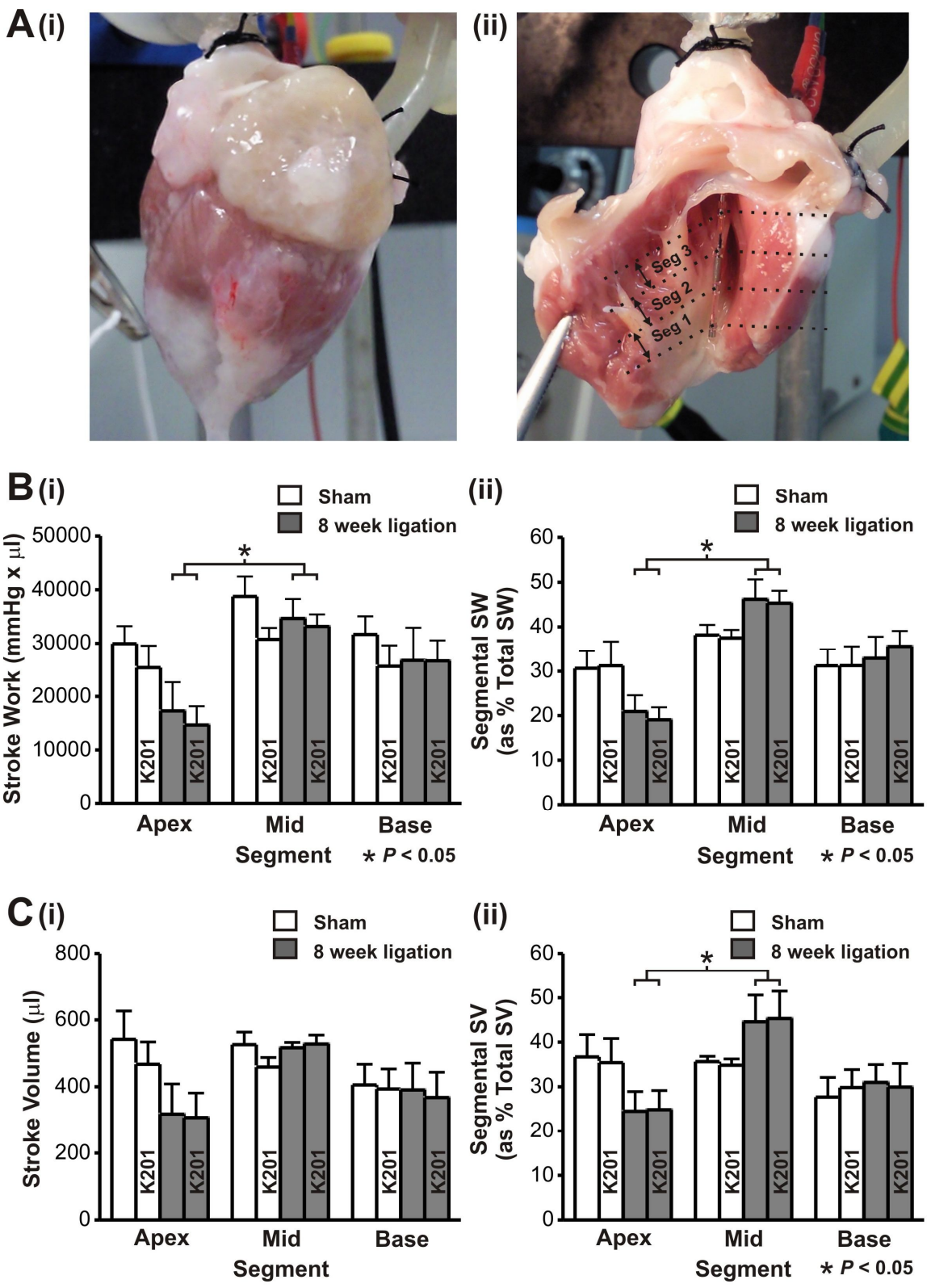

Figure 5.4 Regional function in 8 week ligation vs. sham control hearts. A. 8 week ligation heart intact (i) and opened (ii) showing position of volume segments. B&C. Mean stroke work and stroke volume measured from 3 discrete catheter segments. Left hand panels; mean values ± SEM from each segment before and 9 min after K201. Right hand panels; mean values ± SEM from each segment expressed as % of total (sum of all 3 segments). Sham, n=3; 8 week ligation, n=4.

remaining segments measuring volume within the middle and basal portions of the left ventricular chamber respectively. As shown in Figure 5.4B(i), stroke work for any given segment was not significantly different between sham or 8 week ligation hearts, although there was a tendency for apical stroke work to be lower in the 8 week ligation group. There were no significant differences between segments in the sham control group, however within the 8 week ligation, apical stroke work (17283.87 ± 5401.09 mmHg*µl. μl^{-1}) was significantly lower than that of the mid chamber (34655.62 ± 3628.33 mmHg*µl.μl^{-1}; $P < 0.05$). A similar trend emerged when segmental stroke work was expressed as a % of total stroke work (Figure 5.4B(ii)). The % contribution of each region to the total stroke work was similar before and 9 minutes after perfusion with 1.0 µM K201 in both groups. Stroke volume (Figure 5.4C(i)) in the apical region from sham controls tended to be higher than that of the 8 week ligation hearts, but this did not reach significance. The % contribution of each segment to total stroke volume was not significantly different in the sham controls, but was significantly lower in the apical region of 8 week ligation hearts (24.48 ± 4.80 %) in comparison to the mid chamber region (44.56 ± 6.03 %; $P < 0.05$). 1.0 µM K201 did not significantly alter the contribution of each region to the total stroke volume in either group, suggesting that there is no regional effect of K201.

5.4 Discussion

5.4.1 K201 is negatively inotropic in sham operated hearts but not in infarcted hearts

The 1, 4-benzothiazepine derivative, K201 has been shown to prevent the adverse effects of pacing-induced left ventricular remodelling in the canine heart and result in improved function in a mouse myocardial infarction model of heart failure when chronically administered during the period of induction (Wehrens *et al.*, 2005; Yano *et al.*, 2003). The effects of K201 are not however, limited to cardiac tissue. Improved skeletal muscle function in heart failure has been demonstrated in FKBP12.6$^{-/-}$ mice chronically treated with K201, despite no improvement in cardiac function (Wehrens *et al.*, 2005). K201 has also been shown to enhance glomerular filtration rate and natriuresis *in vivo* in healthy dogs, an effect which is potentially beneficial but which has not yet been described in heart failure models (Lisy & Burnett, Jr., 2006). Therefore, the therapeutic potential of K201 on cardiac function in heart failure models has yet to be studied without the confounding influence of the compounds' systemic effects. Additionally, the aforementioned heart failure models employed chronic administration of K201 during the period of heart failure

induction, but there is little information on the acute effects of the drug following a period of remodelling. In the current study, isolated rabbit hearts which had undergone a coronary artery ligation 8 weeks previously were functionally assessed using a multi-segmental pressure-volume catheter and compared to hearts from sham-operated control animals before and after perfusion with 1.0 μM K201. Prior to K201 administration, baseline functional indices demonstrated that 8 week coronary artery ligation resulted in a reduction in left ventricular relaxation (Figure 5.2(iv)) and ejection fraction (Figure 5.3A(v)), while other indices of contractility did not appear significantly different from controls. Comparison of left ventricular stiffness constants between both groups, as seen in Figure 5.1C, also did not reveal a significant difference. This was believed to be due in part to the low numbers in each group (n = 4; 8 week ligation and sham control). Peak systolic pressure, dP/dt_{max} and aortic flow all tended to be higher in the sham control hearts, and with more numbers in each group it is possible these would have achieved significance. Ng *et al.* (2002) using isolated working rabbit hearts exposed to chronic (8 weeks) coronary artery ligation demonstrated a significant difference in cardiac output (~17%) and peak LV pressure (~10%) between 8 week ligation and sham operated hearts with n-values of 8 for each group (Ng *et al.*, 2002). In the current study, preliminary power calculations suggest that between 10 and 12 hearts per group would be required to report a significant difference in cardiac output and peak pressure between groups.

From the results discussed in Chapter 3, 1.0 μM K201 was shown to be negatively inotropic in hearts from healthy animals, and the same effect was expected to occur in hearts from sham operated animals. The acute effects of K201 on hearts that had undergone coronary artery ligation to produce a myocardial infarction however were not known. From the results shown in Figures 5.2 and 5.3, perfusion with 1.0 μM K201 was more negatively inotropic in sham operated control hearts compared to 8 week ligation hearts, with the effect being most pronounced at 9 minutes post-K201 perfusion. Function did not decline in 8 week ligation animals following addition of K201, with only dP/dt_{max} becoming significantly reduced relative to baseline. Contrary to the findings discussed in chapter 3 and the result hypothesised earlier in this chapter, K201 did not significantly effect cardiac mechanical function in 8 week ligation hearts in contrast to the cardio-depressive response demonstrated in the sham operated control hearts.

5.4.2 The pattern of regional function in isolated working hearts does not alter following perfusion with K201

Stroke volume and stroke work within discrete regions of the left ventricular chamber was assessed using a multi-segmental pressure-volume catheter. The catheter was positioned within the left ventricle such that the first segment lay within the infarcted region as shown in Figure 5.4 A(ii), with the remaining 2 segments spanning the rest of the left ventricular chamber. In the 8 week ligation hearts, the largest area of infarction was found in the apical region. There were no differences in either stroke volume or stroke work within the apex between the 8 week ligation hearts and sham controls, although there was a tendency for both parameters to be lower in 8 week ligation hearts. Increasing the number of hearts in this study may therefore have revealed a significant difference between groups. The % contribution of each segment in the 8 week ligation hearts however was not uniform, and there was a significantly greater contribution from the mid region to total stroke volume and stroke work in comparison to the apical region, while in sham hearts the relative contribution of each segment to total stroke volume/work was similar. The distinct differences in functional response to K201 between groups may have been better understood by a differential regional response between the two groups. For example, K201 may be functionally beneficial in the region closest to infarction, such that the contribution to total function by this region is increased relative to the remaining regions. Figures 5.4 B(ii) and C(ii) show that the relative contribution of each region to total stroke work and stroke volume remain almost identical in both groups before, and 9 min after perfusion with K201, demonstrating that the effect of K201 on cardiac function is similar throughout the myocardium.

5.4.3 Differential response to K201 between 8 week infarct and sham control hearts: Possible mechanisms

It has been well documented that in cardiac disease states such as heart failure, there are marked changes in Ca^{2+} handling mechanisms (Bers *et al.*, 2003; Hasenfuss & Pieske, 2002; Shannon *et al.*, 2003). Heart failure is associated with a reduction in SERCA2a expression and function, as well as altered phospholamban phosphorylation which may work to reduce SR Ca^{2+} content following myocardial infarction and left ventricular dysfunction (Bers *et al.*, 2003). The rabbit model ligation model of left ventricular dysfunction demonstrates the same phenotype (Currie & Smith, 1999) however, while NCX gene and protein expression has also been shown to be upregulated in heart failure

(Hasenfuss *et al.*, 1999; Studer *et al.*, 1994b), previous reports published using the current rabbit ligation model of left ventricular dysfunction have indicated that NCX function is significantly reduced (Quinn *et al.*, 2003). Recently, interest has focused on the relative contribution of altered RyR2 function to cardiac contractile dysfunction in heart failure (Belevych *et al.*, 2007; Shannon *et al.*, 2003; Tateishi *et al.*, 2009). The idea that diastolic Ca^{2+} leak could contribute to heart failure was initiated in a study by Marx *et al.*, (2000) who demonstrated that phosphorylation of RyR2 by PKA resulted in dissociation of a binding protein, FKBP12.6, from the channel complex, an increase in channel open probability (P_o) and the induction of subconductance states (Marx *et al.*, 2000). In intact myocytes from human and canine failing hearts the amount of FKBP12.6 bound to RyR2 was already significantly reduced. The importance of PKA 'hyperphosphorylation' to this mechanism has been hotly debated, with several investigations failing to demonstrate a link between PKA phosphorylation and increased RyR2-mediated Ca^{2+} leak (Bers *et al.*, 2003; Curran *et al.*, 2007). Regardless of the initiating mechanism, the idea that RyR2-mediated SR Ca^{2+} leak can significantly contribute to a reduced SR Ca^{2+} content is also a contentious issue. Shannon *et al*. (2003) assessed SR Ca^{2+} leak in intact myocytes from failing rabbit cardiomyocytes and found it to be increased in heart failure for any given total SR Ca^{2+} content (Shannon *et al.*, 2003). They reasoned that while this mechanism may work in tandem with enhanced NCX function and reduced SR Ca^{2+} uptake to lower SR Ca^{2+} content, data for that particular heart failure model would suggest enhanced NCX function plays a greater role. Belevych *et al*. (2007) reported that SR Ca^{2+} content and fractional Ca^{2+} release were reduced in myocytes from a canine pacing-induced model of heart failure, and attributed this finding to a significantly enhanced SR Ca^{2+} leak, as SR Ca^{2+} uptake was not significantly altered compared to controls and NCX function only upregulated by 30 % (Belevych *et al.*, 2007). A well-documented action of K201 involves its interaction with the RyR2. K201 has been demonstrated to reduce spontaneous SR Ca^{2+} release in ventricular myocytes subjected to Ca^{2+} overload (Hunt *et al.*, 2007; Loughrey *et al.*, 2007). The specific binding site for K201 on the RyR2 has also recently been reported (Yamamoto *et al.*, 2008). If SR Ca^{2+} leak is a significant contributory factor to the reduced SR Ca^{2+} content and loss of inotropy in heart failure, then K201 would likely result in an inhibition of this leak and a partial restoration of cardiac inotropy. In line with this, K201 has been demonstrated to inhibit SR Ca^{2+} leak in failing canine cardiac myocytes, as well as preventing ventricular remodelling associated with a chronic pacing-induced model of heart failure (Yano *et al.*, 2003). K201 has also been shown to restore the rate of Ca^{2+} release in SR vesicles from failing canine cardiomyocytes back towards control levels (Kohno *et al.*, 2003). From the results described in Chapter 3, 1.0 μM K201 is negatively

inotropic in the isolated working rabbit heart. Hearts from 8 week ligation animals however demonstrated a blunted negative inotropic response to K201 in comparison to sham operated controls, with only dP/dt_{max} demonstrating a significant decline from baseline function in the ligated hearts. This may have resulted from a reduction in SR Ca^{2+} leak by K201's interaction with the RyR2 in 8 week ligation hearts. K201 does not only target the RyR2 however, and a number of competing effects may have resulted in the overall action of the drug in 8 week ligation hearts. K201 has been shown to reduce the SR Ca^{2+} uptake via SERCA2a (Loughrey *et al.*, 2007), and several reports have demonstrated a concentration-dependent inhibition of I_{CaL} (Chen *et al.*, 2008; Inagaki *et al.*, 2000b; Kimura *et al.*, 1999) although this does not reach significance in rabbit ventricular myocytes at 1.0 μM (Loughrey *et al.*, 2007).

5.4.4 Alternative mechanisms of K201 action

From the results presented in Chapter 3 application of 1.0 μM K201 in isolated working hearts from healthy rabbits leads to a significant decline in mechanical function and cardiac inotropy. Alternative mechanisms of action may therefore be responsible for divergent effects seen between 8 week myocardial infarction hearts and sham operated controls and it is possible K201 is interacting with an intracellular target that improves function in infarcted hearts.

The levels of nitric oxide (NO) in cardiac tissue have been shown to influence myocardial contractility (Rastaldo *et al.*, 2007). NO is synthesised primarily through several types of NO-synthase; endothelial (e)NOS, neuronal (n)NOS and inducible (i)NOS, the relative expressions and functions of which are believed to be altered in cardiac disease states, including ischaemic heart failure (Rastaldo *et al.*, 2007). Mice in which eNOS has been genetically ablated develop more severe left ventricular dysfunction and remodelling in comparison to wild-type controls (Scherrer-Crosbie *et al.*, 2001). A similar result was also reported in mice lacking expression of nNOS (Dawson *et al.*, 2005). Induction of myocardial infarction in $nNOS^{-/-}$ mice led to left ventricular dilatation and severe functional impairment that developed at a faster rate than left ventricular dysfunction in wild type mice subjected to the same ligation protocol, an effect that was independent of infarct size. In patients with non-ischaemic dilated cardiomyopathy levels of iNOS and eNOS gene expression correlated with severity of LV dysfunction, such that increased expression was associated with greater stroke work and stroke volume (Heymes *et al.*, 1999). In patients with elevated left ventricular end diastolic filling pressures (> 16

mmHg) coronary injection of substance P to stimulate endothelial cell production of NO also resulted in an increase in stroke work and stroke volume, indicative of improved ventricular filling. Kawabata *et al.* (2002) reported that the preservative effects of K201 on metabolism following ischaemia-reperfusion in isolated rabbit hearts were abolished following treatment with the NOS inhibitor L-NAME (Kawabata *et al.*, 2002). A portion of K201's action appears to be mediated through NOS, and upregulation of one or more subtypes of NOS may be acting to improve myocardial relaxation in the current study.

5.4.5 Use of the multi-segmental pressure-volume catheter to assess regional function in the isolated working heart

Multi-segmental pressure-volume analysis has been used in previous studies to assess regional mechanical dyssynchrony (Bleeker *et al.*, 2006; Steendijk *et al.*, 2004; Strum & Pinsky, 2006). Steendijk *et al*. (2004) described the use of this technique in quantification of mechanical dyssynchrony in heart failure patients by identification of altered segmental volume phase relative to the total volume signal (Bleeker *et al.*, 2006; Steendijk *et al.*, 2004). They reported that this approach successfully identified significantly greater mechanical dyssynchrony in congestive heart failure patients with left bundle branch block, compared to coronary artery disease patients presenting essentially preserved left ventricular function. Several conductance-derived indices of mechanical dyssynchrony were also shown to correlate significantly with septal-to-lateral delay, an index of dyssynchrony obtained by tissue Doppler echocardiography (Steendijk *et al.*, 2004). The present investigation reports for the first time the assessment of regional myocardial function in an *ex vivo* rabbit heart preparation. Function was assessed using a 3 segment multi-segmental pressure-volume catheter, with each segment delineating a discrete region of the left ventricular chamber. Regional stroke volume and stroke work were compared between 8 week ligation hearts and sham controls, as well as between each region within groups. Despite the presence of a transmural infarct within the apical region of hearts from 8 week ligation animals, no significant differences in apical stroke volume or stroke work were detected between the 8 week ligation hearts and the sham controls. Stroke work and stroke volume (as a % of total) were however found to be significantly lower in the apical region in comparison to mid region in 8 week ligation hearts, while function in all 3 regions appeared similar in sham controls. Use of the multi-segmental pressure-volume catheter therefore has utility in assessment of regional myocardial function. The groups were comprised of small numbers (sham = 3; 8 week ligation = 4), which may have accounted for the failure in detecting significant differences between groups within the

apical region. It was initially proposed that the blunted negative inotropic response of 8 week ligation hearts to K201 perfusion in comparison to sham controls may have resulted from regionally specific effects of K201 which would presumably alter the contribution of each region to total stroke work/stroke volume relative to other segments measured. However, as the results in Figure 5.4B(ii) & C(ii) demonstrate, regional myocardial contributions to both of these parameters were unchanged following application of K201, suggesting that the effect of K201 was uniform throughout the myocardium.

5.5 Summary

In the present study the effects of acute administration of K201 on mechanical function in a model of left ventricular dysfunction were investigated. Although 1.0 μM K201 did not improve mechanical function in 8 week ligation hearts, a blunted negative inotropic response was found in comparison with sham controls. This may reflect a balance of positive effects of the drug on Ca^{2+} handling mechanisms (improved RyR2 function and decreased SR Ca^{2+} leak) and inhibitory effects (Inhibition of SR Ca^{2+} uptake). Other reported effects of K201 involving stimulation of NOS may also play a role in counterbalancing the negative inotropic effects of the compound however these mechanisms have only been described in models of ischaemia-reperfusion injury and their influence on contractile function following development of myocardial infarction requires further investigation. Novel assessment of regional myocardial stroke volume and stroke work with a multi-segmental pressure-volume catheter in an *ex vivo* rabbit heart preparation demonstrated that K201 showed no regionally specific effects.

6 Pharmacological inhibition of SR Ca^{2+} uptake in the isolated working rabbit heart

6.1 Introduction

Re-sequestration of Ca^{2+} into the sarcoplasmic reticulum (SR) following Ca^{2+}-induced Ca^{2+}-release (CICR) is performed by the Sarco-Endoplasmic Reticulum Ca^{2+}-ATPase, or SERCA. As SR Ca^{2+} content is a crucial determinant of the size of the systolic Ca^{2+} transient and therefore the strength of contraction, the activity of SERCA is critical to the normal regulation of cardiac contractility (Antoons *et al.*, 2003; Periasamy & Huke, 2001). The activity of SERCA2a, the isoform present in cardiac cells, is regulated by an inhibitory protein Phospholamban (PLB). Phosphorylation of PLB by cAMP-mediated protein kinase A, or Ca^{2+}/Calmodulin dependent protein kinases results in a removal of PLB's inhibitory effect and an increase in SR Ca^{2+} uptake by SERCA (Simmerman & Jones, 1998). This effect contributes to the overall positive inotropic and lusitropic effects associated with β-adrenergic stimulation in cardiac muscle, the final outcome of which is an increase in SR Ca^{2+} content (Hussain & Orchard, 1997). In heart failure, a common finding is a reduction in SR Ca^{2+} content and concomitant diminution of the systolic Ca^{2+} transient (Bers *et al.*, 2003; Hasenfuss & Pieske, 2002). Furthermore, there is general agreement that in failing human hearts (Beuckelmann *et al.*, 1992; Hasenfuss *et al.*, 1994a) and animal models of heart failure (Neary *et al.*, 2002a; Yamaguchi *et al.*, 1997) there is a reduction in SR Ca^{2+} uptake which may be attributable to altered SERCA expression or function. Decreased SERCA2a expression and/or function could result in the development of diastolic abnormalities (Kass *et al.*, 2004). NCX expression in some cases is reported to be upregulated in heart failure models (Pogwizd *et al.*, 1999b) which may help to limit diastolic dysfunction but at the same time result in an increased Ca^{2+} efflux during diastole, further contributing to the reduction in SR Ca^{2+} content. Recently, transgenic rat and mouse models displaying upregulated SERCA2a expression, as well as variant isoforms of SERCA (1a, 2b) have allowed further insight into the importance of SR Ca^{2+} uptake to normal cardiac function. More recently inducible knockout of SERCA2a using an *in vivo* murine model has allowed for greater characterisation of the specific role of SERCA2a in maintenance of normal cardiac function (Andersson *et al.*, 2009).

6.1.1 Functional consequences of SERCA2a down-regulation

The SERCA2 gene appears to be absolutely essential for normal development, as it is not possible to create mice with homozygous null mutations of this gene (Ji *et al.*, 2000; Periasamy *et al.*, 1999; Seth *et al.*, 2004). Down-regulation of SERCA2a has been achieved using heterozygous null mutations of the SERCA2 gene with the resulting

phenotype exhibiting decreased SERCA2a mRNA and protein expression (55 % and 35 % respectively), a reduced SR Ca^{2+} uptake and reduction in left ventricular function (Ji *et al.*, 2000; Periasamy *et al.*, 1999). Moreover, Ca^{2+} handling properties are markedly altered in this model, as evidenced by a decline in protein expression but increased phosphorylation of PLB, increased expression and function of NCX, and a reduction in Ca^{2+}_i transient amplitude and SR Ca^{2+} content (Ji *et al.*, 2000). The associated peripheral alterations in Ca^{2+} handling protein expression and function following transgenic down-regulation make it difficult to discern the specific contribution that reduced SERCA2a function makes to impairment of cardiac function. Reduction of SERCA2a expression and its consequences for compensatory upregulation of auxiliary Ca^{2+} transport pathways has been studied in cultured cardiomyocytes using RNA interference (RNAi) (Seth *et al.*, 2004). Reduction of SR Ca^{2+} uptake to 20% of control values 48-72 hours after treatment resulted in increased NCX, stimulating protein 1 (sp1) and myocyte enhancer factor 2 (MEF2) transcription, with no changes detected in sarcolemmal Ca^{2+} ATPase, L-Type Ca^{2+} channel or PLB transcription levels. Most recently, an interesting result was reported by Andersson *et al.* (2009) using an acute tamoxifen-inducible cardiac SERCA2 knockout model in mice (Andersson *et al.*, 2009). 1 week after treatment with tamoxifen SERCA2a protein levels were reduced to 20% of controls, with no detectable SERCA2a in isolated cardiomyocytes after 4 weeks. Assessment of Ca^{2+} handling properties revealed Ca^{2+}_i transients that were significantly reduced in amplitude as well as being heavily reliant on SR-independent Ca^{2+} influx mechanisms, explained in part by a 120% increase in L-type Ca^{2+} current density due to prolonged inactivation times. At 7 weeks SERCA2a knockout mice demonstrated evidence of diastolic dysfunction but surprisingly there were no overt signs of cardiac dysfunction or circulatory failure after 4 weeks, despite reduced cardiac function and near complete absence of SERCA2a expression in the heart. These results suggest that while long term reduction of SERCA2a function eventually results in severe cardiac dysfunction, the short term effects only involve a mild reduction in cardiac function without stimulation of hypertrophic mechanisms (Andersson *et al.*, 2009).

6.1.2 Pharmacological inhibitors may better highlight the role of SERCA2a in normal cardiac function

While these recent studies afford greater insight into the specific role of SERCA2a in regulating cardiac function, *in vivo* manipulation of SERCA2a expression in the heart is accompanied by compensatory changes in the expression and function of Ca^{2+} handling proteins associated with Ca^{2+} transport during the transient. Separating the influence of

compensatory mechanisms from the effects of acute disruption of SERCA2a may provide a better understanding of the specific role this protein plays in normal cardiac function. A number of pharmacological agents exist which inhibit SERCA, the most specific and potent of which is thapsigargin (Kirby *et al.*, 1992; Treiman *et al.*, 1998). While specific inhibition of SR Ca^{2+} uptake using thapsigargin is not possible *in vivo* due to unwanted systemic effects, the isolated working rabbit heart provides a useful model for examining the influence of specific pharmacological SERCA2 inhibition on cardiac function.

6.1.2.1 Thapsigargin: Mechanism of action

The reaction for Ca^{2+} uptake into the SR by SERCA has been described in detail in Chapter 1. Briefly, in the ground state (E_1) there are two high affinity Ca^{2+} transport sites exposed on the cytosolic side of the SR membrane. 2 Ca^{2+} ions bind to this site and in the presence of ATP the Ca_2E_1 complex is phosphorylated to Ca_2E_1-P, resulting in Ca^{2+} ion occlusion, meaning the Ca^{2+} is trapped within the complex and cannot be released to either the SR or the cytosol. A conformational change occurs (E_2 state) whereby the affinity of the phosphorylated ATPase for Ca^{2+} is decreased, causing Ca^{2+} to be released into the SR (Mintz & Guillain, 1997). Sagara *et al.* (1992) reported that thapsigargin was able to inhibit two stages of the ATPase reaction, Ca^{2+} binding and de-phosphorylation of the enzyme (Sagara *et al.*, 1992). The rate of thapsigargin's inhibitory effect on the ATPase was slowed in the presence of Ca^{2+} but markedly increased in the presence of the Ca^{2+} chelator EGTA. Thapsigargin binds to the channel in its low Ca^{2+} affinity (E_2) state, effectively creating a 'dead-end' complex where the pump can no longer be phosphorylated and continue cycling Ca^{2+} into the SR (Sagara *et al.*, 1992). Attempts to identify the binding location for thapsigargin have shown that the M3 segment is an essential requirement (Norregaard *et al.*, 1994). This was highlighted by Xu *et al.* (2004) using COS-1 cells expressing SERCA1 enzymes with specific mutations corresponding to the M3 (Phe-256), M5 (Ile-765) and M7 (Tyr-837) segments which resulted in a reduction in the inhibitory effect of thapsigargin as well as its binding affinity for SERCA (Xu *et al.*, 2004)

6.1.2.2 Comparison of Thapsigargin with alternative pharmacological inhibitors of SERCA

Along with thapsigargin, two other agents have been identified as potent and selective inhibitors of SERCA; Cyclopiazonic acid (CPA) (Goeger *et al.*, 1988; Goeger & Riley, 1989) and 2,5-Di(*Tert*-Butyl)-1,4-Benzohydroquinone (TBQ) (Nakamura *et al.*, 1992).

Thapsigargin possesses the highest affinity for SERCA, with a reported K_d of < 2 pM (Davidson & Varhol, 1995) and near 1:1 stoichiometry with SERCA (Inesi *et al.*, 2005; Sagara & Inesi, 1991). CPA also exhibits a high degree of specificity and can inhibit SERCA in the submicromolar concentration range (Seidler *et al.*, 1989). Both CPA and TBQ inhibition is similar in character to that of thapsigargin albeit with less affinity, involving a stabilization of SERCA enzyme in the E_2 state and formation of a dead end complex (Inesi *et al.*, 2005). TBQ is a far less potent inhibitor of SERCA activity than thapsigargin, with half maximal inhibition occurring at 1.5 μM (Nakamura *et al.*, 1992). Reported non-specific effects of TBQ, including inhibition of L-type Ca^{2+} channels (Nelson *et al.*, 1994) and inwardly rectifying K^+ channels (Hassessian *et al.*, 1994) overlap significantly with its SERCA blocking actions. Furthermore, higher concentrations (0.1 mM) have been shown to inhibit the plasma membrane Ca^{2+} ATPase (Luo *et al.*, 2000), making it difficult to class this compound as a truly selective inhibitor of SR Ca^{2+} uptake. CPA does not appear to exhibit non-specific effects at higher concentrations (Dettbarn & Palade, 1998) however its affinity for SERCA is several orders of magnitude lower than thapsigargin. Thapsigargin therefore represents the most efficacious and selective of the three compounds and as such is the initial compound of choice for pharmacological inhibition of SERCA.

6.1.3 Aims

The study outlined in this chapter aims to investigate the functional consequences of acute pharmacological inhibition of SR Ca^{2+} uptake in the isolated working rabbit heart using the specific inhibitor thapsigargin, and ascertain to what degree contractile function is suppressed by this compound in an isolated working heart preparation. It was hypothesized that inhibition of the SR Ca^{2+} ATPase in the isolated working heart with thapsigargin would result in a significant decline in LV contractility and cardiac output compared to vehicle controls.

6.2 Methods

6.2.1 Isolated working heart setup

Hearts from 10 male New Zealand White rabbits were excised and perfused initially in Langendorff mode on the isolated working heart apparatus as described in the General Methods chapter section 2.1.3. After cannulation of the left atrium working heart mode was initiated and solution was recirculated to perfuse hearts from a fixed volume of 540 ml. Preload was set at 7.4 mmHg and afterload set to 60 mmHg. These settings remained constant throughout the experimental protocol. A pair of platinum subdermal needle electrodes connected to a constant voltage isolated stimulator and train/delay generator, were attached to the right atrial tissue and hearts were paced at 220 beats.min^{-1} throughout the protocol.

6.2.2 Left ventricular function by pressure-volume catheterisation

A 3F Scisense VSL catheter with a recording electrode segment of 19 mm was calibrated as described in the General Methods chapter (See sections 2.2.3 and 2.3.1) and positioned just distal to the aortic cannula. After initiation of working heart perfusion the catheter was advanced slowly past the aortic valves into the left ventricle to obtain continuous recording of pressure and volume throughout the experimental protocol.

6.2.3 Solutions

Perfusion of the isolated working heart was performed using Tyrode's solution, the composition of which is described in General Methods section 2.1.3. A nominally Ca^{2+}-free Tyrode's solution containing 50 μM EGTA was also prepared. This solution was gassed and heated to 37ºC in a water bath before being transferred to a second water-jacketed afterload reservoir attached to the isolated working heart system. Thapsigargin (TG) was dissolved in 0.51 ml DMSO to yield a stock concentration of 3.0 mM. When added to the perfusion reservoir this yielded a final TG concentration of 2.83 μM. This concentration was chosen to ensure enough TG was available to reach all cells within the isolated working heart, but was low enough to avoid any non-specific effects reported with higher (+5 μM) concentrations of TG (Nelson *et al.*, 1994). DMSO was used as the vehicle in the control group. Both solutions were prepared 30 min prior to commencing perfusion of the isolated heart and stored in light-shielded containers until required.

Homogenisation buffer containing a protease/phosphatase inhibitor cocktail was prepared according to the method of Ji *et al*. (1999) (Ji *et al.*, 1999b). The buffer solution was prepared in 10 mM imadazole, pH 7, and contained (in mM) 10 NaF, 1 Na_3VO_4, 2 NaPP, 2 β – GP and 0.05 Calyculin A.

6.2.4 Experimental Protocol

6.2.4.1 Pre-experiment set up

Hearts were split into 2 groups; hearts perfused with TG (n=5) and hearts perfused with vehicle (n=5). Prior to commencing experiments a second, water-jacketed afterload chamber was attached to the working heart system and connected via a length of Tygon tubing to a side-port on the aortic cannula. A 2-way tap at the end of this line separated solution from coming into contact with the rest of the working heart system. The tubing line was primed with nominally Ca^{2+}-free Tyrode's containing 50 μM EGTA and the second afterload chamber (Afterload 2) was filled with this solution before being set at a perfusion pressure of 60 mmHg. For control experiments an additional water-jacketed preload chamber (Preload 2) was attached to the atrial cannula via a side-port arm and 2-way stopcock. This chamber was filled with 250 ml of normal Tyrode's solution containing 2.83 μM TG and set at a perfusion pressure of 7.4 mmHg.

6.2.4.2 Working heart experiments

Following initiation of working heart mode and assessment of parallel conductance with saline bolus injection, hearts in the TG group were allowed to stabilize before 0.51 ml of 3.0 mM TG was added directly to the recirculation reservoir to yield a final TG concentration of 2.83 μM. In vehicle control experiments, 0.51 ml DMSO was added to the recirculating reservoir, yielding a final recirculating DMSO of ~0.09 %. Lights were turned off for the entire duration of working heart perfusion with TG or DMSO vehicle. Coronary flow values were obtained by timed measurements of coronary effluent every 5 min, while LV function and aortic flow were continuously measured until forward flow (aortic flow) reached 0. At this point the peristaltic pump was stopped, the atrial inflow line occluded and coronary perfusion switched from the working heart afterload chamber to Afterload 2, and hearts were perfused in Langendorff mode for 2 min with nominally Ca^{2+}-free Tyrode's solution containing 50 μM EGTA. In control experiments, 0.51 ml of TG vehicle (DMSO) was added directly to the recirculating reservoir and hearts were perfused continuously in working heart mode for a period of 60 min. After 60 min perfusion with the vehicle the atrial inflow line from the isolated working heart preload

chamber was occluded and Preload 2 was opened to perfuse hearts with Tyrode's solution containing 2.83 μM TG for 30 s. This ensured TG was present in homogenate samples from vehicle treated hearts and acted as a further measure of control for subsequent SR Ca^{2+} uptake assays. Preload 2 perfusion was then stopped, and coronary perfusion was switched from the working heart afterload chamber to Afterload 2 as described above for the TG group. Endpoint was defined as the time of aortic flow cessation in the TG group, while in the Vehicle control group endpoint was reached 60 min after addition of the vehicle.

6.2.4.3 Preparation of tissue homogenates

Following 2 min perfusion with nominally Ca^{2+} free 50 μM EGTA Tyrode's solution in both groups, the PV catheter was removed from the left ventricular chamber and a section of left ventricular free wall weighing approximately 1.5 g was cut from the heart; excess fatty tissue was removed. Tissue was weighed before being snap frozen in liquid nitrogen. Tissue was roughly chopped using a clean scalpel blade before being pulverized using a mortar and pestle. Five-times volume of ice-cold homogenization buffer was gradually added during this time, and tissue was homogenized using an Ultraturrax T8 (*Labortechnik*) until no solid pieces of tissue remained. Samples remained on ice to limit protein degradation. The final homogenate was aliquoted into labeled 1.5 ml Eppendorff tubes and stored at -80 ºC prior to subsequent biochemical analysis.

Investigation of SR Ca^{2+} uptake by SERCA2a in tissue homogenate samples using oxalate facilitated Ca^{2+} uptake was performed by Dr Elspeth Elliott, University of Glasgow.

6.2.5 Data recording and statistical analysis

All working heart functional data were recorded on a *Dell* PC using *LabChart* software version 5.5.6 at a sampling rate of 1000 Hz, and analysed offline using *LabChart*'s *Blood Pressure Module* and *LabScribe2.0* software. All results were saved to an external hard drive. Two-sample Student's *t*-test was used to compare values between groups on a number of functional parameters. A *P*-value of < 0.05 was considered statistically significant.

6.3 Results

Perfusion of isolated working hearts with 2.83 μM TG caused a decline in left ventricular function that eventually resulted in premature cessation of forward flow (assessed by aortic flow) in comparison to hearts receiving only the vehicle control. The drug perfusion time in the TG group varied between 7 min and 67 min, with the mean time to cessation of aortic flow 31 ± 11 min. As can be seen in Figure 6.1(i-iii), application of TG led to an initial steep decline in left ventricular function developing over the first 5 minutes of perfusion, followed by a steady state period leading to a gradual decline in function until cessation of aortic flow occurred. Representative pressure-volume loops in Figure 6.1(iv) show the decline in stroke volume at three different timepoints after addition of TG, with the volume trace demonstrating a leftward shift as the time of TG perfusion increases. Mean values for systolic and diastolic functional parameters are also given in table 6.1.

Table 6.1 **Thapsigargin treatment: Left Ventricular Systolic and Diastolic Functional Indices from Isolated Working Rabbit Hearts**

	Pre-addition		Addition + 5 min		Endpoint	
	Vehicle (n=5)	TG (n=5)	Vehicle (n=5)	TG (n=5)	Vehicle (n=5)	TG (n=5)
Parameter						
PSP (mmHg)	106.87 ± 2.83	106.07 ± 1.86	106.20 ± 2.77	92.18 ± 1.39*	99.16 ± 3.78	78.77 ± 1.90*
EDP (mmHg)	9.72 ± 1.83	8.49 ± 1.60	9.97 ± 1.71	12.22 ± 1.24	11.91 ± 1.00	14.19 ± 1.23
dP/dt_{max} ($mmHg.s^{-1}$)	2136.62 ± 164.14	2001.54 ± 206.55	2056.79 ± 131.06	1377.24 ± 58.31*	1744.08 ± 140.28	1024.10 ± 14.35*
dP/dt_{min} ($mmHg.s^{-1}$)	-2156.01 ± 182.18	-2255.47 ± 99.25	-2146.63 ± 150.74	-1596.81 ± 82.08*	-1779.12 ± 89.64	-1242.45 ± 84.84*
Tau (ms)	21.40 ± 0.23	27.80 ± 0.32	21.40 ± 0.24	42.60 ± 0.69*	27.30 ± 0.42	74.70 ± 0.90*
SV (ml)	1.056 ± 0.089	1.173 ± 0.047	1.041 ± 0.079	0.824 ± 0.034	0.876 ± 0.091	0.392 ± 0.017*
AF ($ml.min^{-1}$)	163.08 ± 18.03	180.47 ± 17.76	160.55 ± 15.92	103.06 ± 12.71*	124.57 ± 19.44	n/a
CF ($ml.min^{-1}$)	72.80 ± 5.08	82.00 ± 1.74	72.00 ± 5.22	83.20 ± 2.58	71.20 ± 5.57	81.20 ± 1.74

Table 6.1 Left ventricular function following TG treatment. Left ventricular functional indices in TG (2.83 μM) or DMSO (0.09 %) perfused working rabbit hearts. Endpoint in TG group occurs when aortic flow = 0. In vehicle control, endpoint occurs at 60 min post-addition. PSP; peak systolic pressure, EDP; end diastolic pressure, SV; stroke volume, AF; aortic flow, CF; coronary flow. * $P < 0.05$ TG vs. vehicle.

6.3.1 Effect of TG on systolic functional parameters

Figure 6.2 shows a number of contractile and relaxation parameters 5 min after TG/Vehicle addition and at the endpoint of the experiment, expressed as a percentage of baseline values (defined as 2 min before addition of TG/Vehicle). The mean values are also displayed in table 6.1. No significant change in peak pressure (Figure 6.2 (i)) was evident

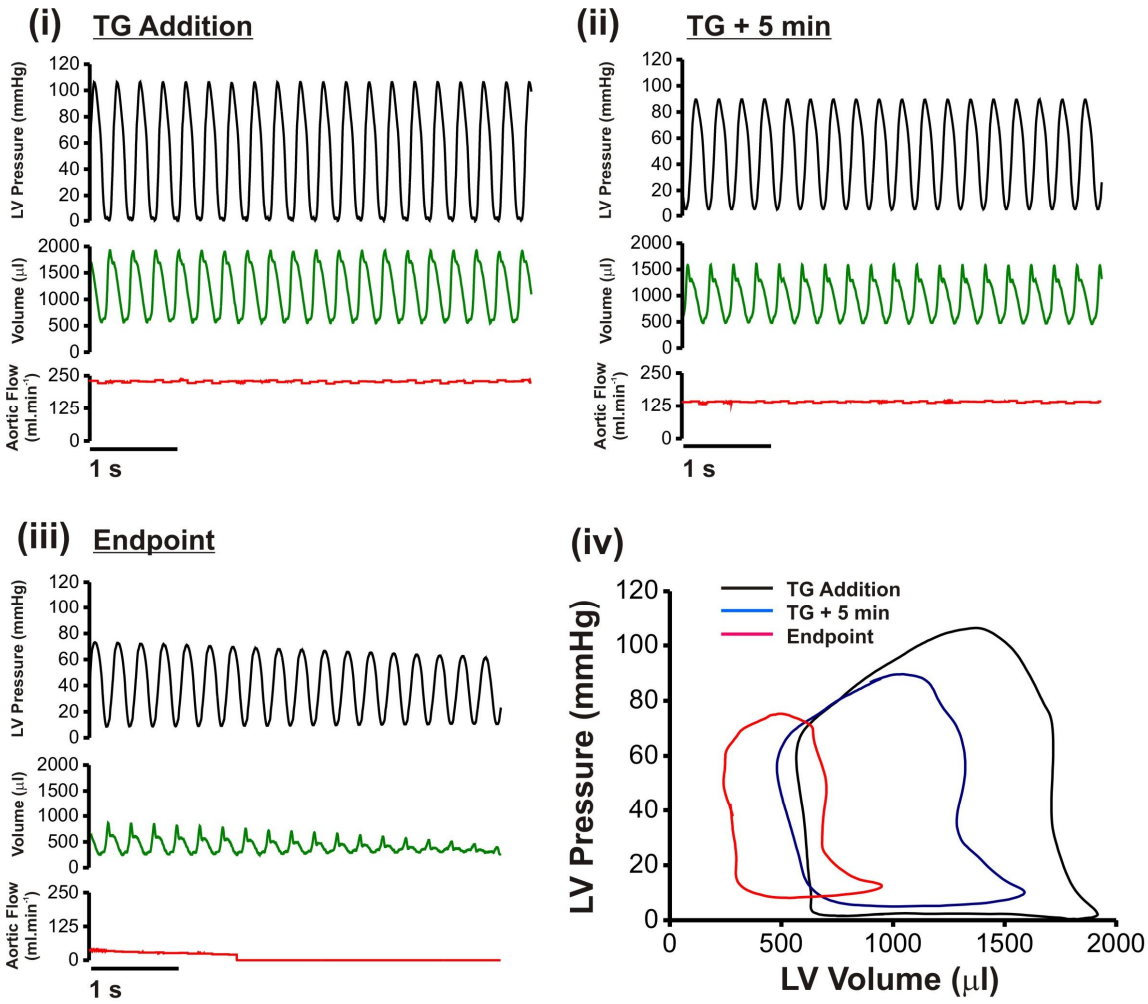

Figure 6.1 Representative pressure, volume and aortic flow recordings (i-iii), and corresponding PV loops (iv), from an isolated working heart perfused with TG.

in vehicle perfused hearts within the 60 min perfusion period. In TG treated hearts however peak pressure fell to 86.96 ± 1.29 % of baseline values 5 min after addition ($P < 0.01$). At the time of aortic flow cessation peak pressure had fallen to 74.36 ± 2.28 % of baseline ($P < 0.01$). 60 min of perfusion with the vehicle control resulted in a significant drop in dP/dt_{max} to 81.57 ± 1.25 % of baseline values ($P < 0.01$), but there was no change present after 5 min. However, dP/dt_{max} (Figure 6.2(ii)) was significantly depressed in the TG treated group at 5 min post addition (70.58 ± 4.53 % of baseline; $P < 0.01$) and this was even more pronounced at endpoint (53.44 ± 5.62 % of baseline).

6.3.2 Effect of Thapsigargin on diastolic functional parameters

TG also caused a significant increase in LVEDP (Figure 6.2(iii)) by endpoint (189.25 ± 30.99 % of control; $P < 0.05$). Perfusion of the vehicle control did not significantly alter LVEDP at either time point. A significant decline in dP/dt_{min} was seen after 60 min

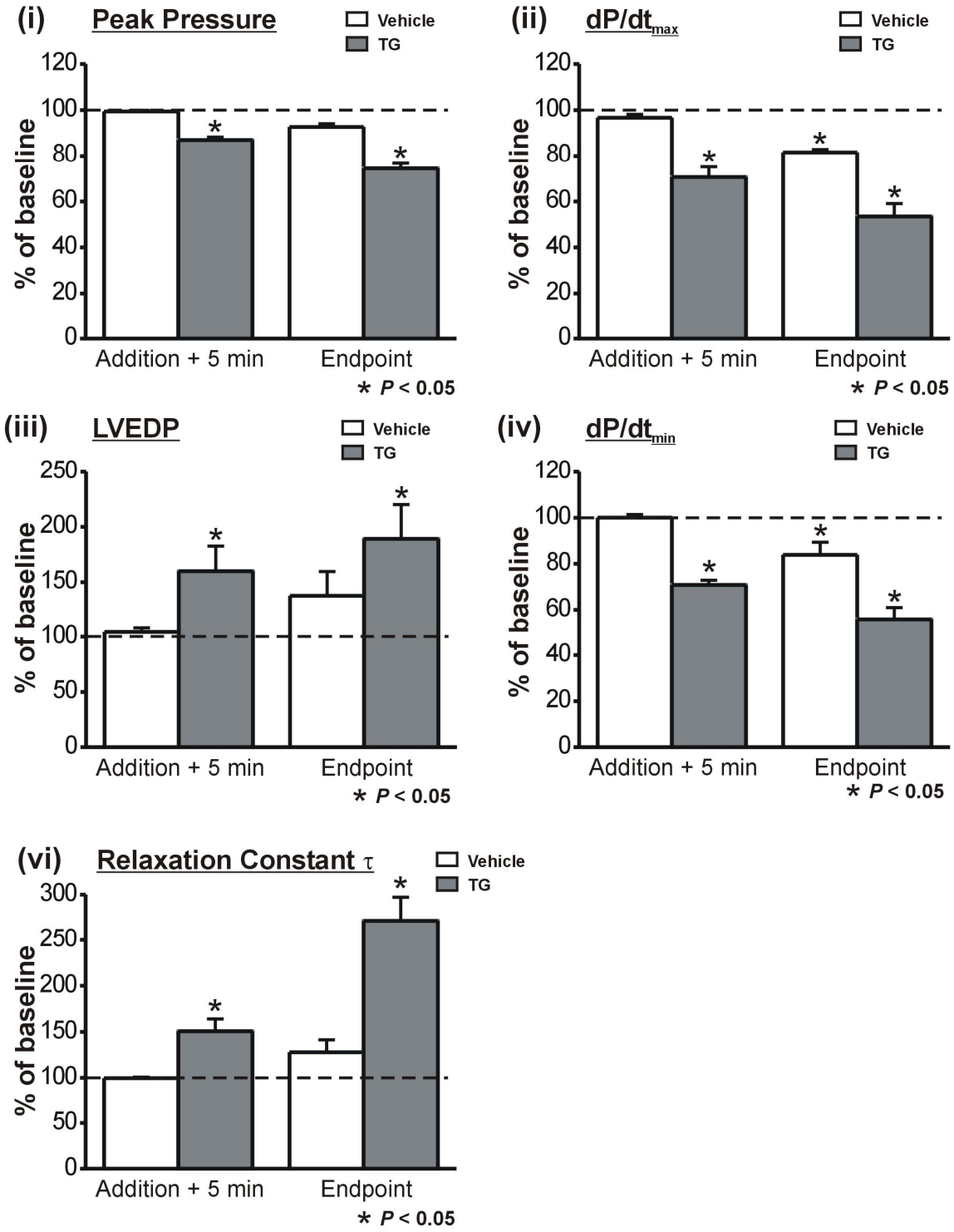

Figure 6.2 Ventricular function following TG treatment. Pressure, contractility and relaxation indices in the isolated working rabbit heart 5 min after addition of TG (Grey bars, n=5) or vehicle (white bars, n=5) and at the endpoint of the protocol. All values expressed as a % of baseline (mean + SEM), indicated by dashed line. Significance tested using paired Student's *t*-test.

vehicle perfusion (83.88 ± 5.47 % of baseline; $P < 0.05$) but not after 5 min. In TG treated hearts dP/dt_{min} (Figure 6.2(iv)) was significantly depressed after 5 min, falling to 70.81 ± 2.01% of baseline ($P < 0.001$), and declining further still (55.84 ± 5.08 % of baseline; $P < 0.001$) by the endpoint. The relaxation constant τ (Figure 6.2(v)) was unchanged in vehicle

treated hearts but significantly prolonged vs. baseline following TG perfusion, increasing to 150.66 ± 13.37 % after 5 min ($P < 0.05$), and to 271.28 ± 25.88 % at the endpoint ($P < 0.01$).

6.3.3 Effect of Thapsigargin on left ventricular volume parameters

Relative changes in volume in the isolated working heart following treatment with TG and vehicle are plotted in Figure 6.3. While there was a significant fall in aortic flow (Figure 6.3A(i))in the vehicle control at endpoint (76.15 ± 6.77 % of baseline; $P < 0.05$) no change was evident 5 min after addition. Aortic flow in the TG treated hearts fell to 56.60 ± 1.51 % of baseline 5 min after TG addition ($P < 0.001$) and, as described above was no longer measureable at the endpoint. Neither the TG nor vehicle treatments influenced coronary flow (Figure 6.3A(ii)) suggesting that reduced perfusion did not play a role in the drop in performance seen in either group. The relative end systolic and end diastolic volumes expressed as a % of baseline are plotted in Figure 6.3A(iii) and (iv) respectively. While 60 min of perfusion with the vehicle control resulted in a small but significant rise in EDV (105.59 ± 0.85 % of baseline; $P < 0.01$) and ESV (115.71 ± 3.91 % of baseline; $P < 0.05$), there was no change evident after 5 min. EDV demonstrated a significant drop from baseline values in TG perfused hearts 5 min after TG addition. At the time of aortic flow cessation EDV had fallen further, to 71.65 ± 2.08 % of baseline ($P < 0.001$). Similarly ESV had fallen to 77.25 ± 2.10 % of baseline ($P < 0.001$) by the endpoint. This tendency for EDV (and correspondingly ESV) to fall during TG perfusion suggests an impairment of ventricular filling. As predicted from the fall in aortic flow, stroke volume (Figure 6.3A(v)) was also significantly reduced 5 min after application of TG (to 70.21 ± 0.41 % of pre-addition values; $P < 0.001$) while no significant change was found in the vehicle control. At endpoint, stroke volume in the TG group had fallen to 33.59 ± 2.28 % of pre-addition values ($P < 0.001$). Stroke volume was significantly reduced in the vehicle control group after 60 min (to 83.02 ± 4.66 %; $P < 0.05$) however this parameter was still significantly elevated in comparison to the TG group at endpoint [0.88 ± 0.09 ml (vehicle) *vs.* 0.39 ± 0.02 ml (TG); $P < 0.01$)].

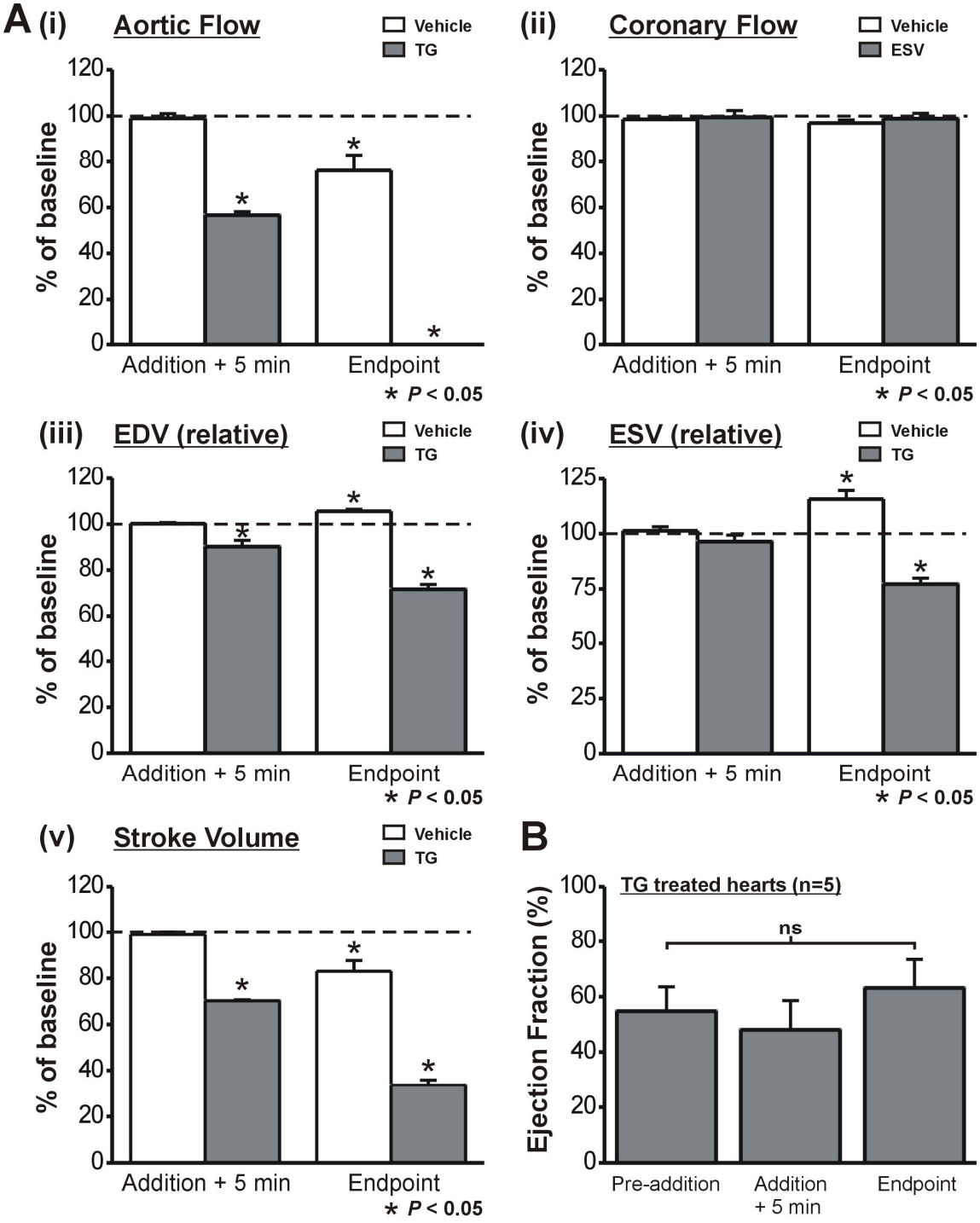

Figure 6.3 Flow and relative volume measurements following application of TG. A(i-v) Flow and volume indices in isolated working rabbit hearts 5 min after addition of TG (Grey bars, n=5) or vehicle (white bars, n=5) and at the endpoint of the protocol. All values expressed as a % of baseline (mean + SEM), indicated by dashed line. B. Ejection fraction in the TG treated group only at pre-TG addition, 5 min after addition, and endpoint.

Assessment of parallel conductance was successfully achieved in 3 of the 5 hearts treated with TG allowing conversion to absolute LV volumes in these hearts. Typical pressure, volume, and aortic flow recordings from an isolated working heart exposed to TG are

shown in Figure 6.1, along with PV loops at the corresponding stages of the protocol. Application of TG led to a decline in both end diastolic and end systolic volume in the isolated working hearts, resulting in a leftward shift in the pressure volume loops relative to steady state (Figure 6.1 (iv)). As a result, stroke volume gradually fell as left ventricular function declined (shown in Figure 6.3A(v)) but ejection fraction (Figure 6.3B) was not significantly altered after 5 min TG perfusion [54.79 ± 8.79 % (pre-addition) vs. 48.04 ± 10.52 % (+ 5 min); $P > 0.05$], and similarly was not significantly altered from baseline immediately prior to cessation of aortic flow [54.79 ± 8.79 % (pre-addition) vs. 63.15 ± 10.31 % (+ 5 min); $P > 0.05$]. These results suggest application of TG causes a significant impairment of left ventricular diastolic filling with relatively preserved ejection fraction.

6.4 Discussion

6.4.1 Acute inhibition of SERCA2a in the isolated working heart leads to left ventricular dysfunction and premature cessation of aortic flow

Thapsigargin is a naturally occurring plant alkaloid that has been shown to selectively inhibit the SERCA family of Ca^{2+} pumps with a high potency (Kirby *et al.*, 1992; Sagara & Inesi, 1991). In the current study, thapsigargin was applied to an isolated working heart model to assess the functional consequences of SERCA2a inhibition. It was found that 2.83 μM TG was sufficient to cause a decline in contractility and relaxation parameters in the isolated working heart, eventually resulting in premature cessation of aortic flow in comparison to vehicle controls. Based on the high potency and specificity of thapsigargin for SERCA these effects are almost certainly the result of inhibition of SR Ca^{2+} uptake and a depletion of the SR Ca^{2+} stores. Thapsigargin did not alter coronary flow at any stage of the protocol suggesting tissue perfusion was not impaired. Perfusion with thapsigargin resulted in a profound depression of left ventricular relaxation, as evidenced by elevated LVEDP, a reduction in dP/dt_{min} and significant prolongation of the relaxation constant τ indicating prolonged relaxation (see Figure 6.2 and table 6.1). Another notable finding was the observed fall in left ventricular end diastolic and end systolic volumes, as represented by the PV loops shown in Figure 6.1(iv), indicative of impaired diastolic left ventricular filling. Reduction in the rate of SR Ca^{2+} uptake has been implicated in impaired relaxation and diastolic dysfunction in heart failure (Kass *et al.*, 2004). In addition, genetic upregulation of SERCA2a expression or ablation of PLB has been demonstrated to result in enhanced SR Ca^{2+} uptake and improved left ventricular function

(Hoshijima *et al.*, 2002; Miyamoto *et al.*, 2000; Muller *et al.*, 2003). In the current study SR Ca^{2+} uptake in an isolated working heart was specifically and acutely inhibited, resulting in impairment of relaxation and the appearance of diastolic abnormalities. These findings support the notion that SR Ca^{2+} uptake by SERCA2a plays a significant regulatory role in normal left ventricular relaxation.

6.4.2 To what degree is SERCA inhibited when cardiac function fails?

In order to characterise the functional role of SERCA2a in the present study it was necessary to study the degree of SERCA inhibition in the isolated working heart at the time of aortic flow cessation. Elliott *et al*. (2009) assessed Ca^{2+} uptake in left ventricular tissue homogenates prepared from hearts perfused with TG and vehicle controls in the current study, using oxalate facilitated Ca^{2+}-uptake (Elliott *et al.*, 2009). The investigators reported that a significant level of Ca^{2+} uptake was detectable in all samples from vehicle control hearts, but that no detectable levels of Ca^{2+} uptake were apparent from TG treated samples. This was true even when protein sample size was 6 times higher than control, indicating that at the time of aortic flow cessation in isolated working hearts SERCA2a activity had been negligible. These findings suggest that while SERCA2a is important in regulating cardiac function, with a particularly important role in relaxation, the function of this protein may be reduced to insignificant levels (<10 %) before the heart can no longer sustain working function. This observation is in agreement with the results of Andersson *et al*. (2009) who demonstrated that in the complete absence of SERCA2 protein, cardiac function is depressed but overt signs of cardiac failure are absent, at least within the first several weeks after SERCA downregulation (Andersson *et al.*, 2009). Important limitations exist in this model with regards to quantifying the specific role of SERCA2a to cardiac function. The inducible knockout, while currently the most acute method of SERCA protein ablation available *in vivo*, is associated with upregulation of other Ca^{2+} handling proteins such as NCX and the L-type Ca^{2+} channel which may be sufficient to compensate for the loss of SR function. Blockade of SERCA2a with TG in the current study is unlikely to be over a sufficient timescale as to be associated with alterations in Ca^{2+} handling protein expression and may therefore prove a more effective model to study the specific role of SERCA2a in regulating cardiac function.

6.4.3 Thapsigargin as a selective inhibitor of SERCA

In order to investigate the role of SR Ca^{2+} uptake to cardiac function using a pharmacological agent it was essential to use a specific inhibitor of SERCA so as to minimise potential for secondary effects to complicate the result. The plant-derived compound thapsigargin (TG) has been demonstrated to possess potent and highly selective inhibitory action on the known isoforms of SERCA. Thastrup *et al*. (1990) demonstrated inhibition of Ca^{2+}-ATPase activity in rat liver microsomes, an effect attributable to blockade of Ca^{2+} uptake into the Endoplasmic reticulum (Thastrup *et al.*, 1990). The high specificity of this compound was reported by Kirby *et al.* (1992) who found that application of TG to intact rat ventricular myocytes resulted in a marked reduction in $[Ca^{2+}]_i$ transient amplitude, a decline in twitch shortening to 22.6 % of control and a greater than 2-fold increase in the $[Ca^{2+}]_i$ transient rate decay constant after approximately 5 min, attributable to a primary reduction in SR Ca^{2+} uptake (Kirby *et al.*, 1992). Oxalate facilitated Ca^{2+} uptake in permeabilised myocytes was inhibited by TG with half-maximal potency in the 10-20 nM range, underlining the high efficacy of this compound. TG was also shown to have no direct influence on sarcolemmal membrane currents or I_{Ca} (Bassani *et al.*, 1993; Kirby *et al.*, 1992). Bassani *et al*. (1993) reported on the rate of TG inhibition in isolated rabbit ventricular myocytes, demonstrating that exposure to 5 μM TG resulted in complete inhibition of the caffeine-induced $[Ca^{2+}]_i$ transient within 90 s. TG has been used to investigate the SR Ca^{2+} uptake rates in rat and rabbit ventricular myocytes, as well as the SERCA pump density (Bassani *et al.*, 1994; Hove-Madsen & Bers, 1993). Furthermore, addition of >5 nmol TG per mg cell protein resulted in complete inhibition of Ca^{2+} uptake after 15 s (Hove-Madsen & Bers, 1993). In the present study, control hearts were perfused with TG at the end of the 60 min in order to eliminate the possibility that TG binding to SERCA was still occurring in the homogenate preparations. Uptake results from Elliott *et al*. (2009) confirmed that SERCA inhibition had not taken place after homogenisation of ventricular tissue as evidenced by the detection of significant levels of Ca^{2+} uptake from these preparations.

Baudet *et al.* (1993) used TG and a second SERCA inhibitor (CPA) to assess the influence of SR Ca^{2+} uptake on twitch force development in multi-cellular muscle preparations (ventricular trabeculae and papillary muscle) (Baudet *et al.*, 1993). It was found that the SR Ca^{2+} content, indirectly assessed using rapid cooling contractures (RCCs) was only reduced by very high [TG] (500 μM) and was still incomplete, as a caffeine and ryanodine sensitive component still remained. This is in apparent contrast to reports using intact

single cells where rapid application of 5 μM TG results in depletion of SR Ca^{2+} content in less than 2 min (Bassani *et al.*, 1994). Nevertheless, Elliott *et al.* (2009) reported that in tissue homogenates from isolated working rabbit hearts used in the current study, oxalate-facilitated SR Ca^{2+} uptake levels were negligible when samples were taken at the time of aortic flow cessation, indicating an almost total inhibition of SERCA2a by TG in a whole heart preparation (Elliott *et al.*, 2009). The apparent discrepancy in these findings is not fully understood, however it is likely that differences in the preparations are responsible, something Baudet *et al.* (1993) cited as being the likely explanation for the discrepancy between results from single cell preparations and their multi-cellular preparation when exposed to similar protocols (Baudet *et al.*, 1993). It is possible that the more physiological perfusion conditions in the isolated working heart facilitate the entry of TG into the intracellular environment. The differences in perfusate temperature (30ºC vs. 37ºC) are unlikely to play a role as significant slowing of TG binding to SERCA is only demonstrable at relatively low temperature (15 ºC) and high pH (8.0) (Sagara *et al.*, 1992). Khandoudi *et al*. (1998) using Langendorff-perfused rabbit hearts, found that 60 min perfusion with 1 μM TG was sufficient to elicit a decrease in peak isovolumetric pressure of ~43 %, an increase in diastolic pressure of ~580 %, and a reduction in dP/dt_{max} by ~50%, however a 45 min exposure to 500 μM TG was required to depress twitch force in isolated superfused trabeculae by 48 %, with rapid cooling contracture (as a measure of SR Ca^{2+} content) only reduced by 62 % (Baudet *et al.*, 1993; Khandoudi *et al.*, 1998). In the current study, 2.83 μM TG was sufficient to reduce dP/dt_{max} to 51.58 % of pre-TG values at the time of aortic flow cessation. Differences between preparations therefore clearly play a role, and lower concentrations of TG in isolated coronary perfused hearts appear to be more effective in reducing contractility than in isolated superfused muscle strips, although the reasons for this are unclear and potentially require further investigation.

6.4.4 Functional decline in DMSO treated hearts following 60 min of perfusion

The data presented in General Methods demonstrated that the current isolated working heart setup was capable of maintaining stable contractile function for 60-90 min with less than a 10% decline in cardiac output by 60 min, in agreement with previously published data. However, in the present investigation vehicle treated controls displayed a significant decline in dP/dt_{max} and dP/dt_{min}, and output (stroke volume/aortic flow) greater than 15%. There are a number of reasons why this may have occurred. The current study employed a pacing rate of 220 $beats.min^{-1}$ for all hearts throughout the protocol to eliminate the

occurrence of pacing breakthrough, while in the longevity experiments all hearts were paced at a lower rate of 200 beats.min^{-1}. The increased work rate in the current study may have therefore contributed to a quicker decline in mechanical function. The presence of 0.1 % DMSO in the perfusion solution for 60 min may also have influenced the longevity of the working heart preparation. DMSO has been demonstrated in guinea pig skeletal muscle preparations to reduce developed stresses and contractility at concentrations as low as 0.007 % (Reid & Moody, 1994). Effects of DMSO on myocardial tissue are species dependent; in dog and cat trabecule and papillary muscle preparations respectively, exposure to 0.5 % DMSO was enough to provoke a negative inotropic response, whereas in rabbit atrial muscle preparations DMSO has been shown to elicit a positive inotropic response at relatively low concentrations (<1 %) but induce negative inotropy at higher concentrations (>3 %) (Shlafer *et al.*, 1974; Spilker, 1970). It is unclear what the direct effects of prolonged exposure to 0.1 % DMSO has on ventricular contractile function in the isolated working rabbit heart. This could have been investigated further by conducting a series of longevity experiments under identical loading and pacing conditions.

6.4.5 Ongoing investigation of the role of SERCA2a in normal cardiac function

The results of this study provide an initial framework for further investigation of the specific role SERCA2a plays in regulating left ventricular function. The protocol used in the current study was successful in creating a model of acute SERCA2a inhibition in the intact rabbit heart where left ventricular function could be monitored throughout. While it was found that at the time of cessation of forward flow in the isolated working rabbit heart SERCA2a function was negligible (Elliott *et al.*, 2009), it is not known at what stage this level of block was achieved. Andersson *et al.* (2009) found that inducible SERCA2a knockout mice demonstrated depressed cardiac function but no overt signs of left ventricular hypertrophy or cardiac failure up to four weeks after SERCA2a levels were undetectable in cardiac tissue (Andersson *et al.*, 2009). This may suggest that hearts can still function in the short term following complete loss of SERCA2a, with only a small depression of cardiac function. Loss of SERCA2a in the above mouse model was also associated with compensatory changes in the expression and function of a number of Ca^{2+} handling components, including the L-type Ca^{2+} channel, NCX and the plasma membrane Ca^{2+}-ATPase (PMCA). The acute nature of SERCA2a inhibition in the current study means that compensatory over-expression of intracellular Ca^{2+} handling components would not be likely to be involved. To better quantify how SERCA2a inhibition alters

regular cardiac function future work using this protocol will also focus on inducing intermediate levels of SERCA2a blockade in the isolated working heart, in order to establish a relationship between the degree of contractile dysfunction and the level of SERCA2a inhibition. This may be accomplished by varying the concentration of TG used to induce blockade and obtaining tissue samples at a set time following addition, or perhaps taking tissue samples at different time points after addition of the same TG concentration. Alternatively, it may be possible to use the degree of reduction in a specific parameter of contractility (for example dP/dt_{max}) to specify the endpoint of an experiment.

6.5 Summary

Blockade of SR Ca^{2+} uptake in the isolated working rabbit heart using the selective SERCA inhibitor thapsigargin led to a decline in left ventricular contractile and relaxation parameters, with hearts demonstrating signs of systolic and diastolic dysfunction, supporting the notion that SR Ca^{2+} uptake plays a prominent role in ventricular relaxation. SERCA2a inhibition with thapsigargin eventually led to cessation of forward flow in the isolated working heart. Subsequent analysis of tissue homogenates revealed that at the time of forward flow cessation SERCA2a activity was negligible (Elliott *et al.*, 2009). These results are in agreement with a previous investigation of prolonged SERCA2a ablation in mice (Andersson *et al.*, 2009).

7 General Discussion

The general aim of this thesis was to investigate the role of the sarcoplasmic reticulum in the mechanical function of an intact, whole heart preparation through pharmacological manipulation of SR Ca^{2+} handling proteins.

…the initial aim of the work described in this thesis was to set up and characterise an isolated working heart preparation using rabbit hearts that would act as a platform for manipulation of SR function using various pharmacological approaches.

To achieve this aim an appropriate whole heart preparation had to be established resembling as close to physiological mechanical function as possible. The isolated working rabbit heart preparation was chosen for this purpose. Non-working Langendorff perfused preparations permit the measurement of contractile function through use of balloon insertion into the left ventricle however such isovolumic contractions are less energetically demanding than *in vivo* ejecting beats and as such are less physiologically representative of heart function. The isolated working rabbit heart performs external work similar to *in vivo* and therefore more closely represents physiological cardiac mechanical function. Mechanical function was characterised using miniaturised pressure-conductance technology, regarded as the gold standard for assessment of ventricular function. Use of this technique in conjunction with an *ex vivo* rabbit heart preparation has not been previously reported and commercially available catheter systems from two companies, Millar and Scisense, were examined to ascertain suitability. Perfusion of isolated working hearts with a modified Tyrode's solution caused saturation of the conductance (and hence volume) signal of the Millar system. The Scisense technology however permitted adjustment of volume signal gain and offset, allowing measurement of relative left ventricular volume changes in an isolated working rabbit heart preparation. Calibration of the relative volume changes to obtain a true volume signal was achieved by calculating parallel conductance through injection of a bolus of 20% saline into the left atrial inflow line, and through calculation of the calibration factor α, which was possible by measuring true cardiac output of the working heart with an ultrasonic flow meter (aortic flow) and timed measurement of coronary effluent (coronary flow). The isolated working rabbit heart preparation was capable of sustaining steady state contractile function under baseline loading conditions (left atrial filling pressure = 7.4 mmHg, afterload = 60 mmHg) for 60-90 min with less than 10% decline in cardiac output, in agreement with previously published data. Pharmacological agents were added to the perfusion fluid reservoir and reached the working heart within 15s. A sampling rate of 1 kHz was sufficient to instantaneously monitor acute changes in left ventricular pressure and volume in the isolated working heart throughout the experimental period.

…the second aim was to characterise working heart mechanical function following exposure to varying concentrations of K201.

The actions of the 1,4-benzothiazepine compound K201 on intracellular Ca^{2+}-handling components of the cardiac myocyte, especially the SR Ca^{2+} release channel RyR2, have been studied extensively using intact and permeabilised ventricular myocytes, as well SR vesicle preparations. The impact on left ventricular mechanical function of the isolated ejecting heart is unknown and was investigated using the current model. 1.0 μM and 3.0 μM led to a significant decline in ventricular contractility and relaxation when normalised to controls. In the case of 3.0 μM the negative inotropic response was so potent that working heart function was unsustainable in several preparations after 2 min. While a significant negative chronotropic effect was noted using 1.0 and 3.0 μM, paced control hearts confirmed that the direct actions of K201 itself on cardiac function and not changes in heart rate, were responsible for the negative inotropic effects of the compound. These findings highlight the need to establish a therapeutic window for K201. A large number of studies indicate 1.0 μM as an optimum concentration for reduction of RyR2 P_o, however this concentration exhibits a negative inotropic effect in normally functioning isolated working hearts and initially this would appear to counter-indicate the use of 1.0 μM for therapeutic strategies utilising K201.

The study then aimed to investigate the influence of acute perfusion of K201 under conditions where SR Ca^{2+} release is thought to be altered; 1) using elevated $[Ca^{2+}]_o$ and β-adrenergic stimulation, known to cause Ca^{2+} overload in intact ventricular myocyte preparations and 2) in a rabbit ligation model of left ventricular dysfunction.

Under conditions which have been shown to cause Ca^{2+} overload and diastolic SR Ca^{2+} release in intact field-stimulated ventricular myocyte preparations (perfusion with 4.5 mM $[Ca^{2+}]_o$ and 150 nM isoproterenol), isolated working rabbit hearts exhibited a transient increase in mechanical function following the first 20s of isoproterenol perfusion. Following this transient phase working hearts demonstrated a decline in contractile function concomitant with a marked increase in interbeat interval variability, resulting in loss of working heart function within the first 600s of isoproterenol perfusion in 6 of 11 hearts. Despite exhibiting clear negative inotropic effects when applied on its own, application of 1.0 μM K201 shortly after isoproterenol perfusion led to a preservation of contractility and relaxation in the isolated working heart. Furthermore, interbeat interval variability was significantly lower in K201-treated hearts at 600s post-ISO compared with non-treated hearts. These results have obvious implications for conditions involving

elevated circulating catecholamines or in conditions where increased frequency of spontaneous diastolic SR Ca^{2+} release is thought to occur. It is important to highlight however, that conditions which result in Ca^{2+} overload are also known to inhibit mitochondrial function and potentially result in loss of ATP production which could also account for the negative inotropic response reported in this study. Previous investigations of ischaemia-reperfusion injury, in which mitochondrial Ca^{2+} overload is believed to play a prominent role, have suggested K201 mediates protection against IR-injury and contractile dysfunction by indirectly influencing mitochondrial K_{ATP} channels, although how this relates to the current study is unknown, and the direct effects of K201 on mitochondrial function warrant further investigation.

Left ventricular dysfunction caused by chronic myocardial infarction is associated with a disruption of SR Ca^{2+} handling proteins, including a reduction in SERCA function and altered ryanodine receptor Ca^{2+} sensitivity leading to an increased rate of diastolic Ca^{2+} leak. Isolated working hearts from rabbits that had undergone coronary artery ligation surgery 8 weeks previously demonstrated a reduction in some indices of mechanical function in comparison to sham operated controls, however diastolic stiffness remained similar between the two groups. Use of a multisegmental pressure-volume catheter was successful in identifying changes in regional left ventricular mechanical function using discrete segmental volumes, demonstrating the potential usefulness of this approach for studying regional dysfunction in rabbit hearts. Sham operated hearts exposed to 1.0 μM K201 exhibited a similar degree of negative inotropism as had been reported for normally functioning hearts in Chapter 3. While it was hypothesised that K201 would exert a similar negative inotropic effect on hearts from the ligation animals, almost all functional indices remained at baseline levels. Only dP/dt_{max} was significantly depressed in comparison to baseline function, and was not reduced to the same degree as in sham operated hearts. This result highlights a dichotomy regarding the influence of K201 on mechanical function between healthy and infarcted hearts. It is possible that inhibition of RyR2 in this model is beneficial to mechanical function by reducing RyR-mediated diastolic Ca^{2+} leak, however this is likely offset by inhibitory effects of K201 on SERCA. It is also possible that other targets of K201 other than SR Ca^{2+} handling proteins (e.g. NOS) are altered following myocardial infarction, and it is important that these offtarget actions are identified to investigate what contribution they make to K201's effects on whole heart mechanical function.

The final set of aims was to assess the contribution of intact SR Ca^{2+} uptake to normal left ventricular contractility and relaxation by perfusion of isolated working hearts with the selective SERCA inhibitor thapsigargin to inhibit Ca^{2+} uptake into the SR.

The consequences of acute inhibition of SR Ca^{2+} uptake on cardiac mechanical function were investigated for the first time using an isolated ejecting heart preparation. Thapsigargin treatment of led to a progressive decline in left ventricular contractility and relaxation, manifest as a leftward shift in the pressure-volume loop, indicative of impaired left ventricular filling. This result emphasised the importance of intact SR Ca^{2+} uptake function for normal left ventricular relaxation. Subsequent Ca^{2+} uptake experiments reported elsewhere revealed that tissue samples taken from hearts treated with TG in the current investigation did not possess a measureable degree of SERCA function, despite previous reports suggesting complete pharmacological SERCA blockade in multicellular preparations was technically difficult to achieve even using thapsigargin concentrations several orders of magnitude higher than those used in the current study. Specific and inducible downregulation of cardiac SERCA2 has been recently demonstrated in a transgenic mouse model resulting in negligible levels of SERCA protein within 1 week and a reduced cardiac pump function but no overt signs of ventricular remodelling within 4 weeks. Compensatory upregulation of other intracellular Ca^{2+} handling proteins occurred in that model, but would be unlikely to play a role in acute pharmacological blockade performed in the isolated working heart. These findings suggest that while SERCA function is critical for maintaining regular systolic and diastolic left ventricular function, functional levels of this protein, and presumably the contribution of the SR to normal contractile function in the isolated working rabbit heart, can be reduced to very low levels before cardiac pump function fails.

Final Conclusion

From the results of this thesis it can be seen that the isolated working heart when paired with miniaturised pressure-conductance technology provides an excellent means of assessing cardiac mechanical function under a variety of different pharmacological and pathological conditions, which can extend to assessment of regional ventricular function using a rabbit heart model. Specific manipulation of SR function using an isolated working heart model provides a better understanding of the critical role SR Ca^{2+} handling plays in mechanical function of the whole heart and may enhance the knowledge already gained from single-cell manipulation of SR proteins.

References

Abe, S., Ohtomo, J., Yamaguchi, I., Tsuchida, E., Fujinuma, T., Sunagawa, K., & Tomoike, H. (1995). Continuous measurement of left ventricular volume in rabbit, using a two-electrode catheter. *Heart Vessels* 10, 138-145.

Abel, R. M. & Reis, R. L. (1970). Effects of coronary blood flow and perfusion pressure on left ventricular contractility in dogs. *Circ.Res.* 27, 961-971.

Afzal, N. & Dhalla, N. S. (1996). Sarcoplasmic reticular Ca^{2+} pump ATPase activity in congestive heart failure due to myocardial infarction. *Can.J.Cardiol.* 12, 1065-1073.

Ai, X., Curran, J. W., Shannon, T. R., Bers, D. M., & Pogwizd, S. M. (2005). Ca^{2+}/calmodulin-dependent protein kinase modulates cardiac ryanodine receptor phosphorylation and sarcoplasmic reticulum Ca^{2+} leak in heart failure. *Circ Res* 97, 1314-1322.

Allen, D. G., Eisner, D. A., Pirolo, J. S., & Smith, G. L. (1985). The relationship between intracellular calcium and contraction in calcium-overloaded ferret papillary muscles. *J.Physiol* 364, 169-182.

Almassy, J., Sztretye, M., Lukacs, B., Dienes, B., Szabo, L., Szentesi, P., Vassort, G., Csernoch, L., & Jona, I. (2008). Effects of K-201 on the calcium pump and calcium release channel of rat skeletal muscle. *Pflugers Arch.* 457, 171-183.

Alousi, A. A. & Johnson, D. C. (1986). Pharmacology of the bipyridines: amrinone and milrinone. *Circulation* 73, III10-III24.

Altamirano, J., Li, Y., DeSantiago, J., Piacentino, V., III, Houser, S. R., & Bers, D. M. (2006). The inotropic effect of cardioactive glycosides in ventricular myocytes requires Na^{+}-Ca^{2+} exchanger function. *J.Physiol* 575, 845-854.

Alto, L. E. & Dhalla, N. S. (1979). Myocardial cation contents during induction of calcium paradox. *Am.J.Physiol* 237, H713-H719.

Andersson, K. B., Birkeland, J. A., Finsen, A. V., Louch, W. E., Sjaastad, I., Wang, Y., Chen, J., Molkentin, J. D., Chien, K. R., Sejersted, O. M., & Christensen, G. (2009). Moderate heart dysfunction in mice with inducible cardiomyocyte-specific excision of the Serca2 gene. ***J.Mol.Cell Cardiol.*** **47, 180-187.**

Antoons, G., Ver, H. M., Raeymaekers, L., Vangheluwe, P., Wuytack, F., & Sipido, K. R. (2003). Ca^{2+} uptake by the sarcoplasmic reticulum in ventricular myocytes of the SERCA2b/b mouse is impaired at higher Ca^{2+} loads only. ***Circ.Res.*** **92, 881-887.**

Araki, Y., Usui, A., Kawaguchi, O., Saito, S., Song, M. H., Akita, T., & Ueda, Y. (2005). Pressure-volume relationship in isolated working heart with crystalloid perfusate in swine and imaging the valve motion. ***Eur.J.Cardiothorac.Surg.*** **28, 435-442.**

Arnold, G., Kosche, F., Miessner, E., Neitzert, A., & Lochner, W. (1968). The importance of the perfusion pressure in the coronary arteries for the contractility and the oxygen consumption of the heart. ***Pflugers Arch.Gesamte Physiol Menschen Tiere*** **299, 339-356.**

Baan, J., Jong, T. T., Kerkhof, P. L., Moene, R. J., van Dijk, A. D., van der Velde, E. T., & Koops, J. (1981). Continuous stroke volume and cardiac output from intra-ventricular dimensions obtained with impedance catheter. ***Cardiovasc.Res.*** **15, 328-334.**

Baan, J., van der Velde, E. T., de Bruin, H. G., Smeenk, G. J., Koops, J., van Dijk, A. D., Temmerman, D., Senden, J., & Buis, B. (1984). Continuous measurement of left ventricular volume in animals and humans by conductance catheter. ***Circulation*** **70, 812-823.**

Baines, C. P. (2009). The mitochondrial permeability transition pore and ischemia-reperfusion injury. ***Basic Res.Cardiol.*** **104, 181-188.**

Baker, D. L., Hashimoto, K., Grupp, I. L., Ji, Y., Reed, T., Loukianov, E., Grupp, G., Bhagwhat, A., Hoit, B., Walsh, R., Marban, E., & Periasamy, M. (1998). Targeted

overexpression of the sarcoplasmic reticulum Ca^{2+}-ATPase increases cardiac contractility in transgenic mouse hearts. *Circ.Res.* 83, 1205-1214.

Baker, J. E., Boerboom, L. E., & Olinger, G. N. (1988). Age-related changes in the ability of hypothermia and cardioplegia to protect ischemic rabbit myocardium. *J.Thorac.Cardiovasc.Surg.* 96, 717-724.

Barcenas-Ruiz, L., Beuckelmann, D. J., & Wier, W. G. (1987). Sodium-calcium exchange in heart: membrane currents and changes in $[Ca^{2+}]_i$. *Science* 238, 1720-1722.

Bassani, J. W., Bassani, R. A., & Bers, D. M. (1993). Twitch-dependent SR Ca accumulation and release in rabbit ventricular myocytes. *Am.J.Physiol* 265, C533-C540.

Bassani, J. W., Bassani, R. A., & Bers, D. M. (1994). Relaxation in rabbit and rat cardiac cells: species-dependent differences in cellular mechanisms. *J.Physiol* 476, 279-293.

Bassani, R. A., Bassani, J. W., & Bers, D. M. (1992). Mitochondrial and sarcolemmal Ca transport reduce $[Ca^{2+}]_i$ during caffeine contractures in rabbit cardiac myocytes. *J.Physiol* 453, 591-608.

Bassani, R. A., Bassani, J. W., & Bers, D. M. (1995). Relaxation in ferret ventricular myocytes: role of the sarcolemmal Ca ATPase. *Pflugers Arch.* 430, 573-578.

Baudet, S., Shaoulian, R., & Bers, D. M. (1993). Effects of thapsigargin and cyclopiazonic acid on twitch force and sarcoplasmic reticulum Ca^{2+} content of rabbit ventricular muscle. *Circ.Res.* 73, 813-819.

Belevych, A., Kubalova, Z., Terentyev, D., Hamlin, R. L., Carnes, C. A., & Gyorke, S. (2007). Enhanced ryanodine receptor-mediated calcium leak determines reduced sarcoplasmic reticulum calcium content in chronic canine heart failure. *Biophys.J.* 93, 4083-4092.

Belz, G. G. (1995). Elastic properties and Windkessel function of the human aorta. *Cardiovasc.Drugs Ther.* 9, 73-83.

Berlin, J. R., Cannell, M. B., & Lederer, W. J. (1989). Cellular origins of the transient inward current in cardiac myocytes. Role of fluctuations and waves of elevated intracellular calcium. *Circ.Res.* 65, 115-126.

Bers, D. M. (1985). Ca influx and sarcoplasmic reticulum Ca release in cardiac muscle activation during postrest recovery. *Am.J.Physiol* 248, H366-H381.

Bers, D. M. (2001). *Excitation-Contraction Coupling and Cardiac Contractile Force,* 2nd ed. Kluwer Academic.

Bers, D. M. (2002). Cardiac excitation-contraction coupling. *Nature* 415, 198-205.

Bers, D. M., Christensen, D. M., & Nguyen, T. X. (1988). Can Ca entry via Na-Ca exchange directly activate cardiac muscle contraction? *J.Mol.Cell Cardiol.* 20, 405-414.

Bers, D. M., Despa, S., & Bossuyt, J. (2006). Regulation of Ca^{2+} and Na^{+} in normal and failing cardiac myocytes. *Ann.N.Y.Acad.Sci.* 1080, 165-177.

Bers, D. M., Eisner, D. A., & Valdivia, H. H. (2003). Sarcoplasmic reticulum Ca^{2+} and heart failure: roles of diastolic leak and Ca^{2+} transport. *Circ.Res.* 93, 487-490.

Bers, D. M. & Perez-Reyes, E. (1999). Ca channels in cardiac myocytes: structure and function in Ca influx and intracellular Ca release. *Cardiovasc.Res.* 42, 339-360.

Bers, D. M. & Stiffel, V. M. (1993). Ratio of ryanodine to dihydropyridine receptors in cardiac and skeletal muscle and implications for E-C coupling. *Am.J.Physiol* 264, 1587-1593.

Beuckelmann, D. J., Nabauer, M., & Erdmann, E. (1992). Intracellular calcium handling in isolated ventricular myocytes from patients with terminal heart failure. *Circulation* 85, 1046-1055.

Beuckelmann, D. J., Nabauer, M., Kruger, C., & Erdmann, E. (1995). Altered diastolic $[Ca^{2+}]_i$ handling in human ventricular myocytes from patients with terminal heart failure. *Am.Heart J.* 129, 684-689.

Beuckelmann, D. J. & Wier, W. G. (1988). Mechanism of release of calcium from sarcoplasmic reticulum of guinea-pig cardiac cells. *J.Physiol* 405, 233-255.

Bindoli, A., Rigobello, M. P., & Galzigna, L. (1989). Toxicity of aminochromes. *Toxicol.Lett.* 48, 3-20.

Blaustein, M. P., Juhaszova, M., & Golovina, V. A. (1998). The cellular mechanism of action of cardiotonic steroids: a new hypothesis. *Clin.Exp.Hypertens.* 20, 691-703.

Bleeker, G. B., Bax, J. J., Steendijk, P., Schalij, M. J., & van der Wall, E. E. (2006). Left ventricular dyssynchrony in patients with heart failure: pathophysiology, diagnosis and treatment. *Nat.Clin.Pract.Cardiovasc.Med.* 3, 213-219.

Bloom, S. & Davis, D. L. (1972). Calcium as mediator of isoproterenol-induced myocardial necrosis. *Am.J.Pathol.* 69, 459-470.

Bouchard, R. A., Clark, R. B., & Giles, W. R. (1995). Effects of action potential duration on excitation-contraction coupling in rat ventricular myocytes. Action potential voltage-clamp measurements. *Circ.Res.* 76, 790-801.

Bove, A. A. & Lynch, P. R. (1970). Radiographic determination of force-velocity-length relationship in the intact dog heart. *J.Appl.Physiol* 29, 884-888.

Boyden, P. A., Dun, W., Barbhaiya, C., & Ter Keurs, H. E. (2004). 2APB- and JTV519(K201)-sensitive micro Ca^{2+} waves in arrhythmogenic Purkinje cells that survive in infarcted canine heart. *Heart Rhythm.* 1, 218-226.

Brandl, C. J., Green, N. M., Korczak, B., & MacLennan, D. H. (1986). Two Ca^{2+} ATPase genes: homologies and mechanistic implications of deduced amino acid sequences. *Cell* 44, 597-607.

Braunwald E (2008). *Heart disease. A textbook of cardiovascular medicine,* 8th ed. W.B. Saunders.

Burkhoff, D., Mirsky, I., & Suga, H. (2005). Assessment of systolic and diastolic ventricular properties via pressure-volume analysis: a guide for clinical, translational, and basic researchers. *Am.J.Physiol Heart Circ.Physiol* 289, H501-H512.

Burkhoff, D., van, d., V, Kass, D., Baan, J., Maughan, W. L., & Sagawa, K. (1985). Accuracy of volume measurement by conductance catheter in isolated, ejecting canine hearts. *Circulation* 72, 440-447.

Capogrossi, M. C., Houser, S. R., Bahinski, A., & Lakatta, E. G. (1987). Synchronous occurrence of spontaneous localized calcium release from the sarcoplasmic reticulum generates action potentials in rat cardiac ventricular myocytes at normal resting membrane potential. *Circ.Res.* 61, 498-503.

Capogrossi, M. C. & Lakatta, E. G. (1985). Frequency modulation and synchronization of spontaneous oscillations in cardiac cells. *Am.J.Physiol* 248, H412-H418.

Capogrossi, M. C., Suarez-Isla, B. A., & Lakatta, E. G. (1986). The interaction of electrically stimulated twitches and spontaneous contractile waves in single cardiac myocytes. *J.Gen.Physiol* 88, 615-633.

Carl, S. L., Felix, K., Caswell, A. H., Brandt, N. R., Ball, W. J., Jr., Vaghy, P. L., Meissner, G., & Ferguson, D. G. (1995). Immunolocalization of sarcolemmal dihydropyridine receptor and sarcoplasmic reticular triadin and ryanodine receptor in rabbit ventricle and atrium. *J.Cell Biol.* 129, 673-682.

Cavagna, M., O'Donnell, J. M., Sumbilla, C., Inesi, G., & Klein, M. G. (2000). Exogenous Ca^{2+}-ATPase isoform effects on Ca^{2+} transients of embryonic chicken and neonatal rat cardiac myocytes. *J.Physiol* 528, 53-63.

Chalmers, J. P., Korner, P. I., & White, S. W. (1967). The effects of haemorrhage in the unanaesthetized rabbit. *J.Physiol* 189, 367-391.

Chapman, R. A. & Tunstall, J. (1980). The interaction of sodium and calcium ions at the cell membrane and the control of contractile strength in frog atrial muscle. *J.Physiol* 305, 109-123.

Chapman, R. A. & Tunstall, J. (1987). The calcium paradox of the heart. *Prog.Biophys.Mol.Biol.* 50, 67-96.

Chemnitius, J. M., Burger, W., & Bing, R. J. (1985). Crystalloid and perfluorochemical perfusates in an isolated working rabbit heart preparation. *Am.J.Physiol* 249, H285-H292.

Chen, V., Chen, Y. H., & Downing, S. E. (1987). An improved isolated working rabbit heart preparation using red cell enhanced perfusate. *Yale J.Biol.Med.* 60, 209-219.

Chen, Y. J., Chen, Y. C., Wongcharoen, W., Lin, C. I., & Chen, S. A. (2008). Effect of K201, a novel antiarrhythmic drug on calcium handling and arrhythmogenic activity of pulmonary vein cardiomyocytes. *Br.J.Pharmacol.* 153, 915-925.

Cheng, H., Lederer, M. R., Lederer, W. J., & Cannell, M. B. (1996). Calcium sparks and $[Ca^{2+}]_i$ waves in cardiac myocytes. *Am.J.Physiol* 270, C148-C159.

Cheng, H., Lederer, W. J., & Cannell, M. B. (1993). Calcium sparks: elementary events underlying excitation-contraction coupling in heart muscle. *Science* 262, 740-744.

Cornea, R. L., Jones, L. R., Autry, J. M., & Thomas, D. D. (1997). Mutation and phosphorylation change the oligomeric structure of phospholamban in lipid bilayers. *Biochemistry* 36, 2960-2967.

Curran, J., Hinton, M. J., Rios, E., Bers, D. M., & Shannon, T. R. (2007). Beta-adrenergic enhancement of sarcoplasmic reticulum calcium leak in cardiac myocytes is mediated by calcium/calmodulin-dependent protein kinase. *Circ.Res.* 100, 391-398.

Currie, S. & Smith, G. L. (1999). Enhanced phosphorylation of phospholamban and downregulation of sarco/endoplasmic reticulum Ca^{2+} ATPase type 2 (SERCA 2) in cardiac sarcoplasmic reticulum from rabbits with heart failure. *Cardiovasc.Res.* 41, 135-146.

Das, D. K., Engelman, R. M., Prasad, M. R., Rousou, J. A., Breyer, R. H., Jones, R., Young, H., & Cordis, G. A. (1989). Improvement of ischemia-reperfusion-induced myocardial dysfunction by modulating calcium-overload using a novel, specific calmodulin antagonist, CGS 9343B. *Biochem.Pharmacol.* 38, 465-471.

Davidson, G. A. & Varhol, R. J. (1995). Kinetics of thapsigargin-Ca^{2+}-ATPase (sarcoplasmic reticulum) interaction reveals a two-step binding mechanism and picomolar inhibition. *J.Biol.Chem.* 270, 11731-11734.

Dawson, D., Lygate, C. A., Zhang, M. H., Hulbert, K., Neubauer, S., & Casadei, B. (2005). nNOS gene deletion exacerbates pathological left ventricular remodeling and functional deterioration after myocardial infarction. *Circulation* 112, 3729-3737.

de Windt, L. J., Willems, J., Reneman, R. S., Van der Vusse, G. J., Arts, T., & Van Bilsen, M. (1999). An improved isolated, left ventricular ejecting, murine heart model. Functional and metabolic evaluation. *Pflugers Arch.* 437, 182-190.

del Monte, F., Williams, E., Lebeche, D., Schmidt, U., Rosenzweig, A., Gwathmey, J. K., Lewandowski, E. D., & Hajjar, R. J. (2001). Improvement in survival and cardiac metabolism after gene transfer of sarcoplasmic reticulum Ca^{2+}-ATPase in a rat model of heart failure. *Circulation* 104, 1424-1429.

Desager, J. P., Leonard, J. P., Vanderbist, M., & Harvengt, C. (1979). Reduced cardiac output and renal blood flow during amitriptyline intoxication in conscious rabbits. *Toxicol.Appl.Pharmacol.* 47, 445-449.

Dettbarn, C. & Palade, P. (1998). Effects of three sarcoplasmic/endoplasmic reticulum Ca^{2+} pump inhibitors on release channels of intracellular stores. *J.Pharmacol.Exp.Ther.* 285, 739-745.

Dhalla, N. S., Yates, J. C., Lee, S. L., & Singh, A. (1978). Functional and subcellular changes in the isolated rat heart perfused with oxidized isoproterenol. *J.Mol.Cell Cardiol.* 10, 31-41.

Diaz, M. E., Trafford, A. W., O'Neill, S. C., & Eisner, D. A. (1997). A measurable reduction of s.r. Ca content follows spontaneous Ca release in rat ventricular myocytes. *Pflugers Arch.* 434, 852-854.

Edwards, A. W., Korner, P. I., & Thorburn, G. D. (1959). The cardiac output of the unanaesthetized rabbit, and the effects of preliminary anaesthesia, environmental temperature and carotid occlusion. *Q.J.Exp.Physiol Cogn Med.Sci.* 44, 309-321.

Elliott, E. B. A., Kelly, A., Rankin, A., Smith, G. L., & Loughrey, C. M. (2009). A quantitative assessment of selective pharmacological inhibition of SERCA in isolated rabbit working hearts. *Biophysical Journal.* 96[3 Suppl 1], 515a.

Elliott, E. B. A., Matsuda, T., Kaneko, N., Loughrey, C. M., & Smith, G. L. (2008). K201 inhibits diastolic Ca^{2+} release and contractions in isolated rat cardiomyocytes without increase in subsequent transient amplitude. *J Biophys* 487, 12-Pos/B331.

Ellison, G. M., Torella, D., Karakikes, I., Purushothaman, S., Curcio, A., Gasparri, C., Indolfi, C., Cable, N. T., Goldspink, D. F., & Nadal-Ginard, B. (2007). Acute beta-adrenergic overload produces myocyte damage through calcium leakage from the ryanodine receptor 2 but spares cardiac stem cells. *J.Biol.Chem.* 282, 11397-11409.

Endoh, M. (2004). Force-frequency relationship in intact mammalian ventricular myocardium: physiological and pathophysiological relevance. *Eur.J.Pharmacol.* 500, 73-86.

Fabiato, A. (1983). Calcium-induced release of calcium from the cardiac sarcoplasmic reticulum. *Am.J Physiol* 245, C1-14.

Fabiato, A. (1985). Time and calcium dependence of activation and inactivation of calcium-induced release of calcium from the sarcoplasmic reticulum of a skinned canine cardiac Purkinje cell. *J.Gen.Physiol* 85, 247-289.

Fabiato, A. & Fabiato, F. (1972). Excitation-contraction coupling of isolated cardiac fibers with disrupted or closed sarcolemmas. Calcium-dependent cyclic and tonic contractions. *Circ.Res.* 31, 293-307.

Fedida, D., Noble, D., Rankin, A. C., & Spindler, A. J. (1987). The arrhythmogenic transient inward current i_{TI} and related contraction in isolated guinea-pig ventricular myocytes. *J.Physiol* 392, 523-542.

Feigl, E. O. (1983). Coronary physiology. *Physiol Rev.* 63, 1-205.

Ferrari, R., Albertini, A., Curello, S., Ceconi, C., Di Lisa, F., Raddino, R., & Visioli, O. (1986). Myocardial recovery during post-ischaemic reperfusion: effects of nifedipine, calcium and magnesium. *J.Mol.Cell Cardiol.* 18, 487-498.

Ferrier, G. R., Moffat, M. P., & Lukas, A. (1985). Possible mechanisms of ventricular arrhythmias elicited by ischemia followed by reperfusion. Studies on isolated canine ventricular tissues. *Circ.Res.* 56, 184-194.

Fill, M., Zahradnikova, A., Villalba-Galea, C. A., Zahradnik, I., Escobar, A. L., & Gyorke, S. (2000). Ryanodine receptor adaptation. *J.Gen.Physiol* 116, 873-882.

Fleckenstein, A., Frey, M., & Fleckenstein-Grun, G. (1983). Consequences of uncontrolled calcium entry and its prevention with calcium antagonists. *Eur.Heart J.* 4 Suppl H, 43-50.

Georgakopoulos, D., Mitzner, W. A., Chen, C. H., Byrne, B. J., Millar, H. D., Hare, J. M., & Kass, D. A. (1998). *In vivo* murine left ventricular pressure-volume relations by miniaturized conductance micromanometry. *Am.J.Physiol* 274, H1416-H1422.

George, C. H. (2008). Sarcoplasmic reticulum Ca^{2+} leak in heart failure: mere observation or functional relevance? *Cardiovasc.Res.* 77, 302-314.

Gillebert, T. C., Leite-Moreira, A. F., & De Hert, S. G. (1997). Relaxation-systolic pressure relation. A load-independent assessment of left ventricular contractility. *Circulation* 95, 745-752.

Gillis, A. M., Kulisz, E., & Mathison, H. J. (1996). Cardiac electrophysiological variables in blood-perfused and buffer-perfused, isolated, working rabbit heart. *Am.J.Physiol* 271, H784-H789.

Goeger, D. E. & Riley, R. T. (1989). Interaction of cyclopiazonic acid with rat skeletal muscle sarcoplasmic reticulum vesicles. Effect on Ca^{2+} binding and Ca^{2+} permeability. *Biochem.Pharmacol.* 38, 3995-4003.

Goeger, D. E., Riley, R. T., Dorner, J. W., & Cole, R. J. (1988). Cyclopiazonic acid inhibition of the Ca^{2+}-transport ATPase in rat skeletal muscle sarcoplasmic reticulum vesicles. *Biochem.Pharmacol.* 37, 978-981.

Goldspink, D. F., Burniston, J. G., Ellison, G. M., Clark, W. A., & Tan, L. B. (2004). Catecholamine-induced apoptosis and necrosis in cardiac and skeletal myocytes of the rat in vivo: the same or separate death pathways? *Exp.Physiol* 89, 407-416.

Greene, A. L., Lalli, M. J., Ji, Y., Babu, G. J., Grupp, I., Sussman, M., & Periasamy, M. (2000). Overexpression of SERCA2b in the heart leads to an increase in

sarcoplasmic reticulum calcium transport function and increased cardiac contractility. *J.Biol.Chem.* 275, 24722-24727.

Grieve, D. J., Cave, A. C., Byrne, J. A., Layland, J., & Shah, A. M. (2004). Analysis of *ex vivo* left ventricular pressure-volume relations in the isolated murine ejecting heart. *Exp.Physiol* 89, 573-582.

Gunter, T. E. & Gunter, K. K. (2001). Uptake of calcium by mitochondria: transport and possible function. *IUBMB.Life* 52, 197-204.

Gunter, T. E. & Pfeiffer, D. R. (1990). Mechanisms by which mitochondria transport calcium. *Am.J.Physiol* 258, 755-786.

Gwathmey, J. K., Copelas, L., MacKinnon, R., Schoen, F. J., Feldman, M. D., Grossman, W., & Morgan, J. P. (1987). Abnormal intracellular calcium handling in myocardium from patients with end-stage heart failure. *Circ.Res.* 61, 70-76.

Hachida, M., Kihara, S., Nonoyama, M., & Koyanagi, H. (1999). Protective effect of JTV519, a new 1,4-benzothiazepine derivative, on prolonged myocardial preservation. *J.Card Surg.* 14, 187-193.

Haft, J. I. (1974). Cardiovascular injury induced by sympathetic catecholamines. *Prog.Cardiovasc.Dis.* 17, 73-86.

Hajjar, R. J., Kang, J. X., Gwathmey, J. K., & Rosenzweig, A. (1997). Physiological effects of adenoviral gene transfer of sarcoplasmic reticulum calcium ATPase in isolated rat myocytes. *Circulation* 95, 423-429.

Harrison, S. M. & Bers, D. M. (1989). Influence of temperature on the calcium sensitivity of the myofilaments of skinned ventricular muscle from the rabbit. *J.Gen.Physiol* 93, 411-428.

Hartley, C. J., Reddy, A. K., & Taffet, G. E. (2008). In-vitro evaluation of sensors and amplifiers to measure left ventricular pressure in mice. *Conf.Proc.IEEE Eng Med.Biol.Soc.* 2008, 965-968.

Hartmann, M. & Decking, U. K. (1999). Blocking Na^+-H^+ exchange by cariporide reduces Na^+-overload in ischemia and is cardioprotective. *J.Mol.Cell Cardiol.* 31, 1985-1995.

Hasenfuss, G. & Pieske, B. (2002). Calcium cycling in congestive heart failure. *J.Mol.Cell Cardiol.* 34, 951-969.

Hasenfuss, G., Reinecke, H., Studer, R., Meyer, M., Pieske, B., Holtz, J., Holubarsch, C., Posival, H., Just, H., & Drexler, H. (1994). Relation between myocardial function and expression of sarcoplasmic reticulum Ca^{2+}-ATPase in failing and nonfailing human myocardium. *Circ.Res.* 75, 434-442.

Hasenfuss, G., Schillinger, W., Lehnart, S. E., Preuss, M., Pieske, B., Maier, L. S., Prestle, J., Minami, K., & Just, H. (1999). Relationship between Na^+-Ca^{2+}-exchanger protein levels and diastolic function of failing human myocardium. *Circulation* 99, 641-648.

Hassessian, H., Vaca, L., & Kunze, D. L. (1994). Blockade of the inward rectifier potassium current by the Ca^{2+}-ATPase inhibitor 2',5'-di(tert-butyl)-1,4-benzohydroquinone (BHQ). *Br.J.Pharmacol.* 112, 1118-1122.

Hasumi, H., Matsuda, R., Shimamoto, K., Hata, Y., & Kaneko, N. (2007). K201, a multi-channel blocker, inhibits clofilium-induced torsades de pointes and attenuates an increase in repolarization. *Eur.J.Pharmacol.* 555, 54-60.

He, H., Giordano, F. J., Hilal-Dandan, R., Choi, D. J., Rockman, H. A., McDonough, P. M., Bluhm, W. F., Meyer, M., Sayen, M. R., Swanson, E., & Dillmann, W. H. (1997). Overexpression of the rat sarcoplasmic reticulum Ca^{2+} ATPase gene in the heart of transgenic mice accelerates calcium transients and cardiac relaxation. *J.Clin.Invest* 100, 380-389.

Hermann, H. P., Zeitz, O., Keweloh, B., Hasenfuss, G., & Janssen, P. M. (2000). Pyruvate potentiates inotropic effects of isoproterenol and Ca^{2+} in rabbit cardiac muscle preparations. *Am.J.Physiol Heart Circ.Physiol* 279, H702-H708.

Herrera, M. C., Olivera, J. M., & Valentinuzzi, M. E. (1999). Parallel conductance estimation by hypertonic dilution method with conductance catheter: effects of the bolus concentration and temperature. *IEEE Trans.Biomed.Eng* 46, 830-837.

Heymes, C., Vanderheyden, M., Bronzwaer, J. G., Shah, A. M., & Paulus, W. J. (1999). Endomyocardial nitric oxide synthase and left ventricular preload reserve in dilated cardiomyopathy. *Circulation* 99, 3009-3016.

Hicks, M. J., Shigekawa, M., & Katz, A. M. (1979). Mechanism by which cyclic adenosine 3':5'-monophosphate-dependent protein kinase stimulates calcium transport in cardiac sarcoplasmic reticulum. *Circ.Res.* 44, 384-391.

Higgins, A. J. & Blackburn, K. J. (1984). Prevention of reperfusion damage in working rat hearts by calcium antagonists and calmodulin antagonists. *J.Mol.Cell Cardiol.* 16, 427-438.

Hobai, I. A. & O'Rourke, B. (2001). Decreased sarcoplasmic reticulum calcium content is responsible for defective excitation-contraction coupling in canine heart failure. *Circulation* 103, 1577-1584.

Holmuhamedov, E. L., Ozcan, C., Jahangir, A., & Terzic, A. (2001). Restoration of Ca^{2+}-inhibited oxidative phosphorylation in cardiac mitochondria by mitochondrial Ca^{2+} unloading. *Mol.Cell Biochem.* 220, 135-140.

Hoshijima, M., Ikeda, Y., Iwanaga, Y., Minamisawa, S., Date, M. O., Gu, Y., Iwatate, M., Li, M., Wang, L., Wilson, J. M., Wang, Y., Ross, J., Jr., & Chien, K. R. (2002). Chronic suppression of heart-failure progression by a pseudophosphorylated mutant of phospholamban via *in vivo* cardiac rAAV gene delivery. *Nat.Med.* 8, 864-871.

Houser, S. R., Piacentino, V., III, & Weisser, J. (2000). Abnormalities of calcium cycling in the hypertrophied and failing heart. *J.Mol.Cell Cardiol.* 32, 1595-1607.

Hove-Madsen, L. & Bers, D. M. (1993). Sarcoplasmic reticulum Ca^{2+} uptake and thapsigargin sensitivity in permeabilized rabbit and rat ventricular myocytes. *Circ.Res.* 73, 820-828.

Hove-Madsen, L., Llach, A., Bayes-Genis, A., Roura, S., Rodriguez, F. E., Aris, A., & Cinca, J. (2004). Atrial fibrillation is associated with increased spontaneous calcium release from the sarcoplasmic reticulum in human atrial myocytes. *Circulation* 110, 1358-1363.

How, O. J., Aasum, E., Kunnathu, S., Severson, D. L., Myhre, E. S., & Larsen, T. S. (2005). Influence of substrate supply on cardiac efficiency, as measured by pressure-volume analysis in *ex vivo* mouse hearts. *Am.J.Physiol Heart Circ.Physiol* 288, H2979-H2985.

Hunt, D. J., Jones, P. P., Wang, R., Chen, W., Bolstad, J., Chen, K., Shimoni, Y., & Chen, S. R. (2007). K201 (JTV519) suppresses spontaneous Ca^{2+} release and [3H]ryanodine binding to RyR2 irrespective of FKBP12.6 association. *Biochem.J.* 404, 431-438.

Hussain, M. & Orchard, C. H. (1997). Sarcoplasmic reticulum Ca^{2+} content, L-type Ca^{2+} current and the Ca^{2+} transient in rat myocytes during beta-adrenergic stimulation. *J.Physiol* 505 (Pt 2), 385-402.

Inagaki, K., Kihara, Y., Hayashida, W., Izumi, T., Iwanaga, Y., Yoneda, T., Takeuchi, Y., Suyama, K., Muso, E., & Sasayama, S. (2000a). Anti-ischemic effect of a novel cardioprotective agent, JTV519, is mediated through specific activation of delta-isoform of protein kinase C in rat ventricular myocardium. *Circulation* 101, 797-804.

Inagaki, K., Kihara, Y., Izumi, T., & Sasayama, S. (2000b). The cardioprotective effects of a new 1,4-benzothiazepine derivative, JTV519, on ischemia/reperfusion-induced Ca^{2+} overload in isolated rat hearts. *Cardiovasc.Drugs Ther.* 14, 489-495.

Inesi, G., Hua, S., Xu, C., Ma, H., Seth, M., Prasad, A. M., & Sumbilla, C. (2005). Studies of Ca^{2+} ATPase (SERCA) inhibition. *J.Bioenerg.Biomembr.* 37, 365-368.

Ito, H., Takaki, M., Yamaguchi, H., Tachibana, H., & Suga, H. (1996). Left ventricular volumetric conductance catheter for rats. *Am.J.Physiol* 270, H1509-H1514.

Ito, K., Shigematsu, S., Sato, T., Abe, T., Li, Y., & Arita, M. (2000). JTV-519, a novel cardioprotective agent, improves the contractile recovery after ischaemia-reperfusion in coronary perfused guinea-pig ventricular muscles. *Br.J.Pharmacol.* 130, 767-776.

Itoi, T. & Lopaschuk, G. D. (1996). Calcium improves mechanical function and carbohydrate metabolism following ischemia in isolated Bi-ventricular working hearts from immature rabbits. *J.Mol.Cell Cardiol.* 28, 1501-1514.

Ji, Y., Lalli, M. J., Babu, G. J., Xu, Y., Kirkpatrick, D. L., Liu, L. H., Chiamvimonvat, N., Walsh, R. A., Shull, G. E., & Periasamy, M. (2000). Disruption of a single copy of the SERCA2 gene results in altered Ca^{2+} homeostasis and cardiomyocyte function. *J.Biol.Chem.* 275, 38073-38080.

Ji, Y., Loukianov, E., Loukianova, T., Jones, L. R., & Periasamy, M. (1999a). SERCA1a can functionally substitute for SERCA2a in the heart. *Am.J.Physiol* 276, H89-H97.

Ji, Y., Loukianov, E., & Periasamy, M. (1999b). Analysis of sarcoplasmic reticulum Ca^{2+} transport and Ca^{2+} ATPase enzymatic properties using mouse cardiac tissue homogenates. *Anal.Biochem.* 269, 236-244.

Joho, S., Ishizaka, S., Sievers, R., Foster, E., Simpson, P. C., & Grossman, W. (2007). Left ventricular pressure-volume relationship in conscious mice. ***Am.J.Physiol Heart Circ.Physiol*** **292, H369-H377.**

Kaneko, N. (1994). New 1,4-Benzothiazepine Derivative, K201, Demonstrates Cardioprotective Effects Against Sudden Cardiac Cell-Death and Intracellular Calcium Blocking Action. ***Drug Development Research*** **33, 429-438.**

Kaneko, N., Matsuda, R., Ohtani, N., Nakajima, T., Arikawa, T., Suzuki, H., Toyoda, S., Kikuchi, M., Hata, Y., Abe, S., Taguchi, I., & Shimamoto, K. (2006). K201 improves norepinephrine-induced diastolic dysfunction with preserved ejection fraction. ***Drug Development Research*** **67, 852-861.**

Kaneko, N., Matsuda, R., Toda, M., & Shimamoto, K. (1997). Inhibition of annexin V-dependent Ca^{2+} movement in large unilamellar vesicles by K201, a new 1,4-benzothiazepine derivative. ***Biochim.Biophys.Acta*** **1330, 1-7.**

Kaprielian, R., Wickenden, A. D., Kassiri, Z., Parker, T. G., Liu, P. P., & Backx, P. H. (1999). Relationship between K channel downregulation and [Ca^{2+}] in rat ventricular myocytes following myocardial infarction. ***J.Physiol*** **517, 229-245.**

Karmazyn, M., Gan, X. T., Humphreys, R. A., Yoshida, H., & Kusumoto, K. (1999). The myocardial Na^{+}-H^{+} exchange: structure, regulation, and its role in heart disease. ***Circ.Res.*** **85, 777-786.**

Kass, D. A. (1992). Clinical evaluation of left heart function by conductance catheter technique. ***Eur.Heart J.*** **13 Suppl E, 57-64.**

Kass, D. A., Bronzwaer, J. G., & Paulus, W. J. (2004). What mechanisms underlie diastolic dysfunction in heart failure? ***Circ.Res.*** **94, 1533-1542.**

Kass, R. S., Lederer, W. J., Tsien, R. W., & Weingart, R. (1978). Role of calcium ions in transient inward currents and aftercontractions induced by strophanthidin in cardiac Purkinje fibres. ***J.Physiol*** **281, 187-208.**

Katra, R. P. & Laurita, K. R. (2005). Cellular mechanism of calcium-mediated triggered activity in the heart. *Circ.Res.* 96, 535-542.

Kawabata, H., Nakagawa, K., & Ishikawa, K. (2002). A novel cardioprotective agent, JTV-519, is abolished by nitric oxide synthase inhibitor on myocardial metabolism in ischemia-reperfused rabbit hearts. *Hypertens.Res.* 25, 303-309.

Kawabata, H., Ryomoto, T., & Ishikawa, K. (2000). Effect of a novel cardioprotective agent, JTV-519, on metabolism, contraction and relaxation in the ischemia-reperfused rabbit heart. *Jpn.Circ.J.* 64, 772-776.

Khandoudi, N., Percevault-Albadine, J., & Bril, A. (1998). Consequences of the inhibition of the sarcoplasmic reticulum calcium ATPase on cardiac function and coronary flow in rabbit isolated perfused heart: role of calcium and nitric oxide. *J.Mol.Cell Cardiol.* 30, 1967-1977.

Khatter, J. C., Agbanyo, M., Navaratnam, S., Nero, B., & Hoeschen, R. J. (1989). Digitalis cardiotoxicity: cellular calcium overload a possible mechanism. *Basic Res.Cardiol.* 84, 553-563.

Kimura, J., Kawahara, M., Sakai, E., Yatabe, J., & Nakanishi, H. (1999). Effects of a novel cardioprotective drug, JTV-519, on membrane currents of guinea pig ventricular myocytes. *Jpn.J.Pharmacol.* 79, 275-281.

Kimura, S., Cameron, J. S., Kozlovskis, P. L., Bassett, A. L., & Myerburg, R. J. (1984). Delayed afterdepolarizations and triggered activity induced in feline Purkinje fibers by alpha-adrenergic stimulation in the presence of elevated calcium levels. *Circulation* 70, 1074-1082.

Kirby, M. S., Sagara, Y., Gaa, S., Inesi, G., Lederer, W. J., & Rogers, T. B. (1992). Thapsigargin inhibits contraction and Ca^{2+} transient in cardiac cells by specific inhibition of the sarcoplasmic reticulum Ca^{2+} pump. *J.Biol.Chem.* 267, 12545-12551.

Kiriyama, K., Kiyosue, T., Wang, J. C., Dohi, K., & Arita, M. (2000). Effects of JTV-519, a novel anti-ischaemic drug, on the delayed rectifier K^+ current in guinea-pig ventricular myocytes. *Naunyn Schmiedebergs Arch.Pharmacol.* 361, 646-653.

Kiss, E., Edes, I., Sato, Y., Luo, W., Liggett, S. B., & Kranias, E. G. (1997). beta-Adrenergic regulation of cAMP and protein phosphorylation in phospholamban-knockout mouse hearts. *Am.J.Physiol* 272, H785-H790.

Koch-Weser, J. & Blinks, J. R. (1963). The influence of the interval between beats on myocardial contractility. *Pharmacol.Rev.* 15, 601-652.

Kohno, M., Yano, M., Kobayashi, S., Doi, M., Oda, T., Tokuhisa, T., Okuda, S., Ohkusa, T., Kohno, M., & Matsuzaki, M. (2003). A new cardioprotective agent, JTV519, improves defective channel gating of ryanodine receptor in heart failure. *Am.J.Physiol Heart Circ.Physiol* 284, H1035-H1042.

Korge, P., Honda, H. M., & Weiss, J. N. (2002). Protection of cardiac mitochondria by diazoxide and protein kinase C: implications for ischemic preconditioning. *Proc.Natl.Acad.Sci.U.S.A* 99, 3312-3317.

Kort, A. A. & Lakatta, E. G. (1984). Calcium-dependent mechanical oscillations occur spontaneously in unstimulated mammalian cardiac tissues. *Circ.Res.* 54, 396-404.

Kumagai, K., Nakashima, H., Gondo, N., & Saku, K. (2003). Antiarrhythmic effects of JTV-519, a novel cardioprotective drug, on atrial fibrillation/flutter in a canine sterile pericarditis model. *J.Cardiovasc.Electrophysiol.* 14, 880-884.

Lalli, M. J., Yong, J., Prasad, V., Hashimoto, K., Plank, D., Babu, G. J., Kirkpatrick, D., Walsh, R. A., Sussman, M., Yatani, A., Marban, E., & Periasamy, M. (2001). Sarcoplasmic reticulum Ca^{2+} atpase (SERCA) 1a structurally substitutes for SERCA2a in the cardiac sarcoplasmic reticulum and increases cardiac Ca^{2+} handling capacity. *Circ.Res.* 89, 160-167.

Lam, E., Martin, M. M., Timerman, A. P., Sabers, C., Fleischer, S., Lukas, T., Abraham, R. T., O'Keefe, S. J., O'Neill, E. A., & Wiederrecht, G. J. (1995). A novel FK506 binding protein can mediate the immunosuppressive effects of FK506 and is associated with the cardiac ryanodine receptor. *J.Biol.Chem.* 270, 26511-26522.

Langer, S. F. (2002). Differential laws of left ventricular isovolumic pressure fall. *Physiol Res.* 51, 1-15.

Lankford, E. B., Kass, D. A., Maughan, W. L., & Shoukas, A. A. (1990). Does volume catheter parallel conductance vary during a cardiac cycle? *Am.J.Physiol* 258, H1933-H1942.

Lederer, W. J., Berlin, J. R., Cohen, N. M., Hadley, R. W., Bers, D. M., & Cannell, M. B. (1990). Excitation-contraction coupling in heart cells. Roles of the sodium-calcium exchange, the calcium current, and the sarcoplasmic reticulum. *Ann.N.Y.Acad.Sci.* 588, 190-206.

Leitch, S. P. & Patterson, D. J. (1994). Interactive effects of K^+, acidosis, and catecholamines on isolated rabbit heart: implications for exercise. *J.Appl.Physiol* 77, 1164-1171.

Leite-Moreira, A. F., Correia-Pinto, J., & Gillebert, T. C. (1999). Afterload induced changes in myocardial relaxation: a mechanism for diastolic dysfunction. *Cardiovasc.Res.* 43, 344-353.

Leite-Moreira, A. F. & Gillebert, T. C. (1994). Nonuniform course of left ventricular pressure fall and its regulation by load and contractile state. *Circulation* 90, 2481-2491.

Lewandowski, E. D., Devous, M. D., Sr., & Nunnally, R. L. (1987). High-energy phosphates and function in isolated, working rabbit hearts. *Am.J.Physiol* 253, H1215-H1223.

Lindner, M., Erdmann, E., & Beuckelmann, D. J. (1998). Calcium content of the sarcoplasmic reticulum in isolated ventricular myocytes from patients with terminal heart failure. *J.Mol.Cell Cardiol.* 30, 743-749.

Lisy, O. & Burnett, J. C., Jr. (2006). New cardioprotective agent K201 is natriuretic and glomerular filtration rate enhancing. *Circulation* 113, 246-251.

Liu, N., Ruan, Y., & Priori, S. G. (2008). Catecholaminergic polymorphic ventricular tachycardia. *Prog.Cardiovasc.Dis.* 51, 23-30.

Liu, Y., Sato, T., Seharaseyon, J., Szewczyk, A., O'Rourke, B., & Marban, E. (1999). Mitochondrial ATP-dependent potassium channels. Viable candidate effectors of ischemic preconditioning. *Ann.N.Y.Acad.Sci.* 874, 27-37.

Logeart, D., Vinet, L., Ragot, T., Heimburger, M., Louedec, L., Michel, J. B., Escoubet, B., & Mercadier, J. J. (2006). Percutaneous intracoronary delivery of SERCA gene increases myocardial function: a tissue Doppler imaging echocardiographic study. *Am.J.Physiol Heart Circ.Physiol* 291, H1773-H1779.

Loughrey, C. M., Otani, N., Seidler, T., Craig, M. A., Matsuda, R., Kaneko, N., & Smith, G. L. (2007). K201 modulates excitation-contraction coupling and spontaneous Ca^{2+} release in normal adult rabbit ventricular cardiomyocytes. *Cardiovasc.Res.* 76, 236-246.

Lukyanenko, V., Gyorke, I., Subramanian, S., Smirnov, A., Wiesner, T. F., & Gyorke, S. (2000). Inhibition of Ca^{2+} sparks by ruthenium red in permeabilized rat ventricular myocytes. *Biophys.J.* 79, 1273-1284.

Luo, D., Nakazawa, M., Yoshida, Y., Cai, J., & Imai, S. (2000). Effects of three different Ca^{2+} pump ATPase inhibitors on evoked contractions in rabbit aorta and activities of Ca^{2+} pump ATPases in porcine aorta. *Gen.Pharmacol.* 34, 211-220.

Luo, W., Grupp, I. L., Harrer, J., Ponniah, S., Grupp, G., Duffy, J. J., Doetschman, T., & Kranias, E. G. (1994). Targeted ablation of the phospholamban gene is

associated with markedly enhanced myocardial contractility and loss of beta-agonist stimulation. *Circ.Res.* 75, 401-409.

Lytton, J., Westlin, M., Burk, S. E., Shull, G. E., & MacLennan, D. H. (1992). Functional comparisons between isoforms of the sarcoplasmic or endoplasmic reticulum family of calcium pumps. *J.Biol.Chem.* 267, 14483-14489.

Maier, L. S., Bers, D. M., & Pieske, B. (2000). Differences in Ca^{2+}-handling and sarcoplasmic reticulum Ca^{2+}-content in isolated rat and rabbit myocardium. *J.Mol.Cell Cardiol.* 32, 2249-2258.

Maier, L. S., Wahl-Schott, C., Horn, W., Weichert, S., Pagel, C., Wagner, S., Dybkova, N., Muller, O. J., Nabauer, M., Franz, W. M., & Pieske, B. (2005). Increased SR Ca^{2+} cycling contributes to improved contractile performance in SERCA2a-overexpressing transgenic rats. *Cardiovasc.Res.* 67, 636-646.

Makinose, M. (1973). Possible functional states of the enzyme of the sarcoplasmic calcium pump. *FEBS Lett.* 37, 140-143.

Mann, D. L., Kent, R. L., Parsons, B., & Cooper, G. (1992). Adrenergic effects on the biology of the adult mammalian cardiocyte. *Circulation* 85, 790-804.

Mann, G. E. (1981). Alterations of myocardial capillary permeability by albumin in the isolated, perfused rabbit heart. *J.Physiol* 319, 311-323.

Marx, S. O., Reiken, S., Hisamatsu, Y., Jayaraman, T., Burkhoff, D., Rosemblit, N., & Marks, A. R. (2000). PKA phosphorylation dissociates FKBP12.6 from the calcium release channel (ryanodine receptor): defective regulation in failing hearts. *Cell* 101, 365-376.

Masuda, M., Chang-Chun, C., Cho, B. C., & Flameng, W. (1994). Coronary reserve and contractile reserve in crystalloid- and blood-perfused rabbit hearts. *Heart Vessels* 9, 175-182.

Matsuoka, S. & Hilgemann, D. W. (1992). Steady-state and dynamic properties of cardiac sodium-calcium exchange. Ion and voltage dependencies of the transport cycle. *J.Gen.Physiol* 100, 963-1001.

Maughan, R. J. (1982). A simple, rapid method for the determination of glucose, lactate, pyruvate, alanine, 3-hydroxybutyrate and acetoacetate on a single 20-µl blood sample. *Clin.Chim.Acta* 122, 231-240.

McCabe, C., Hicks, M. N., Kane, K. A., & Wainwright, C. L. (2005). Electrophysiological and haemodynamic effects of endothelin ETA and ETB receptors in normal and ischaemic working rabbit hearts. *Br.J.Pharmacol.* 146, 118-128.

Meissner, A. & Morgan, J. P. (1995). Contractile dysfunction and abnormal Ca^{2+} modulation during postischemic reperfusion in rat heart. *Am.J.Physiol* 268, H100-H111.

Melzer, W., Schneider, M. F., Simon, B. J., & Szucs, G. (1986). Intramembrane charge movement and calcium release in frog skeletal muscle. *J.Physiol* 373, 481-511.

Meng, H. P. & Pierce, G. N. (1990). Protective effects of 5-(N,N-dimethyl)amiloride on ischemia-reperfusion injury in hearts. *Am.J.Physiol* 258, H1615-H1619.

Merx, M. W. & Schrader, J. (2009). The Working Heart. In *Practical Methods in Cardiovascular Research* pp. 173-189. Springer Berlin Heidelberg.

Milnor, W. R. (1975). Arterial impedance as ventricular afterload. *Circ.Res.* 36, 565-570.

Minamisawa, S., Hoshijima, M., Chu, G., Ward, C. A., Frank, K., Gu, Y., Martone, M. E., Wang, Y., Ross, J., Jr., Kranias, E. G., Giles, W. R., & Chien, K. R. (1999). Chronic phospholamban-sarcoplasmic reticulum calcium ATPase interaction is the critical calcium cycling defect in dilated cardiomyopathy. *Cell* 99, 313-322.

Mintz, E. & Guillain, F. (1997). Ca^{2+} transport by the sarcoplasmic reticulum ATPase. *Biochim.Biophys.Acta* 1318, 52-70.

Miyamae, M., Camacho, S. A., Weiner, M. W., & Figueredo, V. M. (1996). Attenuation of postischemic reperfusion injury is related to prevention of $[Ca^{2+}]_m$ overload in rat hearts. *Am.J.Physiol* 271, H2145-H2153.

Miyamoto, M. I., del Monte, F., Schmidt, U., DiSalvo, T. S., Kang, Z. B., Matsui, T., Guerrero, J. L., Gwathmey, J. K., Rosenzweig, A., & Hajjar, R. J. (2000). Adenoviral gene transfer of SERCA2a improves left-ventricular function in aortic-banded rats in transition to heart failure. *Proc.Natl.Acad.Sci.U.S.A* 97, 793-798.

Miyata, H., Lakatta, E. G., Stern, M. D., & Silverman, H. S. (1992). Relation of mitochondrial and cytosolic free calcium to cardiac myocyte recovery after exposure to anoxia. *Circ.Res.* 71, 605-613.

Mohan, P. & Bloom, S. (1999). Lipolysis is an important determinant of isoproterenol-induced myocardial necrosis. *Cardiovasc.Pathol.* 8, 255-261.

Muller, O. J., Lange, M., Rattunde, H., Lorenzen, H. P., Muller, M., Frey, N., Bittner, C., Simonides, W., Katus, H. A., & Franz, W. M. (2003). Transgenic rat hearts overexpressing SERCA2a show improved contractility under baseline conditions and pressure overload. *Cardiovasc.Res.* 59, 380-389.

Nabauer, M., Callewaert, G., Cleemann, L., & Morad, M. (1989). Regulation of calcium release is gated by calcium current, not gating charge, in cardiac myocytes. *Science* 244, 800-803.

Nakamura, H., Nakasaki, Y., Matsuda, N., & Shigekawa, M. (1992). Inhibition of sarcoplasmic reticulum Ca^{2+}-ATPase by 2,5-di(tert-butyl)-1,4-benzohydroquinone. *J.Biochem.* 112, 750-755.

Nakamura, K., Kusuoka, H., Ambrosio, G., & Becker, L. C. (1993). Glycolysis is necessary to preserve myocardial Ca^{2+} homeostasis during beta-adrenergic stimulation. *Am.J.Physiol* 264, H670-H678.

Nakaya, H., Furusawa, Y., Ogura, T., Tamagawa, M., & Uemura, H. (2000). Inhibitory effects of JTV-519, a novel cardioprotective drug, on potassium currents and experimental atrial fibrillation in guinea-pig hearts. *Br.J.Pharmacol.* 131, 1363-1372.

Neary, P., Duncan, A. M., Cobbe, S. M., & Smith, G. L. (2002). Assessment of sarcoplasmic reticulum Ca^{2+} flux pathways in cardiomyocytes from rabbits with infarct-induced left-ventricular dysfunction. *Pflugers Arch.* 444, 360-371.

Neely, J. R., Liebermeister, H., Battersby, E. J., & Morgan, H. E. (1967). Effect of pressure development on oxygen consumption by isolated rat heart. *Am.J.Physiol* 212, 804-814.

Nelson, E. J., Li, C. C., Bangalore, R., Benson, T., Kass, R. S., & Hinkle, P. M. (1994). Inhibition of L-type calcium-channel activity by thapsigargin and 2,5-t-butylhydroquinone, but not by cyclopiazonic acid. *Biochem.J.* 302 (Pt 1), 147-154.

Neutze, J. M., Wyler, F., & Rudolph, A. M. (1968). Use of radioactive microspheres to assess distribution of cardiac output in rabbits. *Am.J.Physiol* 215, 486-495.

Ng, G. A., Cobbe, S. M., & Smith, G. L. (1998). Non-uniform prolongation of intracellular Ca^{2+} transients recorded from the epicardial surface of isolated hearts from rabbits with heart failure. *Cardiovasc.Res.* 37, 489-502.

Ng, G. A., Hicks, M. N., Cobbe, S. M., & Smith, G. L. (2002). Depressed inotropic response to increased preload in rabbit hearts with left-ventricular dysfunction induced by chronic myocardial infarction. *Pflugers Arch.* 444, 513-522.

Niggli, E. & Lederer, W. J. (1990). Voltage-independent calcium release in heart muscle. *Science* 250, 565-568.

Nishio, M., Ruch, S. W., Kelly, J. E., Aistrup, G. L., Sheehan, K., & Wasserstrom, J. A. (2004). Ouabain increases sarcoplasmic reticulum calcium release in cardiac myocytes. *J.Pharmacol.Exp.Ther.* 308, 1181-1190.

Nishio, M., Ruch, S. W., & Wasserstrom, J. A. (2002). Positive inotropic effects of ouabain in isolated cat ventricular myocytes in sodium-free conditions. *Am.J.Physiol Heart Circ.Physiol* 283, H2045-H2053.

Norregaard, A., Vilsen, B., & Andersen, J. P. (1994). Transmembrane segment M3 is essential to thapsigargin sensitivity of the sarcoplasmic reticulum Ca^{2+}-ATPase. *J.Biol.Chem.* 269, 26598-26601.

O'Donnell, J. M., Fields, A., Xu, X., Chowdhury, S. A., Geenen, D. L., & Bi, J. (2008). Limited functional and metabolic improvements in hypertrophic and healthy rat heart overexpressing the skeletal muscle isoform of SERCA1 by adenoviral gene transfer in vivo. *Am.J.Physiol Heart Circ.Physiol* 295, H2483-H2494.

Obayashi, M., Xiao, B., Stuyvers, B. D., Davidoff, A. W., Mei, J., Chen, S. R., & Ter Keurs, H. E. (2006). Spontaneous diastolic contractions and phosphorylation of the cardiac ryanodine receptor at serine-2808 in congestive heart failure in rat. *Cardiovasc.Res.* 69, 140-151.

Oda, T., Yano, M., Yamamoto, T., Tokuhisa, T., Okuda, S., Doi, M., Ohkusa, T., Ikeda, Y., Kobayashi, S., Ikemoto, N., & Matsuzaki, M. (2005). Defective regulation of interdomain interactions within the ryanodine receptor plays a key role in the pathogenesis of heart failure. *Circulation* 111, 3400-3410.

Ono, K., Yano, M., Ohkusa, T., Kohno, M., Hisaoka, T., Tanigawa, T., Kobayashi, S., Kohno, M., & Matsuzaki, M. (2000). Altered interaction of FKBP12.6 with ryanodine receptor as a cause of abnormal Ca^{2+} release in heart failure. *Cardiovasc.Res* 48, 323-331.

Overend, C. L., Eisner, D. A., & O'Neill, S. C. (1997). The effect of tetracaine on spontaneous Ca^{2+} release and sarcoplasmic reticulum calcium content in rat ventricular myocytes. *J.Physiol* 502 (Pt 3), 471-479.

Pacher, P., Mabley, J. G., Liaudet, L., Evgenov, O. V., Marton, A., Hasko, G., Kollai, M., & Szabo, C. (2004). Left ventricular pressure-volume relationship in a rat model of advanced aging-associated heart failure. *Am.J.Physiol Heart Circ.Physiol* 287, H2132-H2137.

Pacher, P., Nagayama, T., Mukhopadhyay, P., Batkai, S., & Kass, D. A. (2008). Measurement of cardiac function using pressure-volume conductance catheter technique in mice and rats. *Nat.Protoc.* 3, 1422-1434.

Page, E. & Surdyk-Droske, M. (1979). Distribution, surface density, and membrane area of diadic junctional contacts between plasma membrane and terminal cisterns in mammalian ventricle. *Circ.Res.* 45, 260-267.

Pankucsi, C., Varro, A., & Nanasi, P. P. (1996). Three distinct components of the negative inotropic action of lidocaine in dog Purkinje fiber. *Gen.Pharmacol.* 27, 69-71.

Parker, I., Zang, W. J., & Wier, W. G. (1996). Ca^{2+} sparks involving multiple Ca^{2+} release sites along Z-lines in rat heart cells. *J.Physiol* 497, 31-38.

Periasamy, M. & Huke, S. (2001). SERCA pump level is a critical determinant of Ca^{2+} homeostasis and cardiac contractility. *J.Mol.Cell Cardiol.* 33, 1053-1063.

Periasamy, M. & Kalyanasundaram, A. (2007). SERCA pump isoforms: their role in calcium transport and disease. *Muscle Nerve* 35, 430-442.

Periasamy, M., Reed, T. D., Liu, L. H., Ji, Y., Loukianov, E., Paul, R. J., Nieman, M. L., Riddle, T., Duffy, J. J., Doetschman, T., Lorenz, J. N., & Shull, G. E. (1999). Impaired cardiac performance in heterozygous mice with a null mutation in the sarco(endo)plasmic reticulum Ca^{2+}-ATPase isoform 2 (SERCA2) gene. *J.Biol.Chem.* 274, 2556-2562.

Persoon-Rothert, M., van der Valk-Kokshoorn EJ, Egas-Kenniphaas, J. M., Mauve, I., & van der, L. A. (1989). Isoproterenol-induced cytotoxicity in neonatal rat heart cell cultures is mediated by free radical formation. ***J.Mol.Cell Cardiol.*** **21, 1285-1291.**

Pieske, B., Maier, L. S., Bers, D. M., & Hasenfuss, G. (1999). Ca^{2+} handling and sarcoplasmic reticulum Ca^{2+} content in isolated failing and nonfailing human myocardium. ***Circ.Res.*** **85, 38-46.**

Pinsky, M. R., Perlini, S., Solda, P. L., Pantaleo, P., Calciati, A., & Bernardi, L. (1996). Dynamic right and left ventricular interactions in the rabbit: simultaneous measurement of ventricular pressure-volume loops. ***J.Crit Care*** **11, 65-76.**

Podesser, B., Hausleithner, V., Seitelberger, R., Wollenek, G., Wolner, E., & Steiert, H. (1993). New developments in the isolated working heart: a comparison of neonatal, immature, and adult rabbits after sixty minutes of ischemia in respect to hemodynamic and biochemical parameters. ***J.Pharmacol.Toxicol.Methods*** **30, 189-196.**

Podesser, B. K., Hallstrom, S., Schima, H., Huber, L., Weisser, J., Kroner, A., Furst, W., & Wolner, E. (1999). The erythrocyte-perfused "working heart" model: hemodynamic and metabolic performance in comparison to crystalloid perfused hearts. ***J.Pharmacol.Toxicol.Methods*** **41, 9-15.**

Pogwizd, S. M., Qi, M., Yuan, W., Samarel, A. M., & Bers, D. M. (1999). Upregulation of Na^{+}/Ca^{2+} exchanger expression and function in an arrhythmogenic rabbit model of heart failure. ***Circ.Res.*** **85, 1009-1019.**

Puglisi, J. L., Yuan, W., Bassani, J. W., & Bers, D. M. (1999). Ca^{2+} influx through Ca^{2+} channels in rabbit ventricular myocytes during action potential clamp: influence of temperature. ***Circ.Res.*** **85, 7-16.**

Pye, M. P., Black, M., & Cobbe, S. M. (1996). Comparison of in vivo and in vitro haemodynamic function in experimental heart failure: use of echocardiography. ***Cardiovasc.Res.*** **31, 873-881.**

Quinn, F. R., Currie, S., Duncan, A. M., Miller, S., Sayeed, R., Cobbe, S. M., & Smith, G. L. (2003). Myocardial infarction causes increased expression but decreased activity of the myocardial Na^{+}-Ca^{2+} exchanger in the rabbit. ***J.Physiol*** **553, 229-242.**

Ramos, K., Combs, A. B., & Acosta, D. (1984). Role of calcium in isoproterenol cytotoxicity to cultured myocardial cells. ***Biochem.Pharmacol.*** **33, 1989-1992.**

Rastaldo, R., Pagliaro, P., Cappello, S., Penna, C., Mancardi, D., Westerhof, N., & Losano, G. (2007). Nitric oxide and cardiac function. ***Life Sci.*** **81, 779-793.**

Reid, M. B. & Moody, M. R. (1994). Dimethyl sulfoxide depresses skeletal muscle contractility. ***J.Appl.Physiol*** **76, 2186-2190.**

Reiken, S., Gaburjakova, M., Guatimosim, S., Gomez, A. M., D'Armiento, J., Burkhoff, D., Wang, J., Vassort, G., Lederer, W. J., & Marks, A. R. (2003). Protein kinase A phosphorylation of the cardiac calcium release channel (ryanodine receptor) in normal and failing hearts. Role of phosphatases and response to isoproterenol. ***J.Biol.Chem.*** **278, 444-453.**

Remiao, F., Carvalho, M., Carmo, H., Carvalho, F., & Bastos, M. L. (2002). Cu^{2+}-induced isoproterenol oxidation into isoprenochrome in adult rat calcium-tolerant cardiomyocytes. ***Chem.Res.Toxicol.*** **15, 861-869.**

Ritter, O. & Neyses, L. (2003). The molecular basis of myocardial hypertrophy and heart failure. ***Trends Mol.Med.*** **9, 313-321.**

Rona, G. (1985). Catecholamine cardiotoxicity. ***J.Mol.Cell Cardiol.*** **17, 291-306.**

Royse, C. F. & Royse, A. G. (2005). The myocardial and vascular effects of bupivacaine, levobupivacaine, and ropivacaine using pressure volume loops. ***Anesth.Analg.*** **101, 679-87, table.**

Ruiz-Meana, M., Garcia-Dorado, D., Pina, P., Inserte, J., Agullo, L., & Soler-Soler, J. (2003). Cariporide preserves mitochondrial proton gradient and delays ATP

depletion in cardiomyocytes during ischemic conditions. *Am.J.Physiol Heart Circ.Physiol* 285, H999-1006.

Sagara, Y. & Inesi, G. (1991). Inhibition of the sarcoplasmic reticulum Ca^{2+} transport ATPase by thapsigargin at subnanomolar concentrations. *J.Biol.Chem.* 266, 13503-13506.

Sagara, Y., Wade, J. B., & Inesi, G. (1992). A conformational mechanism for formation of a dead-end complex by the sarcoplasmic reticulum ATPase with thapsigargin. *J.Biol.Chem.* 267, 1286-1292.

Sagawa, T., Sagawa, K., Kelly, J. E., Tsushima, R. G., & Wasserstrom, J. A. (2002). Activation of cardiac ryanodine receptors by cardiac glycosides. *Am.J.Physiol Heart Circ.Physiol* 282, H1118-H1126.

Santana, L. F., Kranias, E. G., & Lederer, W. J. (1997). Calcium sparks and excitation-contraction coupling in phospholamban-deficient mouse ventricular myocytes. *J.Physiol* 503, 21-29.

Satoh, H., Ginsburg, K. S., Qing, K., Terada, H., Hayashi, H., & Bers, D. M. (2000). KB-R7943 block of Ca^{2+} influx via Na^{+}/Ca^{2+} exchange does not alter twitches or glycoside inotropy but prevents Ca^{2+} overload in rat ventricular myocytes. *Circulation* 101, 1441-1446.

Scherrer-Crosbie, M., Ullrich, R., Bloch, K. D., Nakajima, H., Nasseri, B., Aretz, H. T., Lindsey, M. L., Vancon, A. C., Huang, P. L., Lee, R. T., Zapol, W. M., & Picard, M. H. (2001). Endothelial nitric oxide synthase limits left ventricular remodeling after myocardial infarction in mice. *Circulation* 104, 1286-1291.

Schlotthauer, K. & Bers, D. M. (2000). Sarcoplasmic reticulum Ca^{2+} release causes myocyte depolarization. Underlying mechanism and threshold for triggered action potentials. *Circ.Res.* 87, 774-780.

Schmidt, H. D. (2001). Isolated working rat heart adaptation after abrupt changes in extracellular Ca^{2+} concentration. *Res.Exp.Med.(Berl)* 200, 107-124.

Schmidt, U., Hajjar, R. J., Helm, P. A., Kim, C. S., Doye, A. A., & Gwathmey, J. K. (1998). Contribution of abnormal sarcoplasmic reticulum ATPase activity to systolic and diastolic dysfunction in human heart failure. *J.Mol.Cell Cardiol.* 30, 1929-1937.

Scholz, H. (1983). Pharmacological actions of various inotropic agents. *Eur.Heart J.* 4 Suppl A, 161-172.

Segel, L. D. & Ensunsa, J. L. (1988). Albumin improves stability and longevity of perfluorochemical-perfused hearts. *Am.J.Physiol* 254, H1105-H1112.

Segers, P., Georgakopoulos, D., Afanasyeva, M., Champion, H. C., Judge, D. P., Millar, H. D., Verdonck, P., Kass, D. A., Stergiopulos, N., & Westerhof, N. (2005). Conductance catheter-based assessment of arterial input impedance, arterial function, and ventricular-vascular interaction in mice. *Am.J.Physiol Heart Circ.Physiol* 288, H1157-H1164.

Seidler, N. W., Jona, I., Vegh, M., & Martonosi, A. (1989). Cyclopiazonic acid is a specific inhibitor of the Ca^{2+}-ATPase of sarcoplasmic reticulum. *J.Biol.Chem.* 264, 17816-17823.

Seth, M., Sumbilla, C., Mullen, S. P., Lewis, D., Klein, M. G., Hussain, A., Soboloff, J., Gill, D. L., & Inesi, G. (2004). Sarco(endo)plasmic reticulum Ca^{2+} ATPase (SERCA) gene silencing and remodeling of the Ca^{2+} signaling mechanism in cardiac myocytes. *Proc.Natl.Acad.Sci.U.S.A* 101, 16683-16688.

Shannon, T. R., Pogwizd, S. M., & Bers, D. M. (2003). Elevated sarcoplasmic reticulum Ca^{2+} leak in intact ventricular myocytes from rabbits in heart failure. *Circ.Res.* 93, 592-594.

Sheu, S. S. & Lederer, W. J. (1985). Lidocaine's negative inotropic and antiarrhythmic actions. Dependence on shortening of action potential duration and reduction of intracellular sodium activity. *Circ.Res.* 57, 578-590.

Shizukuda, Y., Buttrick, P. M., Geenen, D. L., Borczuk, A. C., Kitsis, R. N., & Sonnenblick, E. H. (1998). beta-adrenergic stimulation causes cardiocyte apoptosis: influence of tachycardia and hypertrophy. *Am.J.Physiol* 275, H961-H968.

Shlafer, M., Matheny, J. L., & Karow, A. M., Jr. (1974). Cardiac inotropism of dimethyl sulphoxide: osmotic effects and interactions with calcium ion. *Eur.J.Pharmacol.* 28, 276-287.

Simmerman, H. K. & Jones, L. R. (1998). Phospholamban: protein structure, mechanism of action, and role in cardiac function. *Physiol Rev.* 78, 921-947.

Skrzypiec-Spring, M., Grotthus, B., Szelag, A., & Schulz, R. (2007). Isolated heart perfusion according to Langendorff---still viable in the new millennium. *J.Pharmacol.Toxicol.Methods* 55, 113-126.

Sobie, E. A., Dilly, K. W., dos Santos, C. J., Lederer, W. J., & Jafri, M. S. (2002). Termination of cardiac Ca^{2+} sparks: an investigative mathematical model of calcium-induced calcium release. *Biophys.J.* 83, 59-78.

Solda, P. L., Perlini, S., Piepoli, M., Grandi, A., Paroni, G., Barzizza, F., Finardi, G., & Bernardi, L. (1990). Measuring left ventricular dimensions by conductance catheter in the rabbit. *Eur.Heart J.* 11, 925-935.

Somani, P., Laddu, A. R., & Hardm, H. F. (1970). Nutritional circulation in the heart. 3. Effect of isoproterenol and beta adrenergic blockade on myocardial hemodynamics and rubicium-86 extraction in the isolated supported heart preparation. *J.Pharmacol.Exp.Ther.* 175, 577-592.

Spilker, B. (1970). Inotropic actions of dipolar aprotic solvents. *J.Pharmacol.Exp.Ther.* 175, 361-367.

Stange, M., Xu, L., Balshaw, D., Yamaguchi, N., & Meissner, G. (2003). Characterization of recombinant skeletal muscle (Ser-2843) and cardiac muscle (Ser-2809) ryanodine receptor phosphorylation mutants. *J.Biol.Chem.* 278, 51693-51702.

Steendijk, P. & Baan, J. (2000). Comparison of intravenous and pulmonary artery injections of hypertonic saline for the assessment of conductance catheter parallel conductance. *Cardiovasc.Res.* 46, 82-89.

Steendijk, P., Staal, E., Jukema, J. W., & Baan, J. (2001). Hypertonic saline method accurately determines parallel conductance for dual-field conductance catheter. *Am.J.Physiol Heart Circ.Physiol* 281, H755-H763.

Steendijk, P., Tulner, S. A., Schreuder, J. J., Bax, J. J., van Erven, L., van der Wall, E. E., Dion, R. A., Schalij, M. J., & Baan, J. (2004). Quantification of left ventricular mechanical dyssynchrony by conductance catheter in heart failure patients. *Am.J.Physiol Heart Circ.Physiol* 286, H723-H730.

Steendijk, P., van der Velde, E. T., & Baan, J. (1993). Left ventricular stroke volume by single and dual excitation of conductance catheter in dogs. *Am.J.Physiol* 264, H2198-H2207.

Stern, M. D. (1992). Theory of excitation-contraction coupling in cardiac muscle. *Biophys.J.* 63, 497-517.

Stern, M. D., Capogrossi, M. C., & Lakatta, E. G. (1988). Spontaneous calcium release from the sarcoplasmic reticulum in myocardial cells: mechanisms and consequences. *Cell Calcium* 9, 247-256.

Stromer, H., de Groot, M. C., Horn, M., Faul, C., Leupold, A., Morgan, J. P., Scholz, W., & Neubauer, S. (2000). Na^+/H^+ exchange inhibition with HOE642 improves postischemic recovery due to attenuation of Ca^{2+} overload and prolonged acidosis on reperfusion. *Circulation* 101, 2749-2755.

Strum, D. P. & Pinsky, M. R. (2006). Modeling ischemia-induced dyssynchronous myocardial contraction. *Anesth.Analg.* 103, 846-853.

Studer, R., Reinecke, H., Bilger, J., Eschenhagen, T., Bohm, M., Hasenfuss, G., Just, H., Holtz, J., & Drexler, H. (1994). Gene expression of the cardiac Na^+-Ca^{2+} exchanger in end-stage human heart failure. *Circ.Res.* 75, 443-453.

Suga, H. & Sagawa, K. (1974). Instantaneous pressure-volume relationships and their ratio in the excised, supported canine left ventricle. *Circ.Res.* 35, 117-126.

Suga, H., Sagawa, K., & Shoukas, A. A. (1973). Load independence of the instantaneous pressure-volume ratio of the canine left ventricle and effects of epinephrine and heart rate on the ratio. *Circ.Res.* 32, 314-322.

Sunagawa, K., Maughan, W. L., Burkhoff, D., & Sagawa, K. (1983). Left ventricular interaction with arterial load studied in isolated canine ventricle. *Am.J.Physiol* 245, H773-H780.

Sutherland, F. J. & Hearse, D. J. (2000). The isolated blood and perfusion fluid perfused heart. *Pharmacol.Res.* 41, 613-627.

Tada, M. (2003). Calcium cycling proteins of the cardiac sarcoplasmic reticulum - Molecular regulation of the phospholamban-SERCA Ca^{2+} pump system and its pathophysiological consequences. *Circ.J.* 67, 729-737.

Talukder, M. A., Kalyanasundaram, A., Zhao, X., Zuo, L., Bhupathy, P., Babu, G. J., Cardounel, A. J., Periasamy, M., & Zweier, J. L. (2007). Expression of SERCA isoform with faster Ca^{2+} transport properties improves postischemic cardiac function and Ca^{2+} handling and decreases myocardial infarction. *Am.J.Physiol Heart Circ.Physiol* 293, H2418-H2428.

Tani, M. (1990). Mechanisms of Ca^{2+} overload in reperfused ischemic myocardium. *Annu.Rev.Physiol* 52, 543-559.

Tateishi, H., Yano, M., Mochizuki, M., Suetomi, T., Ono, M., Xu, X., Uchinoumi, H., Okuda, S., Oda, T., Kobayashi, S., Yamamoto, T., Ikeda, Y., Ohkusa, T., Ikemoto, N., & Matsuzaki, M. (2009). Defective domain-domain interactions within the ryanodine receptor as a critical cause of diastolic Ca^{2+} leak in failing hearts. *Cardiovasc.Res.* 81, 536-545.

ten Hove, M., van Emous, J. G., & van Echteld, C. J. (2003). Na^+ overload during ischemia and reperfusion in rat hearts: comparison of the Na^+/H^+ exchange blockers EIPA, cariporide and eniporide. *Mol.Cell Biochem.* 250, 47-54.

Terada, H., Hayashi, H., Satoh, H., Katoh, H., & Yamazaki, N. (1994). Simultaneous measurement of $[Na^+]_i$ and Ca^{2+} transients in an isolated myocyte: effects of strophanthidin. *Biochem.Biophys.Res.Commun.* 203, 1050-1056.

Terentyev, D., Kubalova, Z., Valle, G., Nori, A., Vedamoorthyrao, S., Terentyeva, R., Viatchenko-Karpinski, S., Bers, D. M., Williams, S. C., Volpe, P., & Gyorke, S. (2008). Modulation of SR Ca^{2+} release by luminal Ca^{2+} and calsequestrin in cardiac myocytes: effects of CASQ2 mutations linked to sudden cardiac death. *Biophys.J.* 95, 2037-2048.

Terentyev, D., Viatchenko-Karpinski, S., Valdivia, H. H., Escobar, A. L., & Gyorke, S. (2002). Luminal Ca^{2+} controls termination and refractory behavior of Ca^{2+}-induced Ca^{2+} release in cardiac myocytes. *Circ Res* 91, 414-420.

Thastrup, O., Cullen, P. J., Drobak, B. K., Hanley, M. R., & Dawson, A. P. (1990). Thapsigargin, a tumor promoter, discharges intracellular Ca^{2+} stores by specific inhibition of the endoplasmic reticulum Ca^{2+}-ATPase. *Proc.Natl.Acad.Sci.U.S.A* 87, 2466-2470.

Timerman, A. P., Onoue, H., Xin, H. B., Barg, S., Copello, J., Wiederrecht, G., & Fleischer, S. (1996). Selective binding of FKBP12.6 by the cardiac ryanodine receptor. *J Biol.Chem.* 271, 20385-20391.

Toda, T., Kadono, T., Hoshiai, M., Eguchi, Y., Nakazawa, S., Nakazawa, H., Higashijima, N., & Ishida, H. (2007). Na^+/H^+ exchanger inhibitor cariporide attenuates the mitochondrial Ca^{2+} overload and PTP opening. *Am.J.Physiol Heart Circ.Physiol* 293, H3517-H3523.

Toischer, K., Lehnart, S. E., Tenderich, G., Milting, H., Korfer, R., Schmitto, J. D., Schondube, F. A., Kaneko, N., Loughrey, C. M., Smith, G. L., Hasenfuss, G., & Seidler, T. (2009). K201 improves aspects of the contractile performance of human failing myocardium via reduction in Ca^{2+} leak from the sarcoplasmic reticulum. *Basic Res.Cardiol.*

Trafford, A. W., Diaz, M. E., & Eisner, D. A. (1998). Stimulation of Ca-induced Ca release only transiently increases the systolic Ca transient: measurements of Ca fluxes and sarcoplasmic reticulum Ca. *Cardiovasc.Res.* 37, 710-717.

Treiman, M., Caspersen, C., & Christensen, S. B. (1998). A tool coming of age: thapsigargin as an inhibitor of sarco-endoplasmic reticulum Ca^{2+}-ATPases. *Trends Pharmacol.Sci.* 19, 131-135.

Urschel, C. W., Covell, J. W., Sonnenblick, E. H., Ross, J., Jr., & Braunwald, E. (1968). Effects of decreased aortic compliance on performance of the left ventricle. *Am.J.Physiol* 214, 298-304.

Valdeolmillos, M., O'Neill, S. C., Smith, G. L., & Eisner, D. A. (1989). Calcium-induced calcium release activates contraction in intact cardiac cells. *Pflugers Arch.* 413, 676-678.

Van Bilsen, M., Snoeckx, L. H., Arts, T., Van der Vusse, G. J., & Reneman, R. S. (1991). Performance of the isolated, ejecting heart: effects of aortic impedance and exogenous substrates. *Pflugers Arch.* 419, 7-12.

Vanagt, W. Y., Cornelussen, R. N., Baynham, T. C., van Hunnik, A., Poulina, Q. P., Babiker, F., Spinelli, J., Delhaas, T., & Prinzen, F. W. (2007). Pacing-induced

dyssynchrony during early reperfusion reduces infarct size. *J.Am.Coll.Cardiol.* 49, 1813-1819.

Vangheluwe, P., Sipido, K. R., Raeymaekers, L., & Wuytack, F. (2006a). New perspectives on the role of SERCA2's Ca^{2+} affinity in cardiac function. *Biochim.Biophys.Acta* 1763, 1216-1228.

Vangheluwe, P., Tjwa, M., Van Den, B. A., Louch, W. E., Beullens, M., Dode, L., Carmeliet, P., Kranias, E., Herijgers, P., Sipido, K. R., Raeymaekers, L., & Wuytack, F. (2006b). A SERCA2 pump with an increased Ca^{2+} affinity can lead to severe cardiac hypertrophy, stress intolerance and reduced life span. *J.Mol.Cell Cardiol.* 41, 308-317.

Vassalle, M. & Lin, C. I. (2004). Calcium overload and cardiac function. *J.Biomed.Sci.* 11, 542-565.

Venetucci, L. A., Trafford, A. W., Diaz, M. E., O'Neill, S. C., & Eisner, D. A. (2006). Reducing ryanodine receptor open probability as a means to abolish spontaneous Ca^{2+} release and increase Ca^{2+} transient amplitude in adult ventricular myocytes. *Circ.Res.* 98, 1299-1305.

Ver, H. M., Heymans, S., Antoons, G., Reed, T., Periasamy, M., Awede, B., Lebacq, J., Vangheluwe, P., Dewerchin, M., Collen, D., Sipido, K., Carmeliet, P., & Wuytack, F. (2001). Replacement of the muscle-specific sarcoplasmic reticulum Ca^{2+}-ATPase isoform SERCA2a by the nonmuscle SERCA2b homologue causes mild concentric hypertrophy and impairs contraction-relaxation of the heart. *Circ.Res.* 89, 838-846.

Verboomen, H., Wuytack, F., De Smedt, H., Himpens, B., & Casteels, R. (1992). Functional difference between SERCA2a and SERCA2b Ca^{2+} pumps and their modulation by phospholamban. *Biochem.J.* 286 (Pt 2), 591-595.

Verboomen, H., Wuytack, F., Van den, B. L., Mertens, L., & Casteels, R. (1994). The functional importance of the extreme C-terminal tail in the gene 2 organellar Ca^{2+}-transport ATPase (SERCA2a/b). *Biochem.J.* 303 (Pt 3), 979-984.

Verkerk, A. O., Veldkamp, M. W., Bouman, L. N., & van Ginneken, A. C. (2000). Calcium-activated Cl^- current contributes to delayed afterdepolarizations in single Purkinje and ventricular myocytes. *Circulation* 101, 2639-2644.

Wehrens, X. H., Lehnart, S. E., Reiken, S., van der, N. R., Morales, R., Sun, J., Cheng, Z., Deng, S. X., de Windt, L. J., Landry, D. W., & Marks, A. R. (2005). Enhancing calstabin binding to ryanodine receptors improves cardiac and skeletal muscle function in heart failure. *Proc.Natl.Acad.Sci.U.S.A* 102, 9607-9612.

Wehrens, X. H., Lehnart, S. E., Reiken, S. R., Deng, S. X., Vest, J. A., Cervantes, D., Coromilas, J., Landry, D. W., & Marks, A. R. (2004). Protection from cardiac arrhythmia through ryanodine receptor-stabilizing protein calstabin2. *Science* 304, 292-296.

Wei, C. L., Valvano, J. W., Feldman, M. D., & Pearce, J. A. (2005). Nonlinear conductance-volume relationship for murine conductance catheter measurement system. *IEEE Trans.Biomed.Eng* 52, 1654-1661.

Wettwer, E., Christ, T., Dobrev, D., & Ravens, U. (2007). Novel anti-arrhythmic agents for the treatment of atrial fibrillation. *Curr.Opin.Pharmacol.* 7, 214-218.

Wibo, M., Bravo, G., & Godfraind, T. (1991). Postnatal maturation of excitation-contraction coupling in rat ventricle in relation to the subcellular localization and surface density of 1,4-dihydropyridine and ryanodine receptors. *Circ.Res.* 68, 662-673.

Wu, C. C., Skalak, T. C., Schwenk, T. R., Mahler, C. M., Anne, A., Finnerty, P. W., Haber, H. L., Weikle, R. M., & Feldman, M. D. (1997). Accuracy of the conductance catheter for measurement of ventricular volumes seen clinically: effects of electric field homogeneity and parallel conductance. *IEEE Trans.Biomed.Eng* 44, 266-277.

Xiao, B., Sutherland, C., Walsh, M. P., & Chen, S. R. (2004). Protein kinase A phosphorylation at serine-2808 of the cardiac Ca^{2+}-release channel (ryanodine

receptor) does not dissociate 12.6-kDa FK506-binding protein (FKBP12.6). ***Circ.Res.*** **94, 487-495.**

Xu, C., Ma, H., Inesi, G., Al Shawi, M. K., & Toyoshima, C. (2004). Specific structural requirements for the inhibitory effect of thapsigargin on the Ca^{2+} ATPase SERCA. ***J.Biol.Chem.*** **279, 17973-17979.**

Yamaguchi, F., Sanbe, A., & Takeo, S. (1997). Cardiac sarcoplasmic reticular function in rats with chronic heart failure following myocardial infarction. ***J.Mol.Cell Cardiol.*** **29, 753-763.**

Yamamoto, T., Yano, M., Xu, X., Uchinoumi, H., Tateishi, H., Mochizuki, M., Oda, T., Kobayashi, S., Ikemoto, N., & Matsuzaki, M. (2008). Identification of target domains of the cardiac ryanodine receptor to correct channel disorder in failing hearts. ***Circulation*** **117, 762-772.**

Yang, B., Larson, D. F., Beischel, J., Kelly, R., Shi, J., & Watson, R. R. (2001). Validation of conductance catheter system for quantification of murine pressure-volume loops. ***J.Invest Surg.*** **14, 341-355.**

Yano, M., Kobayashi, S., Kohno, M., Doi, M., Tokuhisa, T., Okuda, S., Suetsugu, M., Hisaoka, T., Obayashi, M., Ohkusa, T., Kohno, M., & Matsuzaki, M. (2003). FKBP12.6-mediated stabilization of calcium-release channel (ryanodine receptor) as a novel therapeutic strategy against heart failure. ***Circulation*** **107, 477-484.**

Yano, M., Ono, K., Ohkusa, T., Suetsugu, M., Kohno, M., Hisaoka, T., Kobayashi, S., Hisamatsu, Y., Yamamoto, T., Kohno, M., Noguchi, N., Takasawa, S., Okamoto, H., & Matsuzaki, M. (2000). Altered stoichiometry of FKBP12.6 versus ryanodine receptor as a cause of abnormal Ca^{2+} leak through ryanodine receptor in heart failure. ***Circulation*** **102, 2131-2136.**

Yano, M., Yamamoto, T., Ikeda, Y., & Matsuzaki, M. (2006). Mechanisms of Disease: ryanodine receptor defects in heart failure and fatal arrhythmia. ***Nat.Clin.Pract.Cardiovasc.Med.*** **3, 43-52.**

Yates, J. C., Beamish, R. E., & Dhalla, N. S. (1981). Ventricular dysfunction and necrosis produced by adrenochrome metabolite of epinephrine: relation to pathogenesis of catecholamine cardiomyopathy. *Am.Heart J.* 102, 210-221.

Ytrehus, K., Liu, Y., & Downey, J. M. (1994). Preconditioning protects ischemic rabbit heart by protein kinase C activation. *Am.J.Physiol* 266, H1145-H1152.

Yuan, W., Ginsburg, K. S., & Bers, D. M. (1996). Comparison of sarcolemmal calcium channel current in rabbit and rat ventricular myocytes. *J.Physiol* 493 (3), 733-746.

Zahradnikova, A., Dura, M., & Gyorke, S. (1999). Modal gating transitions in cardiac ryanodine receptors during increases of Ca^{2+} concentration produced by photolysis of caged Ca^{2+}. *Pflugers Arch.* 438, 283-288.

Zima, A. V., Picht, E., Bers, D. M., & Blatter, L. A. (2008). Termination of cardiac Ca^{2+} sparks: role of intra-SR $[Ca^{2+}]$, release flux, and intra-SR Ca^{2+} diffusion. *Circ.Res.* 103, 105-115.

Zimmer, H. G. & Millar, H. D. (1998). Technology and application of ultraminiature catheter pressure transducers. *Can.J.Cardiol.* 14, 1259-1266.

Zimmerman, A. N. & Hulsmann, W. C. (1966). Paradoxical influence of calcium ions on the permeability of the cell membranes of the isolated rat heart. *Nature* 211, 646-647.

Zygmunt, A. C., Goodrow, R. J., & Weigel, C. M. (1998). I_{NaCa} and $I_{Cl(Ca)}$ contribute to isoproterenol-induced delayed after depolarizations in midmyocardial cells. *Am.J.Physiol* 275, H1979-H1992.